The geology of the Mozambique belt and the Zimbabwe craton around Manica, Western Mozambique.

By

Antonio dos Santos Tcheco Manhica

Submitted in partial fulfilment of the requirements for the degree

Magister Scientia

in the Faculty of Science

University of Pretoria

Pretoria

August 1998

1998

I Hereby certify that this thesis is my own work except where specifically acknowledged and that this thesis has not been submitted elsewhere for the purposes of being awarded a degree.

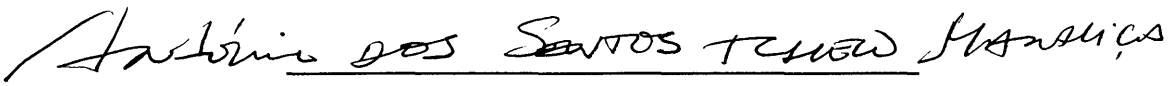

Acknowledgments

Various institutions and organizations have given support of one form or other for the realization of this project for the MSc. degree. Among these, some merit special mention.

Anglo American Prospecting Service (AAPS) funded all field expenses including subsistence and gave logistical support by means of transport and field material and equipment as required. In addition, they provided the necessary funds for accommodation and subsistence while in Pretoria. For all this support I whish to extend my sincere gratitude to this organization and, in particular, to Mr. Roy Corrans, Consultant Geologist and Director of the New Mining Business of which AAPS is part, and to Mr. Steve Marsh, then Head of AAPS, Clayville Office.

To fulfill the requirements for candidateship to this Msc. degree, I completed my Bsc. (Hons). at the Department of Geology, University of Pretoria, with full financial support from the Council for Geoscience in Pretoria. This support was extended to the first year of my MSc. studies. For this I fell in debt with this institution and, in particular, with Dr. Frick, the Director of the Council for Geoscience.

Major and trace elements analyses as well as microprobe and X-Ray Diffraction investigations were done at the laboratories of the Department of Geology of the University of Pretoria with the expenses covered by the department. For this reason I thank the Department and, in particular, Prof. de Waal, in his capacity as Head of the Department, for permitting this. Mrs M. Loubser, the analyst in the X-Ray fluorescence section, Mrs. S. Verryn who performed the XRD analyses and the late Mr. A.V. Atanasov who assisted in the microprobe analyses are thanked for their help.

I thank the Minister of Mineral Resources and Energy of Mozambique for allowing me to take a study leave, the National Director of Geology for the continued multidisciplinary support and the Provincial Director of Mineral Resources and Energy in Manica, Mr. Abdurremane Materia Machon, for the extremely useful logistic support while in the province.

I wish to express my unmeasurable gratitudes to Prof. Geoff Grantham who, not only gave the necessary academic guidance in his capacity as supervisor, but also made sure that all other necessary conditions were there for normal progress of the study. His comments into my various versions of the thesis, helped to bring the thesis to a level of acceptability not only technically but also in terms of language. I thank him, in addition, for financial support from his FRD grant which contributed to the radiogenic isotope studies, the rare earth element analyses and subsistence during 1998.

Prof. Snyman is thanked for his assistance in his capacity as co-supervisor and for the comments and suggestions made in the thesis.

Finally, my achievements would not have been possible if I did not enjoy support and encouragement from my family. So to you Paula, Danilo and Gisela I dedicate this thesis.

THE GEOLOGY OF THE MOZAMBIQUE BELT AND THE ZIMBABWE CRATON AROUND MANICA, WESTERN MOZAMBIQUE

Table of contents

List of Figures **Page no.**

List of Tables **Page no.**

List of appendices

1. Table showing samples per lithological unit, locality and coordinates of samples used in geochronology, geothermobarometry and thermochronology
2. Table of microprobe analyses of minerals used in the thermobarometry
3. Description of analytical techniques

THE GEOLOGY OF THE MOZAMBIQUE BELT AND THE ZIMBABWE CRATON AROUND MANICA, WESTERN MOZAMBIQUE.

Abstract

The study area comprises the Archaean Manica Greenstone Belt and the Vumba Granite Gneiss, the Proterozoic Messica Granite Gneiss of the Zimbabwe Craton, the possibly allochthonous metasedimentary sequence of the Frontier Formation, the granitoids of the Mozambique Metamorphic Province, which are subdivided into Vanduzi Migmatite Gneiss, the Chimoio Granodiorite Gneiss, the Nhansipfe Granitic Orthogneiss and the Pan-African Tchinhadzandze Granodiorite Gneiss. The rock sequences in the two provinces are cut by mafic intrusions.

The greenstone belt comprises mafic to ultramafic and pelitic schists and serpentinites of the Macequece Formation and metasediments of the M'Beza/Vengo Formation. The mafic to ultramafic schists and the serpentinites have chemical signatures of komatiites. The Vumba Granite Gneiss comprises the northern and southern Vumba granitoids dated at 3885±255 Ma, and 2527±632 Ma respectively. They vary from metaluminous to peraluminous, have normative QAP compositions of granodiorites and monzogranites and chemical signatures of mantle fractionates and volcanic-arc granitoids. The Early Proterozoic Messica Granite Gneiss is 2348±267 Ma old, is metaluminous and has QAP compositions of monzogranites and chemical signatures suggesting a crustal source and a volcanic-arc environment. The Frontier Formation comprises quartzite and pelitic schists. The Vanduzi Migmatite Gneiss comprises stromatic and stictolithic types. Two mineral assemblages are distinguished as they contain either garnet or hornblende. The Mid-Proterozoic Chimoio Granodioritic Gneiss is 1236±201 Ma old. It is granodioritic and metaluminous with a chemical signature of volcanic-arc granitoids. The Late Proterozoic Nhansipfe Granitic Orthogneiss is dated at 981±83 Ma and varies from metaluminous to peraluminous. The Rb, Nb and Y contents are typical of within-plate granitoids, whereas Ga, Zr, Al, Ce and Y are typical of A-type granitoids. The age of the mafic intrusions falls between ~500 and ~1100 Ma. The rocks typically contain plagioclase, hornblende and clinopyroxene with or without garnet and orthopyroxene. The chemistry of the rocks is typical of sub-alkaline tholeiites. The Tchinhadzandze Granodiorite Gneiss may be part of a Pan-African event which lasted till ~450-~500 Ma. The normative feldspar compositions and Rb, Ba and Sr contents are typical of granodiorites. It is metaluminous and has Rb, Y and Nb contents typical of volcanic-arc granitoids.

The planar fabrics in the Archaean granite-greenstone belt are characterized by E-W to SW-NE strikes and steep dips to N and S and to NW and SE. The mineral lineations and fold axes plunge 60° and 30° respectively towards the E. Within the Mozambique belt, around the central part and in the extreme east of the study area, the planar fabrics have essentially N-S strikes and steep dips to E and W in contrast with complex deformation observed in the migmatites and megacrystic granitoids.

The study area can be subdivided into three metamorphic blocks, namely, one of low-grade greenschist facies, one of medium-grade amphibolite facies and a third block of high-grade metamorphism.

Uittreksel

Die studiegebied behels die Argeïese Manica Groensteengordel en die Vumba Granietgneis, die Proterosoiëse Messica Graniet Gneis van die Zimbabwe-kraton, die moontlik allochtone metasedimentêre opeenvolging van die Frontier Formasie, die granitoïede van die Mosambiek Metamorfe Provinsie wat onderverdeel word in die Vanduzi Migmatiet Gneis, die Chimoio Granodioriet Gneis, die Nhansipfe Granitiese Ortogneis en die Pan-Afrikaanse Tchinhadzandze Granodioriet Gneis. Die gesteente-opeenvolgings in die twee provinsies word gesny deur mafiese indringings.

Die groensteengordel bestaan uit mafiese tot ultramafiese en pelitiese skiste en serpentiniete van die Macequece Formasie en metasedimente van die M'Beza/Vengo Formasie. Die mafiese tot ultramafiese skiste en die serpentiniete het chemiese kenmerke van komatiïete. Die Vumba Graniet Gneis bestaan uit die noordelike en suidelike Vumba granitoïede wat op 3885±225 Ma en 2527±632 Ma onderskeidelik gedateer is. Hulle varieer van metalumineus tot peralumineus, het normatiewe QAP samestellings van granodioriete en monsograniete en chemiese kenmerke van mantelfraksionate en vulkaniese-boog granitoïede. Die Vroeg-Proterosoïese Messica Graniet Gneis is 2348±267 Ma oud, is metalumineus, het QAP samestellings van monsograniete en chemiese kenmerke wat op korsoorsprong en vulkaniese-boog granitoïede dui. Die Frontier Formasie bestaan uit kwartsiet en pelitiese skis. Die Vanduzi Migmatiet Gneis behels stromatiese en stiktolitiese tipes. Twee mineraalversamelings word onderskei deurdat hulle óf granaat óf horingblende bevat. Die Middel-Proterosoïese Chimoio Granodioriet Gneis is 1236±201Ma oud. Dit is metalumineus en is tipies granodiorities met die chemiese kenmerke van vulkaniese-boog granitoïede. Die Laat-Proterosoïese Nhansipfe Granitiese Ortogneis is gedateer op 981±83 Ma en wissel van metalumineus tot peralumineus. Die Rb-, Nb- en Y-inhoud is tipies van intraplaat granitoïde, en die Ga-, Zr-, Al-, Ce- en Y-inhoud is tipies van A-tipe granitoïede. Die ouderdom van die mafiese intrussies lê tussen ~500 en ~1100Ma. Die gesteentes bevat tipies plagioklaas, horingblende en klinopirokseen met of sonder granaat en ortopirokseen. Die chemie van die gesteentes is tipies van subalkaliese tholeïïete. Die Tchinhadzandze Granodioriet Gneis is moontlik deel van 'n Pan-Afrikaanse gebeurtenis wat tot ~450-~500 Ma geduur het. Die normatiewe veldspaat-samestellings en die Rb-, Ba- en Sr-inhoud is tipies van granodioriet. Dit is metalumineus en het Rb-, Y- en Nb-inhoude tipies van vulkaniese-boog granitoïede.

Die vlakkige maaksels in die Argeïese graniet-groensteengordel word gekenmerk deur O-W tot SW-NO strekkings en steil hellings na N en S en na NW en SO. Die mineraallineasies en plooi-asse duik 60° en 30° onderskeidelik na die Ooste. In die Mosambiekgordel, naby die middel en in die ooste van die studiegebied, strek die vlakkige maaksels in wese N-S en hel steil na die Ooste en Weste, in teenstelling met die komplekse vervorming wat in die migmatiete en megakristiese granitoïede gesien word.

Die studiegebied kan in drie metamorfe terreine onderverdeel word, naamlik een van laegraadse groenskisfasies, een van mediumgraadse amfibolietfasies en 'n derde van hoëgraadse metamorfose.

THE GEOLOGY OF THE MOZAMBIQUE BELT AND THE ZIMBABWE CRATON AROUND MANICA, WESTERN MOZAMBIQUE.

Chapter 1

INTRODUCTION

1.1 Introduction

The geology of Mozambique is poorly known. Published geological maps include the 1987 1:1000 000 map of the whole country, the 1969 1:250 000 maps which largely cover the Precambrian terrains and several generations of 1:50 000 maps of mining districts. For some of the mines 1:10 000 maps were produced. In general, detailed studies have been confined to the mines themselves, emphasising largely economic aspects with little or no extension to the surrounding areas. Few specialized studies concentrating on tectonics and structural geology have so far been undertaken. This situation has inhibited correlation of the geology of Mozambique with that of surrounding countries such as South Africa, Zimbabwe, Swaziland, Zambia and Tanzania.

The geographic position of Mozambique in the framework of Gondwana, makes the country a geologically important terrain particularly because it contains boundaries between cratonic and mobile belt terrains. The deformation and metamorphism contributing to the Mozambique Metamorphic Province is viewed as originating during the amalgamation of Gondwana (Moyes *et al.*, 1993; Dalziel, 1991).

It was decided, therefore, that a study of the geology of the boundary between the Zimbabwe Craton and the Mozambique Metamorphic Province with emphasis on the Mozambique Metamorphic Province, would make a valuable contribution towards the understanding of geological processes that took place in the region and in Gondwana.

1.2 Regional geological setting

The study area includes part of the Archaean to Early Proterozoic-age Zimbabwe Craton and the Late Proterozoic-age Mozambique Metamorphic Province (Fig. 1.1). The Zimbabwe Craton forms part of the Kalahari Craton which also includes the Archaean-age Kaapvaal Craton and Limpopo Metamorphic Province. These entities stabilised far earlier than the central, northeastern and northwestern African cratons that stabilised during the Proterozoic (Petters, 1991, p.10-11). The Mozambique Metamorphic Province forms part of a Grenvillian-age (~1100 Ma±100 Ma) metamorphic terrain which was accreted onto the Kalahari Craton in southern Africa at that time (Fig. 1.1).

Reconstructions of Gondwana suggest that this Grenvillian-age belt continues southwards through western Dronning Maud Land, Antarctica, where it changes to a south-easterly direction and continues

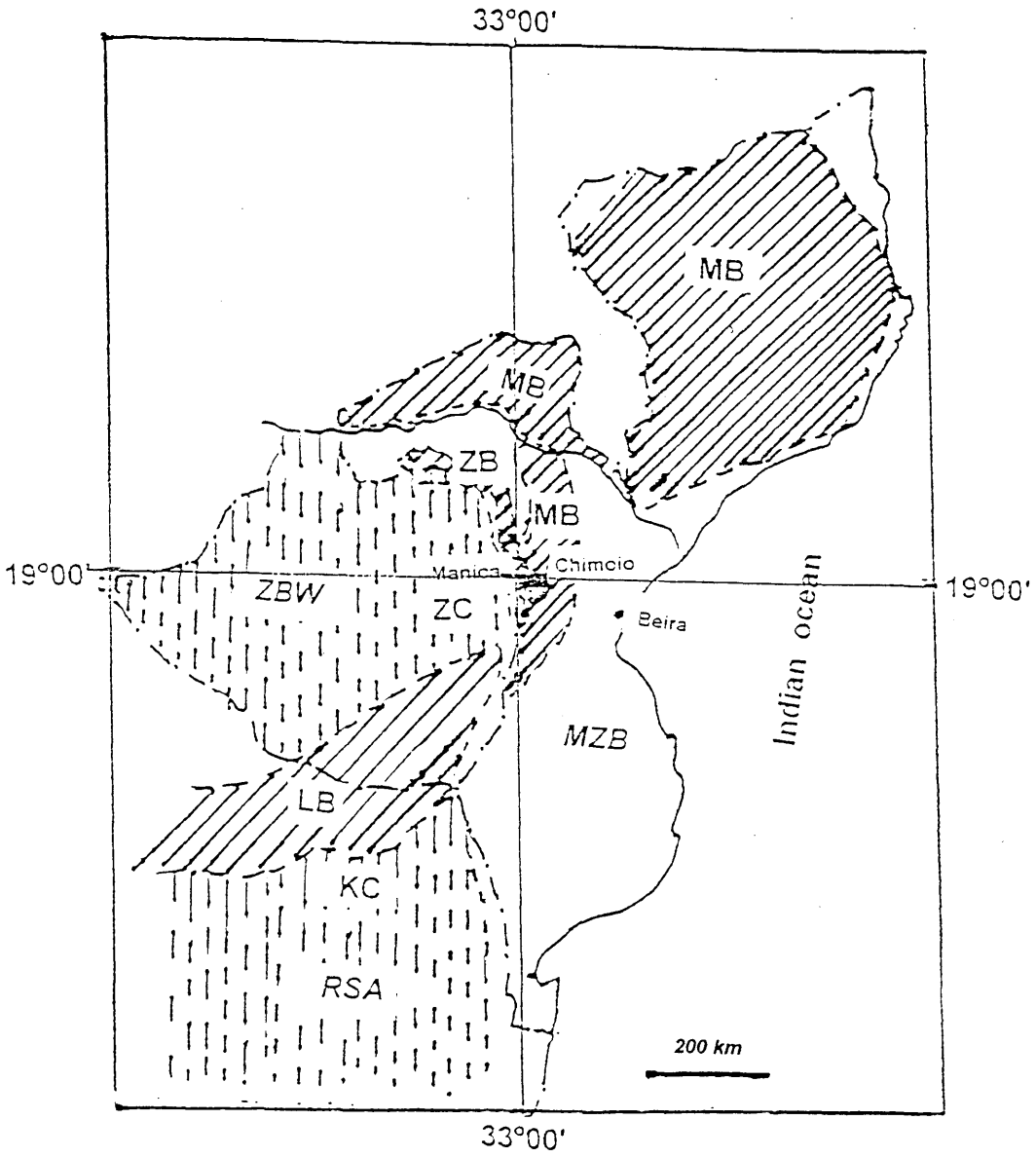

Figure 1.1: Location of the study area shown in the context of the regional geological structure of southern Africa. Adapted from Afonso (1978), Petters (1991) and Dirks *et al.* (1998) data. LB- Limpopo Metamorphic Province MB- Mozambique Metamorphic Province, ZB- Mid-Zambezi Metamorphic Province, ZC- Zimbabwe Province and KC- Kaapvaal Province. ZBW- Zimbabwe, RSA- South Africa and MZB- Mozambique.

into the Natal Metamorphic Province where the rocks become obscured by later Phanerozoic cover sequences (Grantham *et al.* 1988; Groenewald *et al.*, 1991).

1.3 Previous geological work

The study area has been the subject of several geological and metallogenic studies since the beginning of the 20th century, particularly concentrating on Archaean gold deposits which are hosted in the Manica Greenstone Belt. Few of these studies have been formally published.

Phaup (1937), gives an outline of the geology of the Umtali (Zimbabwe) area which describes extensions into Zimbabwe of the Manica (Mozambique) gold belt. In this outline he describes the rock types, structure, tectonics and genesis of the belt. Phaup (1937) reported the main lithological units as comprising the Archaean Greenstone Series which included talc-schist and serpentinites, the M'Beza Sedimentary Series, comprising successively a basal conglomerate, grits, greywacke, arkose, phylites, slates and conglomerate composed of greywacke pebbles. He also described granite batholiths with fine-grained margins grading to coarse grained gneissic granite at the centre of the batholiths. Vail (1964) described the Umkondo System adjacent to the southern part of study area and indicated that it consisted of undeformed, unmetamorphosed sediments. Oberholzer (1964) described the lithostratigraphy of the Archaean Manica Group as consisting of the Macequece Formation which is composed of ultrabasic rocks correlated with the Bulawayan Group in Zimbabwe, and the M'Beza/Vengo Formation, a metasedimentary sequence correlated with the Shamvaian Group of Zimbabwe. Vail (1965) used the K-Ar method to determine ages of biotite in the Gairezi Group gneiss and in the Frontier Formation schist in Macossa (localities adjacent to the study area) and obtained mineral resetting ages of 525±20 and 526±30 respectively. A mineral resetting age of 465±20 in muscovite from the Chicamba quartzite (Frontier Formation, within the study area) was also determined by Vail (1965). A comprehensive geologic investigation involving photogeology and field mapping of Precambrian terrains in the Manica province was undertaken during the 1960's by Araujo and Gouveia (1965) and culminated with the publication of a map. On this map the Precambrian geology is subdivided into (1) the greenschist facies or low grade Archaean Manica System, which includes talc-schists, serpentinites, greenstones and gneisses as well as banded quartzites of the Macequece Series and conglomerates, greywackes and schists of the Vengo Series, (2) the medium to high grade Proterozoic Barue Formation which is composed of granitoid gneisses, metadolerites and amphibolites and (3) the Umkondo System which includes micaschists, quartzites and schists of the Frontier Formation and carbonates, hornfels, schists and quartzites of the Umkondo Formation. They distinguished three types of gneisses, namely, migmatitic, granitic and granite gneisses.

As a result of work done by a multidisciplinary team in the mid sixties, the Servicos de Geologia e Minas da Provincia de Mocambique (1969), Published the "Carta Geologica da Regiao de Vila Manica-Vila Gouveia, Grau Quadrado 1833, scale 1: 250 000". This map shows a detailed distribution and relationship of lithological units and was taken as the main reference in selecting the present study area. Obretenov (1977) described the geology of Manica as part of a survey into the mining in the region. His study mostly confirmed data from previous authors and correlated the Manica Group with the Shamvaian Group in Zimbabwe. He described the rocks of the M'Beza/Vengo Formation as being meta-argilites, black schist, sericite schist and argillaceous schist, meta-

greywacke, meta-arkose and meta-conglomerate. In addition, he included a quartzitic unit at the top of Macequece Formation but conceded this to be controversial and suggested the existence of at least three types of these quartzites. As part of a large scale geologic survey, the area was studied by Hunting, a consulting company, in 1984. The study included aerogeophysics and photogeology with ground control and defined the Matambo Group (Barr *et al.,* 1983). Pinna *et al.* (1986) distinguished greenstones, granitoids and metasediments of the Archaean Manica Group, metasediments of the Frontier Formation which is included in the Gairezi Group, and granitoids of the Madzuire and Matambo Groups which are included in the Mozambique Belt in the study area. More recently a PhD study on the Manica Greenstone Belt and adjacent granitoids by Manuel (1992) describes the geology, petrography, geochemistry and ore deposits. Using chemistry and petrography, he subdivided the granitoid rocks into tonalites, granodiorites and adamellites and further showed the granitoids as being Middle to Late Archaean in age. He also described the basic to ultrabasic rocks of the Manica Greenstone belt as peridotitic and basaltic komatiites, serpentinites, metabasalts and gabbros and confirmed their low grade metamorphism. Based on these age determinations and other several Late Archaean ages of granites, felsites and stromatolites, a stratigraphic column for the Manica region was produced and a correlation with the Zimbabwe Craton ages made. Thus, the older granitoids are correlated with the Sebakwian whereas the younger granitoids as well as felsites and greenstones are correlated to the Bulawayan Group. Manuel (1992) describes conglomerate occurrences in the Zambuzi Valley, monomictic metaconglomerate of serpentinite in the Isitaca and Seymour areas and polymictic conglomerate of metabasalt, serpentinite, komatiite, schist, quartzite and granites in the Penhalonga, Monarch and Chua areas. Schwarz (1994), studied a detailed section through the "Vengo Group" and reported the following lithological sequence from top to bottom:

4. Dolostone sequence, with stromatolites and archaeocyathids,
3. Unit of weathered residue enriched in manganese (Mn),
2. Metaclastic rocks,
1. Metavolcanic rocks

The metaclastic rocks are characterized by an alternating sequence of fine and coarse grained layers that include volcanic rocks.

In conclusion, it is apparent that much of the previous work conducted in the study area concentrated largely on the Manica Greenstone Belt and to a lesser extent on its surrounding granitoid gneisses. Consequently this study will devote more attention to the boundary relationships between the Zimbabwe Craton and the Mozambique Metamorphic Province and to the geology of the latter.

Chapter 2

LITHOSTRATIGRAPHY

2.1 Introduction

This chapter describes the stratigraphic framework used in this thesis. The stratigraphic framework and nomenclature used are based on the previous work done in the study area and described in the previous chapter, as well as those field relationships recorded in this study. The field relationships are described in this chapter. Figure 2.1 (p. 6) shows the distribution of the lithological units. Sample localities are shown on Figure 2.2 and the actual samples are indicated in Appendix 1. The stratigraphic framework is outlined in Table 2.1.

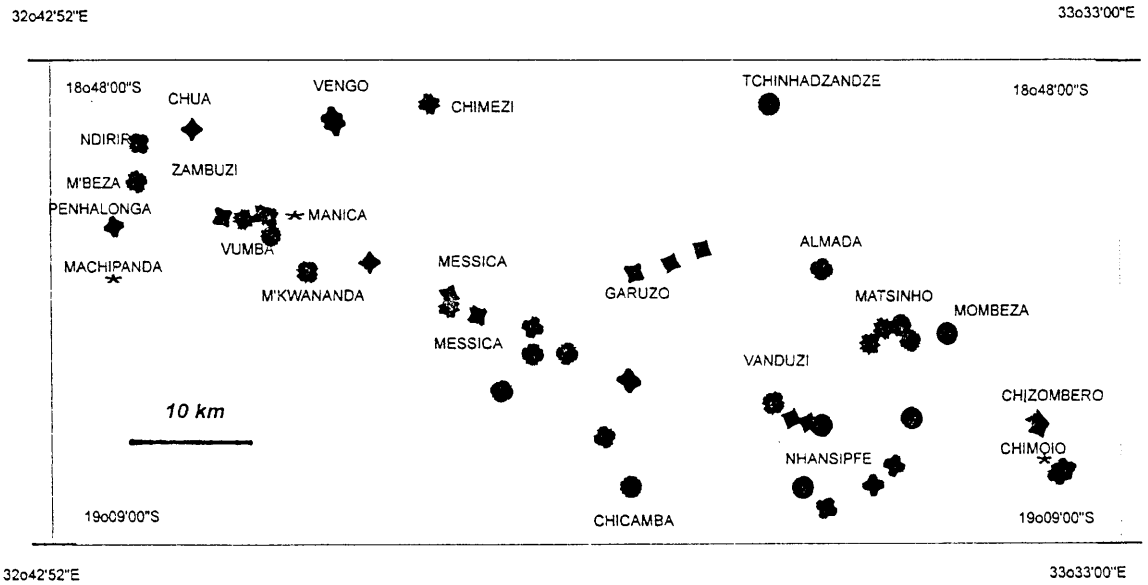

Figure 2.2: Sampling locality map. Locality names are those known to the locals and may be different from the official denominations. Star symbols represent main towns. The others represent sampling localities and due their differences to the number of samples taken in each locality.

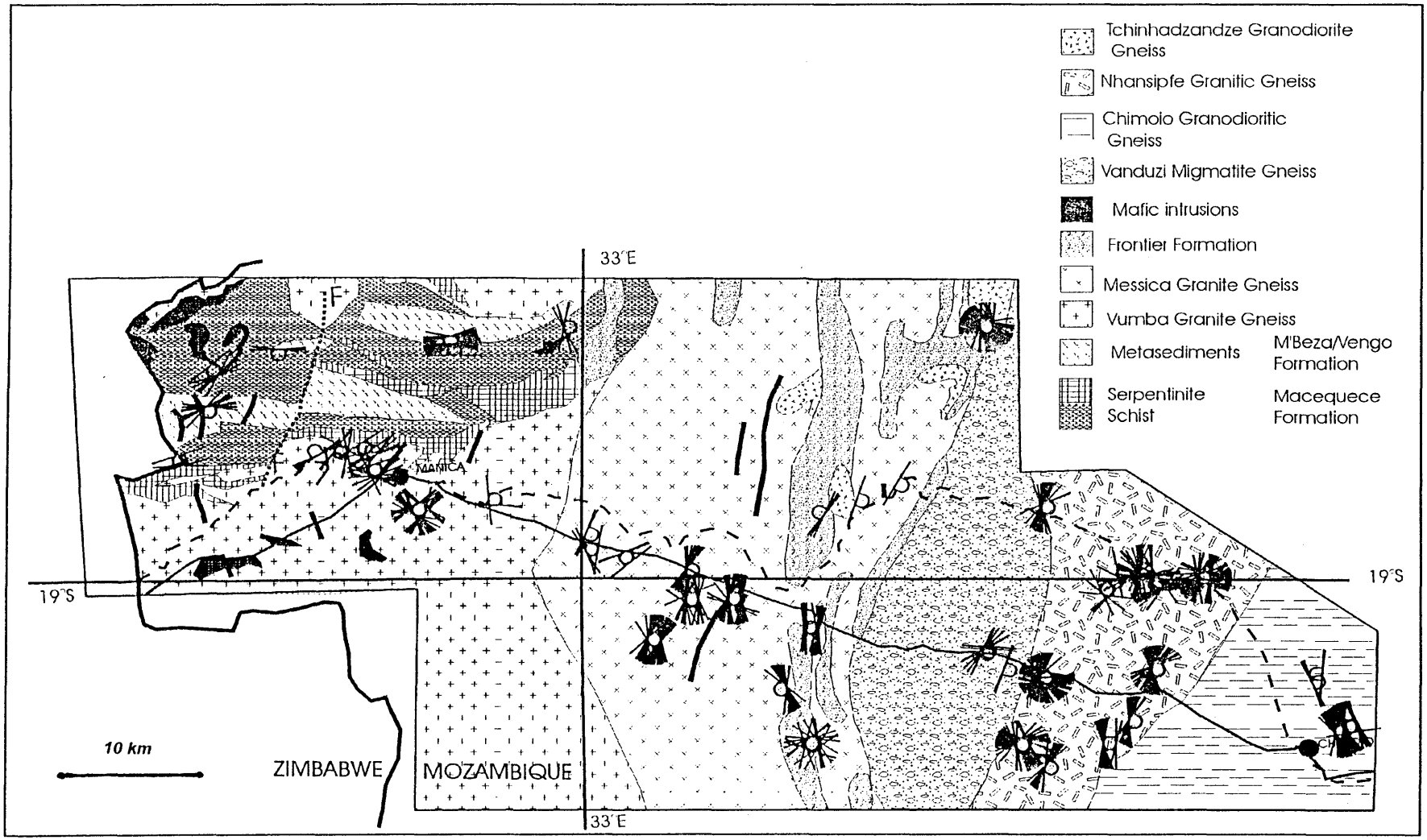

Figure 2.1: Major lithological units and planar fabrics directions within the study area. Broken and full lines across the map represent the railway and the main road respectively. Geologic map after Gouveia *et al.* (1968) with additions from present study.

Table 2.1: Stratigraphic framework of lithological units. Compiled using present study data and data from Oberlholzer (1964), Gouveia *et al.* (1968), Pinna *et al.* (1986) and Manuel (1992).

tectonic block	geologic formation	lithological unit	age
Late-Mozambique Belt	Young Granite	Tchinhadzandze Grano-diorite Gneiss Mafic Dykes	?
Mozambique Belt	---------- ? Madzuire Group Matambo Group	Nhansipfe Granitic Orthogneiss Chimoio Granodioritic Gneiss Vanduzi Migmatite Gneiss	~980 Ma ~1200 Ma
Pre-Mozambique belt	Gairezi Group	Frontier Formation pelitic schist, quartzite	?
Zimbabwe Craton		Messica Granite Gneiss	~2300 Ma
		M'Beza/Vengo Formation greywackes, shales, pelitic schists, congolmerates metaconglomerates	?
		South Vumba Granite Gneiss	~2500 Ma Manuel (1992)
	Manica Group	Macequece Formation mafic to ultramafic schists, felsic schists, serpentinites	~2800 Ma Manuel (1992)
		North Vumba Granitic Gneiss	~3400 Ma Manuel (1992)

Outcrops in the study area are very poor with few relationships between the various units being exposed. Access is also severely restricted because of a limited road network and the uncertainty of the distribution of landmines.

The Archaean granite-greenstone terrain occupies about one third of the study area in the western part. The greenstone lithological units include the M'Beza/Vengo and Macequece Formations which strike approximately E-W to NE-SW in the north-western part of the study area (Fig. 2.1). Exposures of the Vumba Granite Gneiss are found north and south of the greenstone (Fig. 2.1). Both the greenstones and the Vumba Granite Gneiss form steep hilly topography. East of the greenstones and the Vumba Granite Gneiss, the Messica Granite Gneiss is exposed and forms more subdued topography. The metasediments of the Frontier Formation locally overly the greenstone lithologies, the Vumba Granitic Gneiss and the Messica Granite Gneiss. The main exposures of the Frontier Formation form prominent N-S ridges, particularly as a consequence of highly resistant quartzites. East of the Messica Granite Gneiss, migmatitic gneisses of widely varying composition which constitute the

Vanduzi Migmatite Gneiss are exposed. To the east of the migmatites, the megacrystic Nhansipfe Granitic Orthogneiss forms an extensive body. Finally, the eastern extremity of the area is underlain by the Chimoio Granodioritic Gneiss. Small (1-2 km in diameter) plutons of Tchinhadzandze Granodiorite Gneiss are distributed in the centre of the study area and are hosted by the Messica Granite Gneiss although no intrusive contacts were seen. The planar fabric in the granite is variable and is weakly developed compared to the surrounding Messica Granite Gneiss and consequently the Tchinhadzandze Granodiorite Gneiss is viewed as being emplaced either after the fabric-forming event or as being late syn-tectonic.

2.2 Field Distribution and Age of Major Lithostratigraphic Units

The oldest rocks dated in the study area are the northern Vumba granitoids (Manuel, 1992). However, because enclaves of the Macequece Formation rocks are seen in the surrounding granitoids (Phaup, 1937), the former must, at least in part, be even older. In addition Phaup (1937) recorded fine-grained granite where the granites are in contact with the ultramafic rocks of the Macequece Formation which he interpreted to represent a chilled margin and he also reported two generations of granitic rocks. Manuel (1992) also determined two ages of granites from the Vumba granitoids using the Rb/Sr method. A suite of samples from granitoids exposed north of the Manica Greenstone Belt yielded an age of 3385±255 Ma whereas samples from granitoids south of the Manica Greenstone Belt yielded 2527±632 Ma (Manuel, 1992). Meta-volcanic horizons within the Manica Greenstone Belt have yielded a Rb/Sr date of 2801±42 Ma. Age relationships within the ultramafic rocks of the Macequece Formation in the Manica Greenstone belt are difficult to determine due to structural complexity. However, Manuel (1992) suggested that the ultramafic rocks are older than the pelitic schist because the latter schists contain granite clasts. The metasediments of the Mbeza/Vengo Formation are obviously younger than the oldest granitoids because the meta-conglomerates contain clasts of the granitoids. Oberholzer (1964) indicated that the second generation of granitoids is younger than the metasediments of the Mbeza/Vengo Formation because the granites intrude the metasediments. A Rb/Sr study of the Messica Granite Gneiss suggests an age 2348±267 Ma and therefore represents a younger, Early Proterozoic-age granite. No contacts between the Messica Granite Gneiss and the Vumba granitoids were seen. However the style of deformation in the former is simpler suggesting that it is less deformed and consequently is probably younger than the Vumba granitoids. Figure 2.1 shows that the metasediments of the Frontier Formation are restricted to areas underlain by the Macequece Formation, the Vumba Granite Gneiss and the Messica Granite Gneiss. Afonso (1974) described an angular unconformity between rocks of the Umkondo Group and the underlying folded and metamorphosed strata of the Frontier Formation. Barr *et al.* (1983) confirmed the age relationship during photogeological studies which established that the Umkondo overlies part of Gairezi Group which includes the Frontier Formation. Allsopp *et al.* (1989) suggested that the Umkondo Group has a minimum age of ~1089Ma based on Rb/Sr ages of biotite in mafic intrusions into the Umkondo Group. Mafic dykes intrude the Manica Greenstone Belt, the surrounding granitoids and the metasediments of

the Frontier Formation (Carta Geologica Vila Manica-Vila Gouveia 1:250 000*)*. More recently, Pinna *et al.* (1986) indicates that the age of post- Umkondo dolerites vary between 1100-500 Ma (K/Ar dating) and suggested that the Umkondo Group may be the southern equivalent of the Roan Supergroup in Zambia formed at
~1150 Ma. Given the present uncertainty, all that can be said is that the Frontier Formation has an emplacement age younger than the ~2300 Ma of the underlying Messica Granite Gneiss and older than the ~1089 Ma Umkondo which overlies it.

The Chimoio Granodioritic Gneiss gave an age of 1236±202 Ma, older than the Nhansipfe Granitic Orthogneiss with an age of 981±83 Ma, and is incorporated into the Madzuire Group. The younger granitic intrusions are termed the Tchinhadzandze Granodiorite Gneiss.

Chapter 3

MANICA GREENSTONE BELT

3.1 Introduction

The Manica Greenstone Belt comprises rocks of the Macequece and M'Beza/Vengo Formations and both units belong to the Archaean Manica Group and constitute the continuation into Mozambique of the Zimbabwe's Mutare greenstone belt. The M'Beza/Vengo Formation comprises two units, namely, M'Beza and Vengo sequences and lies discordantly on schists and serpentinites of the Macequece Formation. The M'Beza/Vengo Formation comprises pelitic schist, conglomerates, greywackes, shales and their metamorphic equivalents.

3.2 Field Description

3.2.1 Macequece Formation

The Macequece Formation (Fig. 2.1) consists of interlayered Mg-rich and pelitic rocks which show varying degrees of deformation. The highly strained varieties have strong schistose planar fabrics whereas in some areas the rocks are undeformed but metamorphosed to low grades.

The schists occur in the central part of the greenstone belt and share boundaries with metasediments, quartzite, serpentinite and granitoid rocks towards the centre and periphery respectively. The schists are cut by mafic intrusions and are interlayered with banded iron formation (BIF). Four different types of schist were identified, namely, talc-chlorite, quartz-sericite, andalusite-chloritoid and actinolite schists.

The talc-chlorite schists are green with white streaks consisting of talc. Mineralogically they contain talc, chlorite, carbonate and opaque minerals. Two alternating layers are commonly distinguishable, namely, greenish layers, composed of chlorite and light brown layers composed of carbonate. The thicknesses of these layers are$\leq$3 mm . Talc occurs within these layers as a fine material locally forming small lenses. Carbonate, talc and chlorite are fine-grained with the phyllosilicates exhibiting a preferred orientation defining a strong schistosity.

The actinolite/tremolite schist occurs as layers of generally greenish colour and is commonly associated and intercalated with talc-chlorite schist. Mineralogically it contains actinolite/tremolite, talc and chlorite and opaque minerals. It is medium-grained.

The major occurrences of the serpentinite and serpentine-talc-magnesite hornfels are exposed in the southern part of the granite-greenstone belt and commonly occur associated with schists with which they share geological boundaries (Fig.2.1). They are also intruded by mafic rocks. Mineralogically the serpentinite contains serpentine minerals (mostly antigorite), chlorite, carbonate and opaque minerals. It is massive, equigranular and fine-grained. Serpentine-talc-magnesite hornfels have the same mineralogical composition as serpentinite but exhibit a porphyroblastic texture whereby

medium-grained antigorite and carbonate are set in a fine matrix of talc.

The quartz-sericite schists occur in several localities in the Manica Greenstone belt, and in the Penhalonga locality (Fig. 2.2) are associated with banded iron formation (BIF). They vary in colour from greenish to pink with white patches of quartzo-feldspathic material (Fig. 3.1). Two group of minerals form the bulk of the rock, namely, the fine-grained pinkish quartz+sericite with subordinate green chlorite. Texturally the rocks exhibit medium- to coarse-grained quartzo-feldspathic mineral fragments in a fine-grained schistose matrix consisting of quartz, sericite and chlorite.

The andalusite-chloritoid schists are exposed around the Ndirire locality (Fig. 2.2) as loose blocks of float up to 3 metres in size. These blocks overly talc-chlorite schist, but their position in the stratigraphy is uncertain. The rock is greenish, being composed of layers of fuchsitic quartzite separated by thin (up to 5 mm thick) layers of brownish chloritoid and andalusite. The crystals of andalusite are long and prismatic. Mineralogically the rock contains fine-grained quartz and fuchsite with medium to coarse-grained chloritoid and andalusite. The rock is intensely deformed (Fig. 3.2).

Figure 3.1: Pinkish quartz-sericite schist intercalated with dark brown banded iron formation in the foreground.

Figure 3.2: Folding in the andalusite-chloritoid schist. Note the fine brownish layers containing the andalusite and chloritoid.

3.2.2 M'Beza/Vengo Formation

The M'Beza/Vengo Formation is a metasedimentary sequence that discordantly overlies the Macequece Formation in the southern and northern parts of the Manica Greenstone Belt (Fig. 2.1) (Oberlholzer, 1964, p. 2-3). Lithologically, the M'Beza/Vengo Formation is characterized by a layered sequence of polymictic metaconglomerate containing clasts of schist, serpentinite, quartzite and granite pebbles with chloritic argillaceous cement (Manuel, 1992), meta-argilites, black schist, sericite and argillaceous schists, metagreywackes and metarkoses (Obretenov, 1977, p.11-12). Locally carbonate lenses occur intercalated with the schist. The metashales are laminated with the laminae being defined by different colours and composition and vary from whitish through yellow to greenish and are of variable thickness (from less than to 4 millimeters). Intercalated in the metashales are thin layers of metagreywacke up to 10 mm thick . Towards the middle part of the Vengo area (Fig. 2.2), a sequence of very fine-grained brownish to black rocks interlayered with metaconglomerate are exposed. The fine-grained rocks are foliated with the foliation dipping towards the S. Locally, the rocks have undergone polyphase deformation seen as early symmetric folds of an earlier stage that were subsequently overturned to form recumbent folds which in turn were deformed to cylindric, open and box folds. At the Chua locality the sequence contains concordant whitish lenses of carbonate. Locally, the metaconglomerate clasts are deformed and define an E-W foliation with steep dips towards the south.

3.3 Petrography

Undeformed hornfels, schists and shales were investigated. The grain sizes of these rocks vary from very fine-grained (<0.25 mm) through medium (≥1≤2 mm) to coarse-grained (≥2 mm) rocks. XRD was used in determining the mineralogy of the fine-grained rocks and in discriminating between the carbonates and serpentine bearing varieties. Compositionaly the greenstone rocks comprise talc-chlorite schists, quartz-sericite schists, chloritoid-andalusite schists and carbonate-antigorite hornfels within the Macequece Formation and pelitic schist and metashales (phyllites) within the M'Beza/Vengo Formation.

Talc-Chlorite Schists and Carbonate-Antigorite Fels

Mineralogically (Table 3.1) the schists consist of fine grained chlorite, carbonate and opaque minerals. The last two occur in a fine-grained matrix of talc and chlorite.

Table 3.1: Mineralogical composition of talc-chlorite schists and carbonate antigorite fels. Atg- antigorite, Chl- chlorite, Dol- dolomite, Tr- tremolite/actinolite, Tlc- talc and Opm- opaque minerals. Numbers inside the cells represent mineral proportions in percentage.

Sample	Atg	Chl	Dol	Tr	Tlc	Opm	rock type
ba	75	10	10	-	-	5	fels
ma	75	15	5	2	-	4	fels
mb	80	10	5	-	-	5	fels
mc	70	20	8	-	-	2	fels
scg	65	-	15	-	15	5	fels
8	60	-	20	-	15	5	fels
epsc1	-	50	10	-	39	1	schist
26aga	-	50	10	-	38	2	schist
26agb	-	46	12	-	40	2	schist

Chlorite occurs as flakes and/or fibrous aggregates, and in non-sheared rocks the crystals lie in criss-cross directions. Twinned carbonate, which consists of dolomite that predominates over magnesite, occurs as isolated xenoblastic grains in general, but also as interlocking, locally elongated grains when in veins. Opaque minerals are generally associated with chlorite and exhibit sub- to idiomorphic habit (Fig. 3.3). The schistosity is defined by the preferred orientation of chlorite and talc which form fine alternating bands. Chlorite wraps around pre-tectonic opaque minerals and, where microfractures are present, it invades these minerals and, together with carbonate minerals, forms pressure shadows around them (Fig. 3.4), which suggests that the schists have been polymetamorphosed (Spry, 1969, p. 309).

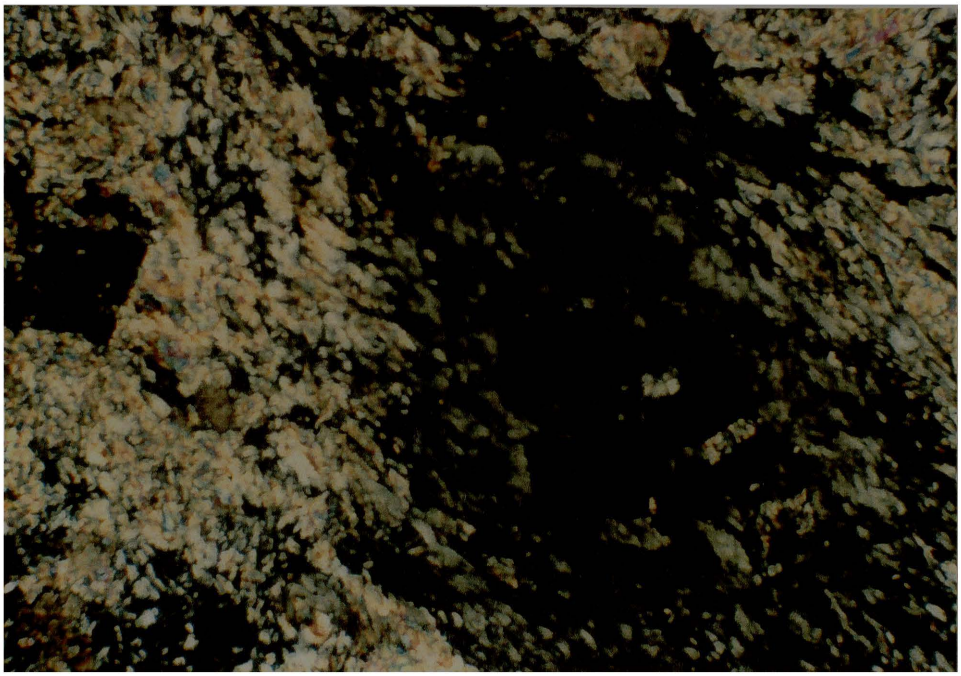

Figure 3.3: Sub-to idioblastic opaque minerals associated with fine-grained chlorite (dark grey) and talc (high birefringence). Crossed nicols, width of field 3 mm.

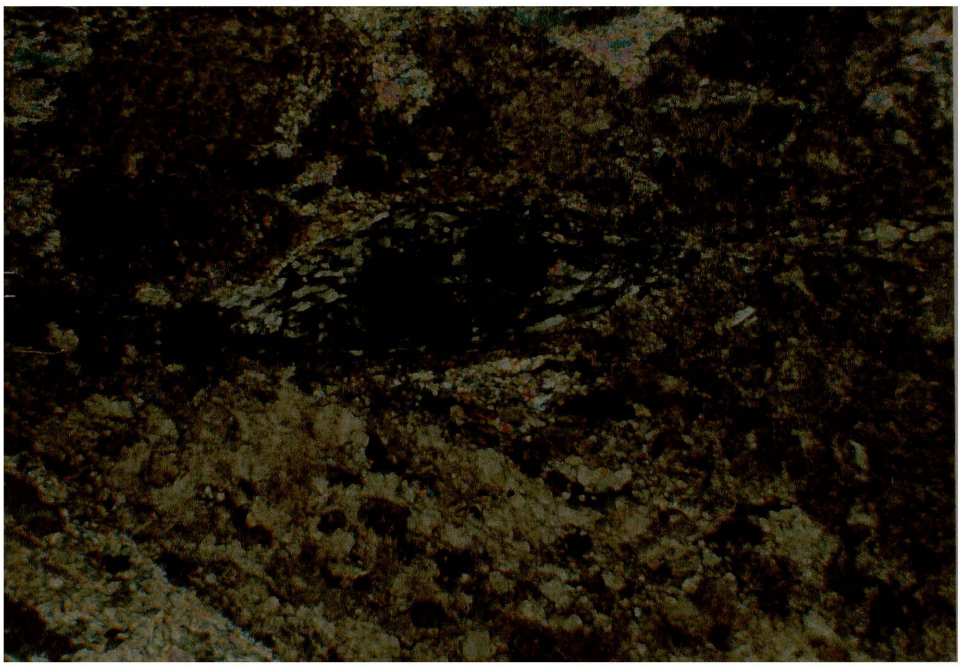

Figure 3.4: Chlorite and carbonate wrapping around and invading opaque minerals. Highly birefringent talc at the top of the picture. Crossed nicols, width of field of view 7 mm.

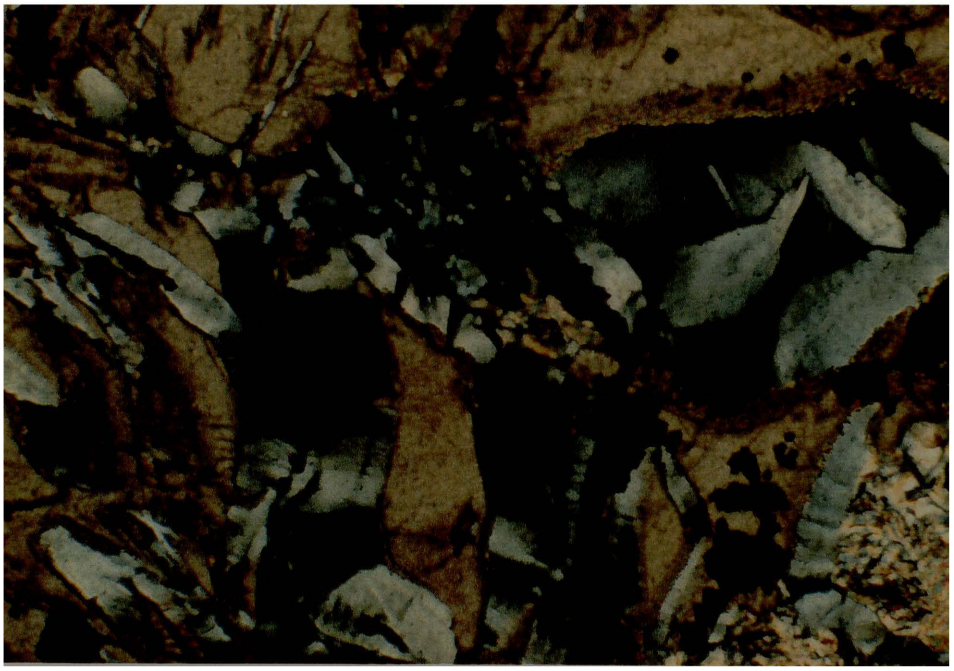

Figure 3.5: Medium-grained carbonate (brown), antigorite (light to dark grey), fine-grained chlorite (grey, top centre) and fine-grained idioblastic opaque minerals (black) locally filling cracks. Crossed nicols, width of field 3 mm.

The carbonate-antigorite serpentinite exhibits a very uniform mineralogical composition (Table 3.1) throughout the study area. The samples vary from massive fine (ma, mb, mc and ba) to medium (scg and 8) grained. Antigorite is fine to medium-grained with varying morphology. In the fine-grained serpentinite, antigorite forms the matrix. Carbonate, mostly dolomite, occurs as isolated grains, as fine- to medium-grained aggregates and locally, small veins. Chlorite occurs as scattered flakes. Rare fibrous chrysotile occurs within antigorite. Actinolite is very rare and occurs as fine prismatic crystals. Talc is represented by fine grains and, together with fine-grained antigorite, forms the matrix in the medium-grained serpentinite (Fig. 3.5). Opaque minerals vary in shape from idioblastic to xenoblastic and commonly fill cracks in serpentine and carbonate (Fig. 3.5) but also occur as isolated grains.

Quartz-Sericite and Chloritoid-Andalusite Schists

The mineralogy of these rocks is shown in Table 3.2.

Quartz-sericite schists consist of angular quartz, sub- to idioblastic chloritoid, chlorite and xenoblastic opaque minerals set in a schistose matrix of very fine-grained quartz and sericite. Chloritoid exhibits polysynthetic twinning and hour glass zoning. Quartz occurs in veins as fine and coarse grains and as granoblastic-polygonal aggregates which represent crushed pre-existing quartz grains. Evidence of this is the presence of strained quartz with some coarse grains having recrystallized to form finer grained aggregates.

Table 3.2: Mineralogical assemblages of quartz-sericite and chloritoid-andalusite schist.

Sample	Qtz	And	Cld	Chl	Ser	Fuc	Opm	rock type
fsc1	54	-	10	5	30	-	1	Qtz-sericite schist
fsc2	65	-	2	20	12	-	1	Qtz-sericite schist
qznd1	20	5	25	2	18	25	5	Cld-andalusite schist

Cld- chloritoid, And- andalusite, Qtz- quartz, Ser- sericite Fuc- fuchsite and Opm- opaque minerals. Numbers inside the cells represent mineral proportions in percentage.

Chloritoid-andalusite schists consist of coarse-grained idioblastic chloritoid and andalusite randomly distributed in a schistose matrix of fuchsite (chromium bearing green mica) and very fine-grained quartz, chlorite, sericite and opaque minerals (Fig.3.6). Quartz occurs as elongate grains in fine bands and as equant grains in aggregates. Fuchsite forms very fine bands that flow around the quartz grains and define the schistosity. Chloritoid exhibits polysynthetic twinning and hour glass zoning (Spry, 1969, p.169-170) and, along cracks, is altered to green mica which forms the matrix (Fig.3.6). It also contains inclusions of fuchsite and quartz. Andalusite, occurring in much smaller proportions than chloritoid, exhibits idiomorphic habits. Locally, it is altered to very fine-grained sericite.

Figure 3.6: Medium-grained idiomorphic chloritoid grain exhibiting hour glass zoning (faintly visible) in a matrix of fuchsite. Crossed nicols, width of field 3 mm.

Pelitic Schist and Metashale

The mineralogy of these rocks is shown in Table 3.3.

Table 3.3: Mineralogical composition of some samples of M'Beza/Vengo Formation.

sample	Qtz	Chl	Ser	Gr	Mag
21sc	x	-	x	x	-
mbsh	x	x	-	-	x
zash	x	x	-	-	x

Mineral abbreviation as in Table 3.2. Mag- magnetite and Gr- graphite. X indicate mineral occurrence.

A common characteristic of these rocks is their very fine grain size and because of this textural characteristic, XRD (X-ray diffraction) was used for qualitative mineralogical identification (Table 3.3). Quartz predominates over sericite and chlorite. Samples from the M'Beza sequence (mbsh and zash) have chlorite as the other major component whereas in the Vengo sequence it is sericite. The rocks from the Vengo sequence are graphitic.

3.4 Chemistry

Four analyses from the present study and 13 from Manuel (1992) of mafic to ultramafic rocks will be used to describe the chemistry of these rocks (Table 3.4). Due to high contents of volatiles, the analyses from this study have yielded low totals varying from 96 to 98 wt% and, therefore, they have been recalculated to 100 wt%.

In general, the rocks are characterized by low SiO_2 and Al_2O_3 contents and high but variable MgO contents which is compatible with their mafic to ultramafic character. The mafic to ultramafic character is also reflected in high Ni and Cr contents and low Li, Sr, Rb, Ba, Y, Nb and Zr contents.

Table 3.4: Chemical composition of Macequece Formations rocks.

Samp	MA	EPSC	SCG	8	20340 A		152	119	104	95	14279	140	1	413	20428	69	192
SiO_2	47.56	48.26	45.71	48.09	47.69	45.94	46.44	47.02	53.39	55.67	48.55	46.64	50.16	45.4	51.59	51.36	51.3
Al_2O_3	2.87	1.91	0.37	3.27	3.6	2.81	7.0	2.46	3.95	5.15	3.76	4.28	7.11	7.8	5.12	7.05	5.98
Fe_2O_3	1.74	2.12	1.77	2.05	4.56	4.41	2.58	2.29	2.84	3.10	2.56	2.88	3.03	2.22	2.53	3.11	2.64
FeO	7.77	7.27	8.10	9.17	12.20	11.64	7.10	6.20	4.33	4.85	6.75	7.63	7.59	6.18	6.22	7.66	6.54
MgO	39.41	36.20	43.81	34.35	20.49	25.62	32.14	40.02	32.67	28.17	33.79	33.49	24.42	30.6	21.56	21.46	25.81
CaO	0.39	3.86	0.02	2.71	8.36	6.67	3.47	0.05	0.06	1.28	2.28	2.5	5.6	6.4	10.89	7.49	5.74
Na_2O	0.00	0.00	0.00	0.00	0.41	0.47	0.07	nd	nd	nd	0.04	0.26	0.18	0.1	0.11	0.1	0.07
K_2O	0.04	0.00	0.00	0.00	0.04	0.06	0.02	0.1	4.63	3.9	0.02	0.09	0.02	0.09	nd	0.02	0.01
TiO_2	0.11	0.17	0.07	0.21	0.69	0.59	0.16	0.13	0.15	0.24	0.2	0.26	0.22	0.2	0.17	0.31	0.17
P_2O_5	0.01	0.01	0.00	0.01	0.03	0.05	0.02	nd	nd	0.02	0.02	0.03	0.05	nd	0.02	0.01	nd
MnO	0.11	0.18	0.15	0.15	0.27	0.21	0.13	0.05	0.07	0.07	0.15	0.15	0.17	0.1	0.17	0.7	0.1
Total	100.00	100.00	100.00	100.00	98.34	98.47	99.13	98.32	102.09	102.45	98.12	98.21	98.55	99.09	98.38	99.27	98.36
Ba	5	10	10	12	20	22	22	28	44	7	37	36	18	100	15	21	16
Co	103	66	120	106	105	101	62	77	72	57	74	79	76	92	68	24	62
Cr	4106	1783	1545	2389	2310	2040	2730	2040	3350	2670	2910	2960	1750	2600	2150	110	100
Cu	17	5	9	19	82	31	nd	6	17	6	nd	nd	nd	nd	172	9	106
Li	1	nd	nd	nd	nd	nd	nd	nd	nd	nd	nd	nd	nd	nd	nd	nd	nd
Nb	1	2	0	3	40	0	3	3	3	3	3	4	3	0	3	3	3
Ni	1883	1723	2668	1715	1862	2557	1486	2139	2019	1606	1689	1587	742	1600	1204	790	1050
Sc	17	15	12	17	Nd	Nd	Nd	Nd	Nd	Nd	Nd	Nd	Nd	Nd	Nd	Nd	Nd
Sr	0	40	0	19	51	67	5	3	3	5	21	12	3	50	7	7	5
Rb	1	0	2	1	4	2	2	1	1	2	1	3	2	nd	2	2	2
V	71	62	36	69	150	200	101	50	80	90	70	70	130	50	100	110	100
Y	3	4	2	6	8	12	3	2	3	25	4	5	8	nd	5	3	3
Zn	45	44	43	45	93	78	63	36	44	63	46	60	130	70	79	569	66
Zr	13	14	10	18	31	30	12	9	13	16	20	28	13	nd	11	23	14

The first four samples were collected and analysed during the present study whereas the remaining data are from Manuel (1992). Nd=not determined and nd=not detected

Al_2O_3, and CaO show an inverse correlation with MgO whereas FeO shows a scatter of data points (Fig. 3.7). The enrichment of samples in Cr and Ni in contrast to V is reflected in the plot of these elements versus MgO (Fig. 3.8). The trend of data is that of positive correlations for Cr and Ni, whereas V is not correlated with MgO or with the other major elements.

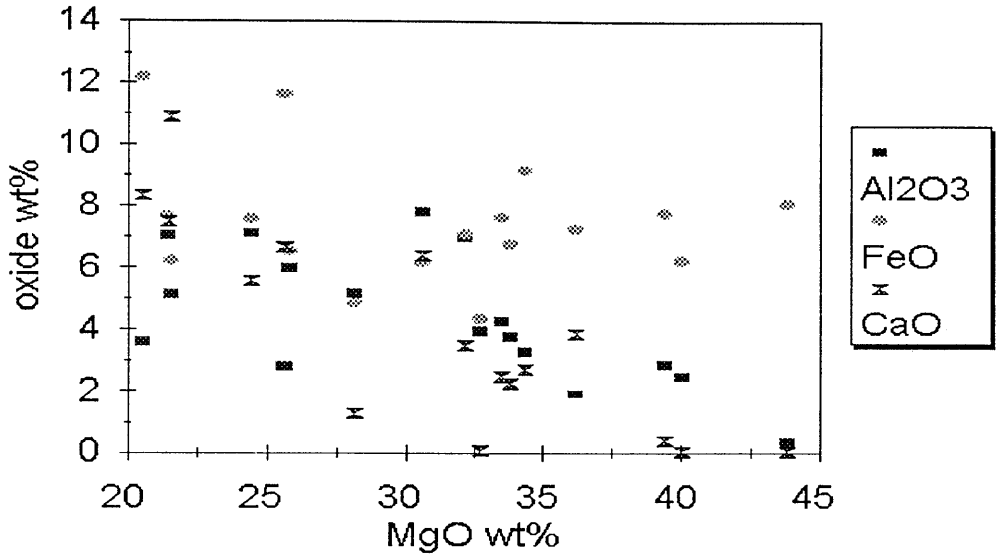

Figure 3.7: Al_2O_3, FeO and CaO versus MgO variation diagram of the mafic to ultramafic rocks.

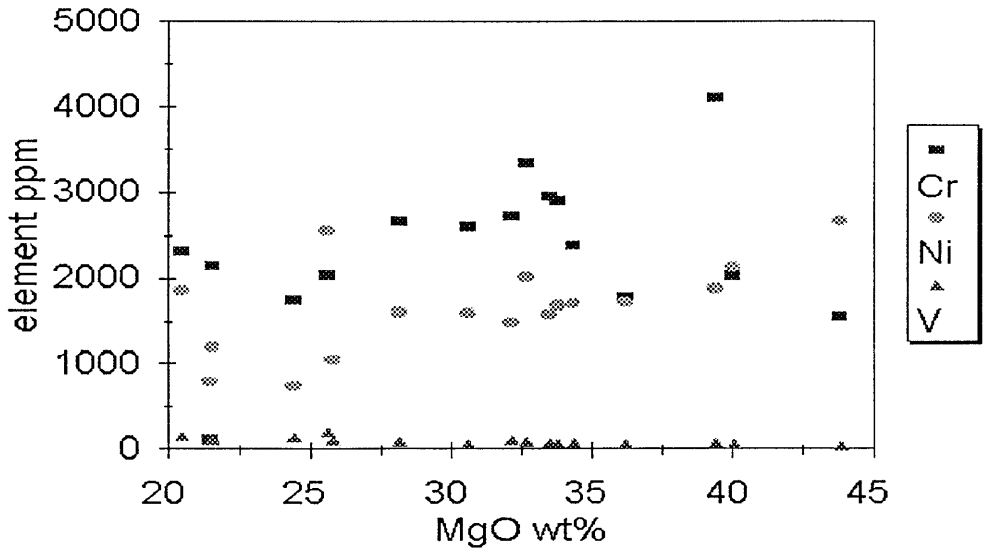

Figure 3.8: Variation diagram of Cr, Ni and V versus MgO of the mafic to ultramafic rocks.

3.5 Interpretation of Metamorphism and Chemistry of Rocks

Based on the mineralogy described above, the rocks of the Macequece Formation can be subdivided into a mafic to ultramafic suite containing chlorite+carbonate+serpentine+talc+tremolite+magnetite and a pelitic suite characterized by quartz+sericite+chloritoid+chlorite+andalusite+fuchsite (Winkler, 1974, p. 151, 206). In Figure 3.9, an ACF diagram confirms that the rocks are rich in magnesium and aluminum respectively, so that they agree with the corresponding fields of meta-ultramafites and metapelites.

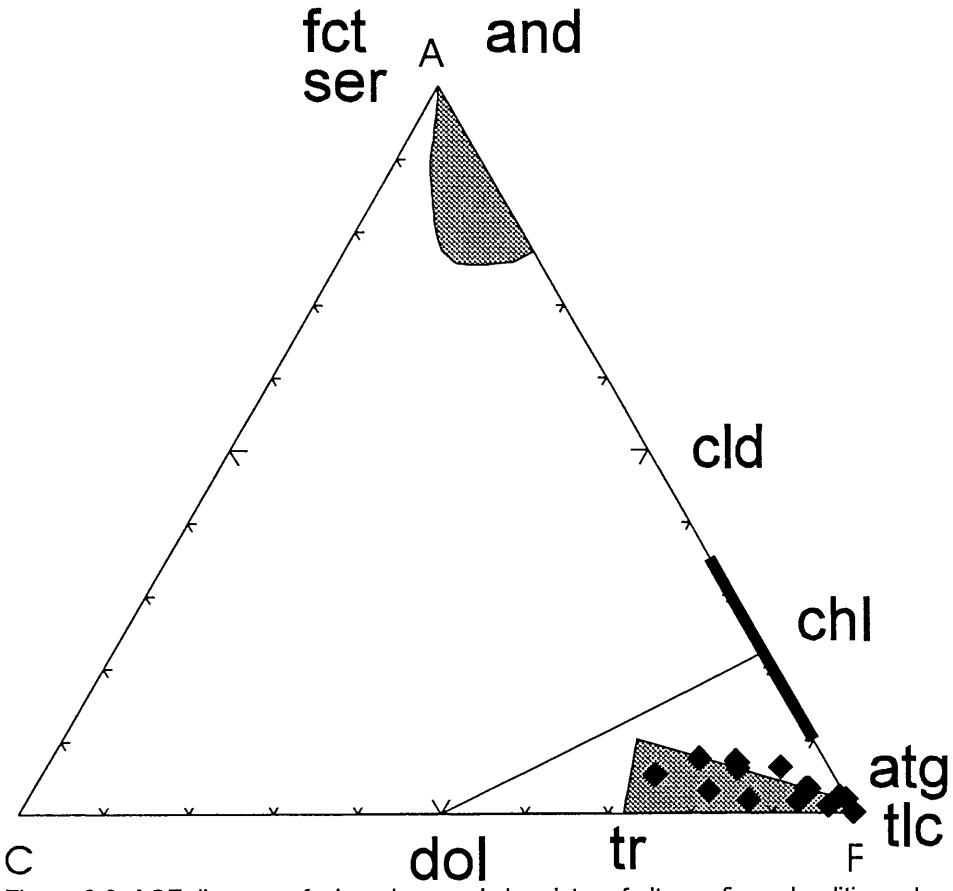

Figure 3.9: ACF diagram of mineralogy and chemistry of ultramafic and pelitic rocks. Shaded areas show field of pelitic and ultramafic compositions. The relevant compositions of the pelitic samples are: 21Sc (SiO_2-67.97; Al_2O_3-20.33; MgO-1.38 and CaO-0.01) and Ndqtz (SiO_2-48.1 and Al_2O_3-40.93). Mineral abbreviations as in Table 3.2. Fct- fuchsite.

3.5.1 Metamorphism

Mafic to Ultramafic Association

The temperature of metamorphism of the association can be constrained using Figure 3.10 and Figure 3.11 in which the phase relationships for ultramafic rocks are shown on TX diagrams (Winkler, 1974, p. 151 ; Bucher and Frey, 1994, p. 165).

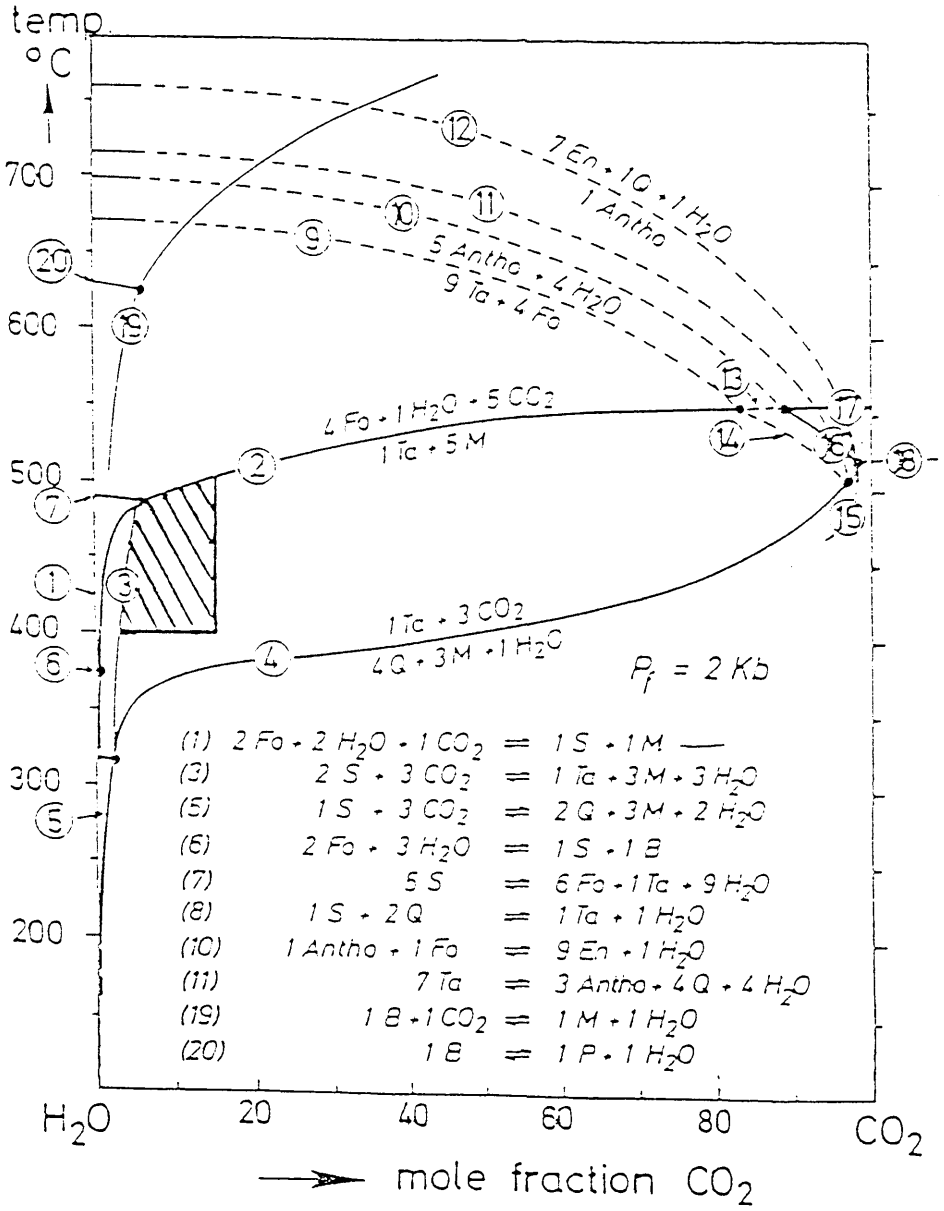

Figure 3.10: Isobaric reaction curves depicting phase relationships in mafic to ultramafic rocks (after Winkler, 1974). The P-T conditions are shown as cross hatched area which is defined by $T \geq 400\ °C \leq 500\ °C$, $XCO_2 \leq 0.14$ and the relevant part of reaction 3.

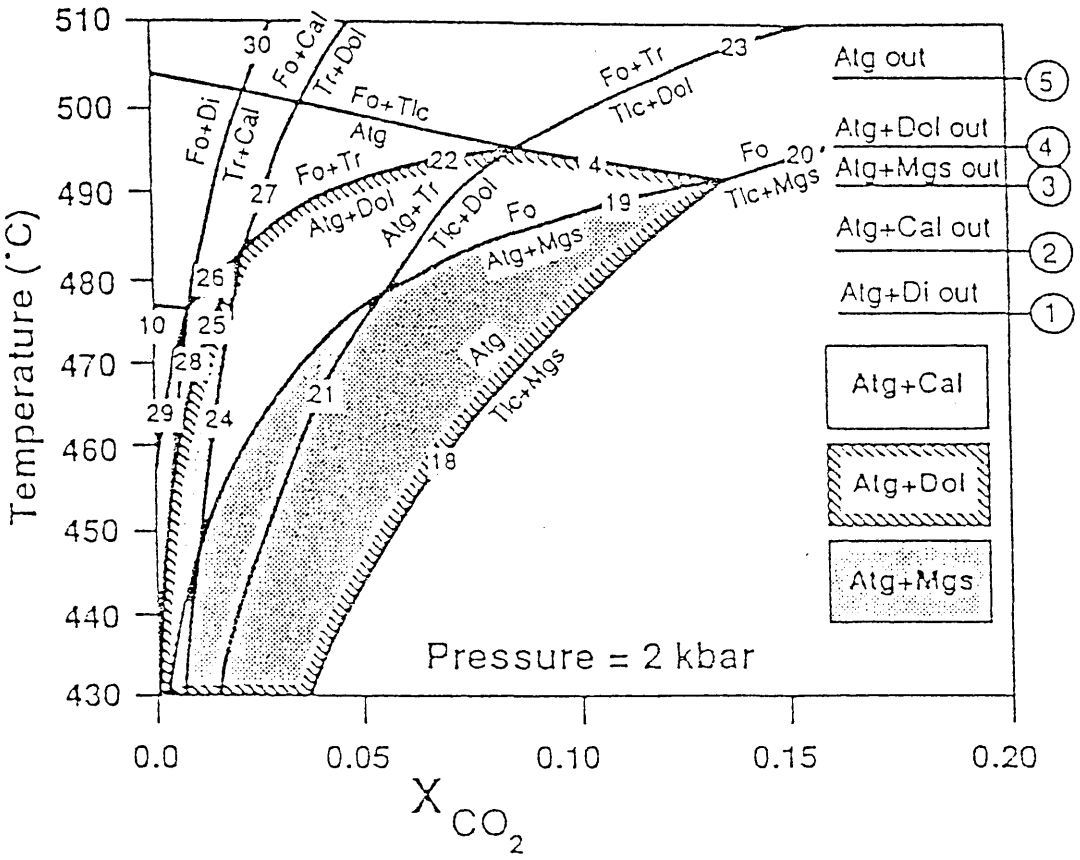

Figure 3.11: Low temperature phase relationship in mafic to ultramafic rocks at isobaric pressure of 2 kbar (after Bucher and Frey, 1994). Relevant P-T conditions are defined by the stippled area.

These figures were selected because they represent relatively low - pressure conditions (2 kbar) as is suggested by the andalusite-bearing pelitic assemblages. The figures show that the minerals recognized are generally stable below 500 °C at 2 Kbar above which olivine would have been expected. In addition, the coexistence of carbonate (dol)+talc+serpentine in some samples (mc, scg, 8) suggests that the fluid phase during metamorphism was a mixture of H_2O and CO_2 with $XCO_2 < 0.14$. These minerals are therefore typical of low grade or greenschist metamorphism.

Pelitic Association

The metamorphic conditions relating to the pelitic association can be interpreted from Figure 3.12 (Yardly, 1989, p. 86) which shows a petrogenetic grid for metamorphosed pelites. The occurrence of andalusite constrains the pressures of metamorphism to below 3.8 kbar and temperatures above ~400 °C below which pyrophyllite would be stable. The occurrence of chloritoid suggests temperatures below ~525 °C above which it would be replaced by staurolite.

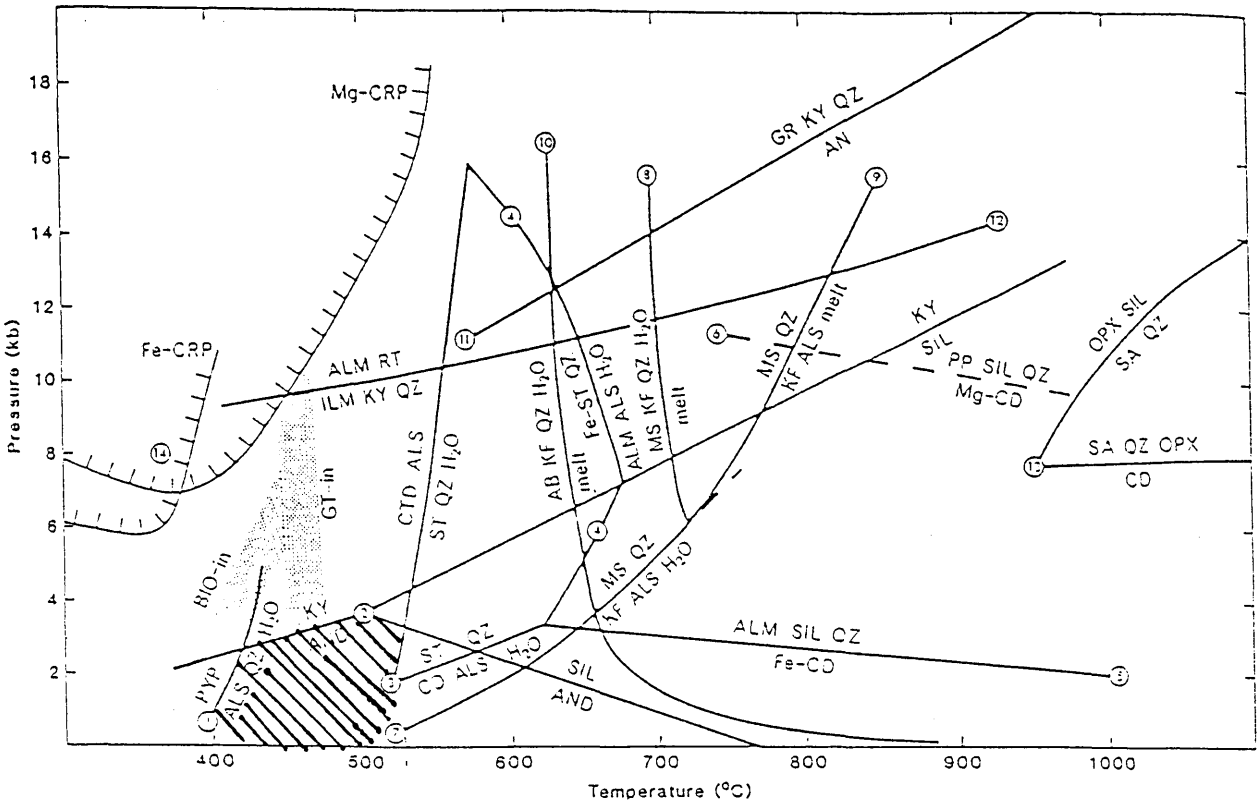

Figure 3.12: Phase relationships in metamorphism of pelitic rocks presented as petrogenetic grid in a PT diagram (after Yardly, 1989).

Considering the intercalated nature of the pelitic and mafic to ultramafic schists, their combined mineral assemblages suggest P-T conditions of between ~400 °C-~500 °C and pressures below 3.8 kbar.

3.5.2 Chemistry

Based on the petrographic data, the chemical composition of samples and the chemical trends described in the previous section, a number of discriminant diagrams are suggested for the interpretation of the nature of the greenstone rocks. Due to limited availability of chemical data, only analyses of mafic to ultramafic rocks will be used.

A plot of chemical data onto the Irvine and Baragar (1971) diagram (Fig. 3.13) shows the trend for MgO enrichment. The analysed samples are characterized by SiO_2 content between 45 and 53 wt% and MgO content above 18 wt%. These parameters are consistent with the definition of the rocks as komatiites (Arndt and Nisbet, 1982). Figure 3.14, after Jensen (1976), supports this with the data plotting in the field of peridotitic komatiites. The low Na_2O+K_2O and TiO_2 contents are also typical of komattiites (Le Maitre, 1989) (Fig.3.15).

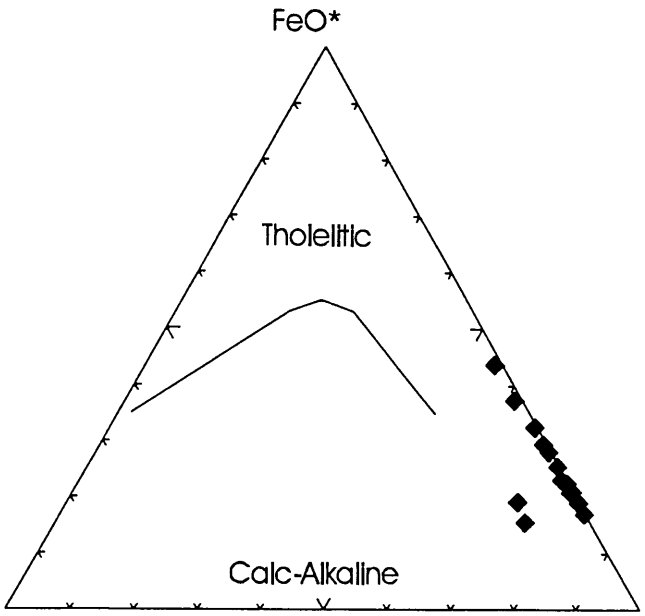

Figure 3.13: Tholeiite versus calc-alkaline series discriminant diagram (after Irvine and Baragar, 1971) of Macequece Formation.

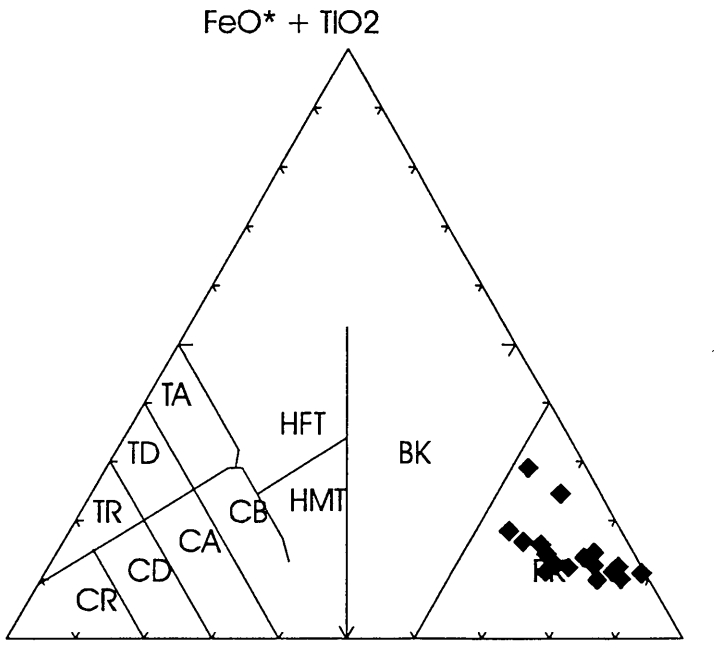

Figure 3.14: Discriminant diagram for tholeiites, komatiites and calc-alkaline fields plotting data of the Macequece Formation (after Jensen, 1976). HF- high iron tholeiites, HM- high magnesium tholeiites, BK- basaltic komatiites, PK- peridotitic komatiites, TR- tholeiitic rhyolites, TD- tholeiitic dacites, TA- tholeiitic andesites, CR- calc-alkaline rhyolites, CD- calc-alkaline dacites, CA- calc-alkaline andesites and CB- calc-alkaline basalts.

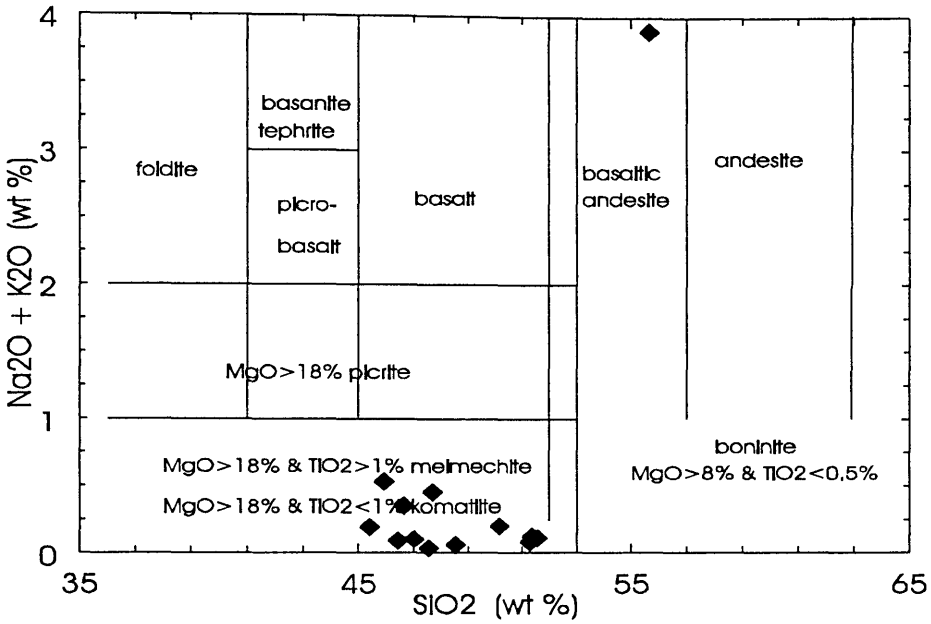

Figure 3.15: Discriminant diagram for various types of basalts (Le Maitre, 1989) of the Macequece Formation.

Chapter 4

ARCHAEAN TO EARLY PROTEROZOIC GRANITOID GNEISSES OF THE ZIMBABWE CRATON

4.1 Introduction

The Archaean to Early Proterozoic granitoids occur within the western half of the study area (Fig. 2.1). Mineralogically two types of rocks were identified, namely, biotite and hornblende bearing varieties. The biotite-bearing rocks occupy most of the area whereas the hornblende gneisses are exposed as small occurrences possibly intrusive into the former.

The Archaean granitoids, which include both mineralogical types, are grouped together as Vumba Granite Gneiss. Two ages were determined in the Vumba granitoids, namely, the 3385±255 Ma and the 2527±632 Ma (Manuel, 1992) north and south of the Manica greenstone belt respectively.

The biotite bearing granitoid gneisses are of Proterozoic age and are grouped into the Messica Granite Gneiss. The Messica Granite Gneiss has an Early Proterozoic age of 2348±267 Ma.

4.2 Field Description

4.2.1 Vumba Granite Gneiss

The Vumba Granite Gneiss surrounds the Manica Greenstone Belt in its northern and southern parts and locally contains inclusions of serpentinite. It is intruded by mafic rocks (Carta Geologica da Regiao de Vila Manica-Vila Gouveia, 1:250 000, 1969) (Fig. 2.1).The Archaean granitoids in Manica have been collectively, but informally, termed the Vumba Granite after the Vumba Mountain. In the Vumba locality, the granitoid varies from homogeneous types to intensely foliated, folded, and jointed varieties and is cut by quartz and quartzo-feldspathic veins and dolerite dykes. The gneiss contains plagïoclase in excess of K-feldspar, quartz and locally chloritized biotite and hornblende. The gneisses are equigranular
medium-grained. In the M'Kwananda area, a strong planar fabric is developed. Here, the rock is intensely sheared, banded and cut by quartzo-feldspathic veins, foliated, folded and faulted and contains enclaves of fine-grained foliated amphibolite (Fig. 4.1). The planar foliation defined by preferred orientation of biotite and hornblende, is faulted and folded suggesting polyphase deformation in this granitoid. In Gecua, east of Vumba locality (Fig. 2.2), the granitoid is homogeneous. It is grey with black spots, with mineralogy consisting of grey plagioclase, quartz and hornblende. It is coarse-grained and has a planar the foliation defined by porphyritic euhedral hornblende grains up to 10 mm long.

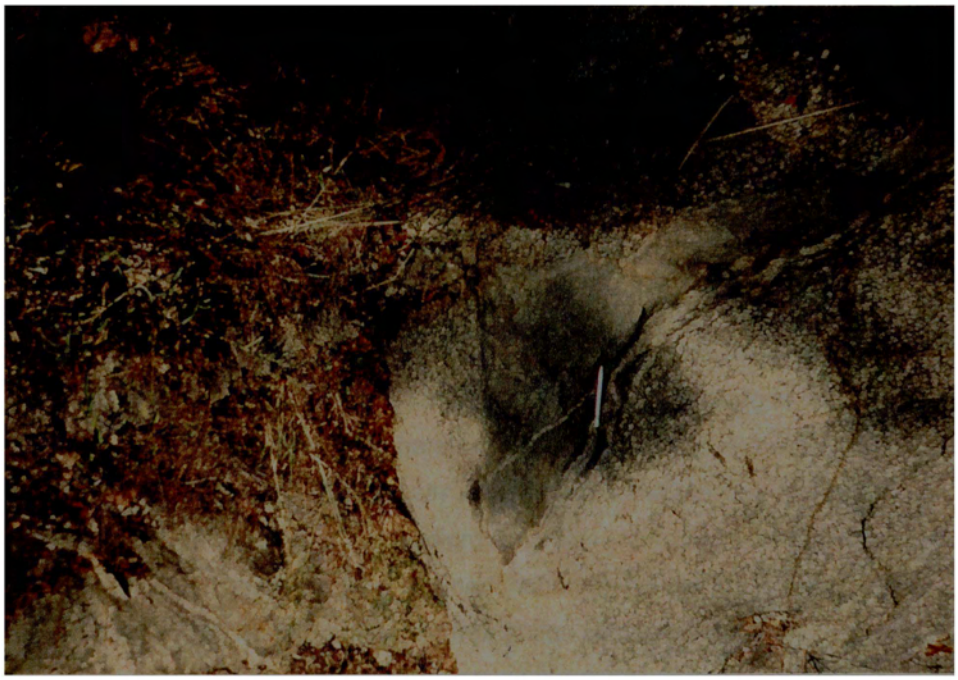

Figure 4.1: Fine-grained amphibolitic enclaves in the M'Kwananda exposure of the Vumba Granite Gneiss.

4.2.2 Messica Granite Gneiss

The Messica Granite Gneiss occurs east of the Vumba Granite Gneiss and the Manica Greenstone Belt and shares geologic boundaries with the Mozambique Metamorphic Province migmatites in the east. It is overlain by Frontier Formation metasediments. It is also intruded by mafic dykes along a N-S axis near Garuzo (Fig. 2.2). The formation includes what previous authors described as "remobilised porphyroblastic granite" (Carta Geologica da Regiao de Vila Manica-Vila Gouveia, 1:250 000, 1969; Pinna *et al.*, 1986). This granitoid type is grey to locally pinkish grey. The minerals include plagioclase, porphyritic K-feldspar, quartz and biotite. Porphyritic K-feldspar is easily recognized on weathered surfaces, but is less obvious in fresh rock. The rocks exhibit variable degrees of deformation with the western exposures showing only weak planar fabrics while in some localities appear undeformed. The intensity of fabric increases toward the east where the rock is strongly foliated and locally exhibits augen textures defined by feldspar, which can be up to 25 mm long. Quartz is commonly deformed and elongated parallel to the foliation direction. The foliation is defined by preferred orientation of biotite which wraps around the feldspar augens. The non-porphyritic granitoid has the same minerals as the porphyritic varieties but is medium-grained and less deformed. The foliation varies from being incipient with different orientations to more pervasive and consistent in a N-S direction with steep dips towards both W and E. Towards the extreme east boundary, where the granite is also commonly porphyritic,

two foliations, namely an E-W S_1 fabric and a younger N-S S_2 are distinguishable. The granite is cut by quartz and pegmatitic veins that are commonly oriented N-S. Many exposures of non-porphyritic granite contain mafic enclaves characterized by plagioclase, hornblende and quartz.

4.3 Petrography

The texture of the Vumba Granite Gneiss is typically hypidiomorphic granular (Shelley, 1993, p. 422) except in samples from M'kwananda (MkG, sheared rock) in which a strong foliation has been developed and in the hornblende-bearing varieties in which hornblende shows a preferred orientation. The Vumba Granite Gneiss consists of K-feldspar, plagioclase, quartz, biotite and hornblende and accessory minerals epidote, allanite, sphene, apatite, chlorite and zircon (Fig. 4.2). This mineralogical composition as well as the proportions in which they occur are shown on Table 4.1. Plagioclase exceeds K-feldspar by ~1.5:1 to 2:1 indicating that these rocks are granodioritic to tonalitic in composition. K-feldspar varies in grain size from medium (1-2 mm) to coarse (2-4) and is essentially microcline, locally sericitized and characterized by anhedral grains exhibiting cross-hatch twinning. Plagioclase grains are anhedral, locally saussuritized and are characterized by complex Carlsbad-Albite polysynthetic twins and are medium (±1.5 mm) to coarse (±2 mm) in grain size. Quartz is represented by two types namely, strained, anhedral, medium (±2 mm) to coarse (±2-3 mm) grains and fine-grained (±0.25-0.5 mm) strain-free grains commonly exhibiting a fine-grained granoblastic texture and occurring along cracks and grain boundaries.

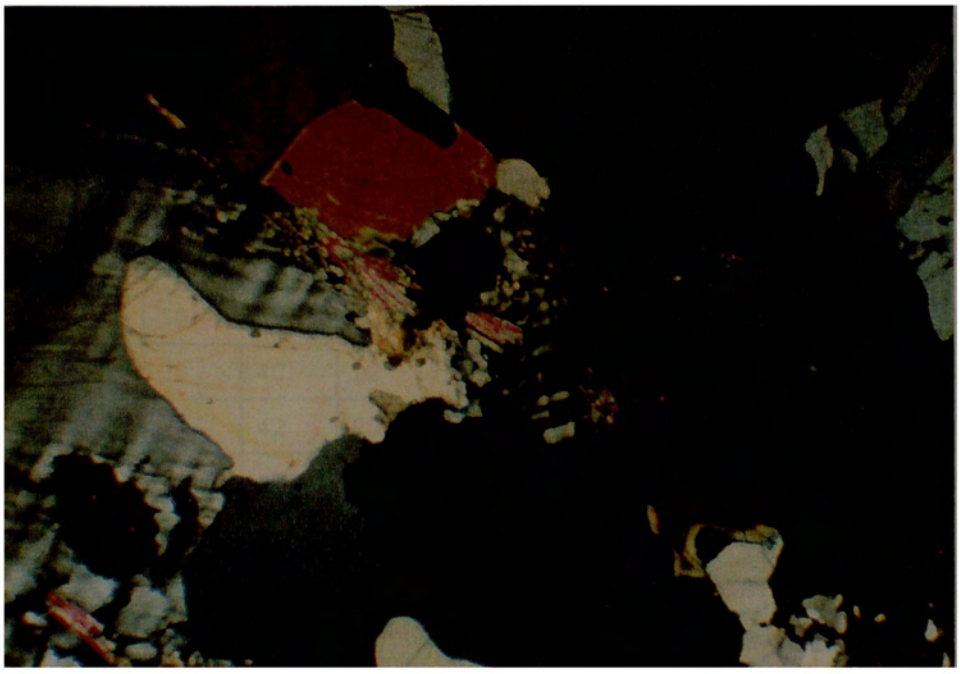

Figure 4.2: Anhedral quartz, microcline (with cross-hatch twinning), plagioclase (with combined polysynthectic and Carlsbad twinning), biotite (locally altered to muscovite and titanite (included in microcline) in the Vumba Granite Gneiss. Crossed nicols, width of field 3.0 mm.

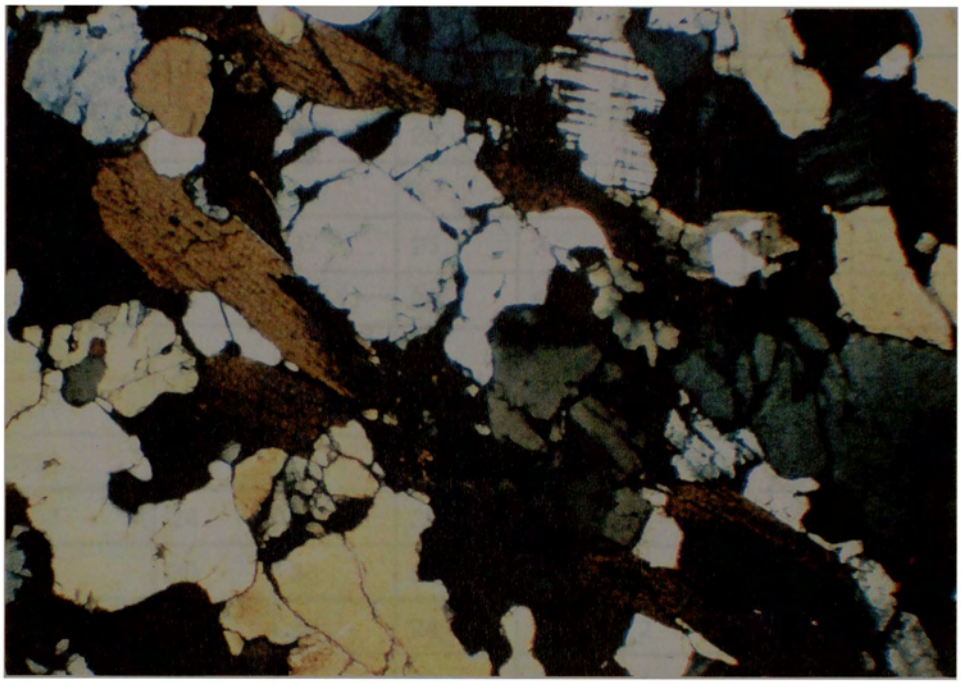

Figure 4.3: Feldspar (with biotite wrapped around) with microcline (exhibiting typical cross-hatch twinning) and fine grains of quartz in the Messica Granite Gneiss. Crossed nicols, width of field 7 mm.

Table 4.1: Mineralogical composition of the Vumba Granite Gneiss.

sample	K-fld	Plg	Qtz	Hbl	Bt	Ep	Ttn	Ap	Aln	Chl	Zr
VGI	20	45	25	2	5	1	1	-	1	-	-
VGII	15	48	30	-	3	1	1	1	1	-	-
VGIII	30	35	30	-	2	-	-	1	1	1	-
VGIV	32	34	28	-	2	1	-	1	-	2	-
VGV	30	35	30	-	2	1	-	1	1	-	-
VG31	20	40	22	8	5	1	1	1	1	-	1
VG32	21	42	20	7	6	1	1	1	1	-	-
VG33	20	46	20	6	5	-	1	-	1	-	1
MpG	25	43	25	-	5	2	-	-	-	-	-
MkG	20	37	20	6	15	1	-	-	1	-	-

Numbers indicate mineral proportions. K-fld- potassic feldspar; Plg- plagioclase, Qtz- quartz, Bt- biotite, Ms- muscovite, Zr- zircon Ttn-titanite, Ep- epidote, Ap- apatite, Aln- allanite Chl- chlorite.

Table 4.2: Mineralogical assemblage of Messica Granite Gneiss. Modal proportion expressed as percentages.

Sample	K-fld	Plg	Qtz	Bt	Ms	Ttn	Opm
PdGr1	22	40	27	6	2	1	2
PdGr2	21	42	28	5	1	2	1
PdGr3	18	40	30	8	1	1	2
PdGr4	26	37	25	7	2	1	2
PdGr5	24	38	28	6	2	1	1
PdGr6	28	34	28	6	2	1	1
CNO1	28	35	30	4	1	1	1
CNO2	27	38	25	5	2	1	2
CNO3	24	38	28	5	3	1	1
CNO4	30	36	22	6	2	2	2
CNO5	28	36	24	7	2	1	2
CNO6	21	42	30	5	1	-	1
MGn3	25	38	25	7	2	1	2
Mgn5	25	42	24	5	2	-	2
M'SKg	28	38	20	12	-	1	1

Abbreviations as in Table 4.1.

These finer grained zones are thought to represent strain-related recrystallisation of the larger grains.

Biotite occurs as isolated grains or grain aggregates and may be subhedral. It is locally poikilitic and partially altered to chlorite. In deformed samples from the M'Kwananda region, biotite together with deformed quartz, defines a planar foliation. Hornblende occurs as euhedral to subhedral coarse grains and exhibits a preferred orientation that defines the foliation. Epidote is commonly associated with plagioclase of which it is a reaction product. Allanite occurs as isolated long pseudohexagonal crystals commonly exhibiting pleochroic haloes or as fine inclusions in plagioclase. Titanite is included in plagioclase and hornblende. Apatite forms euhedral hexagonal crystals included in plagioclase and amphibole. Zircon is included in plagioclase.

The Messica Granite Gneisses are commonly medium-grained equigranular to porphyritic in which feldspars constitute the phenocrysts >5 mm in grain size. The fabric varies from randomly oriented feldspar phenocrysts to one in which strong preferred orientations of deformed quartz and feldspar porphyroclasts are seen (Fig. 4.3) Biotite flakes wrap around the feldspars in the deformed samples similarly defining a planar fabric. Locally, finer quartz and feldspar grains exhibit polygonal textures (Fig. 4.4). Myrmeckite is also common in these granitoids.

The mineralogy of the Messica Granite Gneiss is composed of K-feldspar, plagioclase, quartz, biotite, muscovite, zircon, titanite, apatite and opaque minerals. Table 4.2 provides modal estimates of the mineral proportions. K-feldspar, commonly microcline,is locally perthitic while plagioclase exhibits combined Carlsbad and albite twins. Both feldspars are commonly poikilitic, enclosing finer quartz and feldspar grains, and are anhedral. The grain size is, on average, ±2 mm. Quartz, exhibits irregular crystal faces, is poikilitic with inclusions of finer quartz and feldspar grains and has the same grain size as the feldspars. Biotite occurs as isolated grains or grain aggregates with subhedral grain shapes (Fig. 4.5). Some chloritized biotite grains exhibit needle intergrowths of rutile. Muscovite occurs as small grains associated with biotite (Fig. 4.5) and as inclusions in feldspar. These relationships are interpreted to represent an alteration product resulting from retrogressive reactions. Zircon occurs as isolated prismatic grains. Titanite occurs as short prismatic irregular anhedral isolated grains and as grain aggregates. Apatite commonly occurs as small hexagonal euhedral crystals. Opaque minerals occur as euhedral to anhedral grains, commonly associated with biotite and titanite and, in some cases titanite forms embayments to these opaque minerals grains.

The occurrence of plagioclase-epidote, biotite-muscovite, feldspar-sericite and biotite-chlorite associations is an indication of a subsequent retrogressive metamorphism (hydration reactions) possibly at low grade greenschist facies. The presence of foliation defined by plagioclase porphyroclasts, of strained, elongated coarse quartz and strain-free fine quartz with granoblastic texture suggests deformation and metamorphism.

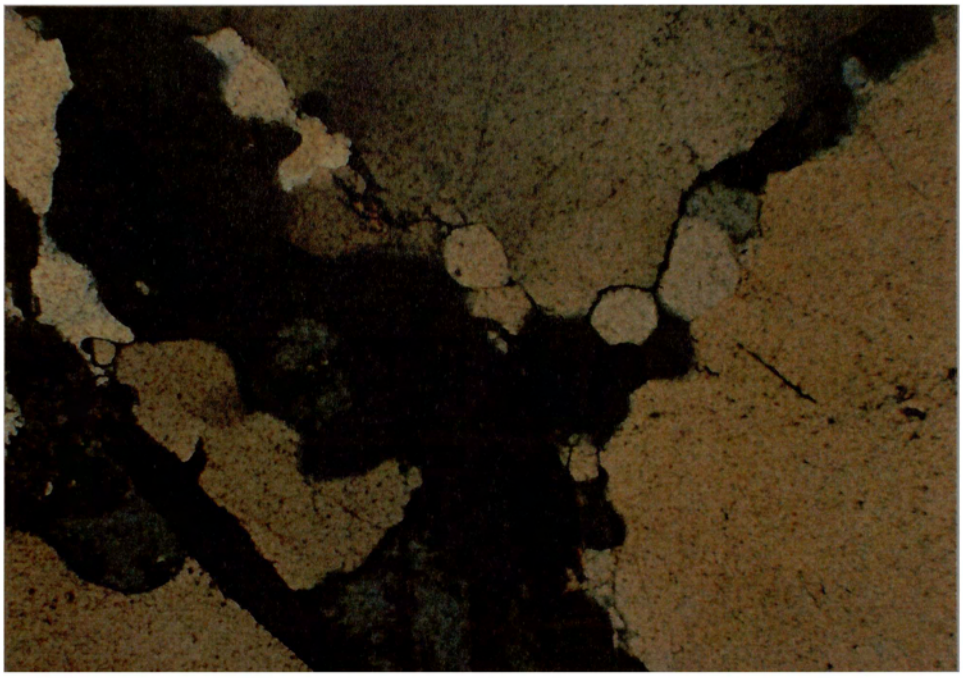

Figure 4.4: Fine quartz grains exhibiting polygonal texture in the Messica Granite Gneiss. Crossed nicols, width of field 3 mm.

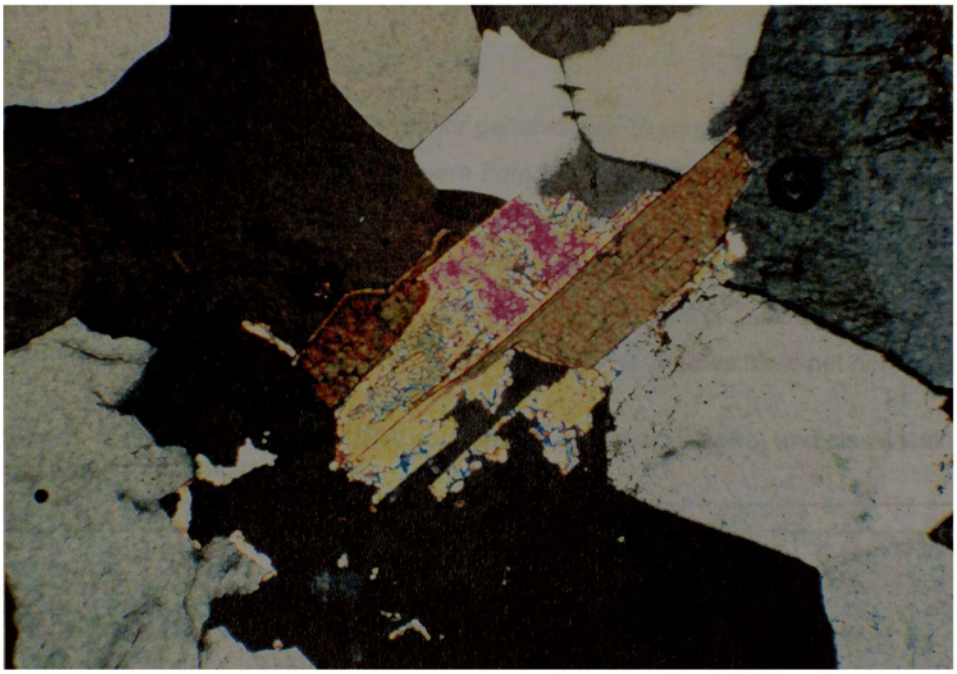

Figure 4.5: Biotite laths occurring at quartz grain boundaries in the Messica Granite Gneiss. The intervening grain with high interference colours is muscovite. Crossed nicols, width of field 3. mm.

4.4 Chemistry

4.4.1 Introduction

Twenty one samples were analysed for geochemical characterization of the Archaean to Early Proterozoic granitoids. Of these, nine were from the Vumba and the remaining twelve from the Messica granitoids. In addition data of 10 samples from the Vumba Granite Gneiss, analysed by Manuel (1992) are also included. The major element and normative data are shown in Table 4.3, the trace element and the REE data in Table 4.4 and the radiogenic isotope data in Tables 4.5 and 4.6 .Analyses of some samples have low totals that are attributed to the fact that volatiles have not been determined.

Table 4.3: Major elements and CIPW normative compositions (norm) and classification of Archaean to Early Proterozoic granitoids.

SAMP	VGR3-1	VGR3-2	VGR3-3	VGR3-4	VGR3-5	VGR3-6	VGRI	VGRIII	VGRIV	127	90	81
SiO_2	65.64	66.66	66.3	66.24	66.52	64.87	70.35	75.43	73.34	70.85	67.95	72.4
Al_2O_3	16.14	16.87	15.92	16.96	15.89	15.61	14.44	12.33	13.62	13.66	15.84	14.61
Fe_2O_3	1.67	1.63	1.68	1.61	1.66	1.62	1.06	0.43	0.68	1.45	1.44	1.19
FeO	2.55	2.58	2.67	2.56	2.60	2.59	1.65	0.49	0.79	2.57	2.30	1.75
MgO	1.6	1.65	1.71	1.62	1.67	1.64	0.76	0.14	0.22	1.6	1.4	0.55
CaO	4.36	4.31	4.37	4.38	4.34	4.47	3.27	0.5	1.03	3.68	4.2	2.62
Na_2O	4.09	3.9	3.88	3.85	3.93	3.93	4.19	3.49	3.36	2.99	3.64	4.08
K_2O	2.2	2.06	2.06	2.11	2.15	2.04	1.75	4.94	4.94	1.77	2.11	2.16
TiO_2	0.48	0.48	0.49	0.48	0.49	0.49	0.32	0.1	0.19	0.45	0.41	0.23
P_2O_5	0.16	0.16	0.17	0.16	0.17	0.17	0.12	0.03	0.06	0.11	0.12	0.06
MnO	0.06	0.06	0.07	0.06	0.06	0.06	0.03	0.02	0.04	0.06	0.06	0.05
total	98.95	100.36	99.32	100.03	99.48	97.49	97.94	97.9	98.27	99.23	99.47	99.64
norm												
Q	21.16	23.46	23.15	23.05	23.02	21.78	30.57	34.72	32.05	35.32	26.71	33.16
Or	13.03	12.2	12.2	12.5	12.73	12.08	10.37	29.25	29.32	10.49	12.5	12.8
Ab	34.61	33	32.83	32.57	33.25	33.25	35.45	29.53	28.43	25.3	30.8	34.52
An	19.18	20.57	19.93	20.93	19.36	18.91	15.41	2.46	4.91	17.74	20.29	12.78
Di	1.34	0	0.71	0	1.07	1.95	0.35	0	0	0	0	0
Hy	5.97	6.83	6.75	6.73	6.34	5.86	3.4	0.77	1.21	6.87	5.97	3.32
Mt	2.42	2.37	2.44	2.34	2.41	2.35	1.54	0.62	0.98	2.11	2.08	1.72
Il	0.91	0.91	0.93	0.91	0.93	0.93	0.61	0.19	0.36	0.85	0.78	0.44
Ap	0.38	0.38	0.41	0.38	0.41	0.41	0.29	0.07	0.15	0.26	0.29	0.14
Q	24	26	26	26	26	25	33	36	34	40	30	36
A	15	14	14	14	14	14	11	30	31	12	14	14
P	61	60	60	60	60	61	55	33	35	48	57	51
rock	granod	granod	granod	granod	granod	granod	granod	mzgr	mnzgr	granod	granod	granod

SAMP	150	124	14	253	403	404	406	M'SKGn	PDGR1	PDGR2	PDGR3
SiO_2	68.04	71.08	72.45	74.03	74.31	77.44	75.96	70.32	71.04	71.31	71.16
Al_2O_3	16.37	14.95	14.24	13.49	14.27	12.88	12.89	14.5	14.17	14.35	14.2
Fe_2O_3	1.40	1.34	1.20	0.67	1.06	0.65	1.03	0.93	1.03	1.12	0.98
FeO	2.14	1.93	1.67	0.87	1.52	0.81	1.42	1.09	1.16	1.27	1.09
MgO	1.34	1.16	1.08	0.4	0.47	0.11	0.06	0.64	0.62	0.64	0.54
CaO	3.69	1.78	1.53	1.56	2.47	1.08	1.63	1.54	1.67	1.75	1.63
Na_2O	3.96	4.92	4.18	3.49	4.35	3.8	4.12	3.62	3.62	3.75	3.68
K_2O	2.25	1.62	2.62	3.88	1.98	3.73	2.52	4.73	5.19	4.98	5.27
TiO_2	0.4	0.41	0.32	0.23	0.22	0.09	0.16	0.27	0.31	0.32	0.32
P_2O_5	0.1	0.09	0.08	0.04	0.06	0.03	0.03	0.1	0.11	0.09	0.11
MnO	0.04	0.05	0.06	0.04	0.05	0.02	0.04	0.02	0.03	0.03	0.02
total	99.73	99.62	99.43	98.75	100.76	100.64	100.14	97.76	98.95	99.61	99

norm	150	124	14	253	403	404	406 M'SKGn	PDGR1	PDGR2	PDGR3
Q	25.66	30.05	32.6	34.62	34.77	38.22	38.2	26.62	25.54	25.55	25.32
Or	13.33	9.59	15.52	22.98	11.74	22.09	14.92	28.02	30.73	29.48	31.2
Ab	33.51	41.63	35.37	29.53	36.8	32.15	34.86	30.63	30.63	31.73	31.14
An	17.92	8.43	7.26	7.68	12	5.29	8.05	7.31	7.1	7.63	6.68
Di	0	0	0	0	0	0	0	0	0.64	0.64	0.82
Cm	0.01	0	0	0	0.01	0	0.01	0	0	0	0
Hy	5.51	4.74	4.34	1.73	2.82	1.1	1.4	2.44	2.06	2.22	1.65
Mt	2.04	1.95	1.75	0.98	1.53	0.95	0.15	1.34	1.5	1.63	1.43
Il	0.76	0.78	0.61	0.44	0.42	0.17	0.3	0.51	0.59	0.61	0.61
Ap	0.24	0.22	0.19	0.1	0.14	0.07	0.07	0.24	0.27	0.22	0.27
Q	28	34	36	37	36	39	40	29	27	27	27
A	15	11	17	24	12	23	16	30	33	31	33
P	57	56	47	39	51	38	45	41	40	42	40
rock e	granod	granod	granod	mzgr	granod	mnzgr	granod	mzgr	mzgr	mzgr	mzgr

SAMP	PDGR4	PDGR5	PDGR6	CNOGN1	CNOGN2	CNOGN3	CNOGN4	CNOGN5
SiO_2	72.08	71.98	70.91	72.5	74.14	73.56	71.97	71.71
Al_2O_3	14.6	14.86	14.84	14.36	13.82	13.53	15.03	14.1
Fe_2O_3	0.94	0.69	0.90	0.82	0.68	0.79	0.81	0.78
FeO	1.03	0.73	1.01	0.78	0.74	0.83	0.88	0.90
MgO	0.53	0.51	0.58	0.33	0.35	0.37	0.47	0.44
CaO	1.51	1.88	1.56	1.45	1.5	1.51	1.63	1.59
Na_2O	3.67	3.88	3.77	3.6	3.56	3.64	3.77	3.5
K_2O	5.21	5.42	5.13	6.64	5.3	5.66	5.35	4.99
TiO_2	0.28	0.25	0.29	0.23	0.21	0.23	0.26	0.24
P_2O_5	0.09	0.09	0.09	0.07	0.07	0.07	0.09	0.08
MnO	0.02	0.02	0.02	0.02	0.02	0.02	0.02	0.02
total	99.96	100.31	99.1	100.8	100.39	100.21	100.28	98.35
norm								
Q	26.52	24.19	24.92	23.17	29.48	27.47	25.21	27.96
Or	30.84	32.09	30.37	39.3	31.38	33.51	31.68	29.54
Ab	31.05	32.83	31.9	30.46	30.12	30.8	31.9	29.61
An	7.22	7.14	7.46	3.39	6.08	3.85	7.78	7.61
Di	0	1.55	0	2.59	0.95	2.82	0	0
Hy	2.03	0.93	2.11	0	0.91	0.1	1.72	1.76
Mt	1.36	1	1.31	1.19	0.98	1.15	1.18	1.13
Il	0.53	0.47	0.55	0.44	0.4	0.44	0.49	0.46
Ap	0.22	0.22	0.22	0.17	0.17	0.17	0.22	0.19
Q	28	25	26	24	30	29	26	30
A	32	33	32	41	32	35	33	31
P	40	42	42	35	37	36	41	39
rock	mzgr	mzgr	mzgr	mzgr	mzgr	mzgr	mzgr	mzgr

Samples from m'skagn throughout cnogn5 are from Messica granitoid and the remaining from Vumba granitoids. mzgr- monzogranite and granod- granodiorite.

4.4.2 Major Element Chemistry

The rocks are typically granitoids with SiO_2 contents 65-76 %, Al_2O_3 12-18 % and (FeO_{total}+ MgO)< 6 %. Na_2O contents in the Vumba and Messica Granite Gneiss are similar (Fig. 4.6). However, the Messica Granite Gneiss has higher K_2O contents of 5-5.5wt% compared to values of 3.5-4 wt% in the Vumba Granite Gneiss. K_2O contents in the Vumba Granite Gneiss show a marginal increase with increasing SiO_2 (Fig. 4.6).

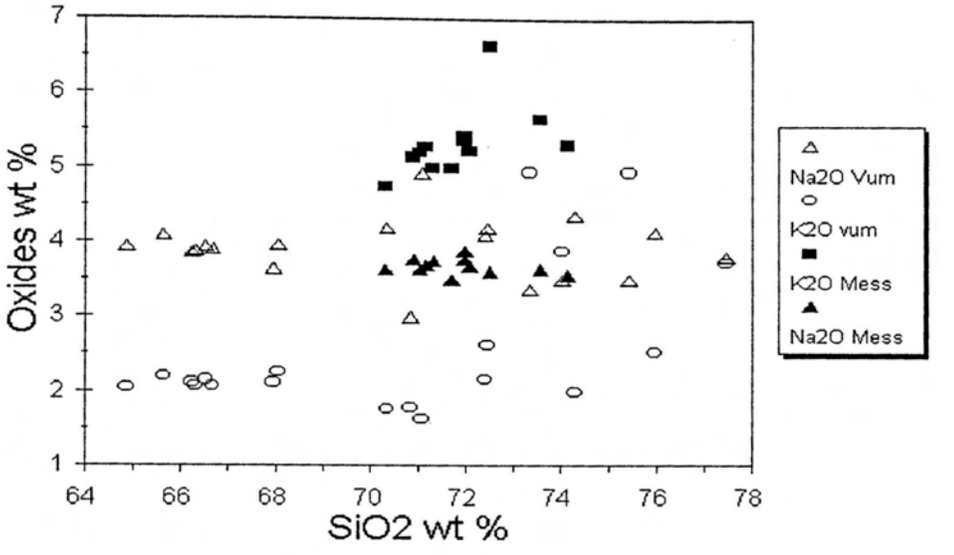

Figure 4.6: Variation diagram plotting Na_2O and K_2O versus SiO_2. Vum- Vumba Granite Gneiss and Mess- Messica Granite Gneiss.

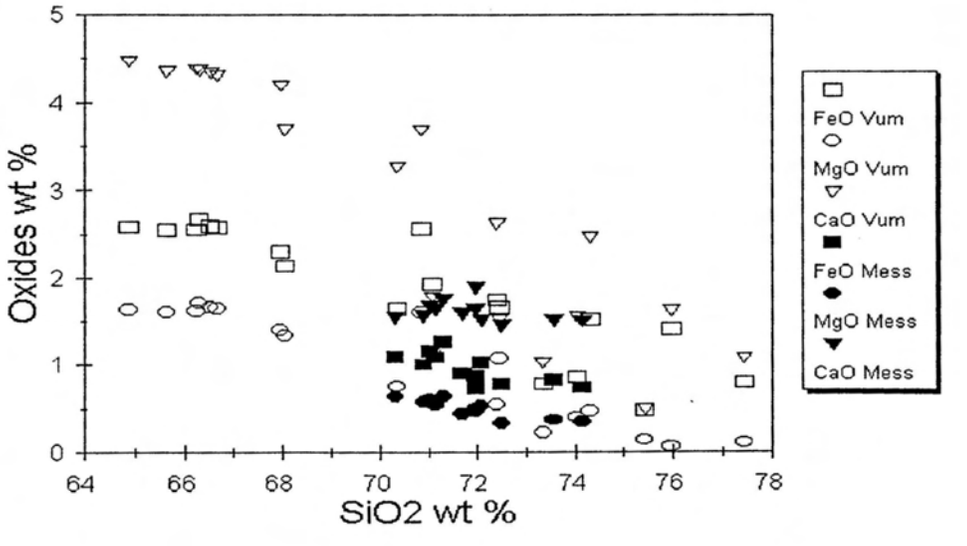

Figure 4.7: Variation diagram plotting FeO, MgO and CaO. Symbols as in Figure 4.6

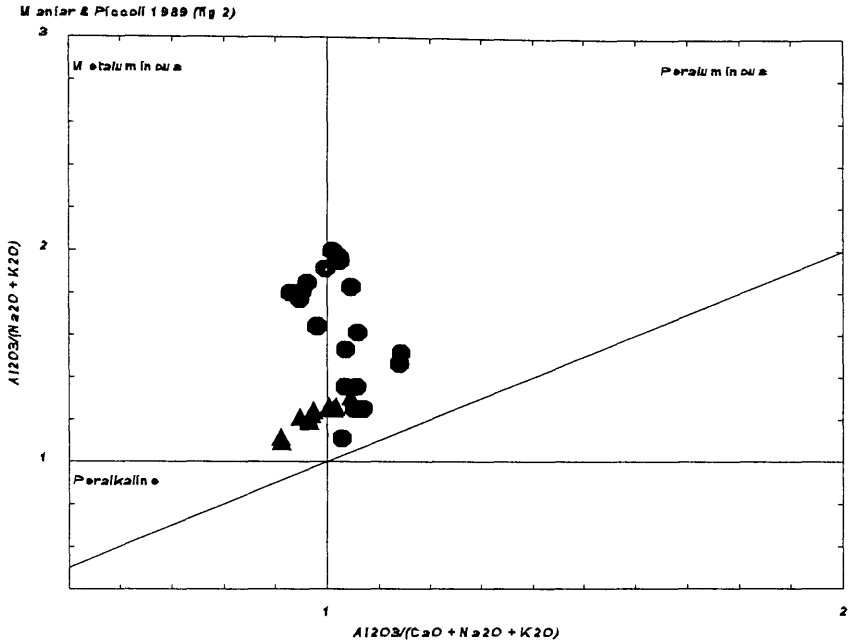

Figure 4.8: Aluminum-saturation ratios diagram (after Shand, 1947) of the Vumba (filled circles) and the Messica (filled up triangles) Granite Gneisses.

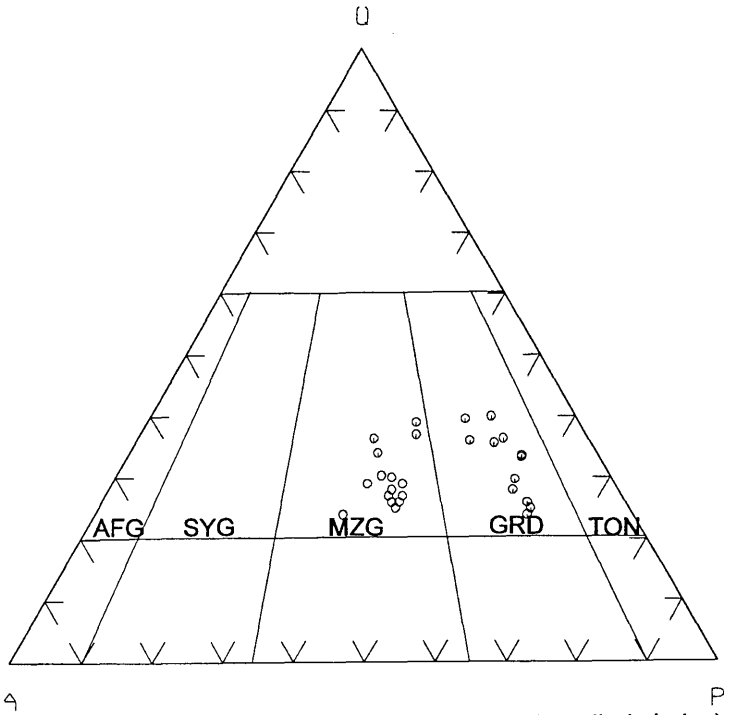

Figure 4.9: Streckeisen (1976) QAP plot of Vumba (filled circles) and Messica granitoids (open circles). AFG- alkali feldspar granite, SYG- syenogranite, MZG- monzogranite, GRD- granodiorite, TON- tonalite.

The variation diagram in Figure 4.7 shows that the Messica granitoids compared with the Vumba granitoids are characterized by lower contents of FeO, MgO and CaO and a more limited SiO_2 composition. In addition, it is observed that the oxide contents decrease with increase in SiO_2 giving rise to negative correlations. CaO contents of the Vumba Granite Gneiss are significantly higher than those for the Messica Granite Gneiss (Fig. 4.7). The combined contents of total alkalis, CaO and Al_2O_3, result in the granites varying from metaluminous to peraluminous on the basis of the aluminum-saturation ratios (Shand,1947) (Fig. 4.8). Similarly ∑FeO contents in the Vumba Granite are distinctly higher than the Messica Granite Gneiss whereas MgO contents are similar to marginally lower than the Messica Granite Gneiss .

On the basis of normative mineralogy in the QAP diagram of Streckeisen (1976) (Fig 4.9), the Vumba granitoids are classified as granodiorites and monzogranites while the Messica granitoids are classified as monzogranite (Table 4.3).

Data plotted in the AFM tholeiite/calc-alkaline discriminant diagram after Irvine & Baragar (1971) (Fig.4.10) suggests that all the granites are typically calc-alkaline. This figure is however not well suited to granitic rocks because, in rocks with high alkali contents with respect to the ferro-magnesian components, all acid rocks plot in the same area within the calc-alkaline field of the AFM diagram. However, the calc-alkaline nature is supported by the Jensen (1976) discriminant diagram (Fig. 4.11) which is better suited to discriminating between calk-alkaline and tholeiitic granitoid rocks.

4.4.3 Trace Element Chemistry

Trace element compositions, including REE, of the Vumba Granite Gneiss are shown in Table 4.4.

Table 4.4: Trace elements compositions of the Messica and Vumba granitoids.

SAMPL	VGR3-1	VGR3-2	VGR3-3	VGR3-4	VGR3-5	VGR3-6	VGRI	VGRIII	VGRIV	127	90	81
Ba	501	482	491	516	538	482	1141	592	564	394	551	472
Li	23	27	26	23	27	25	49	12	16	nd	nd	nd
Nb	6	6	6	6	6	7	6	4	9	nd	nd	nd
Sc	8	8	9	9	9	9	2	2	3	nd	nd	nd
Sr	266	269	266	275	271	277	232	43	107	256	247	131
Rb	64	65	66	65	61	65	61	145	319	73	88	93
Y	14	14	14	16	16	16	5	12	26	Nd	Nd	Nd
Zr	183	176	207	186	171	155	173	91	133	128	152	157
La	17	34	Nd	Nd	Nd	Nd	Nd	Nd	Nd	Nd	Nd	Nd
Ce	32	62	Nd	Nd	Nd	Nd	Nd	Nd	Nd	Nd	Nd	Nd
Pr	4	7	Nd	Nd	Nd	Nd	Nd	Nd	Nd	Nd	Nd	Nd
Nd	15	22	Nd	Nd	Nd	Nd	Nd	Nd	Nd	Nd	Nd	Nd
Sm	3	3	Nd	Nd	Nd	Nd	Nd	Nd	Nd	Nd	Nd	Nd
Eu	1	1	Nd	Nd	Nd	Nd	Nd	Nd	Nd	Nd	Nd	Nd
Gd	2	3	Nd	Nd	Nd	Nd	Nd	Nd	Nd	Nd	Nd	Nd
Dy	2	2	Nd	Nd	Nd	Nd	Nd	Nd	Nd	Nd	Nd	Nd
Ho	0	0	Nd	Nd	Nd	Nd	Nd	Nd	Nd	Nd	Nd	Nd
Er	1	1	Nd	Nd	Nd	Nd	Nd	Nd	Nd	Nd	Nd	Nd
Yb	1	1	Nd	Nd	Nd	Nd	Nd	Nd	Nd	Nd	Nd	Nd
Lu	0	0	Nd	Nd	Nd	Nd	Nd	Nd	Nd	Nd	Nd	Nd

SAMPL	150	124	14	253	403	404	406	MSIKGN	PDGR1	PDGR2	PDGR3	PDGR4
Ba	525	504	505	626	385	422	495	868	938	868	937	918
Li	Nd	Nd	Nd	Nd	Nd	Nd	Nd	19	15	15	13	13
Nb	Nd	Nd	Nd	Nd	Nd	Nd	Nd	5	4	5	6	4
Sc	Nd	Nd	Nd	Nd	Nd	Nd	Nd	2	2	2	2	2
Sr	324	139	149	80	101	36	59	244	203	223	203	204
Rb	77	50	95	132	89	107	78	154	134	126	132	131
Y	Nd	Nd	Nd	Nd	Nd	Nd	Nd	16	7	8	9	7
Zr	135	135	106	130	186	101	210	172	209	229	210	190
La	Nd	Nd	Nd	Nd	Nd	Nd	Nd	Nd	71	90	Nd	Nd
Ce	Nd	Nd	Nd	Nd	Nd	Nd	Nd	Nd	129	165	Nd	Nd
Pr	Nd	Nd	Nd	Nd	Nd	Nd	Nd	Nd	13	16	Nd	Nd
Nd	Nd	Nd	Nd	Nd	Nd	Nd	Nd	Nd	38	49	Nd	Nd
Sm	Nd	Nd	Nd	Nd	Nd	Nd	Nd	Nd	4	6	Nd	Nd
Eu	Nd	Nd	Nd	Nd	Nd	Nd	Nd	Nd	1	1	Nd	Nd
Gd	Nd	Nd	Nd	Nd	Nd	Nd	Nd	Nd	2	3	Nd	Nd
Dy	Nd	Nd	Nd	Nd	Nd	Nd	Nd	Nd	1	2	Nd	Nd
Ho	Nd	Nd	Nd	Nd	Nd	Nd	Nd	Nd	0	0	Nd	Nd
Er	Nd	Nd	Nd	Nd	Nd	Nd	Nd	Nd	0	0	Nd	Nd
Yb	Nd	Nd	Nd	Nd	Nd	Nd	Nd	Nd	0	1	Nd	Nd
Lu	Nd	Nd	Nd	Nd	Nd	Nd	Nd	Nd	0	0	Nd	Nd

SAMPL	PDGR5	PDGR6	CNOGN1	CNOGN2	CNOGN3	CNOGN4	CNOGN5
Ba	901	889	797	772	793	840	710
Li	13	14	13	14	15	15	15
Nb	3	4	4	4	4	4	4
Sc	2	2	1	2	1	1	2
Sr	253	194	159	158	156	165	154
Rb	132	129	151	142	138	144	135
Y	6	7	7	7	6	5	7
Zr	183	204	189	140	165	190	203
La	Nd	Nd	49.62	78.38	Nd	Nd	Nd
Ce	Nd	Nd	95	149	Nd	Nd	Nd
Pr	Nd	Nd	10	15	Nd	Nd	Nd
Nd	Nd	Nd	32	47	Nd	Nd	Nd
Sm	Nd	Nd	5	6	Nd	Nd	Nd
Eu	Nd	Nd	1	1	Nd	Nd	Nd
Gd	Nd	Nd	2	3	Nd	Nd	Nd
Dy	Nd	Nd	1	1	Nd	Nd	Nd
Ho	Nd	Nd	0	0	Nd	Nd	Nd
Er	Nd	Nd	0	0	Nd	Nd	Nd
Yb	Nd	Nd	0	0	Nd	Nd	Nd
Lu	Nd	Nd	0	0	Nd	Nd	Nd

Nd- not determined and nd- not detected.

Ba, Rb and Zr contents in the Vumba Granite Gneiss are typically lower than in the Messica Granite Gneiss. Conversely, Nb, Y and Sc contents in the Vumba Granite Gneiss are higher compared with the contents in the Messica Granite Gneiss. Sr contents in both granites are similar.

Although it is uncertain to what extent plate tectonic processes operated in the Archaean and Proterozoic times, the differences between the Rb, Nb and Y contents of the Vumba and Messica Granite Gneisses result in the Vumba and Messica Granite Gneisses plotting in the field of the volcanic-arc granitoids of Pearce *et al.* (1984) (Fig. 4.12).

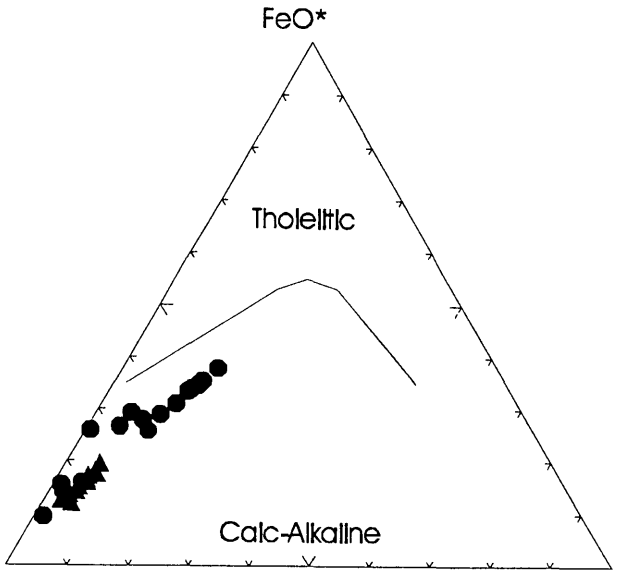

Figure 4.10: Irvine and Baragar (1971) calc-alkaline versus tholeiite discriminant diagram plot of Vumba (filled circles) and Messica (filled triangles) granitoids.

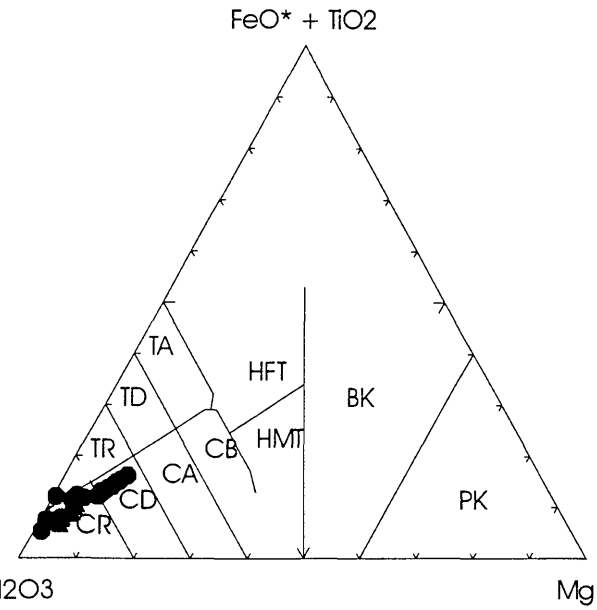

Figure 4.11: Vumba (filled circles) and Messica (filled triangles) granitoids plotted in the Jensen (1976) cationic diagram. TA-tholeiitic andesite, TD-tholeitic dacite, TR-tholeiitic rhyolite, CR- calc-alkaline rhyolite, CD- calc-alkaline dacite, CA- calc-alkaline andesite, CB- calc-alkaline basalt, HHT- high iron tholeiite, HMT- high magnesium tholeiite, BK- basaltic komatiite and PK-peridotitic komatiite.

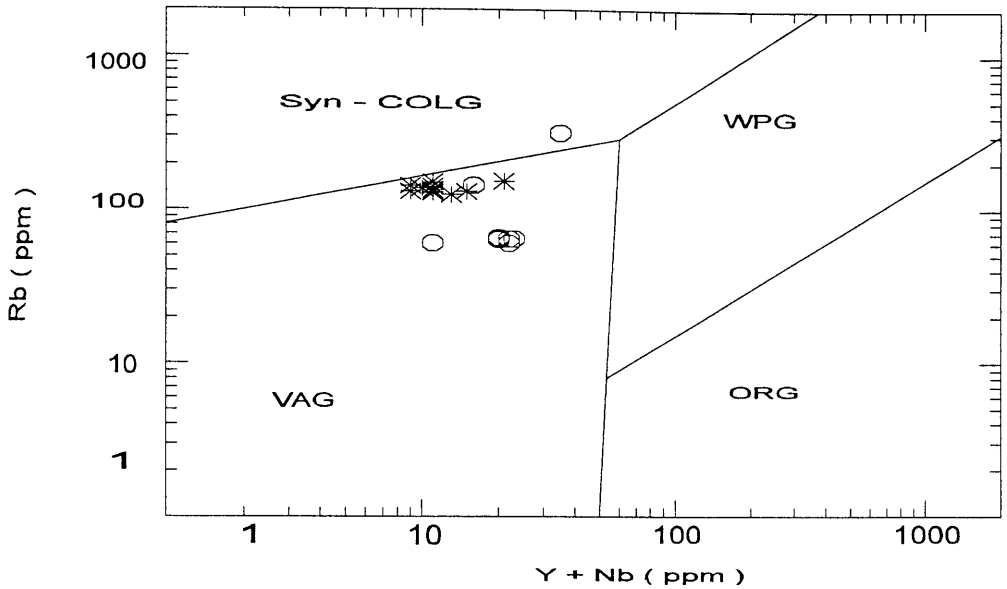

Figure 4.12: Plot of Vumba and Messica granitoids in the tectonic discriminant diagram after Pearce et al (1984). Asterix- Messica granitoids and open circle Vumba granitoids. Syn-Colg- Syn-collisional granitoids, WPG- within-plate granitoids, VAG- volcanic-arc granitoids and ORG- orogenic granitoids.

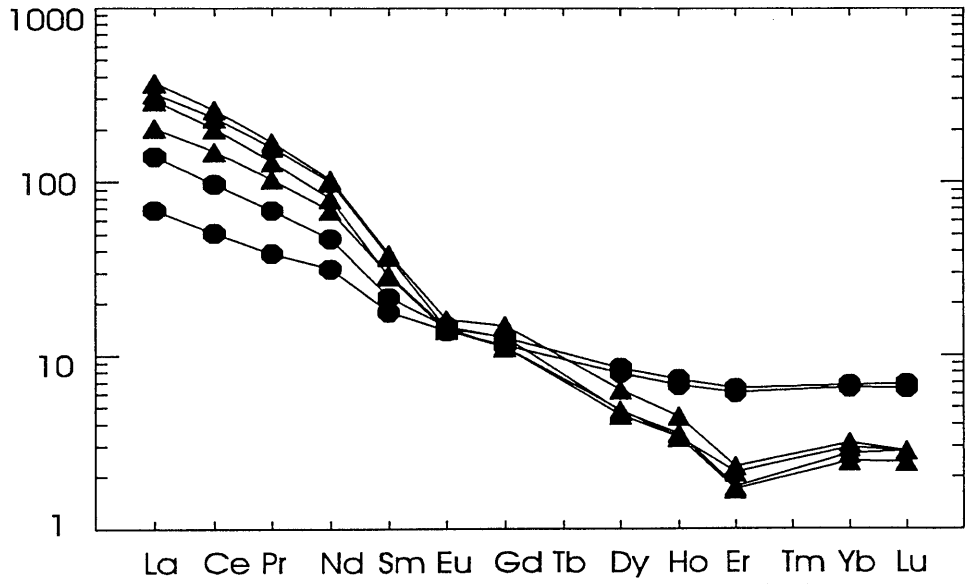

Figure 4.13: Chondrite normalized REE abundance diagram for Vumba (filled circles) and Messica (filled triangles) granitoids.

Six samples from the Vumba and Messica Granite Gneisses were analysed for the REE by Dr. N. Walsh (Royal Holloway, University of London) using the ICP method. The data are presented in the conventional chondrite-normalized diagram (normalising values after Evensen *et al.*, 1978) in Figure 4.13. The Messica Granite Gneiss samples show a pattern characterized by higher light REE and lower heavy REE contents compared to the Vumba Granite Gneiss samples. The Messica Granite Gneiss samples are characterized by a weak negative Eu anomaly suggesting either feldspar fractionation or residual feldspar in the restite whereas the Vumba Granite Gneiss samples have no Eu anomaly suggesting insignificant feldspar fractionation and/or insignificant feldspar residues in the source of the granite. The higher contents of heavy REE in the Vumba Granite Gneiss samples may suggest that garnet and/or hornblende fractionation or garnet and/or hornblende in the restite resulted in the depletion of these elements in the Messica Granite Gneiss compared to the Vumba Granite Gneiss.

4.4.4 Radiogenic isotope chemistry

For whole rock geochronology by the Rb - Sr method, 6 samples of Messica granitoids were analysed during the present study for their contents in Rb and Sr radiogenic isotopes (Table 4.5). The rocks were analysed by Dr. F.J. Kruger at the Bernard Price Institute, University of the Witwatersrand.

Table 4.5: Radiogenic isotope data of Messica granitoids.

Sample	Rb	Sr	$^{87}Rb/^{86}Sr$	$^{87}Sr/^{86}Sr$
pdgr1	134	203	2.0873	0.7824
pdgr2	126	223	1.8155	0.7749
pdgr3	132	203	2.1574	0.7863
pdgr4	131	204	2.0024	0.7797
pdgr5	132	253	1.6790	0.7691
pdgr6	129	194	1.9900	0.7842

Rb and Sr contents are in ppm.

Table 4.6: Radiogenic isotope data of Vumba granitoids.

Sample	Rb	Sr	$^{87}Rb/^{86}Sr$	$^{87}Sr/^{86}Sr$
S365	68	288	0.6820	0.7279
S150	56	279	0.5850	0.7303
S372	68	239	0.8260	0.7365
S90	81	235	1.1140	0.7374
S149	43	46	2.720	0.8122
S373	84	82	3.0780	0.8125
N14	88.2	153.6	1.6720	0.7753
N81	74	127.4	1.6920	0.7792
N407	80.4	74.2	3.180	0.8533
N406	76.8	65.6	3.4350	0.8592
N408	70.9	83.5	2.4830	0.8190

Data are from Manuel (1992). Rb and Sr contents are in ppm. An S prefix to the sample name denotes southern suite whereas an N denotes northern suite.

Regression of the data using the computer program GEODATE , written by Harmer and Eglington (1987) produced an errorchron of 2579Ma ± 468Ma with MSWD=6.611 and an initial $^{87}Sr/^{86}Sr$ =0.7054. Exclusion of sample Pdgr6, which is distinctly displaced from the other points (Fig. 4.14), from the regression calculation yields an isochron of 2348 Ma±267 Ma with MSWD=1.198 and an initial $^{87}Sr/^{86}Sr$ =0.7124. The sample can be excluded due to its apparent alteration and chloritization of biotite which may have affected the distribution of Rb. These data are compared with those of the Vumba granodiorite and tonalites from Manuel (1992) shown in table 4.6. The southern Vumba Granite Gneiss suite of Manuel (1992) was collected close to the Messica Granite Gneiss and the age they yielded (2527 Ma±632) is close to the date of 2348±267 of the Messica granitoids (Fig. 4.14).

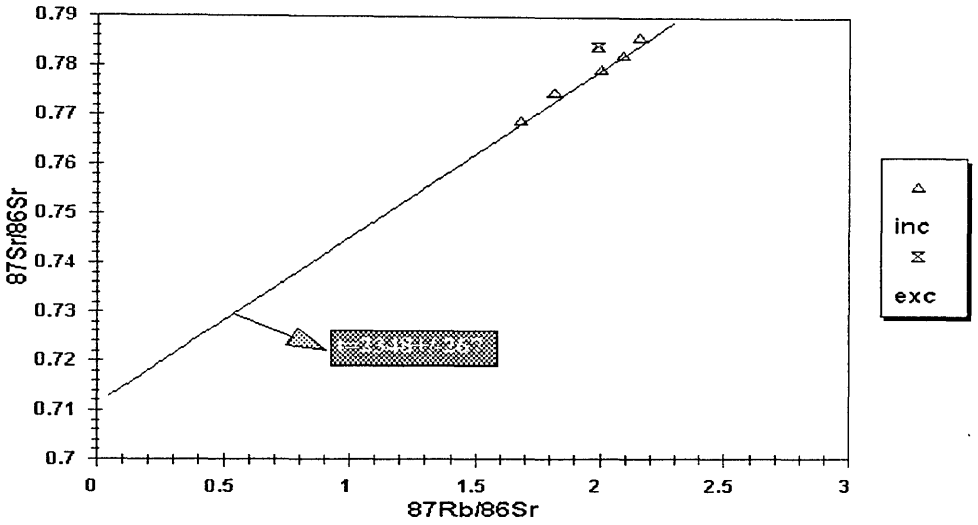

Figure 4.14: Rb/Sr isotopic diagram with the isochron t=2348±267 indicated. inc stands for data included and exc for data excluded.

The Rb contents of the Messica granitoids are ~2X higher than those from the Vumba granodiorites and tonalites whereas Sr is higher in most of the samples from the Vumba granodiorites and tonalites. With the exception of samples 149 and 373, the samples of Messica granitoids are characterized by higher $^{87}Rb/^{86}Sr$ and $^{87}Sr/^{86}Sr$ ratios which is compatible with the Rb and Sr contents in these samples. The oldest granitoids in the study area are located north of the greenstones and were investigated by Manuel (1992) and Table 4.5 shows the corresponding radiogenic isotope analyses. The radiogenic isotope ratios of the oldest Vumba granites are of the same order of magnitude as those of Messica granitoids whereas Rb and Sr contents are approximately half the contents of the Messica Granite Gneiss.

The $^{87}Sr/^{86}Sr_i$ of 0.6947±0.0083 for the ~3385 Ma Vumba granitoids (Manuel, 1992), is similar to 0.6990 ± 0.00003 (McCulloch and Black, 1984) of the bulk earth, here taken as BABI (Basailtic Achondrite Best Initial), suggesting fractionation of these granitoids from the mantle. Conversely, the

^{87}Sr $^{86}Sr_i$ of 0.7124±0.0037 and 0.7122±0.0340 of the younger Messica and Vumba granitoids respectively, are significantly higher than that which granitic crust would have had if it separated from the mantle ca. 2.7 Ga ago (Rollinson, 1993) and higher than today's BABI of 0.7047-0.7050 ratios (Allegre *et al.*, 1983a), suggesting a derivation of these rocks from an environment with continental crust influence. In addition, the fact that the $^{87}Sr/^{86}Sr_i$ ratios of these granitoids are higher than present day's 0.7211 ratio of continental crust (Rollinson, 1993) is an indication that partial melting might have taken place in an already Rb enriched crust which, given the refractory nature of Sr, would give rise to a magma of an even higher relative Rb concentrations.

4.4.5 Discussion and Conclusions

The rocks are classified as granodiorites (Vumba granitoids) and monzogranites (Messica granitoids). Manuel (1992) described the Archaean Vumba granitoid as being tonalites and granodiorites, which combined with the findings of the present study, defines a tonalite-trondhjemite-granodiorite association often abbreviated to TTG (Jahn *et al.*, 1981), provided the definition of trondhjemite as a leucocratic tonalite (Barker, 1979) holds. This association is typical of many Archaean granitoid suits irrespective of their age and geographical position (Martin, 1987; Clarke, 1992, p. 198). Pinna *et al.* (1986), following previous workers, defined the Messica granitoid around Revue river as "remobilised porphyroblastic" and Manuel (1992) described the occurrence of a granite-gneiss north of the greenstones. It was found that the granitoids around the Revue river are typically porphyritic and foliated but are not banded. Elsewhere the Messica granitoid may be foliated but banding is not a common characteristic. In the Vumba granitoids, the hornblende granitoids exhibit a weak foliation defined by preferred orientation of hornblende crystals whereas the M'Kwananda locality shows a strong foliation and folding as well as jointing caused by deformation. Locally small shear zones occur but the common texture is that of a typical granite.

The Archaean TTG radiogenic isotope signatures are similar to those of the mantle (Clarke, 1992, p. 198) so that the initial $^{87}Sr/^{86}Sr_i$ ratio of the older Vumba granitoid of 0.694±0.0089 (Manuel, 1992) which is similar to 0.6989 ± 0.00003 (McCulloch and Black, 1984) of BABI suggests that they are product of mantle fractionation. This suggestion agrees with the results of the investigations into the petrogenesis of Archaean TTG from Eastern Finland carried out by Martin (1987). On the other hand the initial $^{87}Sr/^{86}Sr_i$ ratio of the Messica Granite Gneiss of 0.7124±0.00366 and of the younger late Archaean Vumba Granite Gneiss of 0.7212±0.0340 (Manuel, 1992) are too high and can'nt be assigned a mantle derivation suggesting that these granitoids were derived from a crust already enriched in Rb. The Messica monzogranites are younger and chemically more evolved, with higher $^{87}Sr/^{86}Sr_i$ ratios and a negative Eu anomaly. These characteristics would be consistent with them being a partial melt of a TTG rock suite in which feldspar would have been left in the residue.

In conclusion, it is proposed that the older TTG suite originated as partial melt of basaltic mantle material and the younger Vumba and Messica granitoids originated from partial melting of the older TTG suite.

Chapter 5

FRONTIER FORMATION

5.1 Introduction

The Frontier Formation has been viewed as a supracrustal sequence to the Mozambique Belt by previous workers (eg. Afonso, 1978). During the present study, however, it was found that this metasedimentary sequence only overlies the Early Proterozoic Messica Granite Gneiss around Garuzo and the greenstones in the Chimezi areas respectively (Fig. 2.1). Rocks in the sequence consist of quartzite and pelitic schists. No whole-rock chemical analyses were conducted with only selected minerals being analysed for the purposes of thermobarometry to be discussed later.

5.2 Field Description

The Frontier Formation rocks occur in the Garuzo region where they overlie the Messica Granite Gneiss and in Chimezi where they overlie serpentinites and schist of the Macequece Formation. In both localities, the exposures are oriented N-S (Fig. 2.1). The Frontier Formation consists of quartzite and mica schist. Quartzite is the predominant rock type and forms prominent ridges, very resistant to erosion (Fig. 5.1). Muscovite flakes exhibit a preferred foliation. Quartz grains are deformed and elongated along foliation planes. The rock is affected by conjugate joints. Texturally, the quartzite is equigranular coarse-grained. In the Chimezi area, the quartzite is grey and composed of very fine-grained quartz and muscovite interlayered with sillimanite/kyanite schist.

Figure 5.1: Resistant quartzite ridge in the Frontier Formation.

Around Garuzo, the schists are composed of alternating bands and lenses of quartz and sillimanite on one hand, and biotite and garnet on another. Sillimanite and biotite exhibit a preferred orientation. Quartz is deformed along foliation planes. The schist shows folding defined by felsic bands.

5.3 Petrography

Besides microscopic mineral identification, X-Ray diffraction methods were also used, particularly in fine grained samples (samples 31chgr1 and 31chgr2) collected in Chimezi (Fig. 2.2). The rocks have granoblastic and schistose textures in quartzite and mica sillimanite-bearing rocks respectively. They are coarse grained (±2 mm) at Garuzo and very fine grained at Chimezi. The mineralogy of the samples is shown in Table 5.1. The samples are all quartz rich, and they contain sillimanite+biotite and kyanite+sillimanite in Garuzo and Chimezi respectively. Garnet appears in samples from Garuzo whereas sericite is recognised in samples from Chimezi.

Table 5.1: Mineralogical assemblage of the Frontier Formation.

Sample	Qtz	Bt	Sil	Ky	Grt	Ms	Ser	Opm
GQZ	64	10	24	-	1	-	-	1
GSC	70	10	20	-	-	-	-	-
GCMX	72	10	15	-	2	-	-	1
GAQZ1	93	-	-	-	-	6	-	1
CHQZ	94	-	-	-	-	5	-	1
31CHQ1	85	-	3	10	-	-	2	-
31CHQ2	87	-	2	8	-	-	3	-

Qtz- quartz, Bt- biotite, Sil- sillimanite, Ky- kyanite, Grt- garnet, Ms- muscovite, Ser- sericite and Opm- opaque minerals.

Three parageneses are recognised, all being quartz-rich. The parageneses are (1) Qtz+Bt+Sil±Grt (2) Qtz+Ms (3) Qtz+Ser±Sil±Ky. Paragenesis (3) characterizes samples from Chimezi and the remaining paragenesis characterize samples from Garuzo. Quartz grains define granoblastic textures and show undulatory extinction resulting from high strain. Some samples have lenticular quartz grains which define a strong schistose planar fabric. Biotite exhibits a strong planar fabric defining a lepidoblastic texture. Sillimanite needles are parallel to biotite flakes with which they are commonly associated and are very fine grained in the west. The foliation defined by sillimanite and biotite wraps around garnet indicating that garnet was pre-tectonic and sillimanite+biotite probably syn-tectonic (Fig. 5.2) (Spry, 1979, p. 252-253; Shelley, 1993, p. 304-307). Kyanite occurs as anhedral fine grains with some larger grains exhibiting the typical two cleavages at about 75°. Irregular garnet grains contain inclusions of quartz. Muscovite occurs as flakes in and along quartz grain boundaries. Sericite is very fine-grained. Opaque minerals occur as fine xenoblastic to idioblastic grains as inclusions in quartz or associated with biotite.

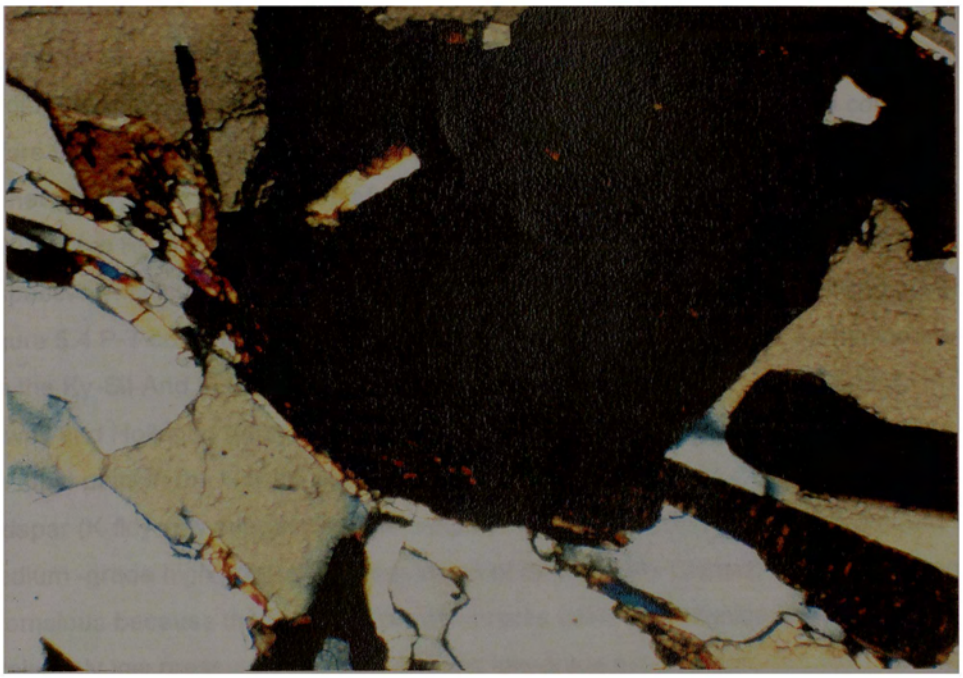

Figure 5.2: Biotite flakes (brown and partially extinct) and sillimanite needles (high birefringence) forming a foliation which wraps around a garnet grain (black). Crossed nicols; width of field 3 mm.

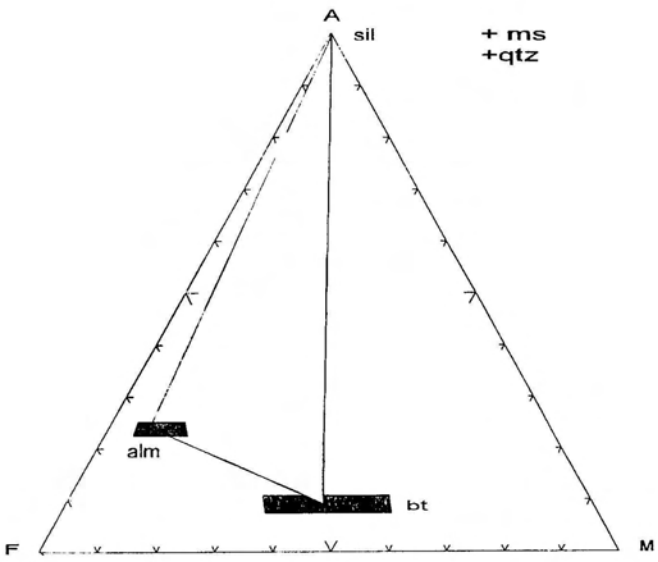

Figure 5.3: The medium- to high-grade mineral assemblage (bt+sil+alm) from the Frontier Formation, around Garuzo, plotted in an AFM diagram. Alm- almandine, bt- biotite, sil- sillimanite, qtz- quartz and ms- muscovite.

5.4 Interpretation

The assemblage (Bt+Sil+Grt) in the presence of quartz and muscovite (Fig. 5.3) is typical of upper medium-grade to high grade metamorphism (Winkler, 1974, p. 216). These conditions were attained before the tectonism/deformation that gave rise to the planar foliation since this wraps around cracked garnet (Spry, 1969). Application of computer programs of Powell and Holland (1988) and Berman (1991), give Ky-And-Sil triple points of P=~4.9 kbar and T=~582 °C, and P=~3.8 kbar and T=~506 °C respectively, calculated on the basis of mineral activities which are entered into the programs. In Figure 5.4 P-T conditions relevant to the metamorphism in the Frontier Formation are shown. Plotted are the Ky-Sil-And triple point and the equilibrium reaction Ms+Qtz->Kfld+Al_2SiO_5+H_2O calculated after Powell and Holland (1988). The diagram suggests that metamorphic conditions were below and above the triple point in the Garuzo and the Chimezi areas respectively. On the other hand, the absence of K-feldspar (K-fld) may suggest that the temperatures were not high enough to produce this mineral. The medium -grade high pressures assemblage of Sil+Ky in the Chimezi area can be considered anomalous because the Frontier Formation rocks overlie the Manica Greenstone Belt rocks which have a relatively low pressure andalusite-bearing low-grade assemblage.

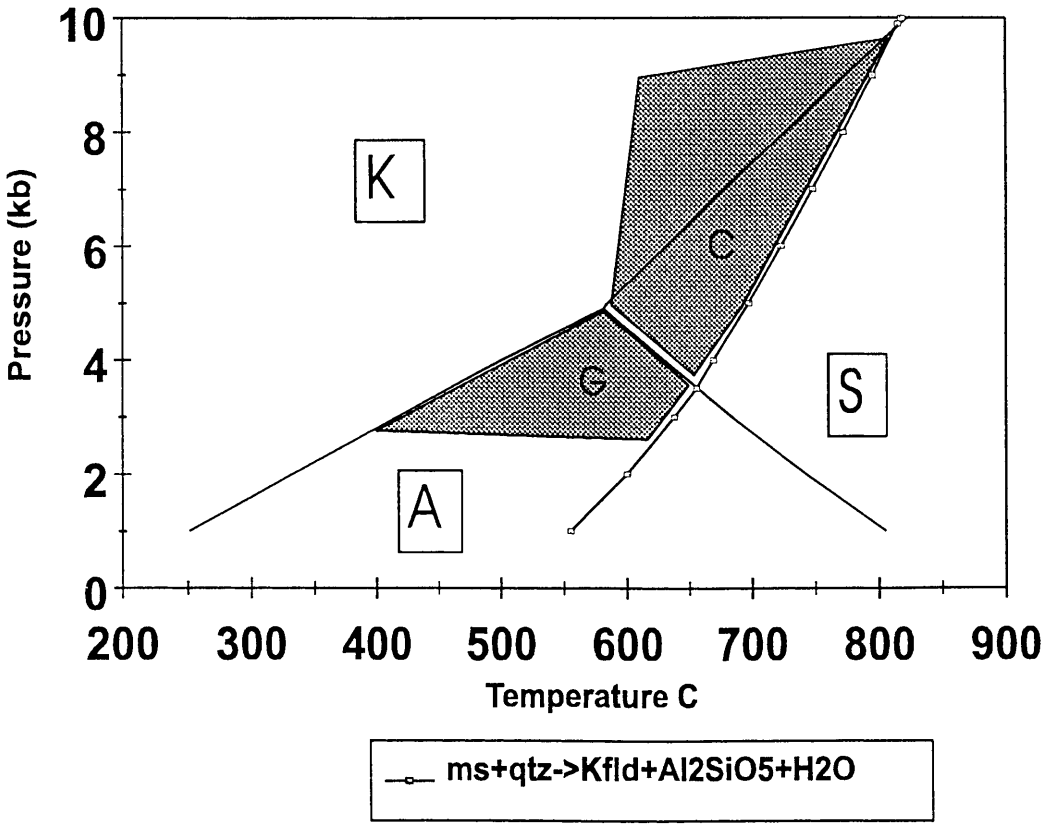

Figure 5.4: P-T conditions relevant to the Frontier Formation metamorphism in the Garuzo (G) and Chimezi (C) areas. And-Sil-Ky triple point as well as the reaction curve are afeter Powell and Holland (1988). Shown also are the fields of stability of kyanite (K), andalusite (A) and sillimanite (S).

Chapter 6

VANDUZI MIGMATITE GNEISS

6.1 Introduction

The Vanduzi Migmatite Gneiss occurs between the Messica Granite Gneiss in the west and the Nhansipfe Granitic Orthogneiss in the east (Fig. 2.1) and partially coincides with the zone of anatexis reflected in the 1:250 000 Carta Geologica da Regiao de Vila Manica-Vila Gouveia (1969) and of migmatites (Pinna *et al.*, 1986). Due to the heterogeneous nature of the rock, no chemical analyses were obtained.

6.2 Field Description

The Vanduzi Migmatite Gneiss is bound to the west by the Messica Granite Gneiss and Frontier Formation and to the east by the megacrystic Nhansipfe Granitic Orthogneiss. Field relationships are poorly exposed with the areas underlain by the Vanduzi Migamatite Gneiss showing very subdued topography. In the biotite-hornblende-quartz-feldspar migmatitic gneiss near the Vanduzi river (Fig. 2.2), large scale migmatisation has occurred which is characterized by layers of leucosome which are folded (Fig. 6.1). Two generations of partial melt layers are developed, being the older one folded and parallel to layering in the paleosome (Fig. 6.1).

Figure 6.1: Two generations of partial melting in the Vanduzi Migmatite Gneiss. Note that the second generation partial melt layers transgress the S_1 foliation and leucosomes.

The younger partial melt lenses are oriented N-S and cross-cuts both the planar fabric in the palaeosome and the earlier migmatitic layers (Fig. 6.1). Both generations of partial melt have mafic melanosomes comprising biotite and hornblende. At other localities, mafic boudins may represent interlayered mafic dykes pulled apart during deformation. Near Matsinho, the Vanduzi Migmatite Gneiss consists of more homogeneous biotite-quartz-feldspar gneiss with two generations of migmatisation recognisable in the field. The older leucosomes are recognised by their folded nature and are characterised by biotite-rich melanosomes whereas the younger melt patches are not deformed, share a common orientation, have no biotite-rich melanosome and are characterised by the presence of garnet in the leucosome (Fig. 6.2).

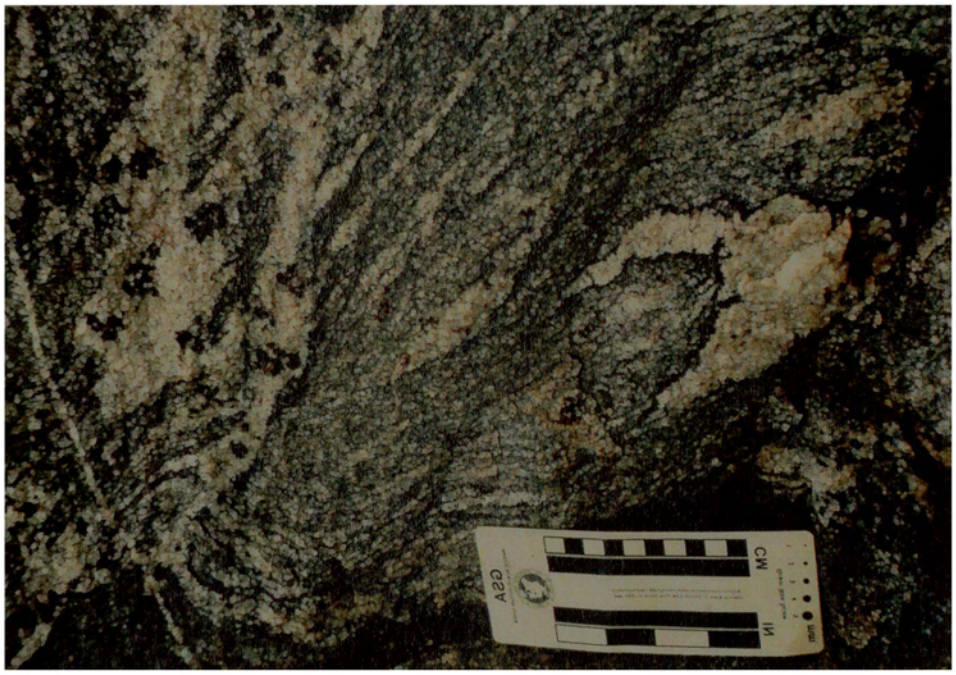

Figure 6.2: First stage stromatic migmatite (right, folded leucosome) and second generation stictolithic migmatite (left leucosomes) near Matsinho. Note garnet grains as part of the partial melt at left.

6.3 Petrography

The mineralogy of the samples is shown in Table 6.1. It is typically granitic being dominated by K-feldspar, plagioclase and quartz with minor amounts of biotite, hornblende and garnet.

The texture of these rocks is typically inequigranular fine- to medium-grained with fine foliated bands of biotite and hornblende interfringed with the granitic leucosome. Locally feldspar and quartz are intergrown to form myrmekite.

Two assemblages are recognized in the samples, namely (1) Plg+Bt+Hbl+K-fld+Qtz and (2) Plg+Bt+Grt+K-fld+Qtz. In assemblage (1) the K-feldspar is microcline, characterized by cross-hatch twinning and minor orthoclase with Carlsbad twinning.

Table 6.1: Mineralogical composition of the Migmatite Gneiss.

samp	K-fld	Plg	Qtz	Bt	Hbl	Ms	Grt	Aln	Ap	Ttn	Opm
mh'gn	35	30	30	4	-	<1	<1	<1	<1	-	-
grR	30	30	30	2	5	-	-	-	-	2	1
nzgg1	32	25	30	5	8	<1	-	<1	<1	<1	<1
mggnv	10	55	25	5	5	<1	-	-	-	-	<1
gr5	45	25	25	3	-	-	1	-	-	-	-

K-fld- potassium feldspar, Qtz- quartz, Plg- plagioclase, Bt- biotite, Hbl- hornblende, Ms- muscovite, Grt- garnet, Aln- allanite, Ttn- titanite, Ap- apatite and Opm- opaque minerals.

The grain size varies from <1-≤2 mm. The plagioclase has a similar grain size, exhibits polysynthetic albite twinning and contains inclusions of quartz, apatite and allanite. Quartz is coarser than the feldspars and has grain sizes varying from >1 to ±2.5 mm and is strained. Biotite is randomly oriented in the granitic leucosome but exhibits preferred orientations in the mafic bands where it defines a foliation together with hornblende. The hornblende is green and locally contains inclusions of quartz, titanite and opaque minerals. Muscovite is rare and commonly occurs as an alteration product of biotite. Allanite is idiomorphic and occurs associated with or as inclusions in plagioclase. Apatite is idiomorphic and occurs as inclusions in plagioclase and hornblende. Titanite is generally associated with hornblende as inclusion in the latter. The samples have low contents of opaque minerals. In assemblage (2) K-feldspar, plagioclase and quartz and the accessory minerals exhibit the same textural characteristics as in (1), but the K-feldspar content is higher leading to overall higher contents of felsic minerals relative to assemblage (1). Biotite occurs randomly in the paleosome and garnet is anhedral and is concentrated in the leucosome.

6.4 Interpretation of Petrography

The mineralogical assemblage of the migmatite gneiss is plotted in a ACF diagram in Figure. 6.3 in which the two mineral associations are distinguishable, namely, (1) Plg+Bt+Hbl+K-fld+Qtz and (2) Plg+Bt+Grt+K-fld+Qtz. The assemblage (1) is typical of mafic- to intermediate igneous rocks whereas the assemblage (2) is typical of semi-pelitic rocks. The association (2) is characterized by a low percentage of ferromagnesian minerals and the occurrence of garnet suggesting that this mineral might have formed by the reaction Bt+Qtz+Ms --->Grt +K-fld+H_2O (in melt).

The combination of granitic bands with bands of biotite and hornblende exhibiting preferred orientation, is typical of migmatites (Pitcher, 1993, p. 238-239) whereby the granitic bands, constituting the leucosome, form as a result of partial melt of feldspars and quartz with the consequent concentration of biotite and hornblende at the margins of these bands. The ferromagnesians (eg. Grt) that are melted or formed in the process are included in the granitic leucosome in which they occur randomly.

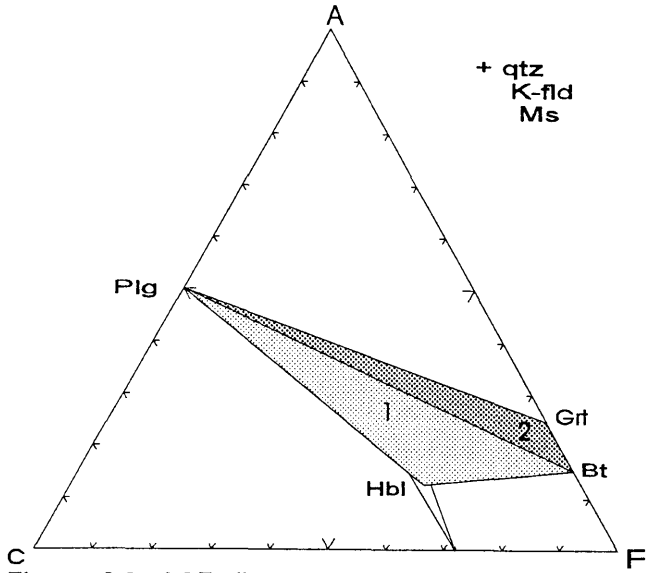

Figure 6.3: ACF diagram of the Vanduzi Migmatite Gneiss mineral assemblage. Plg- plagioclase, K- fld- potassium feldspar, Hbl- hornblende, Grt- garnet Bt- biotite and Ms- muscovite. 1 and 2- reactions as in the main test.

6.5 Leucosome Development History

Migmatites vary in structure from patchy to well layered, stromatic, types (Pitcher, 1993, p. 239). Migmatites are structured into neosome, comprising the newly developed layers of granitic leucosome and melanosome comprising the mafic minerals biotite and hornblende at the margins of the leucosome, and the palaeosome comprising the surviving country rock (Mehnert, 1968, p. 11; Pitcher, 1993, p. 239) (Fig. 6.4).

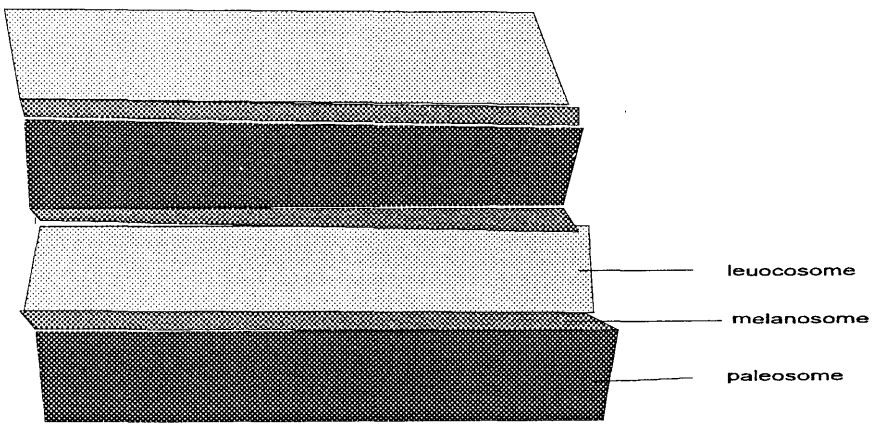

Figure 6.4: Nomenclature of stromatic migmatite (after Mehnert, 1968).

Two types of migmatites are recognized using the classification of Mehnert (1968 p. 18,37) namely stromatic and stictolithic. The stromatic variety is developed in both assemblages (1) and (2) and is characterized by the development of both leucosome and melanosome. The stictolithic variety (flecky gneiss) is only developed in assemblage 2 where the melting reaction of Bt+Qtz+Ms --->Grt+K-fld+H_2O in the melt is considered to have taken place and consequently no melanosome is developed. Both assemblages show two stages of migmatite genesis. Figures 6.1 and 6.2 both show stromatic migmatites characterized by leucosome and melanosome which are deformed. Both figures also show a second generation of migmatization which transgresses the S_1 foliation. In Figure 6.1 the second phase of leucosome development is of a stromatic variety whereas in Figure 6.2 the younger leucosome development is of a stictolithic or flecky gneiss variety.

6.6 Melt P-T Conditions

It is generally accepted that partial melting begins at about 650 °C under pressure of about ≥5 kbar and where $P_{total}=P_{H2O}$ (Pitcher, 1993, p. 239). However, substantial amounts of melt will only be produced as water becomes available from dehydration reactions of minerals and the temperature increases (Mehnert,1987).

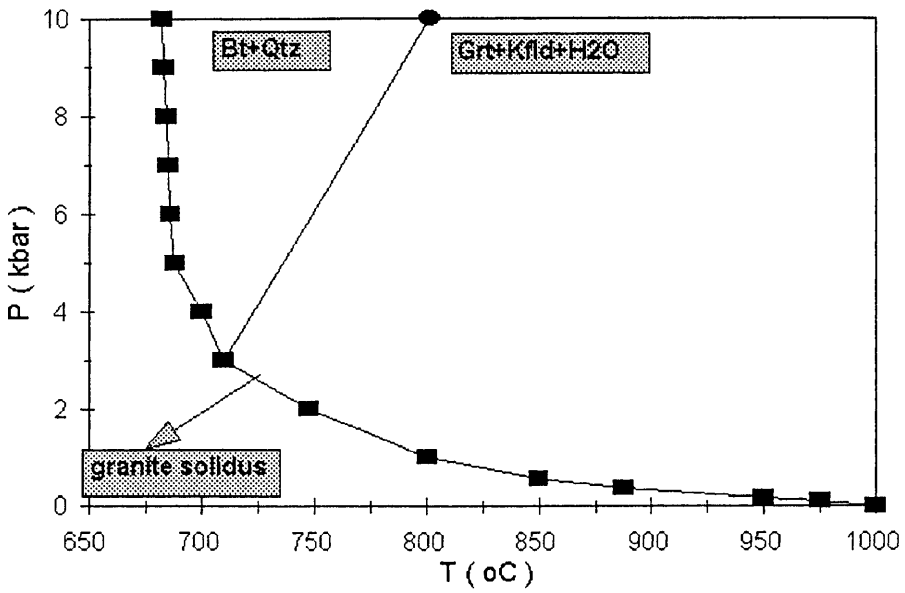

Figure 6.5: Granite solidus for the partial melting during the formation of Vanduzi Migmatitic Gneiss. Solidus data from Ebadi and Johannes (1991) and Johannes and Holtz (1990) and curve redrawn from Johannes, (1985, p. 44).

The structure of the migmatite gneiss near Vanduzi comprises layers of granitic leucosome with mafic selvedges (melanosome) at its margins (Fig. 6.1) suggesting that the melting system did not reach temperatures high enough to melt this mafic phase and incorporate it into the leucosome during first migmatization. These conditions are illustrated by the granite solidus shown in Figure 6.5 for $P_{total}=P_{H2O}$ for a granite with plagioclase $>An_{20}$ (Johannes, 1985). This figure shows that in conditions of minimum temperature melting, only quartzo-feldspatic melts will form the leucosomes whereas in higher temperature garnet may be part of the leucosomes. The occurrence of garnet as part of the leucosome (Fig. 6.2) in assemblage (2) in the migmatite gneiss near Matsinho suggests higher T conditions involving the dehydration melting reaction Bt+Qtz+Ms ---->Grt+K-fld+H_2O (Fig. 6.5).

Chapter 7

CHIMOIO GRANODIORITIC GNEISS

7.1 Introduction

The Chimoio Granodioritic Gneiss underlies the eastern portion of the study area and is named after the town of Chimoio which it underlies. Petrography and geochemistry were conducted on the main body.

7.2 Field Description

The Chimoio Granodioritic Gneiss occurs in the extreme east of the study area (Fig. 2.1) and consists of zones of more homogeneous intermediate biotite-hornblende-quartz-feldspar gneisses interlayered with heterogeneous interlayered amphibolitic and quartzo-feldspathic rocks. The amphibolitic rock is banded and consists of feldspar and quartz (felsic bands) and biotite and hornblende (mafic bands).

Figure 7.1: Sub-horizontal foliation concordant to the layering in the Chimoio Granodioritic Gneiss.

The migmatization is defined by lenticular layering of granitic partial melt bands oriented N-S with melanosome containing biotite and hornblende. Xenolithic biotite-hornblende rich enclaves are common in the intermediate biotite-hornblende-quartz-feldspar gneisses. The intermediate biotite-hornblende-quartz-feldspar gneisses are characterized by sub-horizontal foliation (Fig. 7.1) whereas in the intercalated amphibolite/leucocratic gneiss the foliation tends to be oriented along a NW-SE strike with steep dips towards the NE. The amphibolite and intercalated gneissic and migmatitic bands are intensely deformed resulting in various type of folds and boudins in the leucosome (Fig. 7.2).

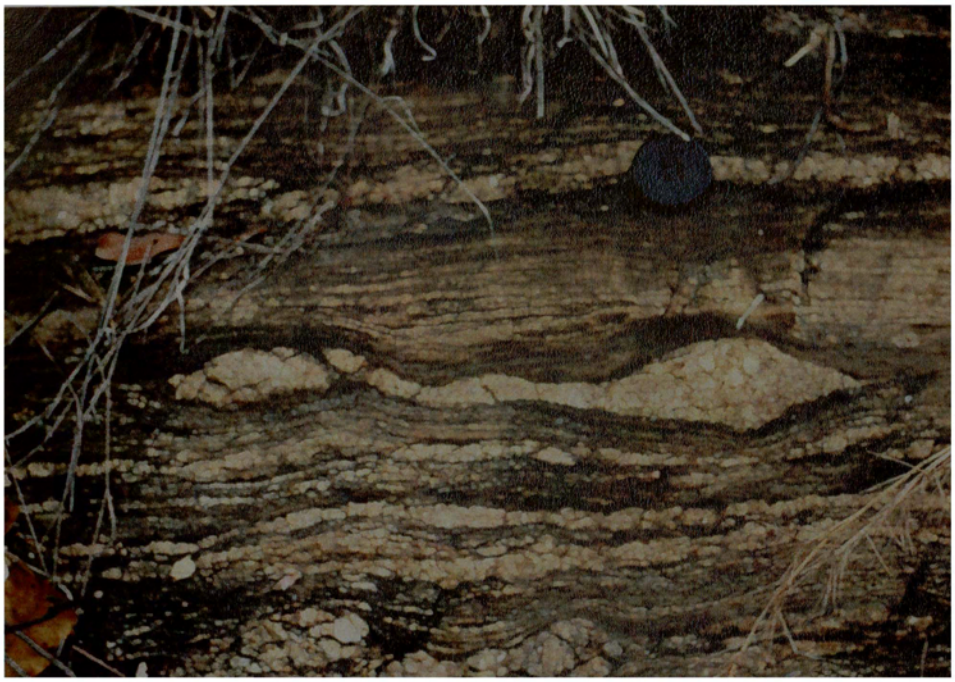

Figure 7.2: Boudinage in the deformed migmatitic gneiss in the Chimoio Granodioritic Gneiss

7.3 Petrography

The mineralogical assemblage of the Chimoio Granodioritic Gneiss consists of plagioclase (48-52%), K-feldspar (20-24%), quartz (8-10%), hornblende (8-12%), biotite (4-8 %) and accessory quantities of opaque minerals, apatite, allanite, muscovite and zircon (Table7.1). The dominant texture is granitic inequigranular medium- to coarse-grained and locally, myrmekites are developed. The samples are poor in quartz and are considerably enriched in hornblende (Fig.7.3) which combined with biotite amounts to a maximum of 22% (Table 7.1).

K-feldspar and plagioclase form equant sub- to anhedral grains exhibiting cross-hatched and Carlsbad and combined Carlsbad-albite twinning respectively. Some grains contain inclusions of fine-grained feldspar, quartz, euhedral apatite and zircon. Some plagioclase grains are unaltered

whereas others are cracked and generally sericitized, with cracks filled with sericite and other fine-grained felsic minerals. Quartz is anhedral, strained and locally, some grains enclose fine feldspar and quartz grains.

Table 7.1: Mineral assemblage of Chimoio Granodioritic Gneiss.

samp	K-fld	Plg	Qtz	Bt	Hbl	Ms	Aln	Zrn	Ap	Opm
cvgna	20	51	12	4	10	-	tr	tr	-	2
cvgnb	22	48	10	5	12	-	tr	tr	tr	2
cvgnc	24	51	10	5	8	1	tr	tr	tr	1
cvgnd	20	52	8	5	12	1	-	tr	tr	1
cvgne	22	48	10	8	11	-	tr	-	tr	1
cvgnf	22	50	8	5	12	-	-	tr	tr	3

K-fld- potassium-feldspar, Qtz- quartz, Plg- plagioclase, Bt- biotite, Hbl- hornblende, Ms- muscovite, Aln- allanite, Zrn- zircon, Ap- apatite and Opm- opaque minerals. tr-proportions less than 1%.

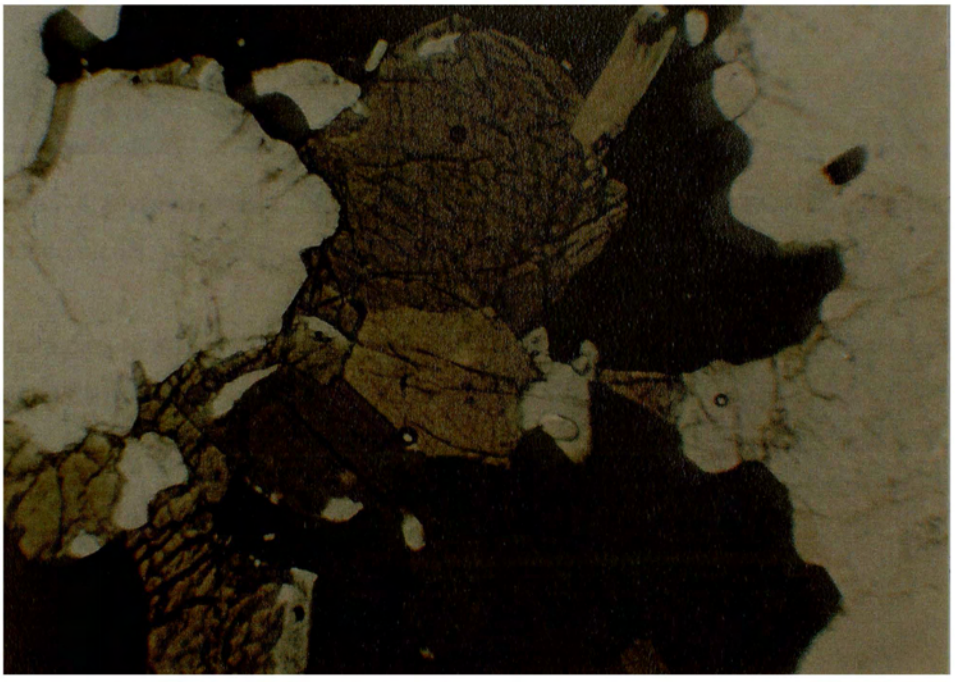

Figure 7.3: Brownish green and buff hornblende, brownish green flakes of biotite and plagioclase (white) in the Chimoio Granodiorite Gneiss. Parallel light, width of field 7 mm.

Finer quartz grains are, in general, unstrained especially those occurring as inclusions. Locally,quartz is intergrown with K-feldspar forming myrmekite (Fig.7.4). Hornblende is poikiloblastic with inclusions of

feldspar, quartz, apatite, zircon and allanite. It is subhedral with green to greenish-brown colours, (Fig. 7.3). Biotite occurs as individual grains or aggregates of flakes with straight sides and generally associated with hornblende. It contains inclusions of fine-grained quartz and feldspar. Muscovite is rare and generally occurs as secondary mineral after biotite and plagioclase.

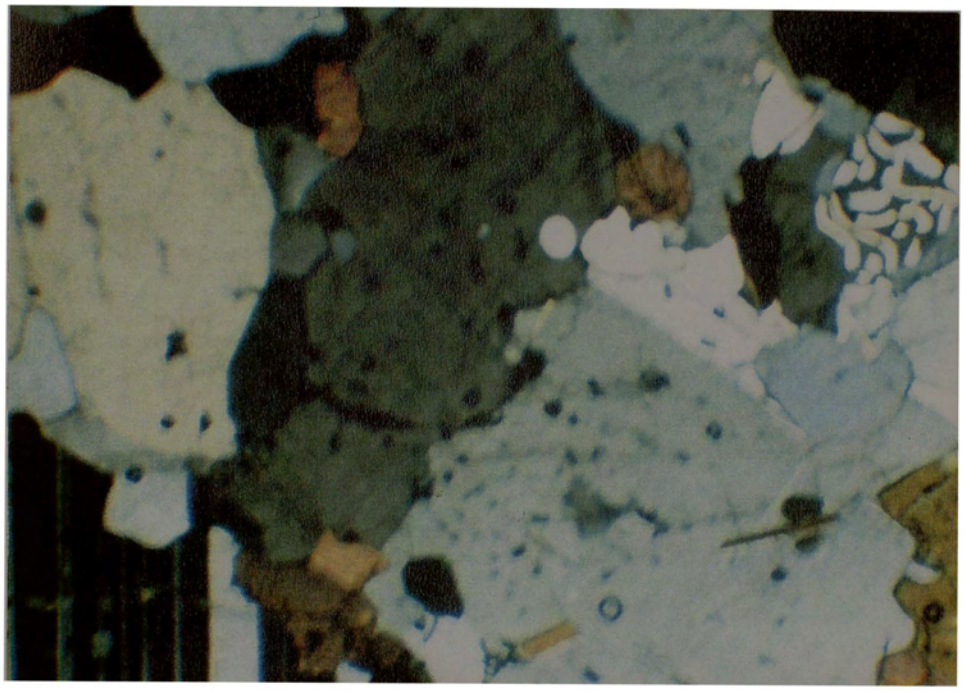

Figure 7.4: Myrmekitic intergrowths (top right) in the gneisses of the Chimoio Granodiritic Gneiss. Crossed nicols, width of field 7 mm.

Allanite occurs as brownish fine grains associated with, or as inclusions in, the ferromagnesian and opaque minerals. When occurring as inclusions, it is commonly euhedral and exhibits concentric zoning. Zircon is short prismatic and is generally enclosed in feldspar and hornblende. Apatite occurs as fine-grained six sided fine grains generally included in feldspar, hornblende and quartz. In addition to these accessory minerals, titanite occurs in trace amounts.

7.3.1 Interpretation of Petrography

The mineralogical assemblage of the Chimoio Granodiorite Gneiss is dominated by plagioclase, K-feldspar , quartz and hornblende as indicated above. The occurrence of hornblende as a metamorphic mineral suggests metamorphism at medium grade amphibolite facies and the plot of this assemblage on an ACF diagram suggests that hornblende, biotite and plagioclase were in equilibrium.

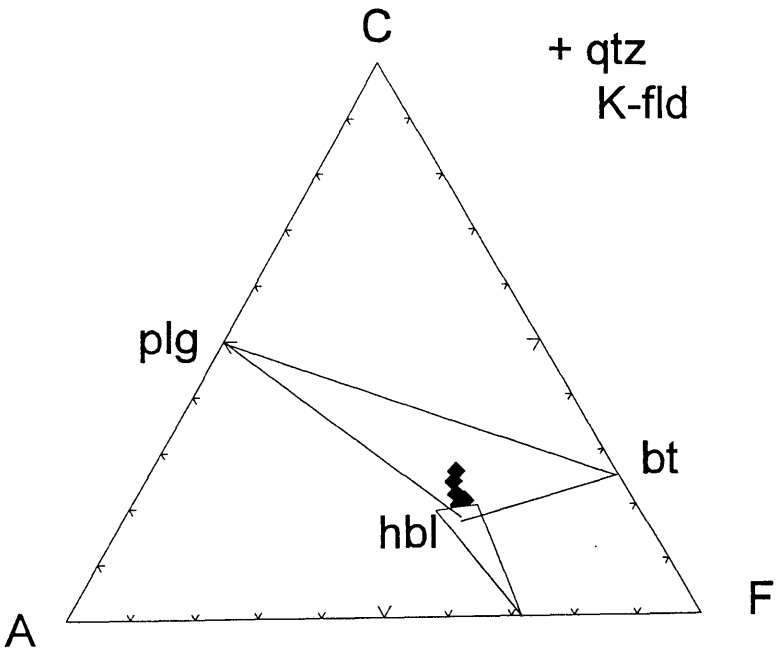

Figure 7.5: ACF diagram showing the equilibrium mineral assemblage of Chimoio Granodioritic Gneiss. Filled squares represent the chemical composition of the samples analysed. plg- Plagioclase, hbl- hornblende, bt- biotite, qtz- quartz and K-feldspar.

7.4 Chemistry

Six samples were analysed for the major and trace elements (Table 7.2) and two samples for the REE (Table 7.3). The same six samples were also subjected to a Rb/Sr isotope study.

7.4.1 Major Element Chemistry

The SiO_2 values do not vary greatly and the contents are intermediate. The samples have similar Al_2O_3 contents. FeO and MgO contents are low and typical of granitoid gneisses. CaO contents are generally greater than both K_2O and Na_2O contents which have similar values. These compositions taken as their equivalent minerals, namely anorthite, K-feldspar and albite, result in the Chimoio gneiss being a granodiorite (Fig. 7.6).

Table 7.2: Major and trace elements and composition A/CNK parameter of the Chimoio Granodioritic Gneiss.

sample	CVGNA	CVGNB	CVGNC	CVGND	CVGNE	CVGNF
SiO2	62.43	58.65	60.89	58.9	58.69	58.81
Al2O3	17.03	16.78	17.97	17.11	17.39	16.47
Fe2O3	2.40	3.20	2.39	3.13	2.94	3.02
FeO	3.22	4.63	3.02	4.42	4.08	4.11
MgO	2.15	2.86	2.12	2.69	2.61	2.68
CaO	4.37	5.82	4.06	5.29	5.34	5.41
Na2O	3.86	3.61	3.76	3.99	3.79	3.95
K2O	3.84	3.63	4.52	3.42	3.79	3.79
TiO2	0.68	0.96	0.72	0.88	0.93	0.92
P2O5	0.32	0.38	0.31	0.38	0.38	0.32
MnO	0.09	0.15	0.09	0.13	0.14	0.13
total	**100.39**	**100.67**	**99.85**	**100.34**	**100.08**	**99.61**
Ba	1851	1813	2016	1318	1685	1735
Li	31	23	32	31	24	24
Nb	10	13	9	13	13	13
Sc	12	17	10	17	14	15
Sr	871	938	820	720	881	913
Rb	104	78	121	95	81	81
Y	23	34	19	33	30	31
Ga	21	23	22	24	21	21
Al	9.02	8.89	9.52	9.06	9.21	8.72
Zr	189	243	177	164	319	245
Y/Nb	2.30	2.62	2.11	2.54	2.31	2.38
A/CNK	0.92	0.82	0.97	0.86	0.87	0.81

Calculation of the parameter Al_2O_3 / $CaO+Na_2O+K_2O$ (Table 7.2) shows that the Chimoio Graonodioritic Gneiss is metaluminous (A/CNK<1 Fig. 7.7). The FeO, MgO, K_2O and Na_2O contents result in the Chimoio Gneiss being typically calc-alkaline in character (Fig. 7.8). TiO_2 and P_2O_5 contents are typical of granitoid gneiss and average 0.9 wt% and 0.34 respectively. A plot of normative quartz (Q), alkali feldspar (A) and plagioclase (P) result in the Chimoio Gneiss being quartz-monzodiorite (Fig. 7.9).

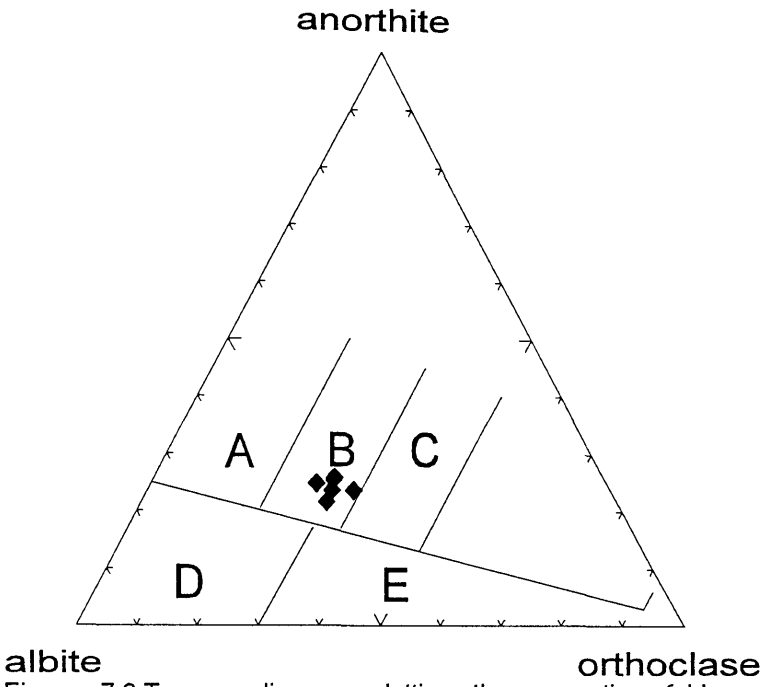

Figure 7.6:Ternary diagram plotting the normative feldspar composition of Chimoio Granodioritic Gneiss. A- tonalite; B- granodiorite; C- Adamelite; D- trondjemite; E- Granite (after Barker,1979).

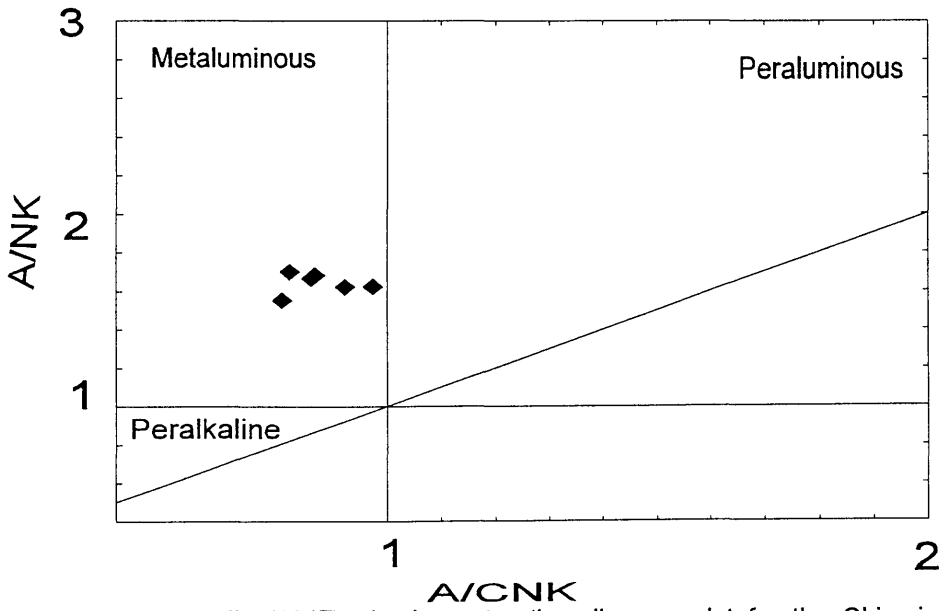

Figure 7.7: Shand's (1947) alumina-saturation diagram plot for the Chimoio Granodioritic Gneiss.

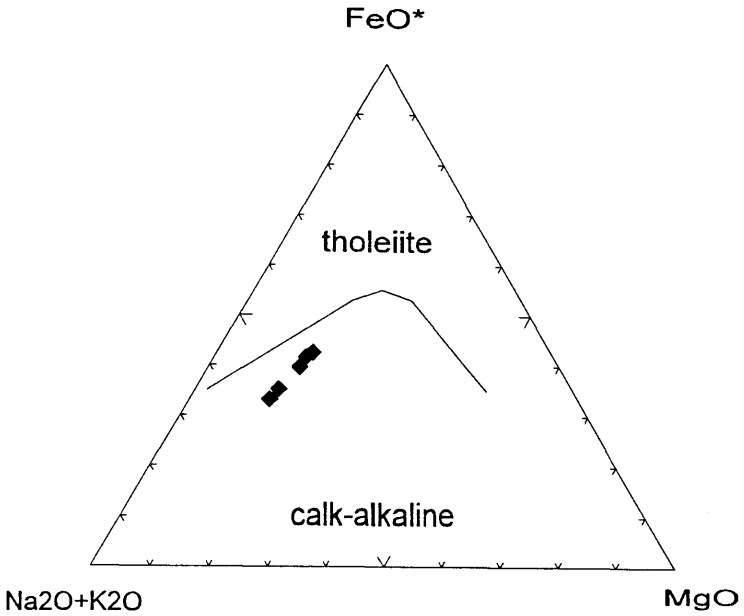

Figure 7.8: Plot of Chimoio gneiss samples into the Irvine and Baragar (1971) diagram for tholeiite and calc-alkaline fields.

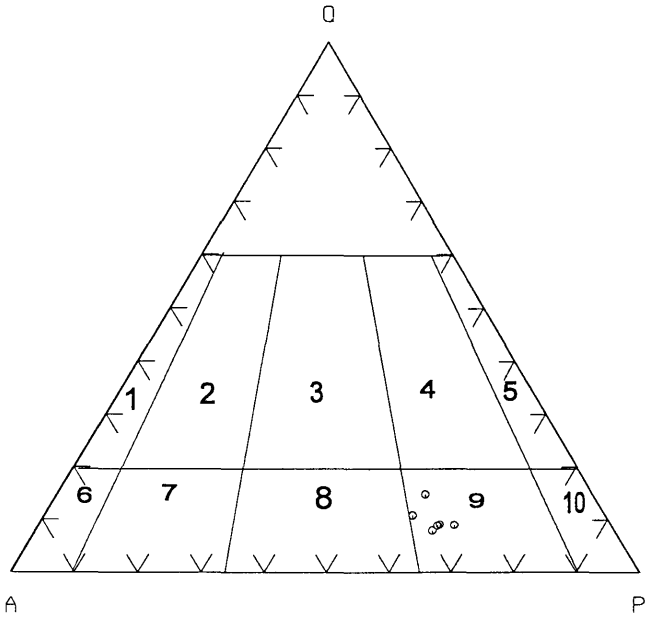

Figure 7.9: Ternary diagram plotting Alkali feldspar (A), plagioclase (P) and quartz (Q) parameters from Chimoio gneiss. Adapted from Streckeisen (1976). 1- alkali feldspar granite; 2- syenogranite; 3- monzogranite; 4- granodiorite; 5- tonalite; 6- quartz alkali feldspar syenite; 7-quartz syenite; 8- quartz monzonite; 9- quartz monzodiorite; 10- quartz diorite.

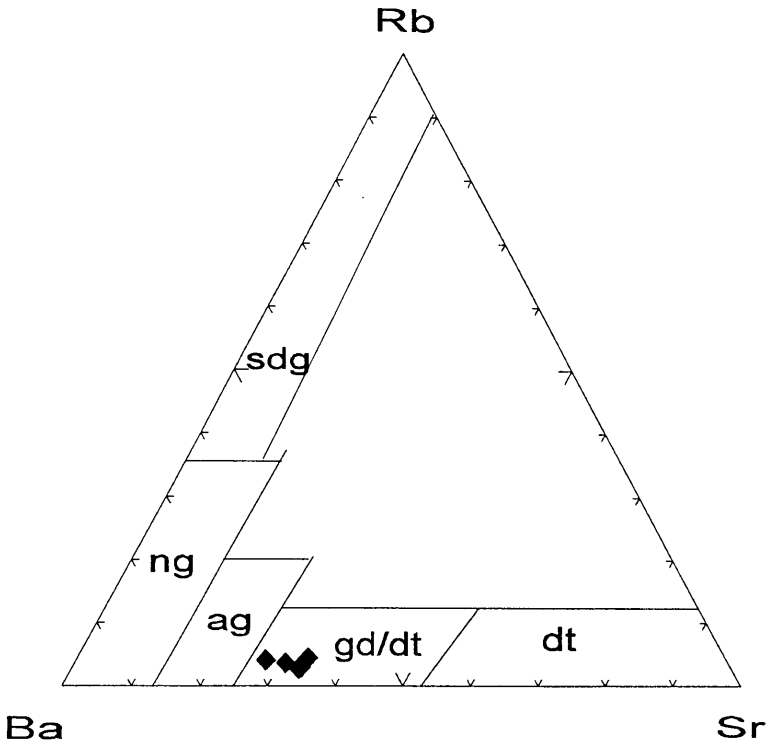

Figure 7.10: Plot of Chimoio Granodioritic Gneiss in the Rb-Ba-Sr diagram (after El Bouseily and El Sokkary (1975). Sdg- strongly differentiated granites; ng- normal granites; ag- anomalous granites; gd/dt- granodiorite and quartz diorite; dt- diorite.

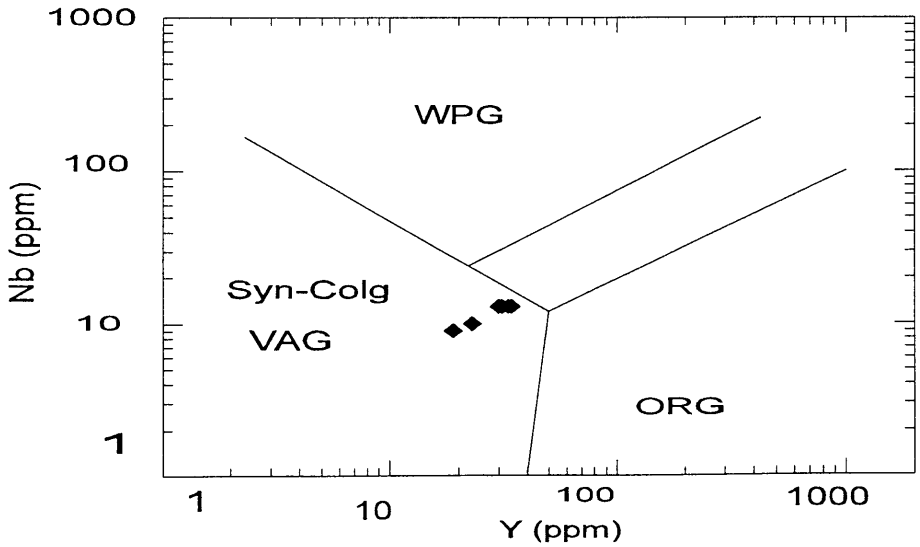

Figure 7.11: Chimoio Granodioritic Gneiss samples plotted into the discriminant diagram for the fields of Within-Plate (WPG), Syn-Collisional (Syn-Colg) and Volcanic - Arc (VAG) and Orogenic (ORG) granitoids (after Pearce *et al.*, 1984).

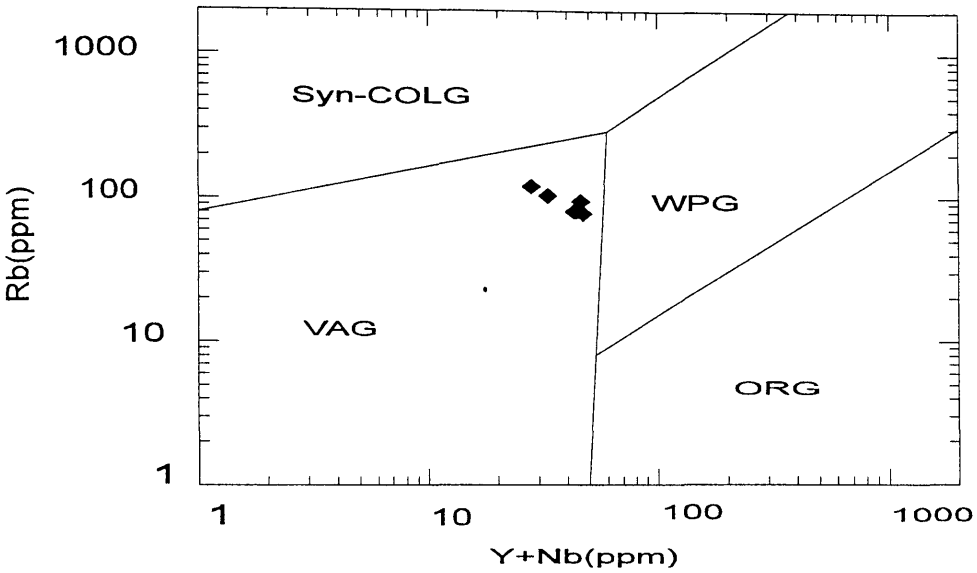

Figure 7.12: Chimoio Granodioritic Gneiss chemical data plotted into the discriminant diagram of Pearce *et al.* (1984). Abbreviation as in Figure 7.11.

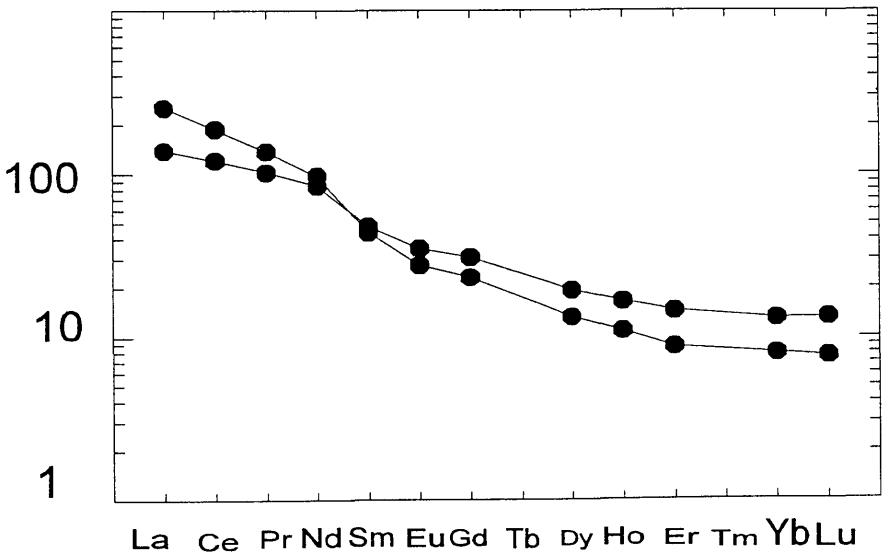

Figure 7.13: REE abundance variation diagram of two samples from Chimoio Granodioritic Gneiss. Normalizing values after Evensen *et al.* (1978).

7.4.2 Trace Element Chemistry

The samples have high Ba and Sr contents but Rb contents are relatively low, a characteristic consistent with the granodioritic nature of the Chimoio granitoids (Fig. 7.10). Sr/Rb ratios are typically 7-10:1 which is consistent with the high plagioclase contents of these gneisses. Zirconium contents are reasonably high and variable. Nb and Y contents are low, a characteristic which is typical of syn-collisional and or volcanic arc granitoids (Fig. 7.11). The Rb, Nb and Y characteristics are typical of volcanic- arc granitoids (Fig. 7.12).

7.4.3 REE Chemistry

The contents of the two samples analysed are shown in Table 7.3 and the chondrite-normalized profiles of samples cvgna and cvgnb are shown in Figure 7.13.

Table 7.3: REE composition of Chimoio Granodioritic Gneiss in ppm.

Sample	La	Ce	Pr	Nd	Sm	Eu	Gd	Dy	Ho	Er	Yb	Lu
CVGNA	62.13	119.9	13.2	46.41	6.78	1.61	4.73	3.37	0.61	1.44	1.27	0.19
CVGNB	33.96	77.34	9.86	40.21	7.41	2.03	6.29	4.9	0.93	2.4	2.08	0.33

The samples have high La_{cn}/Yb_{cn} ratios of about 10:1 resulting in relatively steep REE patterns. The patterns have negligible negative Eu anomalies suggesting that the feldspar fractionation has not played a significant role in the evolution of the gneisses and that plagioclase was not a significant phase in the restitic source of the granitoids.

7.5.4 Radiogenic Rb/Sr Isotope Chemistry

Data of Rb/Sr isotopic study are presented in Table 7.4.

Table 7.4: Radiogenic composition of Chimoio Granodioritic Gneiss.

sample	Rb	Sr	87Rb/86Sr	87Sr/86Sr
cvgna	104	871	0.3523	
cvgnb	78	938	0.2509	0.7105
cvgnc	121	820	0.4088	0.7125
cvgnd	95	720	0.3970	0.71307
cvgne	81	881	0.2694	0.71043
cvgnf	81	913	0.2651	0.7102

Regression of data from the 6 samples using GEODATE (Harmer and Eglington, 1987) using 1.00% and 0.03% errors for the X and Y values respectively yield an errorchron of 1322.22 ± 279 Ma (MSWD 4.995) with $^{87}Sr/^{86}S_i$=0.7054. Exclusion of sample cvgna from the calculation does not materially alter the age or the Ro but results in an isochron of 1236 ± 201Ma (MSWD = 2.221) with Ro=0.7056 (Fig. 7.14). This age places this gneiss between the Messica Granite Gneiss and the Nhansipfe Granitic Orthogneiss to the west.

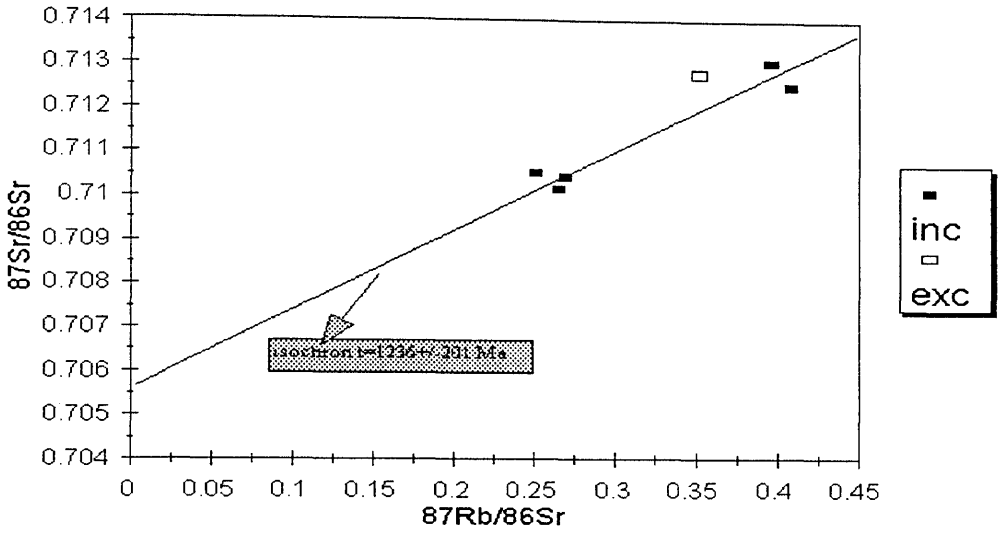

Figure 7.14:Diagram plotting isotopic data of the Chimoio Granodioritic Gneiss. inc indicates included data and exc indicates excluded data.

7.5 Discussion

In Figure 7.6, the Chimoio Granodioritic Gneiss chemical data plot in the field of granodiorite on the basis of feldspar proportions. In this diagram Na_2O, K_2O and CaO are taken as their equivalent minerals albite, orthoclase and anorthite. On the other hand when quartz is taken into account, the gneiss becomes a quartz-monzodiorite, confirming the lower SiO_2 and high CaO nature of this gneiss. Both classifications are acceptable but the granodiorite which is also confirmed by trace elements plot in Figure 7.10 is here preferred. Trace elements chemistry is typical of volcanic-arc granitoids (Fig. 7.12).

Chapter 8

NHANSIPFE GRANITIC ORTHOGNEISS

8.1 Introduction

The Nhansipfe Granitic Orthogneiss is exposed east of the Vanduzi Migmatite Gneiss and west of the Chimoio Granodioritic Gneiss (Fig. 2.1). Previous work did not differentiate this granite from the Messica Granite Gneiss. During the present study mineralogical and textural characteristics, on outcrop scale, enabled its distinction from the Messica Granite Gneiss. A Rb/Sr isotope study confirms the distinction and indicates that the Nhansipfe Granitic Orthogneiss is much younger.

8.2 Field Description

A common characteristic of the granitoids of this unit is the megacrystic size of feldspar crystals. The rock type is commonly an augen gneiss, locally with intercalations of quartzo-feldspathic partial melt bands and pegmatitic veins (Figs. 8.1 and 8.2). The mineralogy includes feldspar, quartz and garnet and biotite and hornblende in the felsic and mafic bands respectively. Garnet occurs as medium-grained aggregates and coarse isolated grains that are locally idioblastic, particularly within the felsic bands. Some feldspar grains, commonly the largest ones, are also idioblastic. The foliation is defined by the preferred orientation of biotite and is deformed around the coarse feldspars porphyroclasts and commonly includes NE-SW S_1 and an approximately N-S S_2 foliations (Fig. 8.3). At Matsinho, the gneiss is intensely folded(Fig. 8.4) and contains mafic fine-grained gneissic enclaves composed of plagioclase, pyroxene, hornblende, and garnet which suggests that the grantoids intruded a mafic rock.

Figure 8.1: Quartzo-feldspathic partial melt bands in the megacrystic Nhansipfe Granitic Orthogneiss.

Figure 8.2: Pegmatitic veins forming intercalated bands in the megacrystic Nhansipfe Granitic Orthogneiss.

Figure 8.3: S_1 and S_2 foliations in the megacrystic Nhansipfe Granitic Orthogneiss near Mombeza.

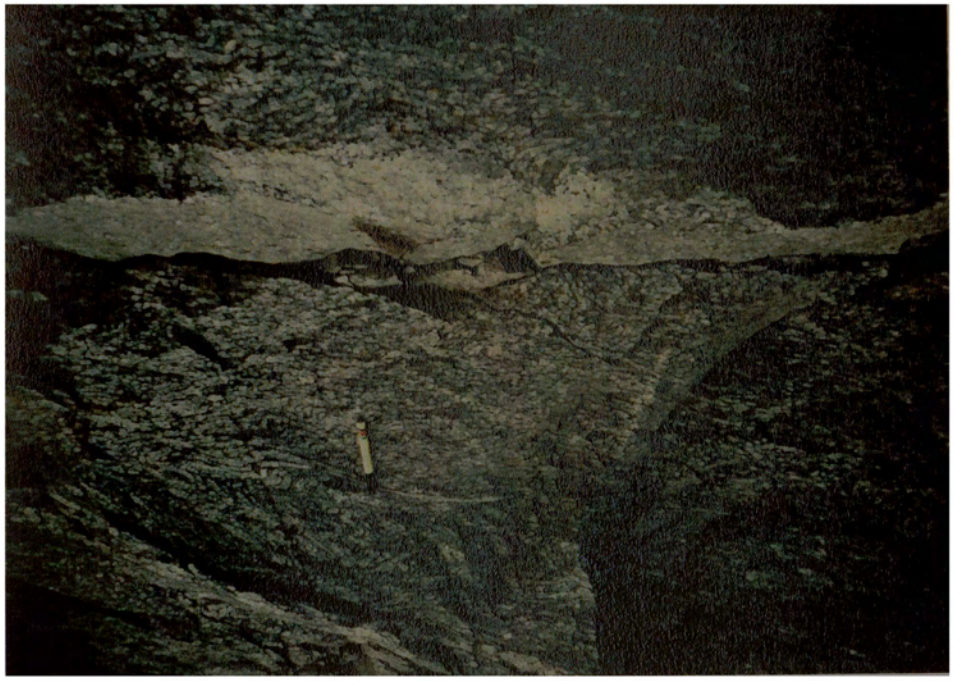

Figure 8.4: Folded foliation in the fine-grained light-coloured gneiss in Matsinho.

Figure 8.5: Folded felsic bands offset by subvertical faults in the megacrystic Nhansipfe Granitic Orthogneiss.

The megacrystic rock is folded, the folds being defined by the felsic bands which are locally offset by subvertical faults (Fig. 8.5). At Chibata, the gneiss contains mafic enclaves consisting of plagioclase, hornblende, pyroxene and garnet. These enclaves are massive fine-grained at the core but, at the contact with the gneiss, are foliated. The gneiss is sheared as indicated by feldspar stretching (Fig. 8.6) and mesoboudins in mafic enclave (Fig. 8.7). Feldspar porphyroclasts suggest a sinistral movement.

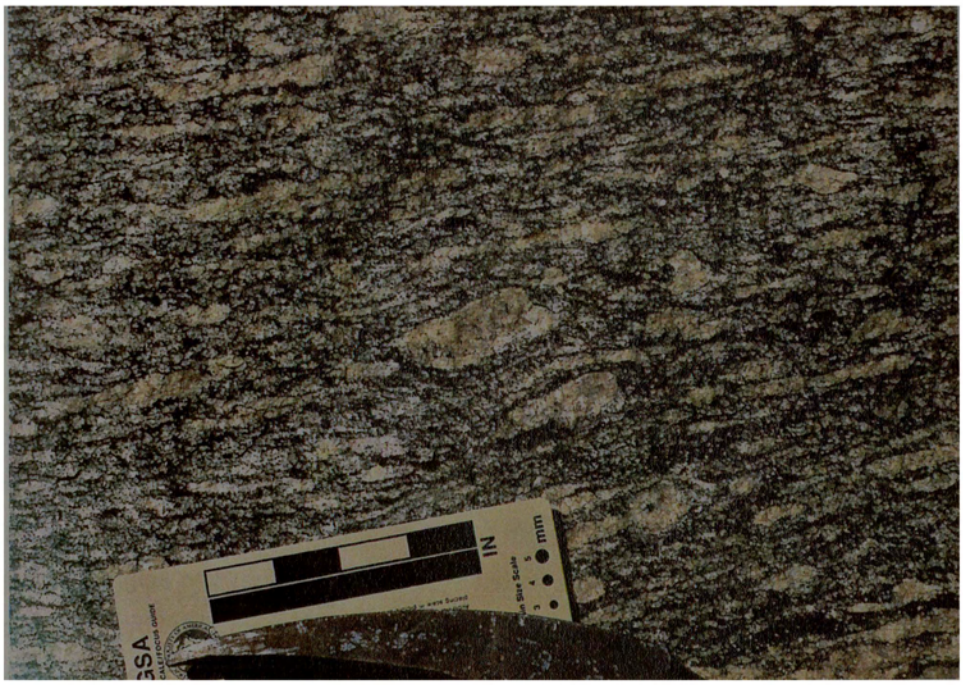

Figure 8.6: Sinistral feldspar porphyroclasts in the megacrystic gneiss near Chibata.

Figure 8.7: Mesoboudins in the mafic enclaves in the megacrystic gneiss near Chibata.

8.3 Petrography

The estimated modes of the minerals in this gneiss are shown in Table 8.1. The mineralogy is dominated by alkali and plagioclase feldspar and quartz. Biotite and hornblende occur in lesser amounts and garnet, titanite, zircon and opaque minerals are accessories. In the Nhansipfe (samples nfgn's) and Mombeza (samples mrgn and mggn's) localities, hornblende is absent. The opaque minerals occur in all samples but their proportions are higher in those samples enriched in ferromagnesian minerals. The rocks are generally inequigranular and are characterised by very coarse-grained feldspar(>3 cm). Samples from the Matsinho (samples mhgn's) and Chibata (samples pcy and grf) localities are fine- to medium-grained possibly due to grain-size reduction caused by deformation. The rocks are generally characterized by a planar fabric defined by the preferred orientation of biotite and/or hornblende. Alternating bands of felsic and mafic minerals, define compositional layering. The texture in the felsic bands is essentially coarse-grained granoblastic whereas within the mafic bands the texture is medium-grained lepidoblastic.

K-feldspar and plagioclase occur as coarse xenoblastic grains. Plagioclase grains are commonly zoned and contain inclusions of finer feldspar and quartz grains. Some are cracked and commonly contain fine grains of sericite and epidote. The coarse feldspars are deformed and elongated along foliation planes and locally form mosaics of non-zoned grains with granoblastic grain boundaries with interfacial angles of about 120°. Locally, the K-feldspar exhibits perthitic textures whereas plagioclase shows antiperthitic intergrowths. Quartz is anhedral and commonly contains inclusions of feldspar. Coarse grains of quartz have undulose extinction and are often partially recrystallised around their margins to fine-grained granoblastic mosaics thereby defining a mortar texture. Quartz is locally intergrown with plagioclase forming myrmekite which partially replaces microcline (Fig. 8.8). Hornblende forms anhedral grains and are generally cracked. The grains contain inclusions of quartz, zircon, titanite and opaque minerals. Some grains show preferred orientation and are deformed and oriented along foliation planes. Biotite occurs as aggregates or isolated flakes and is generally spatially associated with hornblende. In some samples, biotite is the only ferromagnesian phase but when hornblende is present they seem to occur in similar proportions. Biotite flakes exhibit preferred orientation along foliation planes (Fig. 8.9). Garnet is spatially associated with both felsic and ferromagnesian. It occurs as fine grains which are commonly idioblastic, particularly when filling cracks in both feldspar and hornblende. It is also present as coarse xenoblastic grains along grain boundaries or as inclusions in plagioclase and ferromagnesian minerals. Coarse garnet grains are commonly cracked and locally appear mantled by hornblende (Fig.8.10).

Table 8.1: Modal proportion of minerals in the Nhansipfe Granitic Orthogneiss.

sample	K-fld	Plg	Qtz	Hbl	Bt	Ms	Grt	Ttn	Zrn	Ap	Opm
nfgn1	27	34	28	-	10	-	-	-	tr	-	1
nfgn2	30	32	27	-	7	-	2	-	1	-	1
nfgn3	28	30	28	-	10	-	2		1	-	1
nfgn4	28	32	26	-	10	-	2	-	1	-	1
nfgn5	30	33	25	-	8	-	2	-	1	-	1
nfgn6	30	30	26	-	8	-	2	-	1	-	1
mggn1	27	30	28	-	8	-	4	-	1	-	2
mggn2	26	29	30	-	10	-	4		-	-	1
nggn2	30	28	30	-	8	1	2		-	-	1
ndgn1	30	28	30		8	1	3	-	-	-	-
nzgg1	30	30	28	4	6	-		-	1	-	1
nzgn2	28	32	28	4	5	-	-	1	1	-	1
nzgn3	30	30	28	5	5	-	-	-	1	-	1
mrgn	30	33	26	-	8	-	3	-	-	-	-
chgn	30	32	28	-	8	-	2	-	-	-	-
mhgn1	25	28	25	12	8	-	-	-	1	tr	1
mhgn2	23	30	25	10	10	-	-	tr	1	tr	1
mhgr	26	24	30	12	7	-	-	-	-	-	1
mhgn6	25	23	27	12	10	-	-	tr	1	-	2
agn1	30	35	25	4	5	-	-	-	-	tr	1
agn2	30	33	25	5	4	-	-	2	-	tr	1
agn3	28	32	24	8	6	-	-	1	-	-	1
agn4	30	34	25	5	2	-	-	2	-	-	2
agn5	25	30	28	8	2	-	-	2	tr	tr	3
agn6	28	30	28	6	3	-	-	2	-	-	3
pcy	30	30	32	3	1	-	-	tr	1	-	3
mcgr	27	30	28	12	8	-	-	-	tr	-	3

Plg-plagioclase, K-fld- potassium-feldspar, Qtz- quartz, Hbl- hornblende, Bt- biotite, Ms- muscovite, Grt-garnet, Ttn- titanite, Zrn- zircon, ap- apatite and Opm- opaque minerals; tr=trace.

Figure 8.8: Myrmekitic intergrowths in the Nhansipfe Granitic Orthogneiss. Minerals in the photo are microcline (cross-hatch twinning), plagioclase (dark grey) and quartz (yellowish white). Crossed nicols, width of field 3 mm.

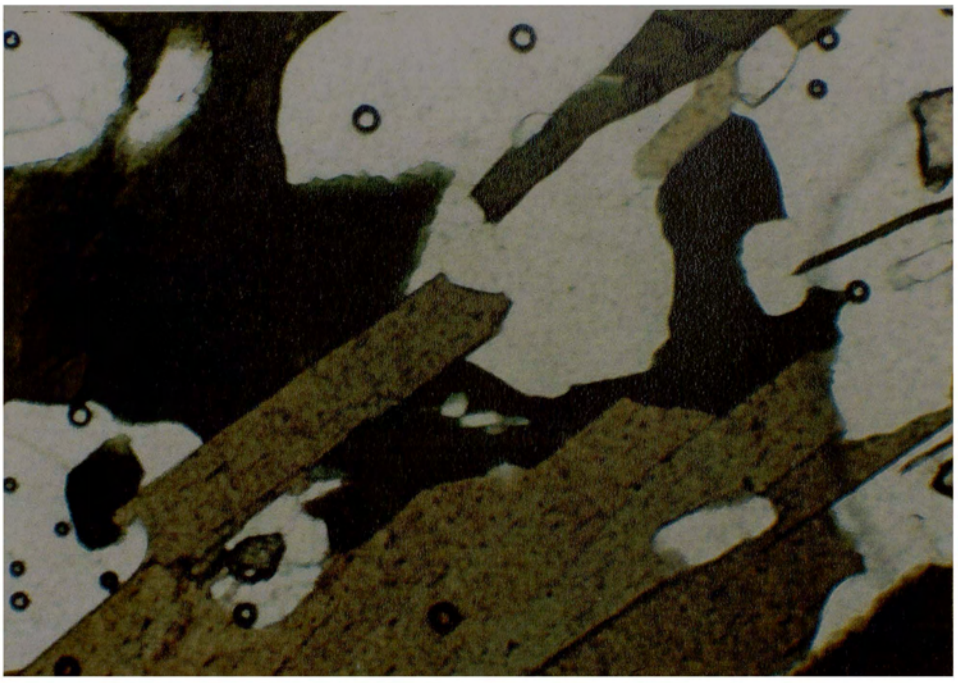

Figure 8.9: Biotite flakes forming planar foliation. Parallel light, width of field 3 mm. Circular spots are air bubles in the epoxy resin.

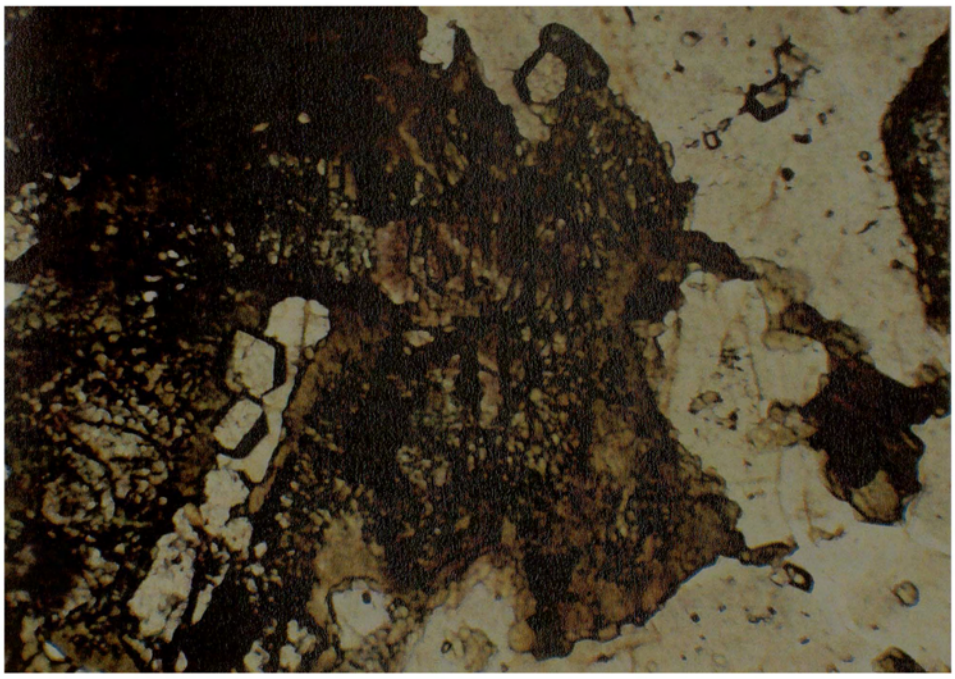

Figure 8.10: Hornblende (brown) mantled xenoblastic and cracked garnet and idioblastic garnet grains (high relief) along plagioclase cracks from the Nhansipfe granitoids. Parallel light, width of field 7 mm.

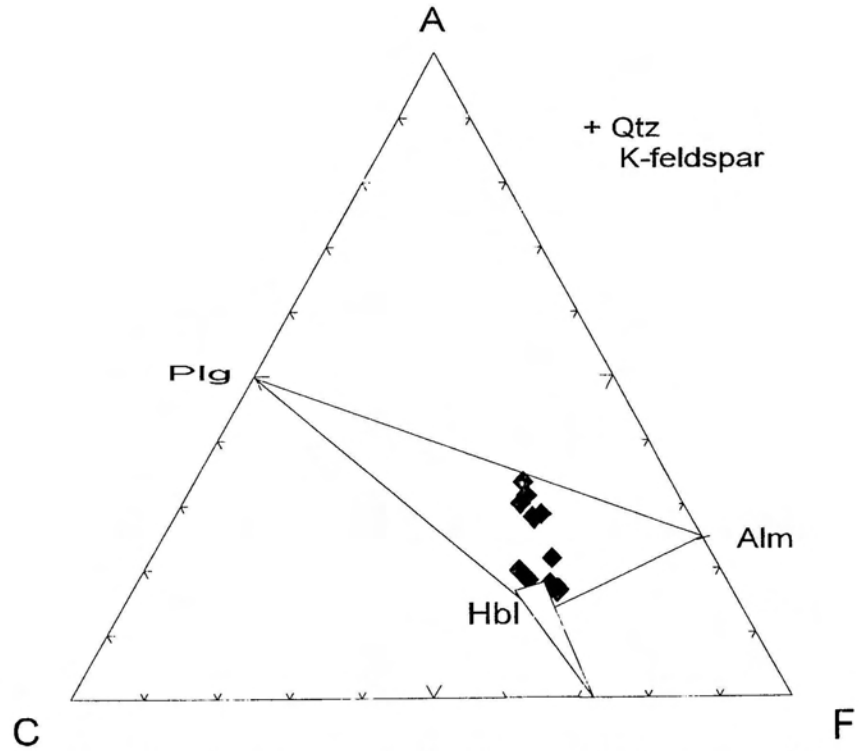

Figure 8.11: ACF diagram plotting the chemistry and showing the equilibrium mineral assemblage of medium-grade amphibolite facies of Nhansipfe Granitic Orthogneiss. Hbl- hornblende, Alm- almandine, Qtz- quartz, K-feldspar- potassium feldspar and Plg- plagioclase.

Titanite is a common accessory mineral in samples enriched with ferromagnesian minerals and is spatially associated with them as fine to coarse-grains. It is also associated with plagioclase. Coarse grains of titanite generally contain inclusions of felsic minerals. Zircon occurs as isolated prismatic grains as inclusions in both felsic and mafic minerals. Apatite is rare but occurs as hexagonal grains usually included in felsic minerals. Opaque minerals occur as sub- to anhedral grains in two ways, namely, as isolated and interstitial grains or grains associated with ferromagnesian minerals.

8.3.1 Interpretation of Petrography

Besides quartz and K-feldspar, the Nhansipfe Granitic Orthogneiss is characterised by the mineral assemblage of plagioclase±hornblende±garnet±biotite (Fig. 8.11). The co-existence of hornblende+garnet+plagioclase (composition ~An_{20}) is typical of medium grade or amphibolite facies metamorphism. The preservation of complex Carlsbad/albite polysynthectic twinning in plagioclase would support an igneous origin for the gneiss (Smith and Mackenzie, 1959). The perthitic textures in orthoclase and antiperthitic textures in plagioclase suggest that the rocks had been subjected to higher temperatures, and have cooled down sufficiently slowly to permit the development of these exsolution textures.

In Figure 8.10, xenoblastic garnet is mantled by hornblende which is in contact with plagioclase, suggesting that the hornblende is produced by a hydration reaction involving garnet and plagioclase. On the other hand, the idioblastic garnet grains could have been produced by a prograde metamorphic reaction involving plagioclase and hornblende. The fact that this garnet does not show any reaction texture, suggests that it was produced at a later stage than the xenoblastic garnet and consequently this would suggest three metamorphic episodes, namely (1) prograde metamorphism to medium-grade amphibolite facies producing garnet and hornblende, (2) retrograde (hydration) metamorphism (reaction of garnet to produce hornblende) and (3) prograde metamorphism (reaction of plagioclase and hornblende to produce the idiomorphic garnet grains).

8.4 Chemistry

8.4.1 Introduction

The major and trace element compositions of 15 analysed samples are shown in Table 8.2 . The rare earth element (REE) compositions of four samples and the Rb/Sr isotopic data are shown in Table 8.3 and 8.4 respectively.

Table 8.2: Major and trace element analyses of samples from the Nhansipfe Granitic Orthogneiss.

SAMPLE	NFGN1	NFGN2	NFGN3	NFGN4	NFGN5	NFGN6	AGN1	AGN3	NZGN	MHGN1	MHGN2	MHGN3	MHGN4	MHGN5	MHGN6
SiO_2	66.11	66.16	66.2	65.95	65.47	65.45	66.3	66.74	65.31	63.3	63.35	63.31	62.67	67.49	63.39
Al_2O_3	15.56	15.36	15.62	15.07	15.63	15.65	14.43	14.57	13.71	14.21	14.08	14.18	14.44	13.62	14.39
Fe_2O_3	2.03	2.28	1.92	2.26	2.17	2.13	2.48	2.34	2.80	3.46	3.54	3.40	3.38	2.67	3.39
FeO	2.88	3.26	2.93	3.38	2.91	3.12	3.00	2.90	4.14	4.82	4.69	4.69	4.70	3.31	4.57
MgO	1.18	1.37	1.28	1.46	1.34	1.32	1.08	1.11	1.26	1.49	1.58	1.47	1.47	0.98	1.54
CaO	2.69	2.83	2.78	3.11	2.87	3.13	3.19	3.27	3.2	3.86	4.15	3.75	3.9	2.88	3.81
Na_2O	2.78	2.98	2.76	3.00	2.98	2.94	3.40	3.44	2.85	3.45	3.77	3.54	3.49	3.26	3.66
K_2O	4.18	3.92	3.54	3.52	4.51	3.74	4.97	4.72	3.76	3.85	3.95	3.84	3.83	4.81	3.91
TiO_2	0.64	0.76	0.74	0.84	0.78	0.73	0.97	0.91	1.06	1.25	1.33	1.25	1.2	0.85	1.3
P_2O_5	0.21	0.27	0.24	0.27	0.26	0.25	0.25	0.24	0.28	0.33	0.34	0.33	0.3	0.21	0.34
MnO	0.06	0.06	0.04	0.05	0.04	0.06	0.1	0.1	0.11	0.14	0.16	0.15	0.14	0.11	0.16
total	98.32	99.25	98.05	98.91	98.96	98.52	100.17	100.34	98.48	100.16	100.94	99.91	99.52	100.19	100.46
Ba	1008	978	747	710	1080	1101	1991	1920	1523	1969	2317	2373	2033	2101	2404
Li	33	41	33	36	36	33	23	24	28	29	23	19	24	28	19
Nb	32	34	34	40	37	34	33	31	32	41	34	32	39	27	33
Sc	8	9	7	8	7	9	14	14	15	18	19	16	16	13	17
Sr	259	250	217	222	259	307	364	365	281	325	391	391	345	299	407
Rb	212	216	211	199	219	209	137	127	99	88	86	106	100	101	82
Y	38	27	22	37	24	27	87	81	81	81	74	69	85	72	72
Ga	23	21	24	24	22	24	21	20	22	22	21	22	23	20	23
Al	8	8	8	8	8	8	8	8	7	8	8	8	8	7	8
Zr	278	295	420	346	319	327	498	395	524	792	743	793	719	620	737

8.4.2 Major Element Chemistry.

The SiO_2 contents of the samples are typically acid (granitic). The samples are enriched in Al_2O_3 with contents and FeO_{total} contents are significantly greater than the MgO contents (~1-1.5wt%) resulting in high Fe/Mg ratios of ~5:1. CaO contents are low. Total alkali contents are >6 wt% with K_2O typically being >Na_2O. Calculation of the parameter $Al_2O_3/CaO+Na_2O+K_2O$ shows that the samples from Nhansipfe locality (nfgn's) are peraluminous (A/CNK >) whereas the remaining are metaluminous (A/CNK <1). The TiO_2 contents are high and vary between 0.64-1.33 wt%. The P_2O_5 contents vary between 0.2-0.3 wt%. Harker variation diagrams of CaO and FeO_{total} contents plotted against SiO_2 show that they decrease with increasing SiO_2 contents resulting in inverse or negative correlations (Fig. 8.12). Similarly TiO_2 and P_2O_5 show decreasing contents with increasing SiO_2 whereas K_2O increases with increasing SiO_2 (Fig. 8.13).

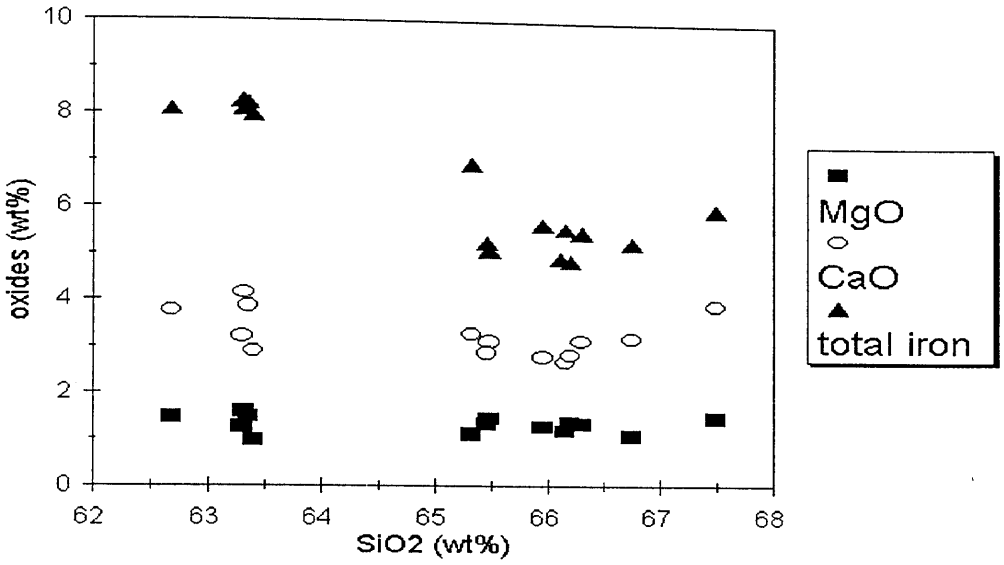

Figure 8.12: Harker variation diagram of MgO, CaO and total iron versus SiO_2 of samples from the Nhansipfe Granitic Gneiss.

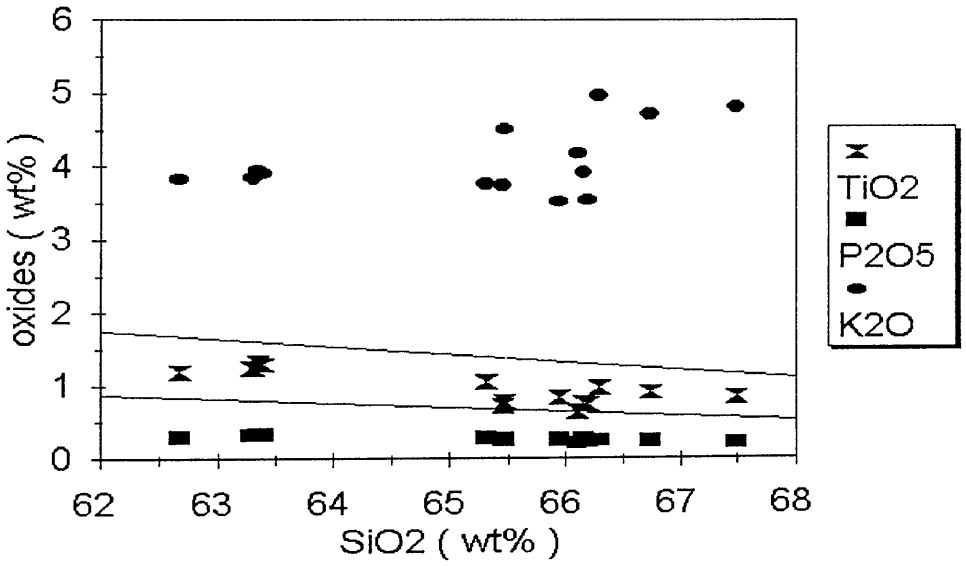

Figure 8.13: Harker variation diagram of TiO_2, P_2O_5 and K_2O vesus SiO_2 from Nhansipfe Granitic Gneiss. Shown are lines of 900 °C and 1000 °C (for 7.5 Kbar) drawn on the basis of TiO_2 contents according to Green and Pearson (1986).

Experimental work by Green and Pearson (1986) on the solubility of TiO_2 in magmas of varying compositions suggests the magma from which the Nhansife Granite originally crystallised was relatively hot, possibly of the order of 900°C. In Fig. 8.13 this is illustrated by lines of 900 °C and 1000 °C drawn on the basis of TiO_2 contents of the analysed samples, and a pressure of 7.5 kbar and according to experiments by Green and Pearson (1986). Similarly, application of saturation surface thermometry utilising the P_2O_5 contents in the samples and the calibration of the solubility of P_2O_5 in magmas of varying SiO_2 contents by Harrison and Watson (1984) suggests that the Nhansife Granite magma had a minimum temperature of ~950-1000 °C (Fig. 8.14) assuming that all the P_2O_5 is partitioned into apatite in stoichiometric proportions and that the apatite enrichment is not a result of crystal accumulation or xenocrystic incorporation. The crystal accumulation is discounted because of the similar contents in rocks of varying SiO_2 composition.

8.4.3 Trace Element Chemistry

The samples typically have high contents of Ba, Zr, Sr, Rb, Nb and Y. The high Zr contents can also be ascribed to high solubility of Zr in high temperature magmas. Zr saturation surface thermometry after Watson and Harrison (1983) indicates that the contents of Zr in the samples would require temperatures of ~800-950 °C (Fig. 8.14) assuming again that the high Zr contents are not the consequence of crystal accumulation or xenocrystic inclusion in the magma. Sr/Rb ratios are low resulting from the relatively high Rb contents, and do not show any systematic variation between ~1:1 and ~3:1. Similarly, the Y/Nb ratio is variable between ~1:1 and ~3:1. The Ba-Sr-Rb contents of the Nhansife gneisses are typical of anomalous granites (Fig. 8.15) suggesting that processes such as metasomatism might have affected the normal distribution of these elements (El Bouseilly and El Sokkary, 1975). The high Rb, Nb and Y contents are typical of within-plate granitoids (Pearce *et al*. 1984) (Fig. 8.16).

8.4.4 REE Chemistry

Four samples were analysed for the rare earth elements (REE) and their contents are shown in Table 8.3. The REE contents are high in Ce, Nd and La.

Table 8.3. Rare earth element analyses of the Nhansife Granitic Orthogneiss in ppm.

Sample	La	Ce	Pr	Nd	Sm	Eu	Gd	Dy	Ho	Er	Yb	Lu
NFGN1	75	147	16	55	8	1	6	6	1	2	2	0
NFGN2	69	136	15	53	8	1	6	5	1	2	2	0
MHGN1	65	150	20	81	15	4	14	13	2	6	6	1
MHGN2	72	154	19	78	14	4	12	11	2	5	5	1

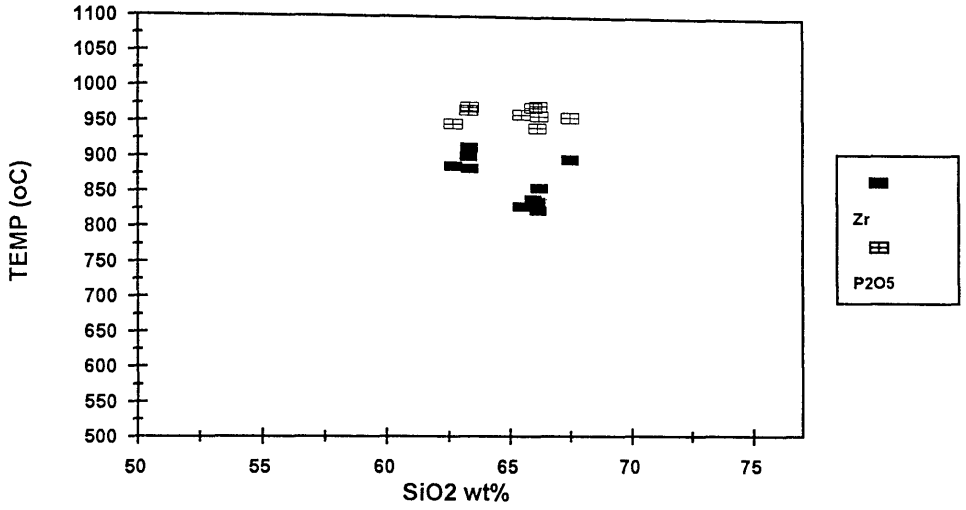

Figure 8.14: Saturation surface thermometry utilising the analysed P_2O_5 and Zr contents of the analysed samples and the solubility calibrations after Harrison and Watson (1984) and Watson and Harrison (1983).

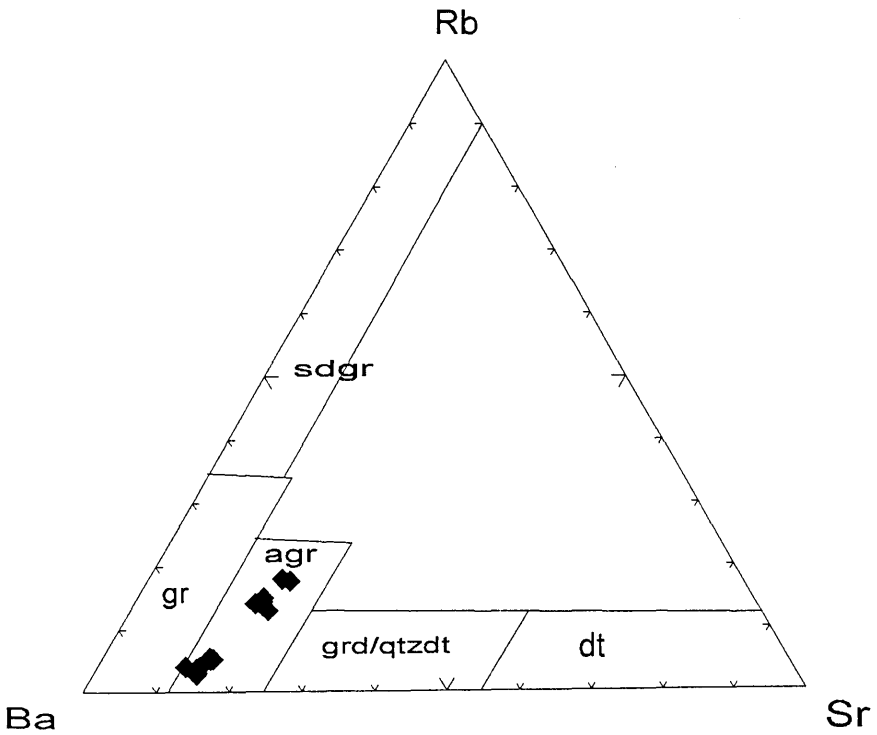

Figure 815: Chemical data plotting in the field of anomalous granites in the diagram after El Bouseily and El Sokkary (1975). Sdgr- strongly differentiated granites; gr- normal granites; agr- anomalous granites; grd- granodiorites; qtzdt- quartz diorites and dt- diorites.

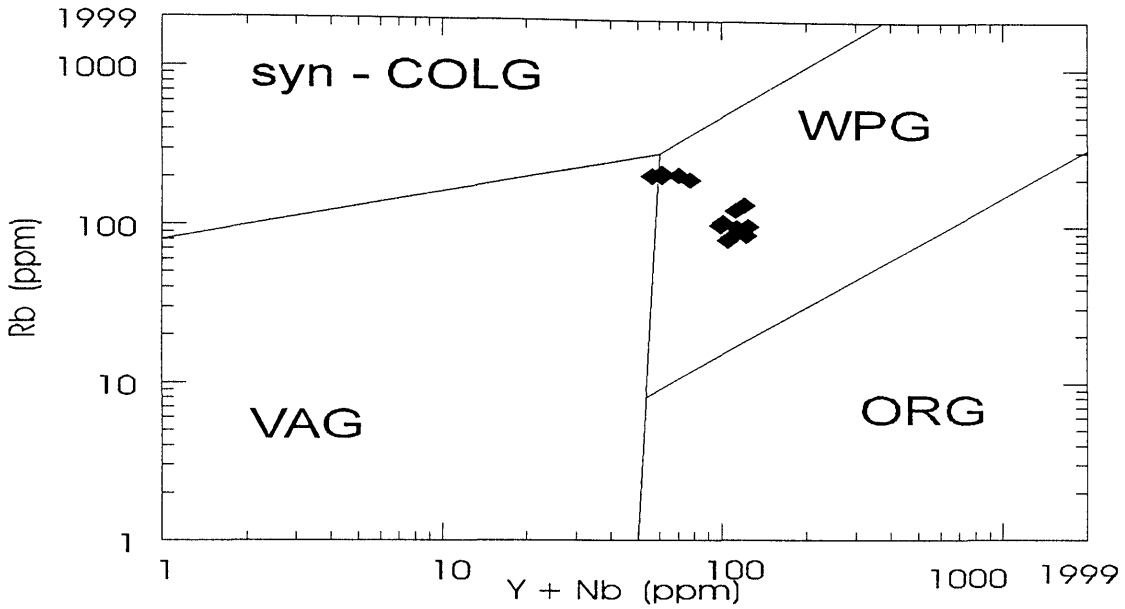

Figure 8.16:Tectonic discriminant diagram of Pearce *et al.* (1984) in which the chemical data of Nhansipfe Granitic Orthogneiss polt in the field of within-plate granitoids. Syn-COLG- syn-collision granites, VAG- volcanic-arc granites, ORG- orogenic granites, WPG- within-plate granites.

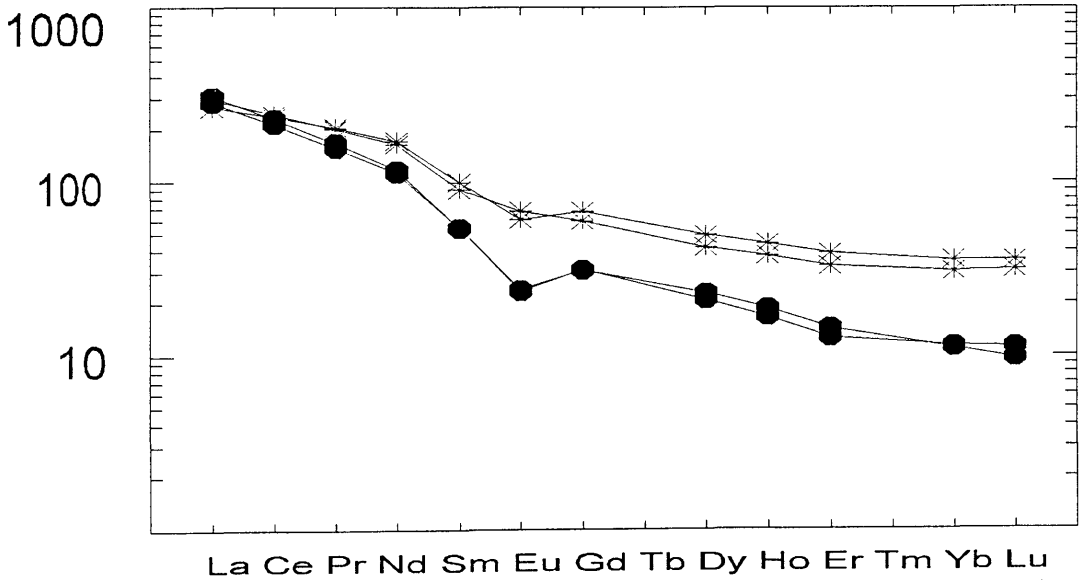

Figure 8.17: REE abundance variation diagram of the Nhansipfe Granitic Orthogneiss. Normalizing values are from Evensen *et al.* (1978) Filled boxes are samples from Nhansipfe and asterix from Matsinho localities respectively.

The conventional chondrite-normalised REE patterns for the 4 samples are shown in Figure 8.17. The REE patterns of the Nhansipfe Granitic Gneisses show a relative enrichment of the LREE relative to the HREE and are characterised by a weak to prominent negative Eu anomaly which is accentuated in the samples from the Nhansipfe locality. These negative Eu anomalies suggests either significant plagioclase feldspar in the restite or depletion of Eu from an evolving magma by fractional crystallization of plagioclase.

8.4.5 Radiogenic Rb/Sr isotope chemistry

A study of the Rb/Sr isotopes was conducted on the 6 samples labelled NFGN 1-6 (Table 8.4). Regression of the data from the 6 samples using the GEODATE (Harmer and Eglington, 1987) using 1% and 0.01% errors for the X and Y values respectively yields an errorchron of 969Ma ± 141 (MSWD 7.711) with R_o=0.7158. Exclusion of the data for sample nfgn2 from the calculation does not significantly alter the age or the R_o and results in an isochron of 981 Ma±83 Ma (MSWD=1.24) with R_o=0.7157 (Fig. 8.18). This age is clearly significantly different to that obtained for the Messica Granite Gneiss to the west.

Table 8.4. Rb/Sr trace element and isotope data from the Nhansife Granitic Gneiss.

sample	Rb(ppm)	Sr(ppm)	$^{87}Rb/^{86}Sr$	$^{87}Sr/^{86}Sr$
nfgn1	211.7	256	2.4023	0.7492
nfgn2	223.1	245.6	2.6392	0.7509
nfgn3	213	232.9	2.6576	0.7525
nfgn4	204.5	211.6	2.8092	0.7552
nfgn5	225.6	251.6	2.6057	0.7527
nfgn6	212.3	297.9	2.0694	0.7448

8.4.6 Discussion and Interpretation of Chemistry

The Nhansipfe granitoids are characterised by high abundance of alkalis, ∑FeO, Fe/Mg ratios and enrichment of Ga, Rb, Nb, Y, Zr, and REE (except Eu) and relatively lower contents of Al_2O_3, MgO, CaO and Sr. These characteristics are typical of A-type granitoids (Whalen, *et al.* 1987; Eby, 1990, 1992). These authors have further utilised various combinations of Zr, Nb, Ce, Y and Ga with CaO and Al_2O_3 to discriminate A-type granites and to subdivide these granites further. The (K_2O+Na_2O/CaO) versus (Zr+Nb+Ce+Y) diagram of Whalen *et al.* (1987) confirms the A-type nature of the granitoids in spite of the fact that Ce data are not available for all the samples (Fig. 8.19). A diagram plotting Zr versus Ga/Al is also considered a very good genetic discriminant for A-type granitoids rocks and has been used successfully by Whalen *et al.* (1987). Data form the present study plot in the field of A-type (Fig. 8. 20).

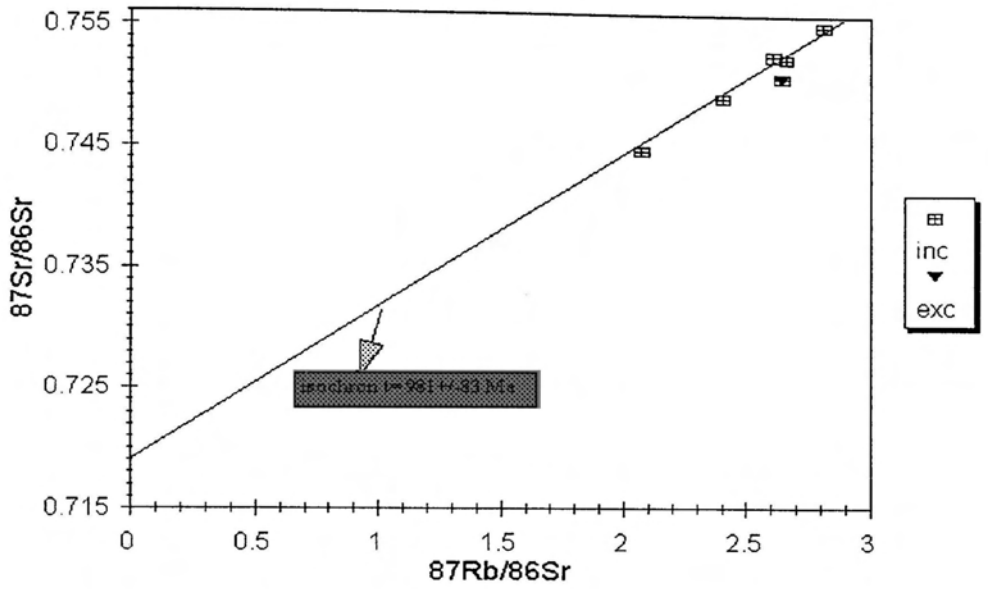

Figure 8.18: Diagram plotting radiogenic isotopic data of Nhansipfe Granitic Orthogneiss. Shown also is the isochon t=981±83 Ma. inc and exc stand for data included and excluded from the regression respectively.

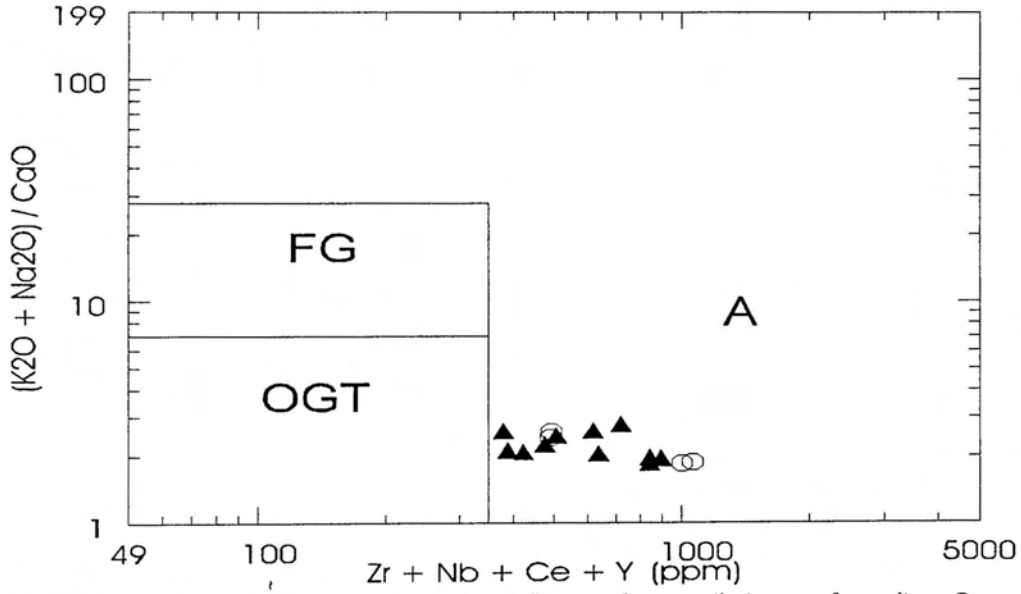

Figure 8.19: Whalen *et al.* (1987) discriminant diagram for genetic types of granites. Open circles represent samples that were analysed for REE including Ce. A- A-type granite field. FG- fractionated felsic granites and OGT- unfractionated orogenic granites.

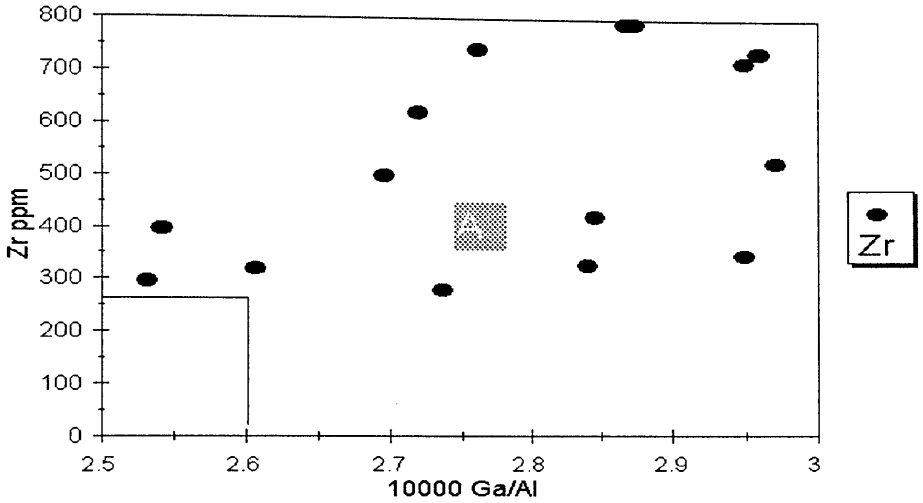

Figure 8.20: Whalen *et al.* (1987) Zr versus Ga/Al discriminant diagram of the Nhansipfe Granitic Orthogneiss plotting in the field of A- type granites (A).

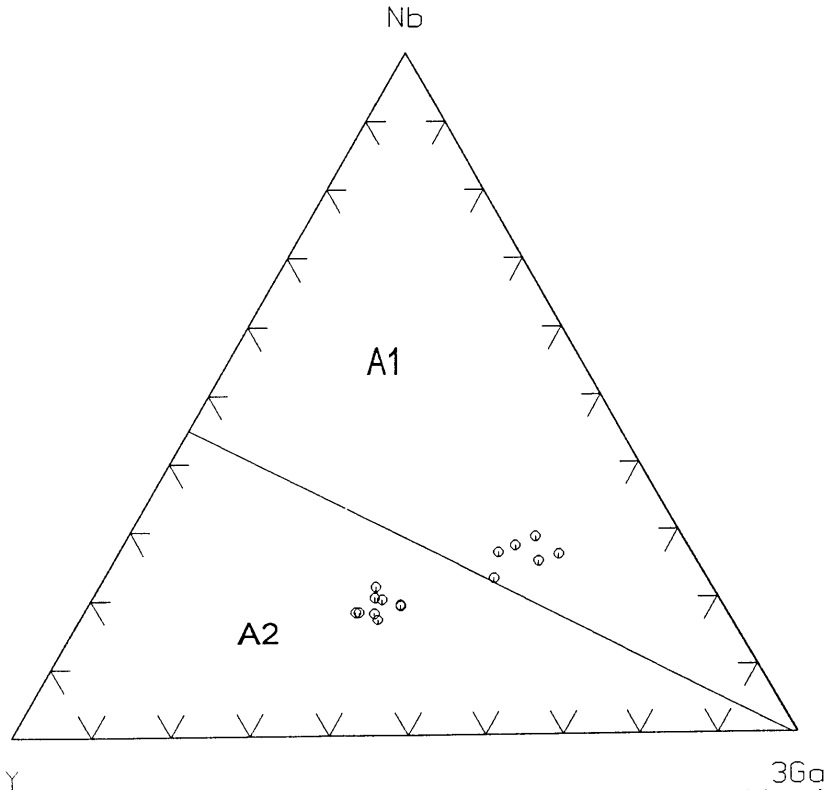

Figure 8.21: Discrimination of Nhansipfe Granitic Orthogneiss into A1 and A2 types granitoids (after Eby, 1992).

The discrimination of A-type granitoids using chemical criteria has been discussed by Eby (1990) who supported the criteria used by Whalen *et al.* (1987). He adds, however, that this discrimination is only reliable at SiO_2<65 wt% because at higher contents total alkali and CaO concentrations overlap. These parameters are largely met in this study. Eby (1992) further subdivided A-type granites into two groups, namely, A1, derived from sources chemically similar to those of oceanic island basalts, and A2 from sources similar to island arc or continental margin basalts (Eby, 1990, 1992). One way of assessing the existence of these two types of granites is the use of the incompatible elements Ga-Nb-Y discriminant diagram (Eby, 1992) which is shown in Figure 8.21 and in which the subdivision in A1 and A2 is evident. It must be emphasized that this triangular discriminant diagram can be used because the samples plot in the field of within-plate granite of Pearce *et al.* (1984) (Fig. 8.16) and in the A-type granitoids field in the Ga/Al diagram of Whalen *et al.*(1987) (Fig. 20) as required by Eby (1992).

A-type granitoids commonly have been perceived as being anorogenic, i.e., formed from magmatic processes unrelated to any orogen (eg. Pearce *et al.*, 1984). This concept has been critically challenged in recent times. For instance, Eby (1990) stated that A-type granitoids occur in within-plates or in plate margins during terminal stages of subduction-related orogeny. More recently, Windley (1993) discussed the problem related with anorogenic magmatism and suggests that a better understanding of this process can only be achieved if anorogenic magmatism is investigated in association with a local orogen.

The Nhansipfe Granitic Orthogneiss occurs within an area which includes the Proterozoic Chimoio Granodioritic Gneiss which plots in the volcanic-arc granites (VAG) field in the discriminant diagram of Pearce *et al.* (1984). It is, therefore, suggested that the Nhansipfe Granitic Orthogneiss has been formed from partial melting of a crust associated with/or produced during subduction related processes which are typical of a volcanic-arc tectonic environment.

Chapter 9

MAFIC INTRUSIONS

9.1 Introduction

These are intrusive into the Archaean Manica Greenstone Belt and Vumba Granite Gneiss in the west, and the Early and Late Proterozoic Messica Granite Gneiss and Nhansipfe Granitic Orthogneiss in the east respectively. Those in the E commonly form dykes (Fig. 2.1). The intrusions forming dykes in both E and W areas are oriented ~N-S and are, therefore, considered to be coeval. The N-S orientation is similar to the Umkondo Group sills in SE Zimbabwe which are dated at ~1080 Ma old (Allsop *et al.*, 1989). The lack of a strong deformational fabric, typical of the Mozambique Metamorphic Province, in the mafic rocks of the study area suggests that these might not be that old. This assessment could find some support from Pinna *et al.*(1986) who indicated an age of between ~500-~1100 Ma for some post-Umkondo mafic intrusions.

9.2 Field Description

The mafic rocks are intrusive into both the Archaean Zimbabwe Craton and the Proterozoic Mozambique Metamorphic Province, occurring mostly as dykes in the latter (Fig. 2.1). They vary from gabbros to dolerites and have a similar mineralogical composition characterized by white plagioclase, greenish and stubby clinopyroxene grains and black short prismatic to acicular amphibole grains. They are commonly chloritized, suggesting metamorphism under greenschist facies conditions, and are inequigranular medium-grained. Mafic intrusions within the Mozambique Metamorphic Province, unlike those within the Craton, commonly occur as dykes with N-S orientations and intrude both the granitoids and the metasediments. They are represented by amphibolitic dolerites. They were studied in Garuzo, Chicamba, Mombeza and Vanduzi areas (Figure 2.2). Mineralogically two groups are distinguishable, namely, one in which the mineral assemblage, is dominated by plagioclase, hornblende, pyroxene, quartz, and garnet, and which has a granoblastic metamorphic texture and another group which is characterized by the absence of garnet and relict igneous textures. The former occurs E of the Messica area and the latter to the west. The amphibolites occur as dykes of fine- to medium-grained rocks in the Garuzo, Chicamba, Vanduzi and Mombeza areas (Figure2.2). The foliation in the amphibolite is defined by the preferred orientation of inequant minerals that include hornblende and deformed plagioclase and quartz. Migmatization in amphibolite also took place as is shown in Figure 9.1 in which the migmatization is indicated by planar quartzo-feldspathic leucosomes in an amphibolite dyke intruding a porphyritic foliated granite. The fact that the partial melt patches are parallel to the N-S foliation suggests their development during the second phase of deformation (the first produced a E-W foliation and predates the amphibolite intrusion).

Figure 9.1: Patches of partial melts in the amphibolite intruding a megacrystic granite.

9.3 Petrography

The mineralogy of these rocks is shown in Table 9.1. Two groups of rocks are represented, namely, one with typical igneous ophitic texture and another with metamorphic granoblastic textures.

Table 9.1: Mineral assemblage of mafic rocks. Numbers represent mineral proportions.

sample	Plg	Amp	Cpx	Opx	Qtz	Grt	Chl	Ep	Ttn	Opm	texture
18S	45	40	7	-	-	-	2	1	1	4	igneous
MDo	45	42	5	-	-	-	5	1	-	2	igneous
15M	37	39	15	-	-	-	3	1	-	5	igneous
12T	52	10	30	-	-	-	1	1	1	5	igneous
maamp1	20	60	10	-	1	5	-	-	2	2	metam
maamp	25	56	8	-	1	5	-	-	2	2	metam
maamp2	15	75	1	-	1	-	-	-	5	3	metam
amp*	18	65	8	-	-	-	-	-	8	1	metam
mramp	45	35	4	1	2	8	-	-	3	2	metam
chm	33	62	-	-	2	-	-	-	1	2	metam
mbamp	34	44	8	2	2	5	-	-	3	2	metam

Plg- plagioclase, Amp- amphibole, Cpx- clinopyroxene, Opx- Orthopyroxene, Qtz- quartz, Grt- garnet, Chl- chlorite, Ep- epidote, Ttn- titanite and Opm- opaque minerals; metam- metamorphic.

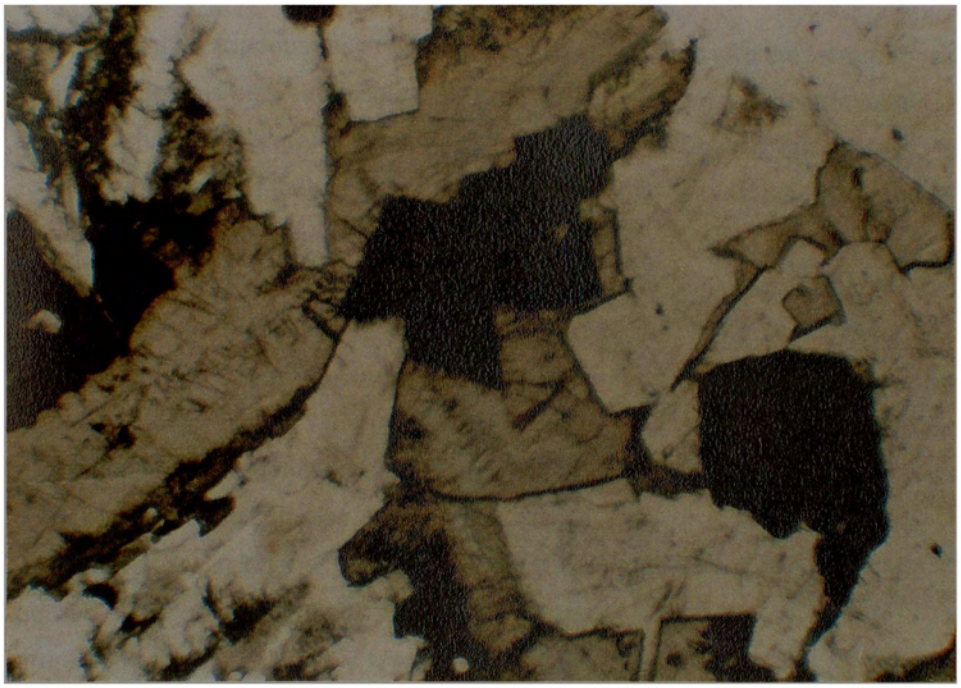

Figure 9.2: Clinopyroxene (brown), plagioclase (white), chlorite (greenish), amphibole (green, top left) and opaque minerals (black) of the igneous mafic rocks. Parallel light, width of field 7 mm.

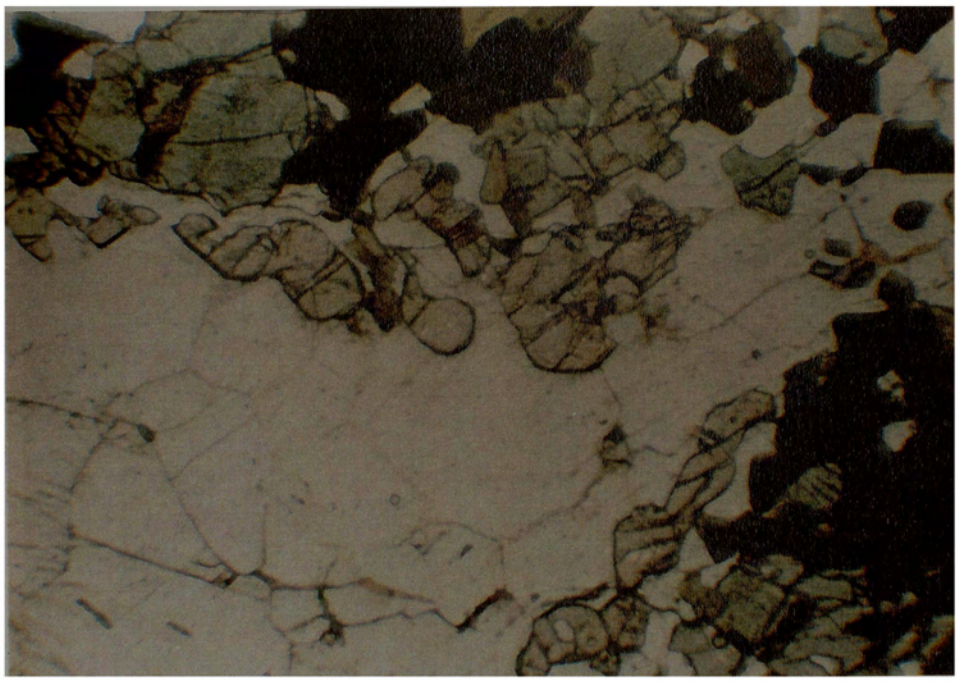

Figure 9.3: Granoblastic-polygonal texture showing plagioclase (white) with 120° triple junctions, adjoining amphibole (green) and xenoblastic garnet (light brown, included in plagioclase) and opaque minerals (black). Parallel light, width of field 7 mm.

In general the igneous rocks are fine- to medium-grained with the ferromagnesian minerals occupying spaces between plagioclase grains (Fig. 9.2) whereas the dominant texture in the metamorphic rocks is granoblastic because of textural re-equilibration (Shelley, 1993, p. 104) (Fig. 9.3).

The mineralogy of these mafic rocks is dominated by plagioclase and amphibole whereas garnet occurs in the metamorphosed equivalents.

The samples are characterized by saussuritization of plagioclase, and chloritization and uralitization of clinopyroxene. Plagioclase is commonly zoned and either represents magmatic disequilibrium during emplacement or disequilibrium during partial metamorphic hydration. The dominant amphibole is actinolite in the rocks with igneous textures and hornblende in the metamorphic rocks whereas pyroxene is represented by clinopyroxene. Small proportions of orthopyroxene and quartz occur in some metamorphic samples.

In samples with igneous textures plagioclase is saussuritized, sericitized and contains inclusions of garnet. Amphibole occurs as idiomorphic to lobate xenomorphic and needle-like grains, some of which are altered to chlorite and enclose grains of plagioclase, epidote and opaque minerals. Pyroxene occurs as euhedral to subhedral grains which commonly show zoning, weak pleochroism and simple twinning. At the grain boundaries some grains are altered to chlorite (Fig. 9.2). Locally it contains small inclusions of plagioclase and appears also as relict grains in rocks where the predominant ferromagnesian mineral is amphibole. Epidote is a minor, but important component and is generally associated with plagioclase in which it occurs as inclusions, as an alteration product. Titanite and opaque minerals accessories and are commonly associated with ferromagnesian silicates.

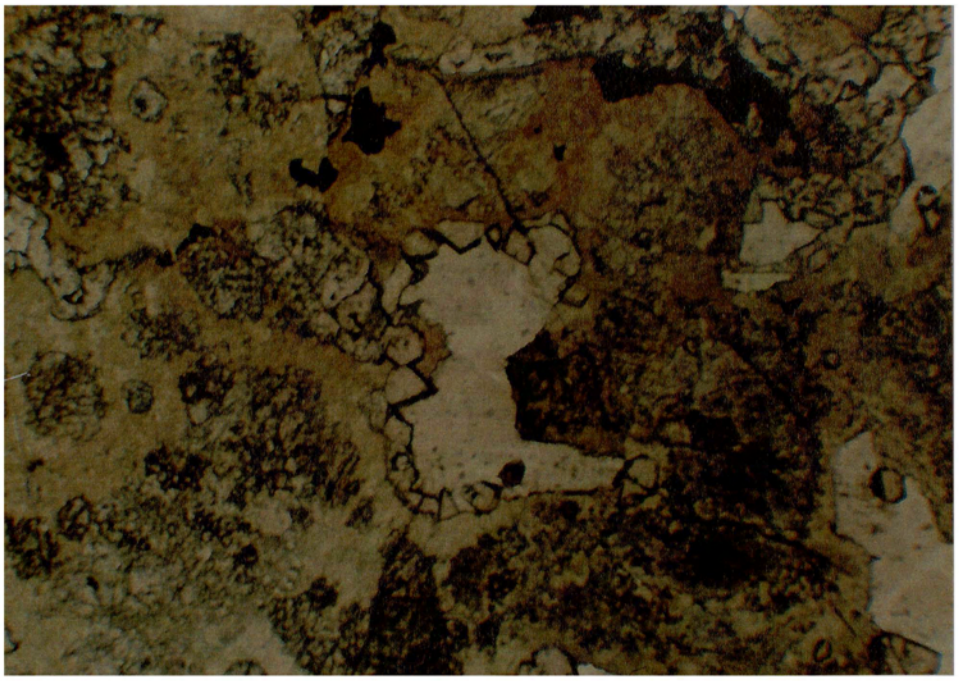

Figure 9.4: Idioblastic fine grained garnet (high relief) associated with both plagioclase (white) and amphibole (green) in the metamorphosed mafic rocks. Parallel light, width of field 7 mm.

Figure 9.5: Xenoblastic grains of garnet with symplectitic inclusions of plagioclase. Parallel light width of field 3 mm.

In the metamorphic rocks plagioclase occurs as sub-idiomorphic rectangular and equant grains exhibiting typical plagioclase twinning. In general the laths are fresh in appearance whereas the equant grains are locally saussuritized, sericitized cracked and filled with inclusions. Amphibole occurs as large grains with irregular faces enclosing finer grains of plagioclase as well as quartz or as equant grains normally showing granoblastic texture. Locally amphibole is altered to chlorite. Clinopyroxene is commonly weakly pleochroic and occurs as brown to reddish brown equant anhedral grains. Rare orthopyroxene is brown, pleochroic and exhibits straight extinction. Garnet occurs as fine-grained idiomorphic grains, commonly associated with plagioclase and amphibole and as coarser xenoblastic grains which contain inclusions of fine plagioclase and, rarely, amphibole and pyroxene grains (Figs. 9.4 and 9.5). Quartz is strained and shows a polygonal texture. Biotite occurs as flakes exhibiting the typical biotite pleochroism. Titanite occurs as irregular aggregates of very fine grains, generally associated with ferromagnesian minerals. Opaque minerals occur as grains with irregular faces commonly associated with the ferromagnesian minerals and titanite which they locally replace.

9.3.1 Interpretation of Petrography

The mineralogy of the samples analysed is typical of mafic rocks (Fig. 9.6).
The mineralogy of samples taken in the west consists of plagioclase±clinopyroxene±amphibole (actinolite)±chlorite±epidote±titanite. This assemblage is typical of basic rocks which have been subjected to low grade metamorphism (Bucher and Frey, 1994, p. 263, 273) (Fig. 9.6.II). In contrast the samples taken further east are characterised by the absence of epidote and actinolite and the presence

of garnet and in some samples, orthopyroxene. The resultant mineral assemblage is typical of basic rocks that have been subjected to medium- to high-grade metamorphism (Bucher and Frey, 1994, p. 263, 278-279) (Fig. 9.6). The occurrence of the common granoblastic texture suggests that the rocks have been recrystallized which is consistent with the medium grade metamorphism.

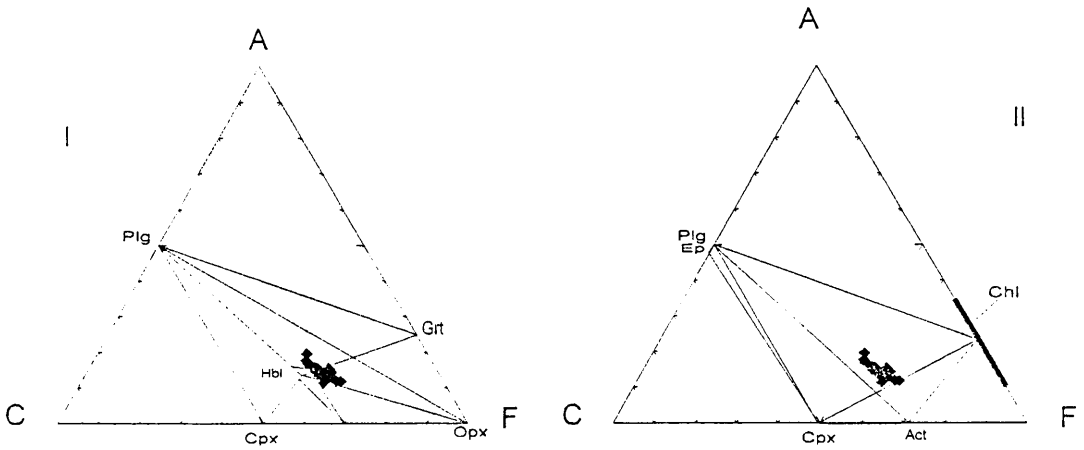

Figure 9.6: ACF diagrams plotting the chemistry and mineralogical assemblages of mafic intrusions. The plotted chemistry is the same in both diagrams. The diagram I shows the mineralogy of high grade metamorphic rocks from the east whereas the diagram II shows mineralogy of the mafic rocks with igneous texture from west.

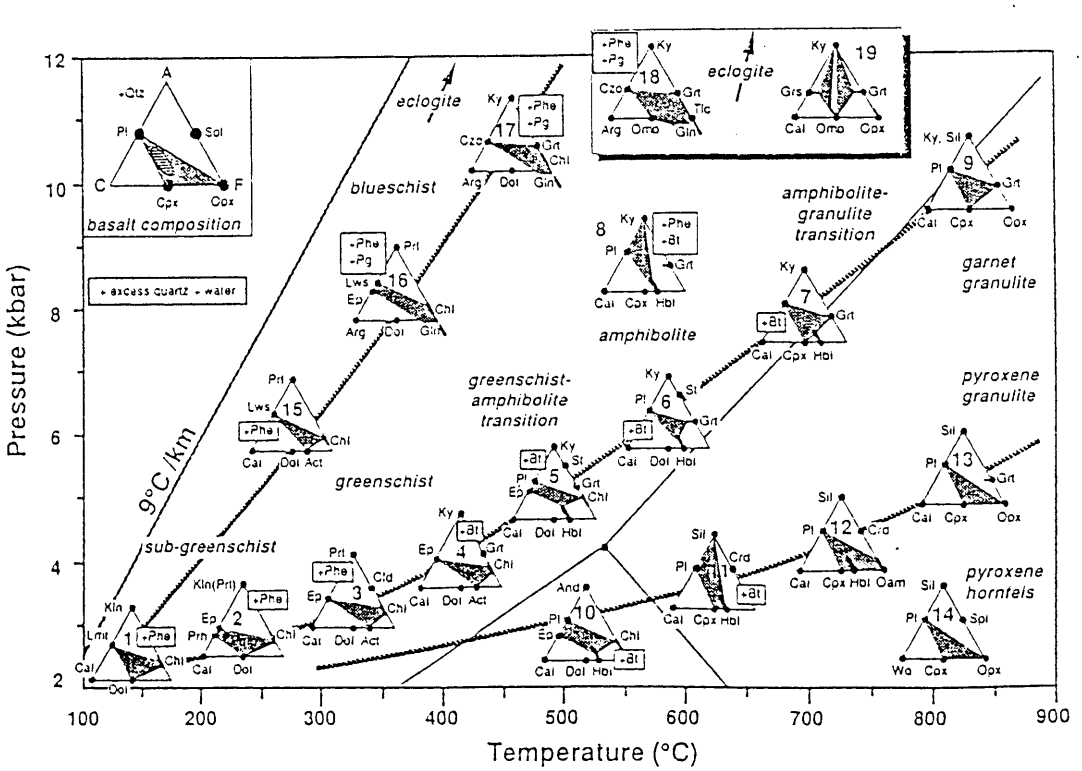

Figure 9.7: Metamorphism of basic rocks represented by the chemographies which are presented as ACF diagrams (after Bucher and Frey, 1994).

Comparing the assemblages of the samples with those from Figure 9.7, it can be seen that the metamorphic grade in the samples increases from chemography 5 (Fig.9.7) in the west, through chemography 6, 7 to one intermediate between chemographies 9 and 13 in the east. The latter chemographies are consistent with the partial melting of a mafic dyke in the east (Figure 9.1). The variation in P-T between chemographies 5 and a point between chemographies 9 and 13 suggests an increase in T from W to E of ~500 °C to ~750 to 800 °C and an increase in P of ~5 to 8 kbar and hence a metamorphic gradient of ~30 °C/Km.

9.4 Chemistry

The geochemical data discussed here are derived from the present study as well as from Manuel (1992). Most of the rocks from Manuel (1992) were described by him as metabasites. The chemical composition of all samples is shown on Table 9.2.

Table 9.2: Chemical composition of mafic intrusions.

SAMP	15M	12T	MDO	18S	MAMP2	MAAMP	MAMP1	99	116	58	158	144	39	233	23	239	38	93	129	6	2
SiO_2	48.89	48.81	48.88	49.44	49.24	50.03	49.16	50.65	51.1	48.08	48.08	50.6	55.46	49.26	51.53	51.46	54.06	50.95	51.59	50.3	50.8
A_2O_3	12.92	15.08	14.07	12.99	13.5	11.69	13.57	13.99	13.66	12.64	14.46	13.81	14.48	12.46	13.52	13.06	14.48	14.06	12.76	13.72	13.2
Fe_2O_3	5.61	5.50	3.26	3.94	3.64	3.87	4.12	4.64	6.19	5.65	4.16	5.52	3.81	6.28	6.13	5.22	3.86	4.29	5.11	4.72	6.0
FeO	12.44	11.79	9.18	10.14	10.19	11.09	11.25	9.33	10.50	10.89	8.29	9.70	6.92	11.38	10.46	9.93	6.75	8.37	10.23	9.22	10.2
MgO	4.69	3.55	8.37	6.65	9.04	8.74	7.66	5.27	3.98	5.34	5.85	4.52	5.83	5.21	3.97	5.92	5.91	7.06	5.49	6.56	3.9
CaO	8.45	8.45	11.02	10.4	10.83	11.87	10.35	10.69	8.26	9.59	10.29	9.41	9.48	8.96	8.26	10.07	9.71	10.56	10.62	9.07	8.6
Na_2O	2.85	3.08	1.68	2.55	2.01	1.86	2.28	2.06	2.69	2.38	2.26	2.55	1.18	2.56	2.62	2.18	1.86	2.19	1.96	2.46	2.6
K_2O	1.31	1.36	0.67	0.44	0.37	0.3	0.29	0.18	1.22	0.78	0.55	1.08	1.19	1.02	1.16	0.48	1.16	0.31	0.15	0.15	1.3
TiO_2	2.24	2.43	0.85	1.81	1.09	1.16	1.3	1.48	2.11	3.16	1.64	1.8	0.77	2.2	2.15	1.31	0.76	1.04	1.36	1.57	2.0
P_2O_5	0.31	0.3	0.06	0.21	0.22	0.08	0.11	0.16	0.26	0.31	0.17	0.22	0.08	0.2	0.22	0.11	0.09	0.09	0.11	0.13	0.2
MnO	0.23	0.22	0.2	0.2	0.22	0.21	0.2	0.2	0.22	0.22	0.19	0.21	0.17	0.24	0.2	0.22	0.17	0.19	0.23	0.19	0.2
total	**99.94**	**100.57**	**98.24**	**98.77**	**100.35**	**100.9**	**100.29**	**98.65**	**100.19**	**99.04**	**95.94**	**99.42**	**99.37**	**99.77**	**100.22**	**99.96**	**98.81**	**99.11**	**99.61**	**98.09**	**99.6**
Ba	335	330	92	154	80	119	139	41	375	186	140	347	344	4	316	99	278	75	43	42	20
Co	63	61	82	66	64	93	86	50	50	60	43	42	40	51	50	48	41	146	43	44	5
Cr	43	44	359	72	272	155	87	80	60	100	100	110	40	70	30	130	50	270	100	150	3
Cu	265	342	94	89	151	169	194	97	246	157	83	266	73	262	219	106	63	77	76	38	17
Nb	13	13	4	11	5	4.4	4.7	5	10	14	8	9	6	9	9	5	7	5	6	8	
Ni	54	45	149	65	141	131	122	88	46	79	64	57	74	59	50	66	73	111	52	67	5
Sc	38	32	44	38	45	51	42	0	0	0	0	0	0	0	0	0	0	0	0	0	
Sr	139	170	94	224	118	112	132	105	142	241	218	140	121	131	155	93	120	95	86	114	15
Rb	46	46	32	12	14	8.5	11	9	46	23	17	40	49	44	75	20	51	19	5	4	7
V	431	568	275	319	303	376	335	340	390	430	280	340	210	490	430	320	190	260	300	330	41
Y	55	52	21	30	25	23	25	28	50	37	22	48	22	36	35	26	21	21	28	36	3
Zn	148	149	5.3	104	98	95	102	95	129	143	88	102	77	112	121	109	76	90	106	112	13
Ga	22	26	15	19	16	18	19	0	0	0	0	0	0	0	0	0	0	0	0	0	
Zr	217	244	54	135	75	70	81	90	195	190	107	159	106	146	164	84	109	72	92	119	14

Samples numbered without letters are from Manuel (1992).

Most of samples are characterized by typical basaltic silica contents, are relatively rich in Al_2O_3 and show a large variation of iron, MgO and TiO_2 contents. Plot of FeO and TiO_2 show linear trends with negative slopes resulting from these elements increasing in relation to decreasing MgO contents (Fig. 9.8). CaO increases sympathetically with MgO suggesting that clinopyroxene fractionation has controlled the CaO/MgO variation. This suggestion is consistent with the clinopyroxene being the dominant pyroxene in the rock samples, particularly those with more or less pristine igneous mineral assemblages.

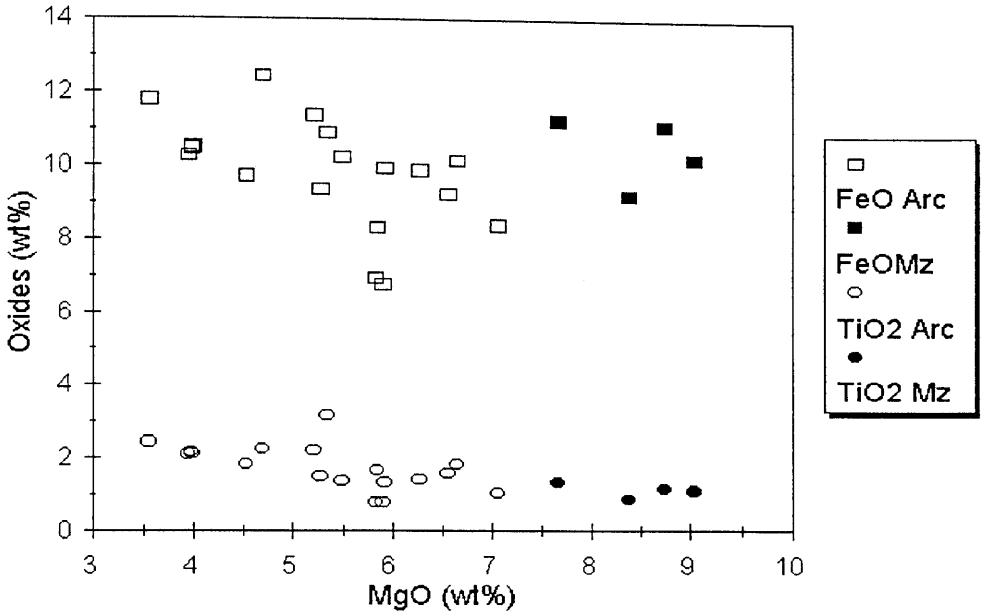

Figure 9.8: Harker diagram of FeO and TiO_2 versus MgO of Mafic intrusions . Mz- samples from Mozambique Belt and Arc- samples from Archaean Granite-Greenstone Belt.

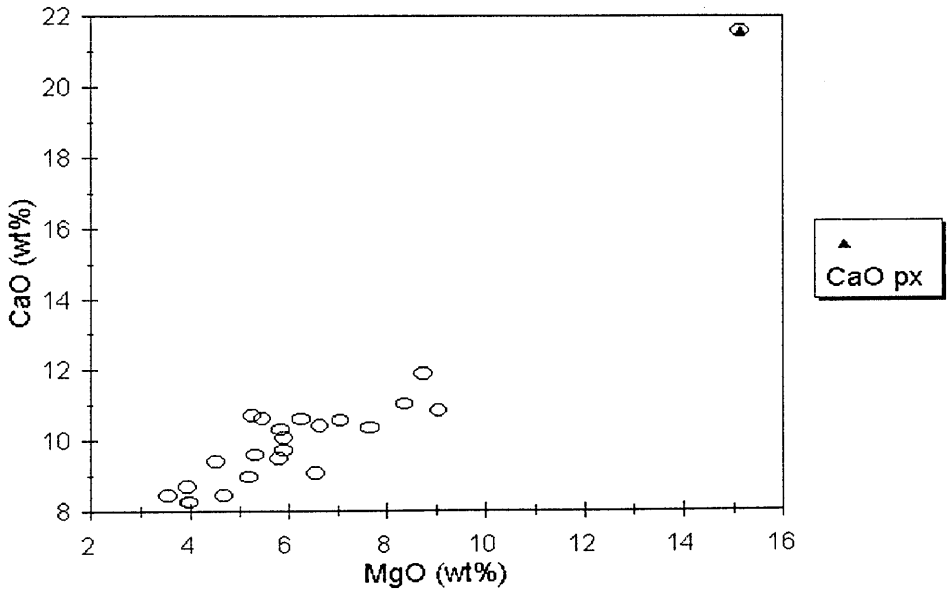

Figure 9.9 CaO versus MgO variation diagram of mafic intrusions. Shown in the diagram is the plot of chemical data of an augite (px) from Deer, Howie and Zussman (1992) (analysis No 8).

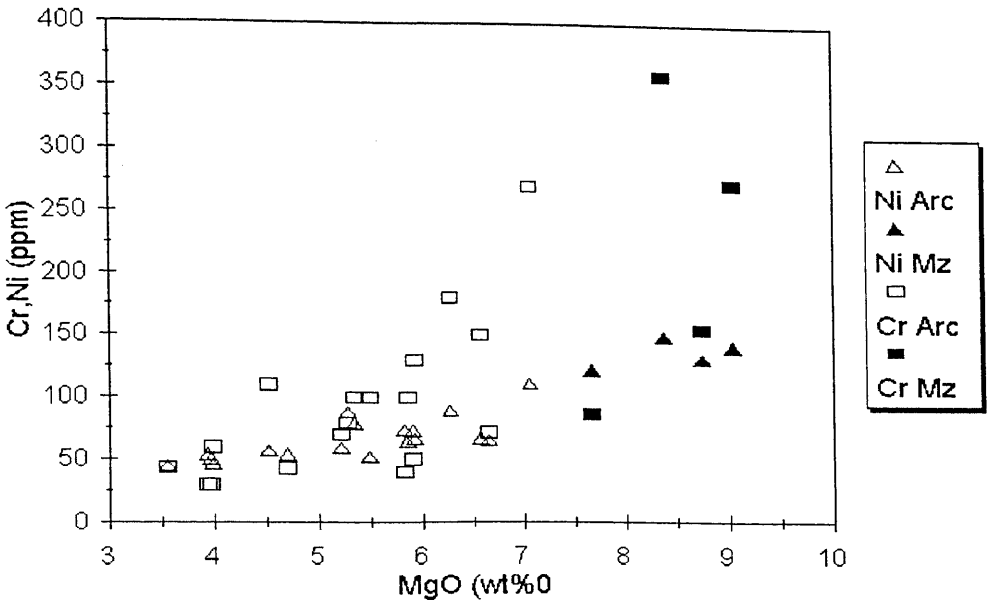

Figure 9.10: Harker diagram plotting Cr and Ni versus MgO of Mafic Intrusions. Abbreviations as in Figure 9.8.

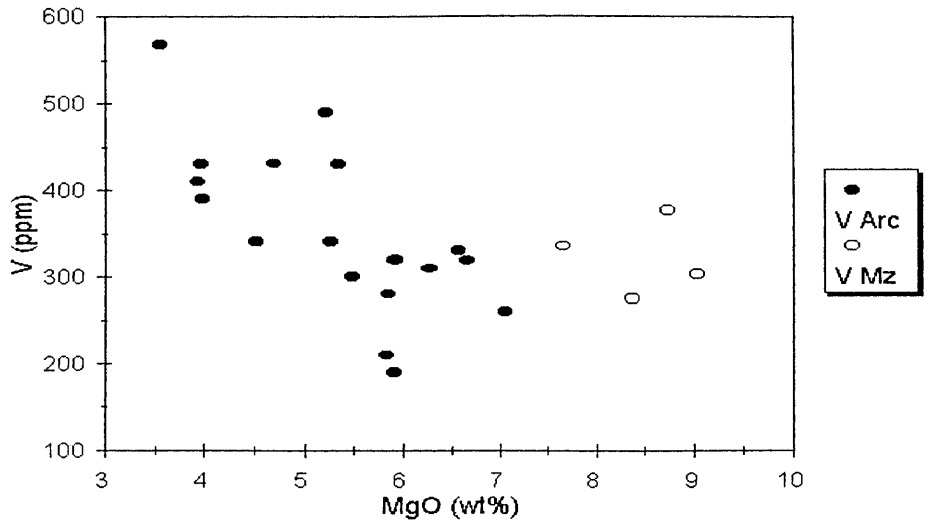

Figure 9.11: Harker diagram plotting V versus MgO of Mafic Intrusions. Abbreviations as in Figure 9.8.

The analyses of an augite from Deer, Howie and Zussman (1992, p. 229) supports this assessment as it plots along the CaO versus MgO trend (Fig. 9.9). Figure 9.10 shows linear variations between Cr and Ni versus MgO. These variations are consistent with clinopyroxene fractionation with both Cr and Ni being strongly fractionated into clinopyroxene (Rollinson, 1993). An inverse correlation between V and MgO is seen (Fig. 9.11), similar to that seen for TiO_2 and FeO versus MgO. These similarities suggest that fractionation of ilmenite and or magnetite have contributed to this variation as these elements are necessary components of these minerals (Rollinson, 1993).

9.4.1 Interpretation of Chemistry

Jensen (1976) described a ternary discriminant diagram to classify rocks ranging from acid volcanics to peridotitic komatiites. In the field of tholeiites, he discriminated between high iron (HFT) and high magnesium (HMT) tholleiites. The samples from the mafic intrusions are all tholeiites and plot mostly in the HFT and a few in the HMT fields (Fig.9.12). Figures 9.13 and 9.14 (Irvine and Baragar,1971) suggest that the mafic intrusions are dominantly sub-alkaline and tholeiites respectively.

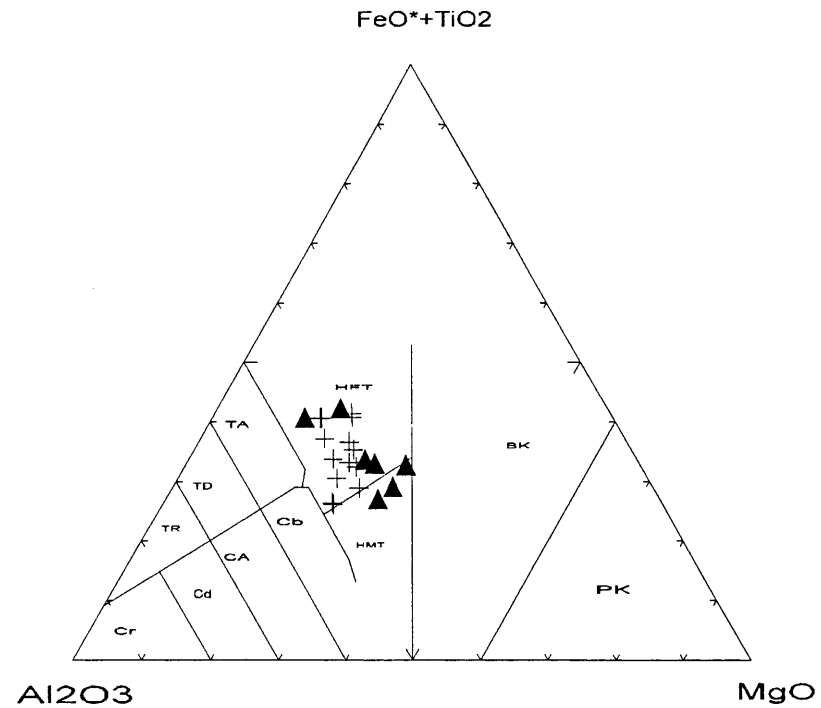

Figure 9.12: Jensen (1976) discriminant diagram plotting chemical data in the fields of high iron (HFT) and high magnesium (HMT) tholeiite fields. Filled up triangles data from Manuel (1992) and crosses, present study. HF- high iron tholeiites, HM- high magnesium tholeiites, BK- basaltic komatiites, PK- peridotitic komatiites, TR- tholeiitic rhyolites, TD- tholeiitic dacites, TA- tholeiitic andesites, CR- calc-alkaline rhyolites, CD- calc-alkaline dacites, CA- calc-alkaline andesites and CB- calc-alkaline basalts.

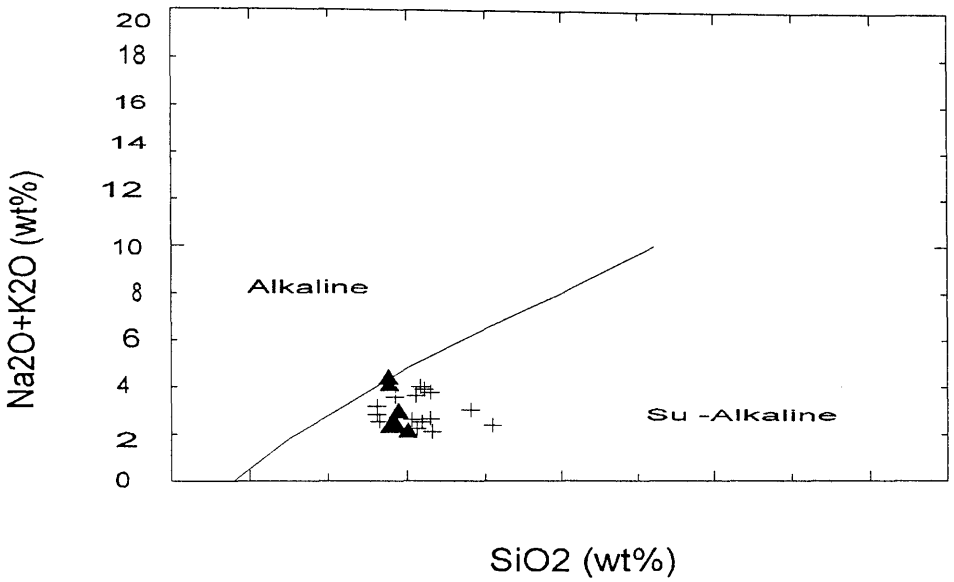

Figure 9.13: Chemical data of mafic intrusions plotting as mostly sub-alkaline (Irvine and Baragar, 1971). Filled up triangles- present study and crosses- Manuel (1992).

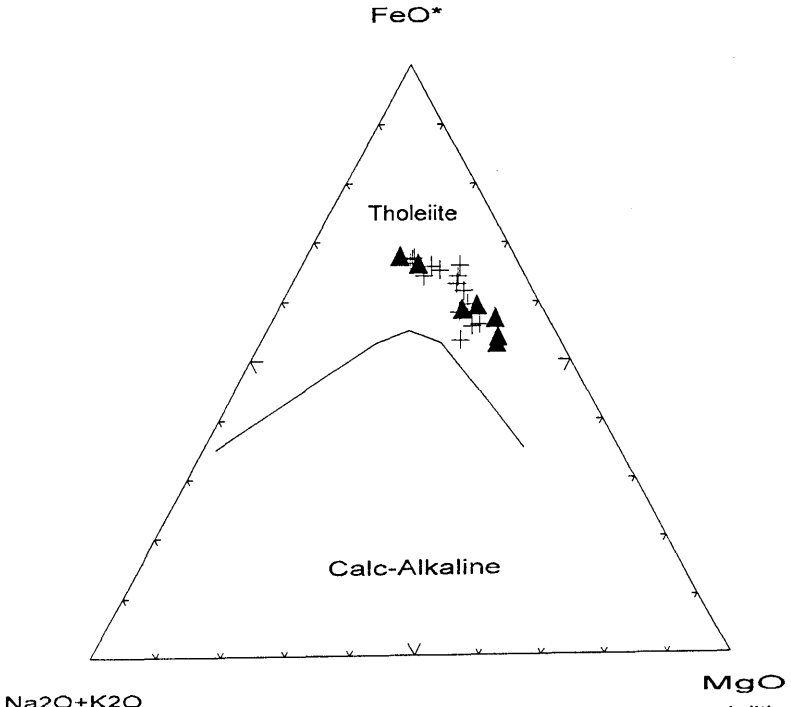

Figure 9.14: Chemical data of Mafic Intrusions indicate a tholeiitic composition in the Irvine and Baragar (1971) discriminant diagram. Symbols as in Figure 9.13.

The analyses of samples 15M and 12T, with igneous textures, Maamp and Maamp2, with metamorphic textures, and 158 and 144 from Manuel (1992) were selected and plotted as spider diagrams (Figs. 9.14 and 9.15). In Figure 9.15 the data are normalized to MORB using values from Pearce (1983) whereas in Figure 9.16 are chondrite normalized using values from Sun (1980). For each diagram it is observed that the samples have similar trends with both diagrams suggesting that their values are 10-100 times higher than those of MORB and chondrites. The trends in these diagrams are similar to those of Pearce (1983) and Sun (1980) respectively for island-arc tholeiitic basalts and are in agreement with Wood (1979) who suggested that in basalts, enrichment in Rb, Ba and K and depletion in Nb is characteristic of island-arc tholeiitic basalts.

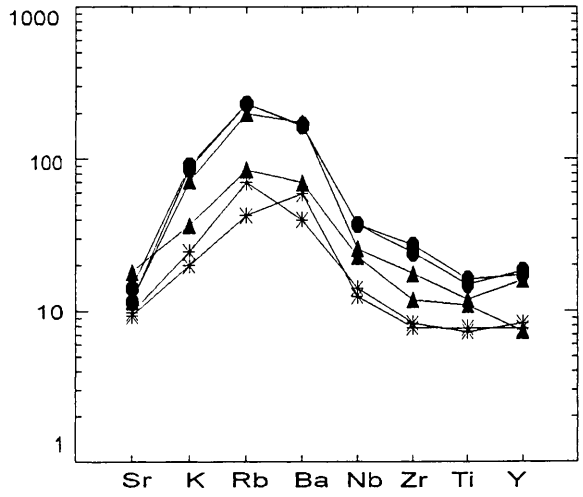

Figure 9.15: MORB normalized trace elements abundance variation diagram. Normalizing data from Pearce (1983). Circles- samples with igneous textures, asterix- samples with metamorphic textures and triangles- analyses from Manuel (1992).

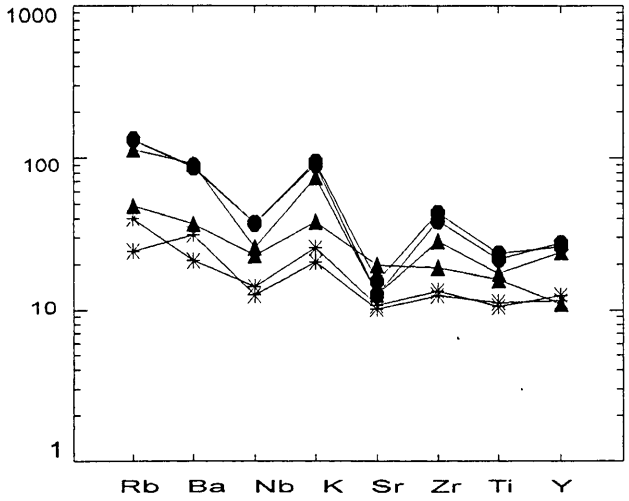

Figure 9.16: Chondrite normalized trace elements abundance variation diagram. Normalizing data from Sun (1980). Circles- samples with igneous textures, asterix- samples with metamorphic textures and triangles- analyses from Manuel (1992).

In conclusion the mafic intrusions comprise two coeval categories of rocks, namely, one occurring within the granite - greenstone belt and characterized by igneous texture and metamorphosed to low grade greenschist facies and another which includes the rocks occurring as dykes within the Mozambique Metamorphic Province and metamorphosed to medium to high grade amphibolite facies. Both rocks have an island-arc tholeiite chemical signature.

Chapter 10

TCHINHADZANDZE GRANODIORITE GNEISS

10.1 Introduction

The Tchinhadzandze Granodiorite Gneiss occurs within an area occupied by the Early Proterozoic Messica Granite Gneiss and the Frontier Formation. The distinctive characteristic of this granite is that it does not show the strong planar fabrics which characterize the eastern exposures of the Messica Granite Gneiss and therefore it is either late- or post-tectonic with respect to that deformation.

10.2 Field Description

This gneiss occurs as bodies generally associated with the metasediments of the Frontier Formation and their better exposures are at Tchinhadzandze (Fig. 2.2). The granite is grey and contains feldspar which predominates over quartz, biotite and hornblende and locally exhibits feldspar phenocrysts. The rock is weakly foliated, and the foliation is, defined by biotite and hornblende randomly oriented. It is weakly jointed and cut by thin quartz-feldspar and pegmatitic veins.

10.3 Petrography

The granite is inequigranular, medium grained (Fig. 10.1), and locally exhibits preferred orientation of biotite and hornblende. The feldspars exhibit perthitic and myrmeckitic intergrowths.
The mineralogy is dominated by plagioclase and includes quartz, K-feldspar, hornblende and biotite. Minor phases are titanite, epidote and zircon (Table 10.1).

Table 10.1: Mineralogical assemblage (proportions of each mineral indicated) of Tchinhadzandze Granodiorite Gneiss.

sample	K-fld	Plg	Qtz	Bt	Hbl	Ep	Ttn
ygr1	24	42	25	4	4	<1	1
ygr2	23	45	22	4	5	-	1
ygr3	22	45	24	3	5	<1	1
ygr4	23	43	23	5	6	<1	-
ygr5	23	42	25	4	5	-	1
ygr6	22	44	24	5	5	<1	-

K-fld- potassium feldspar, Plg- plagioclase, Qtz- quartz, Bt- biotite, Hbl- Hornblende, Ep- epidote and Ttn- titanite.

K-Feldspar occurs as anhedral grains exhibiting cross-hatched (mostly) and Carlsbad twins whereas plagioclase exhibits albite and Carlsbad twinning. Both feldspar types are cracked and contain inclusions of finer quartz and feldspar grains.

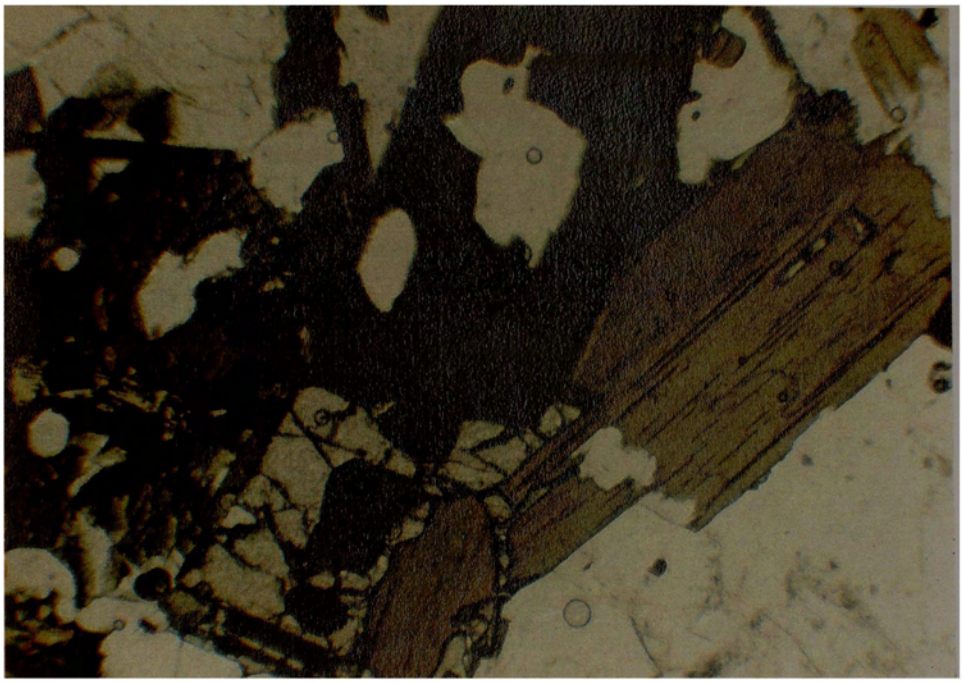

Figure 10.1: Inequigranular medium grained granite gneiss. Minerals shown are feldspar (white), green hornblende containing inclusions of feldspar and quartz, brown biotite and dark grey titanite (high relief) associated with hornblende and biotite. Parallel light, width of field 7 mm.

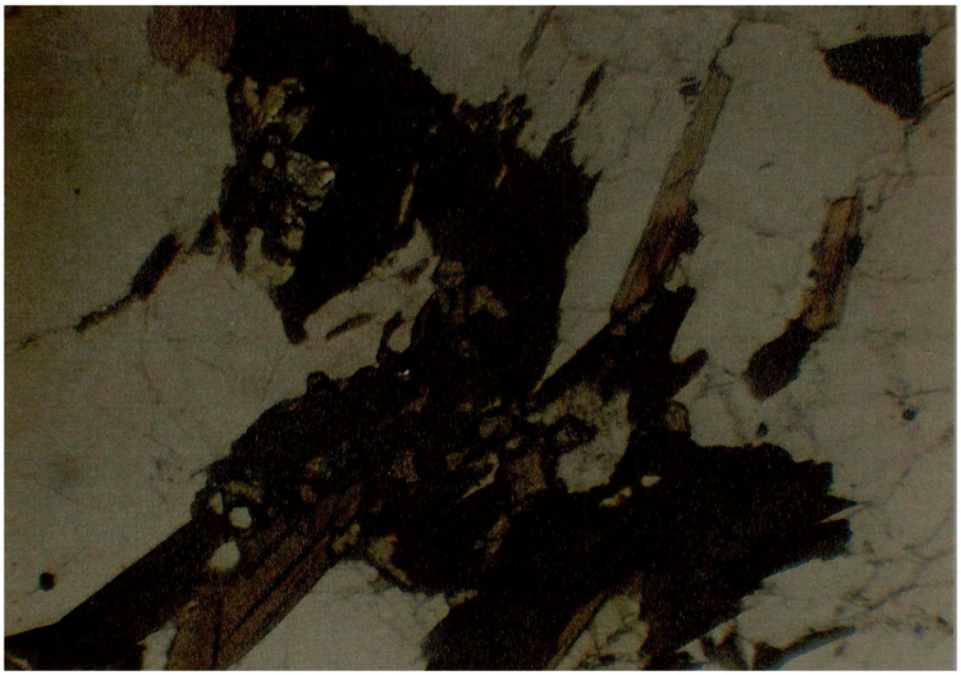

Figure 10.2: Preferred orientation of biotite and hornblende. Note fine-grained titanite (high relief) associated with the hornblende and biotite. Parallel light, width of field 7 mm.

Anhedral quartz contains inclusions of feldspar and shows undulatory extinction indicating that the granite has been strained. Brown biotite forms subhedral grains which locally show preferred orientation. Green hornblende grains, commonly associated with biotite, are subhedral to anhedral and contain inclusions of feldspar, quartz and titanite. (Fig. 10.2). Titanite occurs as fine to medium grains associated with ferromagnesian minerals either along grain boundaries or as inclusions (Fig. 10.2). Epidote occurs as an alteration product of amphibole and plagioclase. Zircon is rare and occurs as prismatic fine grains.

10.4 Chemistry

10.4.1 Introduction

The samples were analysed for major and trace element compositions (Table 10.2) and two of them were analysed for REE (Table 10.3).

10.4.2 Major Element Chemistry

The major element compositions of the samples show little variation. Total iron and MgO contents result in ΣFeO/MgO ratios of ~3:1.

Table 10.2: Major and trace elements analyses of samples from Tchinhadzandze Granodiorite Gneiss.

Sample	YGR1	YGR2	YGR3	YGR4	YGR5	YGR6
SiO_2	70.48	69.17	68.21	69.37	69.51	69.9
$Al_{i2}O_3$	14.7	15.23	15.24	15.13	15.04	14.87
Fe_2O_3	1.19	1.44	1.50	1.25	1.39	1.31
FeO	1.42	1.82	1.90	1.58	1.72	1.60
MgO	1.16	1.36	1.43	1.34	1.33	1.36
CaO	2.28	2.64	2.85	2.5	2.55	2.46
Na_2O	4.02	4.05	3.93	3.91	3.76	4.02
K_2O	4.24	3.82	3.9	3.94	4.26	4.13
TiO_2	0.37	0.41	0.4	0.37	0.4	0.39
P_2O_5	0.14	0.18	0.19	0.17	0.2	0.18
MnO	0.03	0.06	0.05	0.04	0.05	0.05
total	**100.03**	**100.18**	**99.60**	**99.60**	**100.21**	**100.27**
Ba	1612	1351	1548	1539	1634	1550
Co	36	37	36	38	36	43
Cr	33	36	37	33	34	35
Cu	15	5	5	4	7	8
Li	15	16	15	17	15	14
Nb	4	4	5	5	4	4
Ni	18	22	24	25	22	21
Sc	3	5	5	6	6	5
Sr	618	576	620	614	592	616
Rb	86	93	92	88	94	87
V	29	39	40	32	35	36
Y	8	11	11	10	12	12
Zn	162	53	52	47	51	51
Zr	128	182	167	147	213	219
Ga	17	19	20	18	20	19

The Na_2O+CaO contents are ~6 wt% with K_2O ~4 wt% which results in the samples plotting on the boundaries between the granodiorite, adamellite trondhjemite and granite fields in terms of normative albite, orthoclase and anorthite on the Barker (1979) diagram (Figure 10.3). According to Shand's alumina saturation Index the rocks are metaluminous (Fig. 10.4). Although the range of SiO_2 values is small, Harker variation diagrams show linear trends of decreasing Al_2O_3, Fe_2O_3, MgO, FeO and CaO contents with increasing SiO_2 whereas Na_2O and K_2O increase with SiO_2 (Figs. 10.5, 10.6 and 10.7). Low MgO and ΣFeO relative to Σalkalis result in the granite being calc-alkaline in nature (Fig. 10.8).

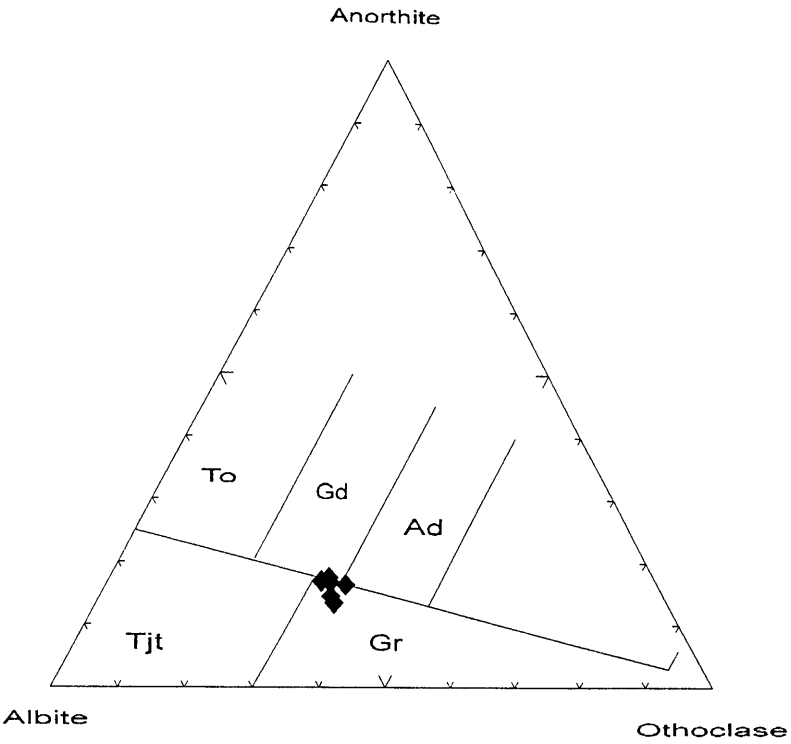

Figure 10.3: Plot of Tchinhadzandze Granodiorite Gneiss in the normative albite, orthoclase and anorthite diagram (after Barker, 1979). The boundary between trondhjemites (Tjt) and granite (Gr) and the boundary between these two fields and the fields of tonalites (To), granodiorite (Gd) and adamellites (Ad) are from O'Connor (1965).

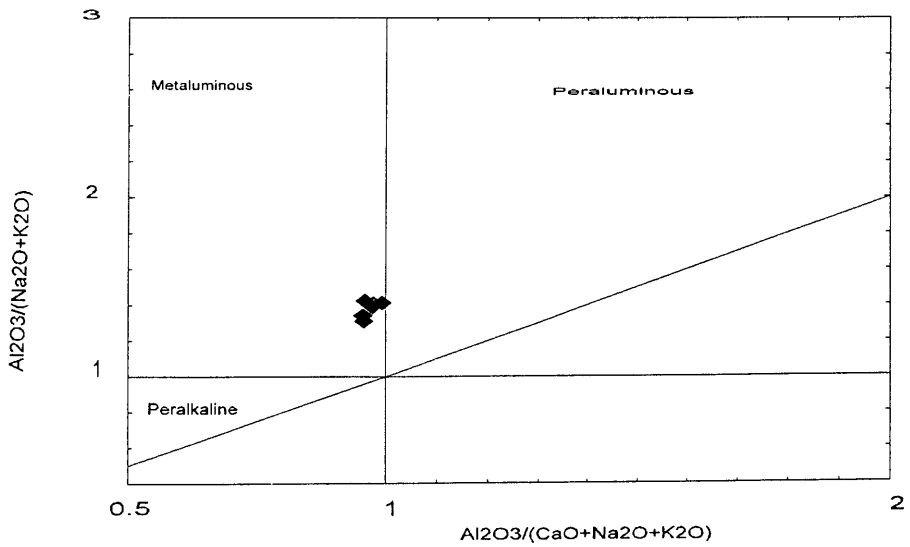

Figure 10.4: Shands 's (1947) alumina saturation Index diagram plotting samples of the Tchinhadzandze Granodiorite Gneiss as metaluminous.

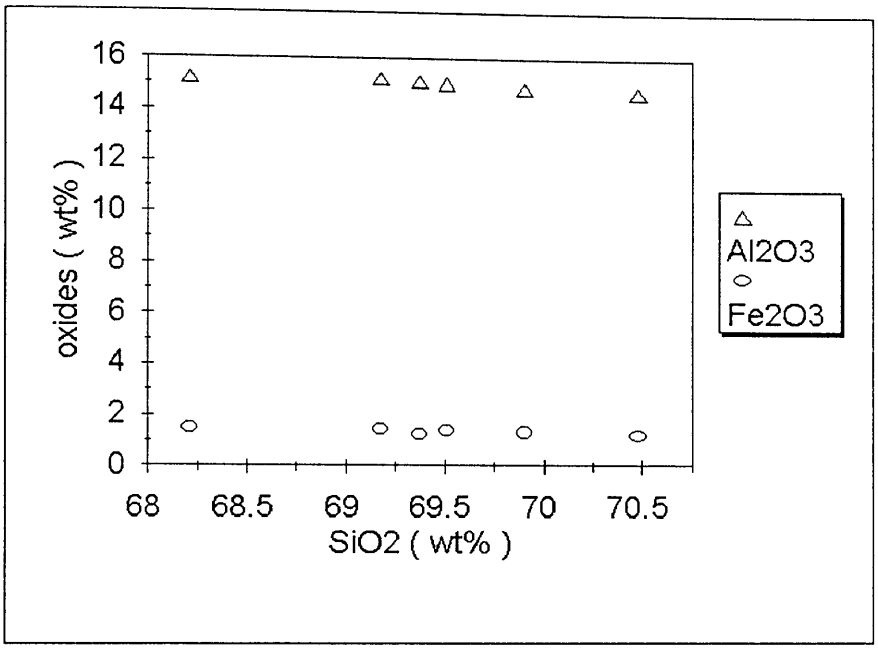

Figure 10.5: Al_2O_3 and Fe_2O_3 versus SiO$_2$ variation diagram of Tchinhadzandze Granodiorite Gneiss.

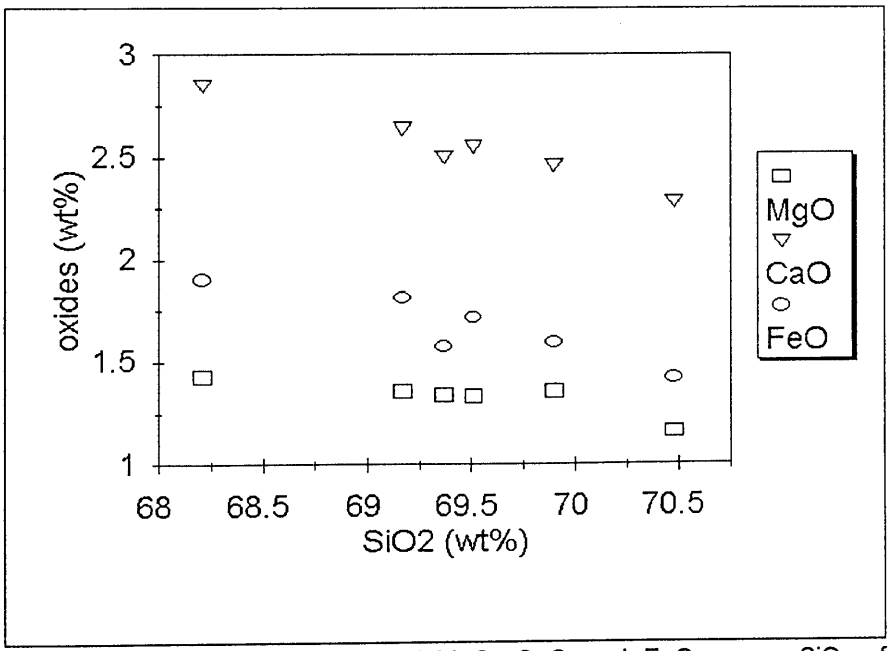

Figure 10.6: Variation diagram of MgO, CaO and FeO versus SiO_2 of Tchinhadzandze Granodiorite Gneiss.

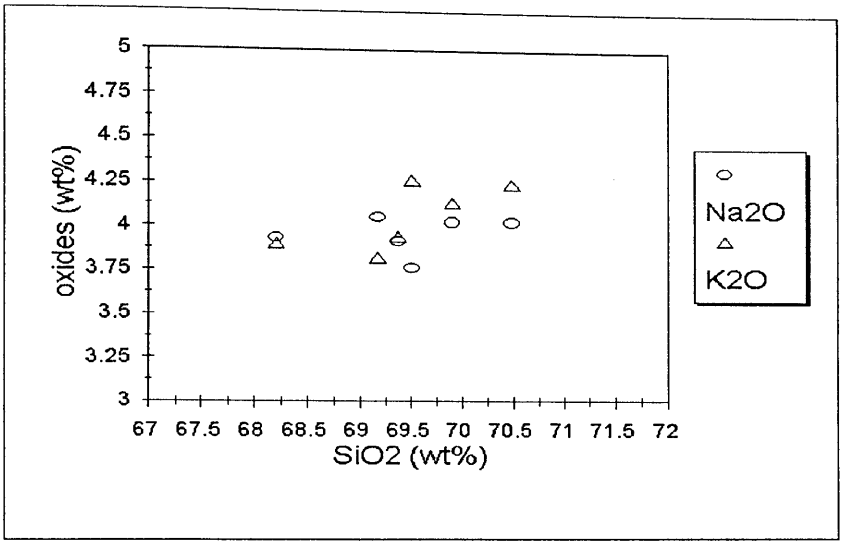

Figure 10.7: Na_2O and K_2O versus SiO_2 variation diagram of the Tchinhadzandze Granodiorite Gneiss.

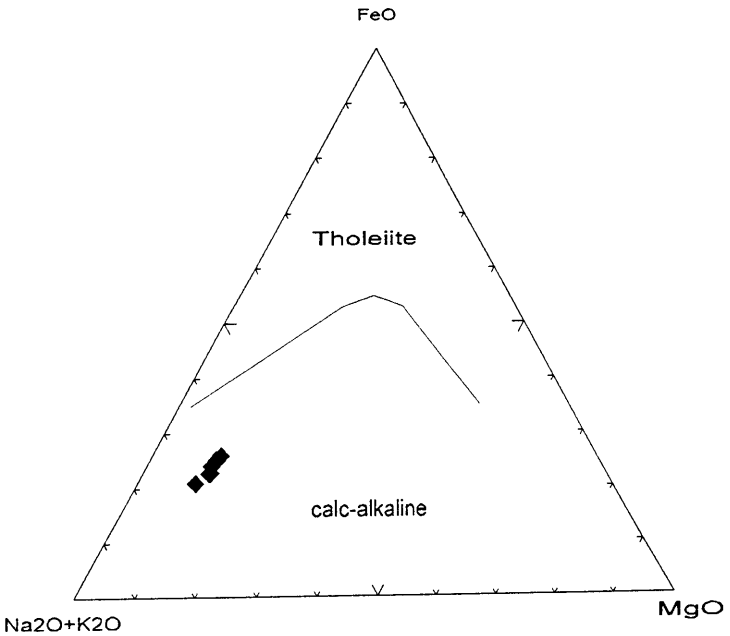

Figure 10.8: Irvine and Baragar (1971) discriminant diagram of the Tchinhadzandze Granodiorite Gneiss. Analyses plot in the field of calc-alkaline.

10.4.3 Trace Element Chemistry

In general the samples show little variation in their trace elements contents. Sr/Rb ratios are high resulting from the relatively low Rb contents and show a systematic variation between ~6:1 and ~7:1. Trace element spidergrams exhibit a pattern characterized by Rb, Ba, K and Sr enrichment relative to Nb, Zr, Ti and Y. This pattern is typical of volcanic-arc granitic magmas (Pearce *et al.*, 1984) (Fig. 10.9).

Two samples were analysed for their contents in rare earth elements (REE) (Table 10.3). The REE contents in this granite are characterized by a relatively high Ce, La and Nd values . The REE patterns for the two samples are shown in Fig. 10.10. The normalizing values are from Evenson *et al.* (1978).The REE patterns are characterized by enrichment of light rare earth elements relative to heavy ones with La_{cn}/Yb_{cn} of ~100, a weak positive Eu anomaly and a flat pattern of the heaviest elements Er, Yb and Lu. The positive Eu anomaly is possibly due to accumulation of Ca-feldspar. The flat HREE pattern may reflect hornblende accumulation in the source rock because the HREE are strongly partitioned into hornblende (Rollinson, 1993).

Table 10.3: Rare earth Element analyses of Tchinhadzandze Granodiorite Gneiss in ppm.

sample	La	Ce	Pr	Nd	Sm	Eu	Gd	Dy	Ho	Er	Yb	Lu
YGR1	38.01	76.27	7.8	25.93	3.48	1.25	2.23	1.24	0.19	0.41	0.39	0.06
YGR2	44.38	104.82	8.98	29.92	4.41	1.27	2.86	1.79	0.29	0.58	0.58	0.08

10.5 Discussion and Conclusion

The Ba-Rb-Sr contents of the Tchinhadzandze rocks are typical of granodiorites (El Bouseilly and El Sokkary, 1975) (Fig. 10.11) and the low Rb contents are typical of granitoids found in volcanic-arc settings (Pearce *et al.* 1984) (Fig. 10.12).

In conclusion, the Tchinhadzandze rocks have normative and chemical compositions of a granodiorite and the random orientation of of the planar fabric in this granite may indicate that the fabric is a flow fabric developed during emplacement.

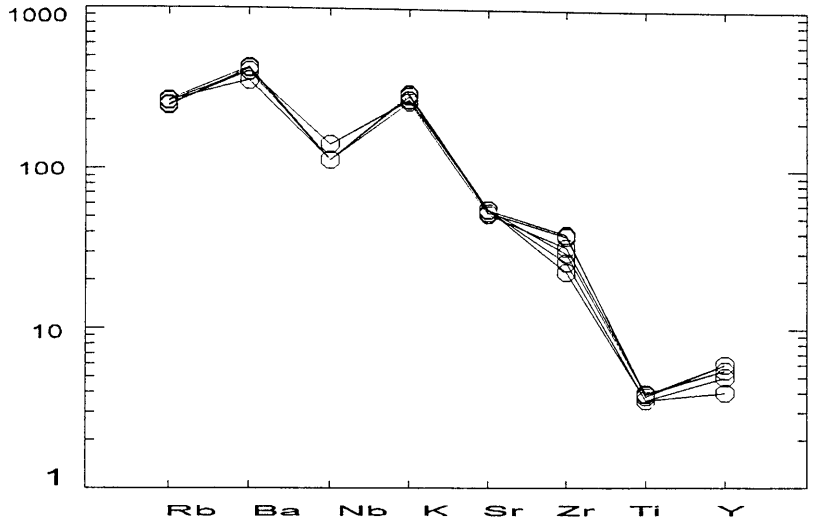

Figure 10.9: Chondrite normalized trace elements abundance variation diagram of Tchinhadzandze Granodiorite Gneiss (normalizing values after Sun, 1980).

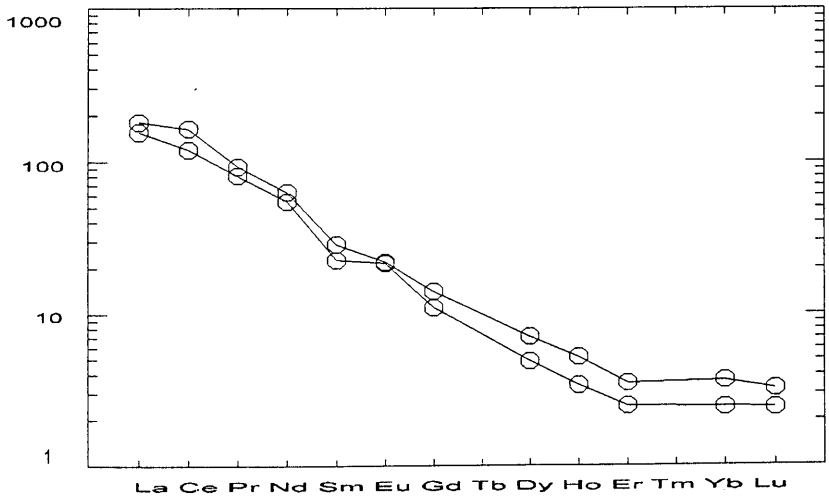

Figure 10.10: Chondrite normalized REE abundance variation diagram of Tchinhadzandze Granodiorite Gneiss (normalizing data after Evenson *et al*. 1978).

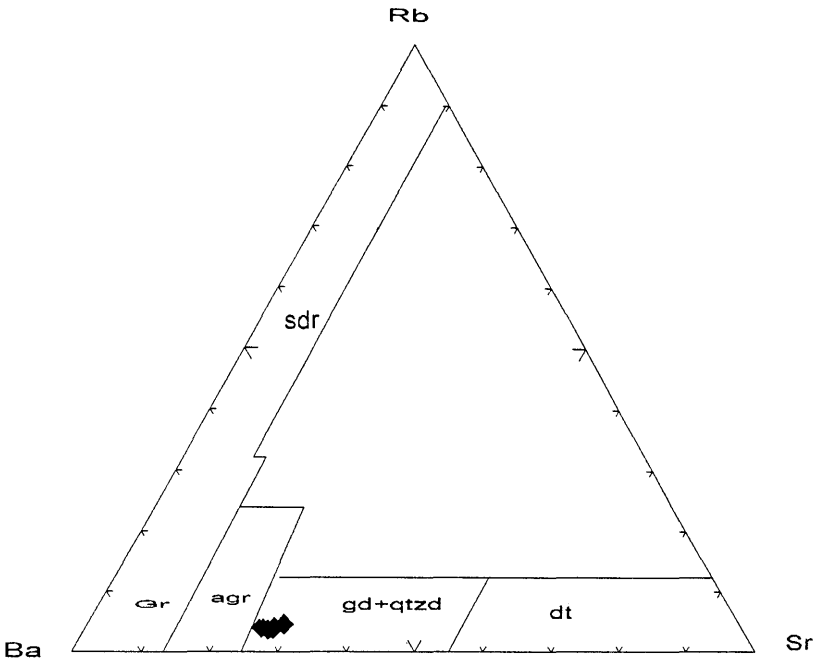

Figure 10.11: Diagram plotting samples in the field of granodiorites and quartz-diorites (after El Bouseily and El Sokkary, 1975). Sdr- strongly differentiated granites, Gr-normal granites, agr- anomalous granites and dt- diorites.

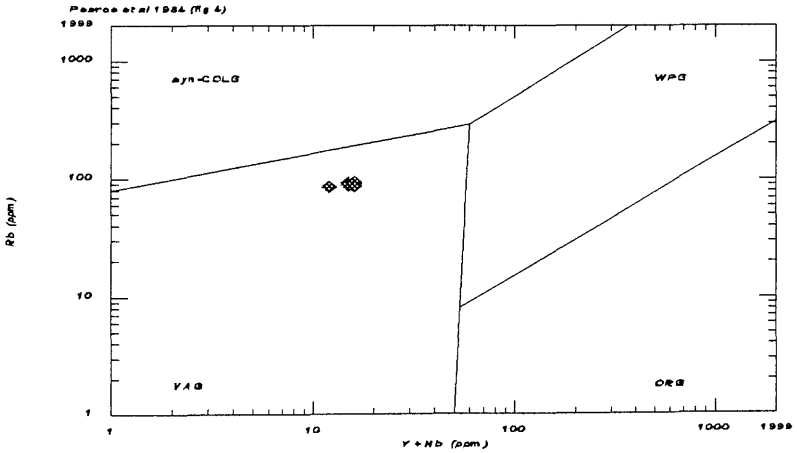

Figure 10.12: Pearce *et al.* (1984) tectonic discriminant diagram for granitoid rocks plotting the samples in the field of VAG (volcanic-arc granitoids). Syn-COLG- syn collisional, WPG- within plate, ORG- orogenic granites.

Chapter 11

STRUCTURAL GEOLOGY

11.1 Introduction

The study area can be subdivided into four structural domains labelled 1 to 4 and shown on the map (Fig. 11.1). The map displays rose diagrams of planar fabric strike directions. Figure 11.1 and the accompanying stereonets (Figs. 11.2, 11.3, 11.4, 11.5, 11.6, 11.7, 11.8, 11.9, 11.10, and 11.11) were prepared using the computer program Spheristat.

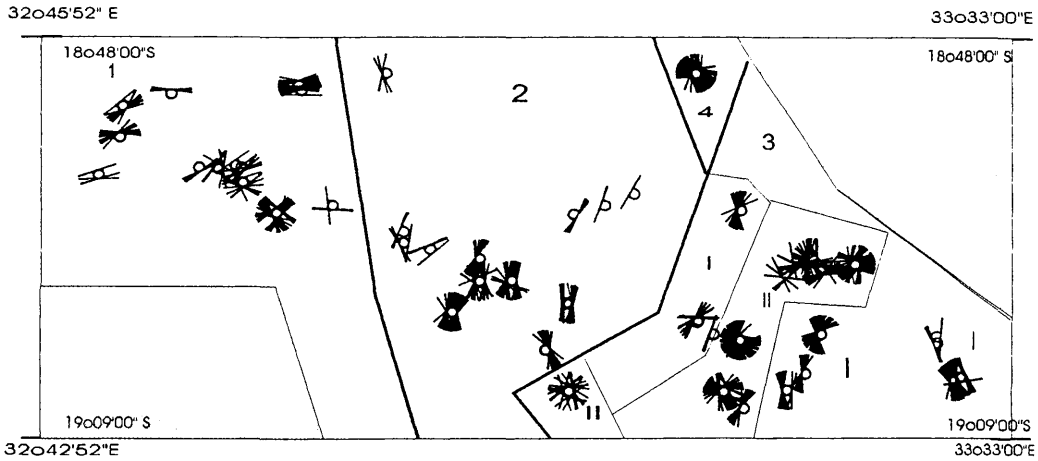

Figure 11.1: Map showing planar fabric strike directions and the subdivision of the study area in domains labelled 1 to 4. Within domain 3, sectors I and II are indicated. In grey are areas not covered by the study. The dimensions of the area are ~(37X88) km^2

11.2 Description of Structures

11.2.1 Domain 1

Comparison of Fig. 11.1 and 2.1 shows that this domain is underlain by the Manica Greenstone Belt and the Vumba Granite Gneiss. Stereonets 11.2, 11.3 and 11.4 represent the planar and linear fabrics measured in the Manica Greenstone Belt, the Vumba Granite Gneiss and the M'Beza/Vengo Formation respectively. The planar fabrics measured include the schistosity in the schists of the Manica Greenstone Belt, the foliations in the Vumba Granite Gneiss and the sedimentary layering in the M'Beza/Vengo Formation. Consequently they include S_o and S_1. The linear fabrics include mineral lineations (Fig. 11.2) and fold axes (Fig. 11.4). The axial plane foliations strike E-W to NE-SW with steep dips to the N and S and NW and SE (Figs. 11.2,11.3 and 11.4). The mineral lineations have a constant trend characterized by plunges of 60° towards 108° in average (Fig. 11.2) and the fold axes have plunges of ~30° towards E (Fig. 11.4). The schistosity has resulted from at least two kinds of movements, namely, a N-S compression and a dip/oblique-slip movement in a SE-NW direction and associated with the steeply dipping lineation (Fig. 11.2). The E-W oriented fold axes suggest that the

folds in the M'Beza/Vengo Formation (Fig. 11.4) were the result of N-S compressional movements.

Two stages of deformation took place, namely, D_1 which involved the development of planar fabrics parallel to primary layering resulting in S_o and S_1 having similar orientations. These fabrics were then folded by D_2 about axes which plunge shallowly to the east at ~30° suggesting N-S compression. Fig. 2.1 shows however that the strike of the foliation in the eastern sector of the Manica Greenstone Belt swings towards a NE-SW orientation.

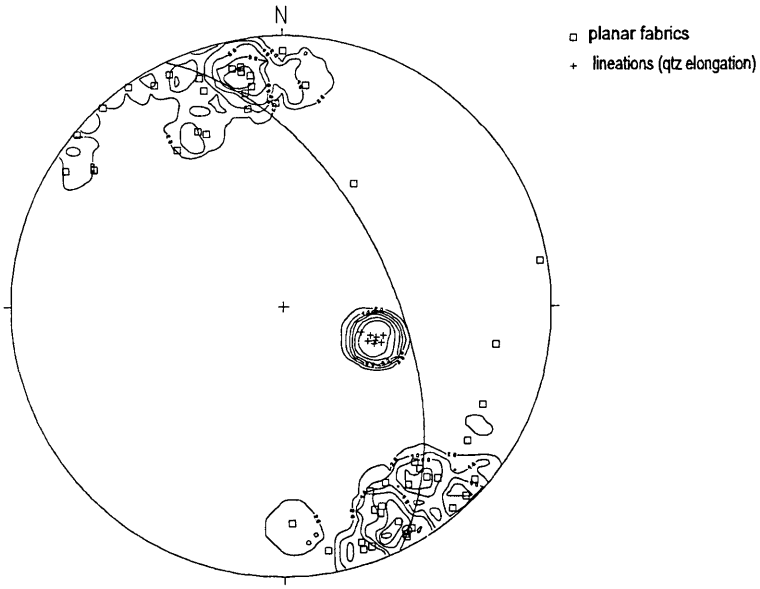

Figure 11.2: Poles to planar fabrics in the Manica Greenstone Belt and quartz elongation lineation in the quartz-sericite schist.

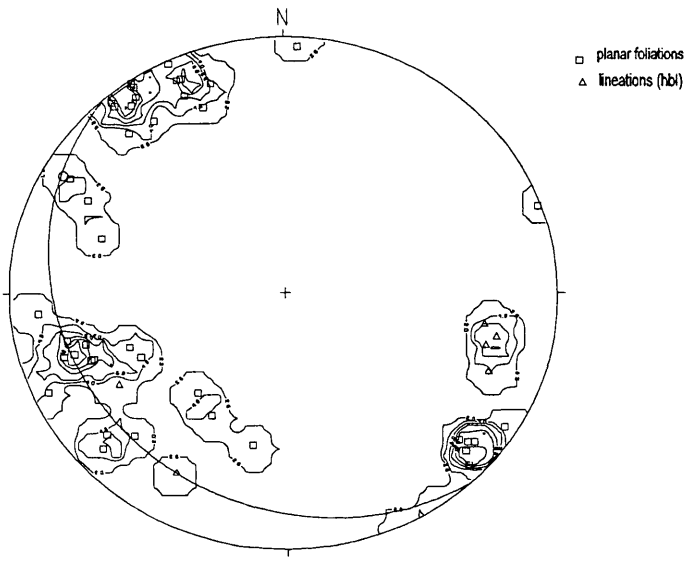

Figure 11.3: Poles to planar fabrics and mineral lineations in the Vumba Granite Gneiss.

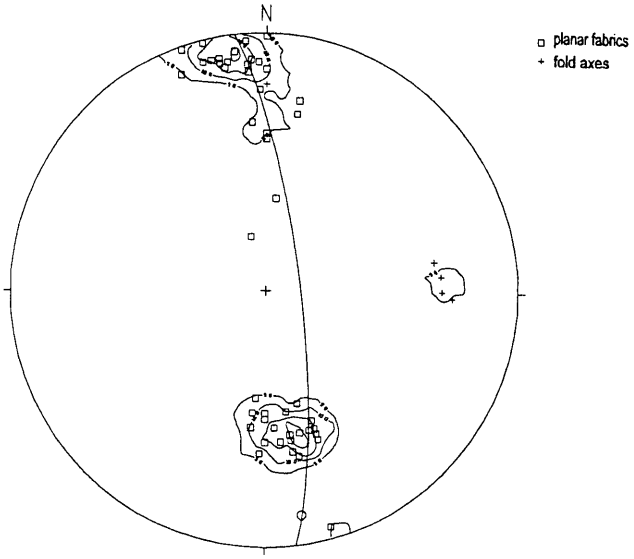

Figure 11.4: Poles to layering and schistosity and fold axes measured in the M'Beza/Vengo Formation.

11.2.2 Domain 2

Comparison of Figures 11.1 and 2.1 shows that this domain is underlain by the Messica Granite Gneiss and the Frontier Formation. Stereonets in Figures 11.5 and 11.6 represent the structural measurements from the Messica Granite Gneiss and the Frontier Formation respectively. In the gneiss, the measured structures are planar fabrics defined by the preferred orientation of biotite and hornblende, and linear elements defined by quartz grains elongation with sub-horizontal plunges towards the north (Fig. 11.5). In the metasediments of the Frontier Formation, the planar fabrics are primary layering (S_o) and foliation (S_1), defined by the development of metamorphic layering. The S_o and S_1 have similar to cross-cutting orientation at small angles. The foliation strikes are dominantly N-S with steep dips towards E and W (dominantly) (Figs. 11.5 and 11.6). The lineation has shallow plunges towards N. The steep planar fabric with associated near-horizontal mineral lineation suggests a N-S strike-slip environment (Hobbs *et al.* 1976, Passchier *et al.*, 1990).It is significant that the E-W planar fabrics in domain 1 are not seen in domain 2 which suggest that these fabrics possibly predate those in domain 2.

11.2.3 Domain 3

Comparison of Figures. 11.1 and 2.1 shows that this domain is underlain by the Vanduzi Migmatite Gneiss, the Nhansipfe Granite Orthogneiss and the Chimoio Granodioritic Gneiss. The stereonet in Figure 11.7 represenst the leucosomes, planar and linear fabrics measured in the Vanduzi Migmatite Gneiss. Stereonets in Figures 11.8 and 11.9 display the data for the planar and linear fabrics respectively, measured in the Nhansipfe Granitic Orthogneiss. The stereonet in Figure 11.10 shows the planar and linear fabrics measured in the Chimoio Granodioritic Gneiss.

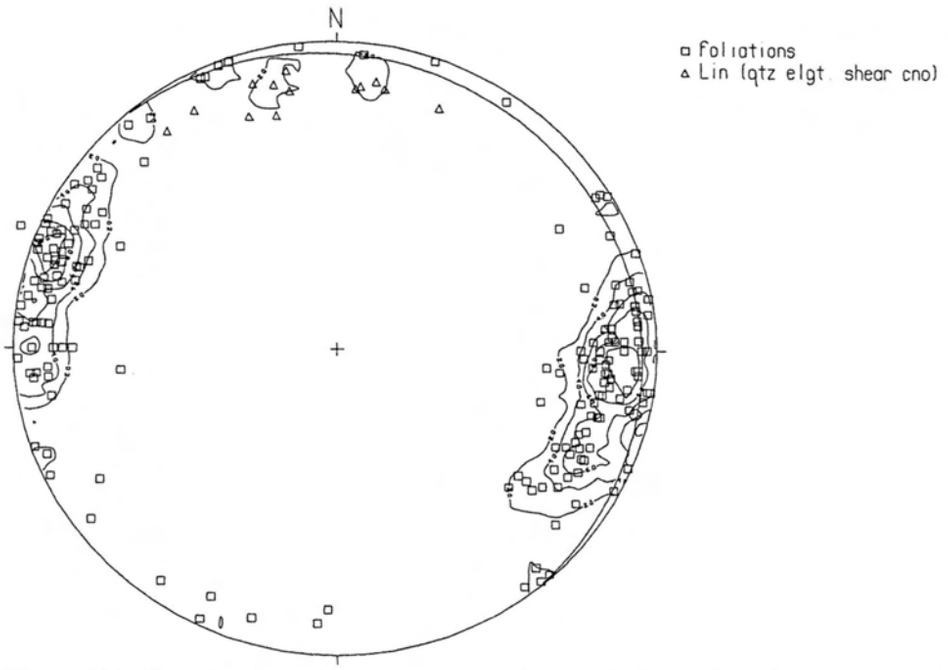

Figure 11.5: Poles to planar foliations and orientation of mineral lineations measured in the Messica Granite Gneiss.

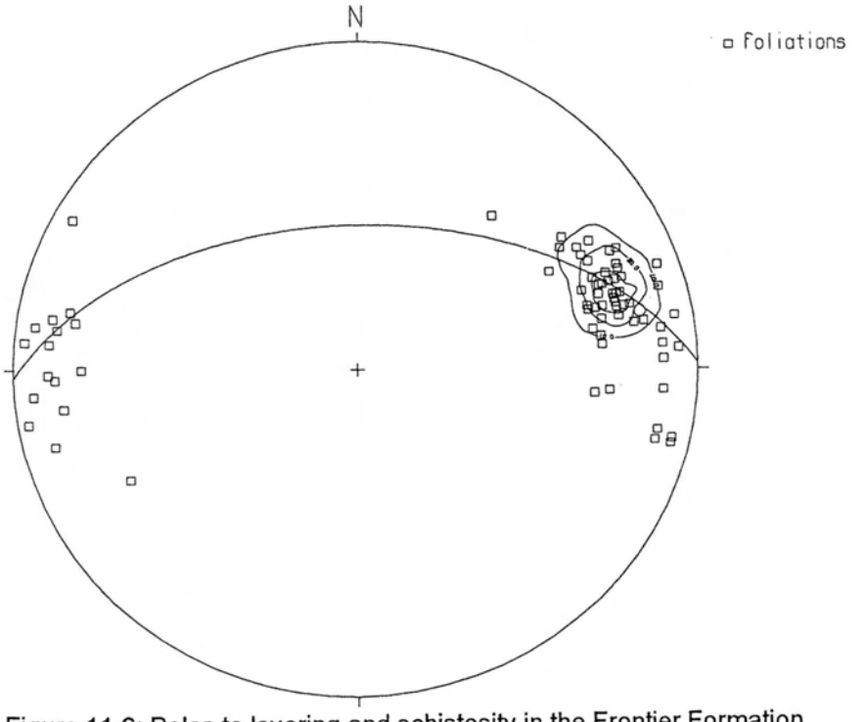

Figure 11.6: Poles to layering and schistosity in the Frontier Formation

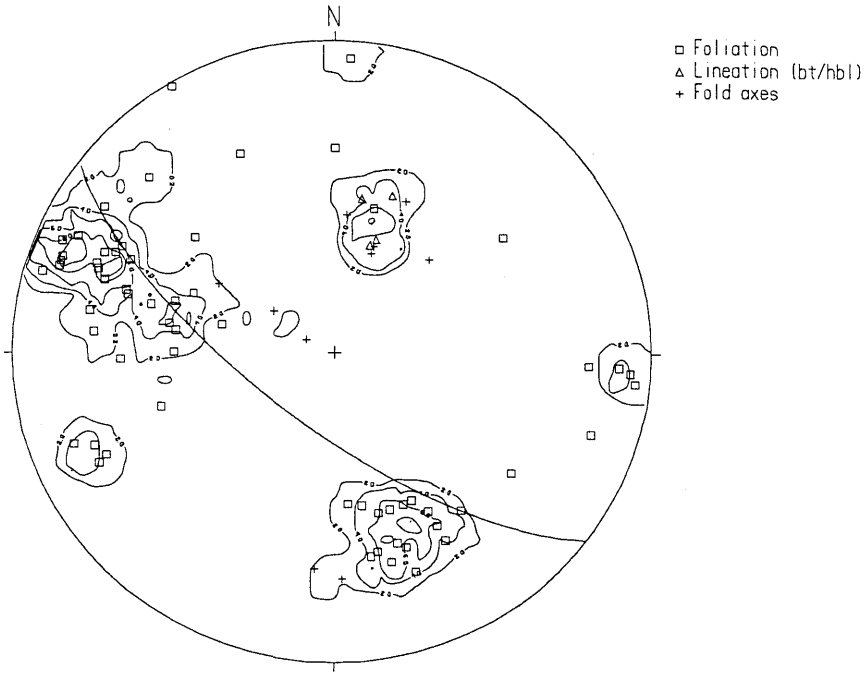

Figure 11. 7: Poles to planar fabrics and lenticular leucosomes and plunge directions of mineral lineations and fold axes in the Vanduzi Migmatite Gneiss.

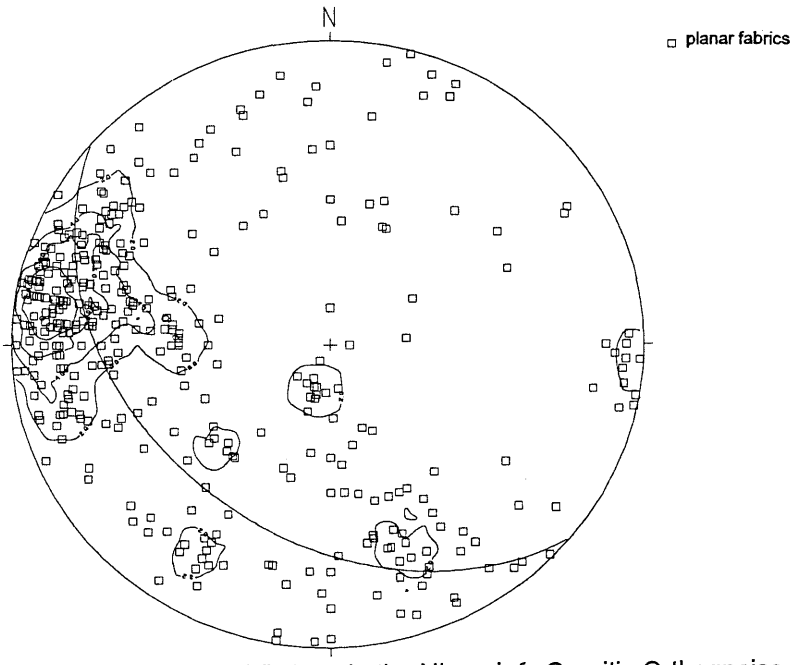

Figure 11.8: Poles to foliations in the Nhansipfe Granitic Orthogneiss.

In the Vanduzi Migmatite Gneiss planar fabrics comprise the primary layering S_0 and two foliations, namely, S_1 with E-W strike and moderate to steep dips towards N and S_2 with N-S strike and steep dips towards E and W. Two sets of leucosomes, correlated with S_1 and S_2 foliations are developed. The linear elements comprise mineral lineations and fold axes. These lineations and fold axes have essentially moderate plunges towards N. (Fig.11.7). The interpretation of this set of structural data suggests that D_1 involved the development of leucosome and planar fabrics parallel to primary layering to result in stage 1 leucosome, S_0 and S_1 having similar orientations. These planar fabrics as well as the leucosome were then folded by D_2 about axes which plunge ~45° towards N by a E-W compression. Apart from the S_2 foliation, the D_2 deformation is also associated with the development of strongly oriented N-S leucosomes. The moderately N plunging mineral lineation, suggests the occurrence of a N-S strike-slip movement.

In the Nhansipfe Granitic Orthogneiss planar fabrics (Fig.11.8) comprise mineral foliations defined by deformed feldspar megacrysts, biotite and hornblende whereas the linear fabrics are mineral lineations and fold axes (Fig. 11.9). The foliation is highly variable with a high concentration with N-S strikes and steep easterly dips. The lineations plunge shallowly to steeply to the NNE. The fold axes have variable orientations which lie crudely along a great circle which strikes NNE (~20°) and dips ~70° ESE.

The stereonet in Figure 11.10 represents planar and linear fabrics measured in the Chimoio Granodiorite Gneiss. The planar fabrics comprises mineral foliations defined by planar orientation of biotite and hornblende and essentially have N-S strikes and steep dips to E and W. Linear fabrics comprise mineral lineations defined by hornblende and biotite, and fold axes which plunge shallowly and moderately, respectively, to the N and S. These observations may suggest that the steep zones have originated from strike-slip deformation.

From Figure 11.1, Domain 3 can be subgrouped into subdomains I and II types. Type I subdomains are characterized by planar fabrics with dominantly N-S strikes. In subdomain type II, the planar fabrics have highly variable strikes. The wide range of foliations is also due to the recognition in the migmatite gneiss terrane of two generations of leucosome development, the first being oriented parallel to S_1 layering which is deformed and folded by S_2 which is oriented N-S. The second leucosome development is oriented N-S.

11.2.4 Domain 4

Comparison of Figure 11.1 and Figure 2.1 shows that this domain is underlain by the plutons of the Tchinhadzandze Granodiorite Gneiss.

Both planar and linear fabrics in these granites are weakly developed and variable. The poles to mineral foliations defined by biotite and hornblende show weak concentrations suggesting a NW-SE planar fabric (Fig. 11.11). The randomness of these foliations may also indicate that the fabric has resulted from primary magmatic flow. The lineations were measured in biotite and hornblende.

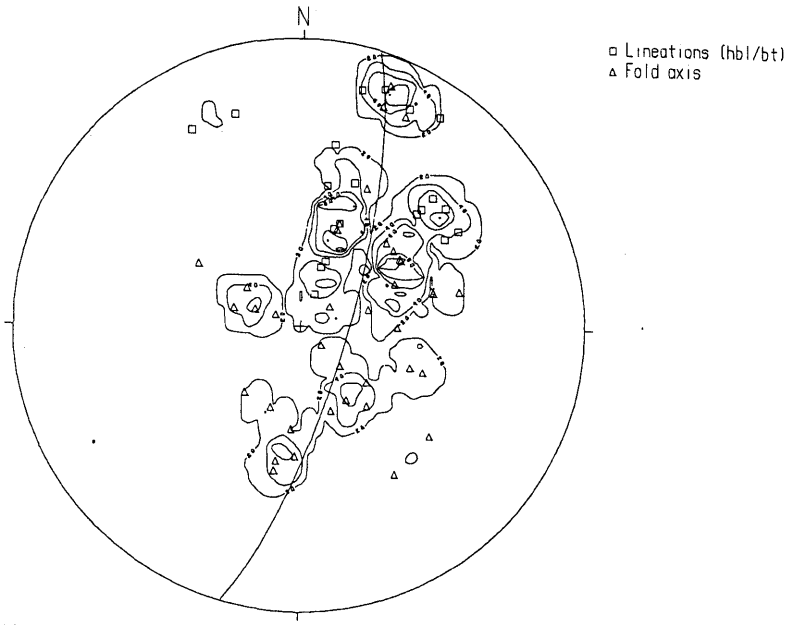

Figure 11.9: Mineral lineations and fold axes measured in the Nhansipfe Granitic Orthogneiss.

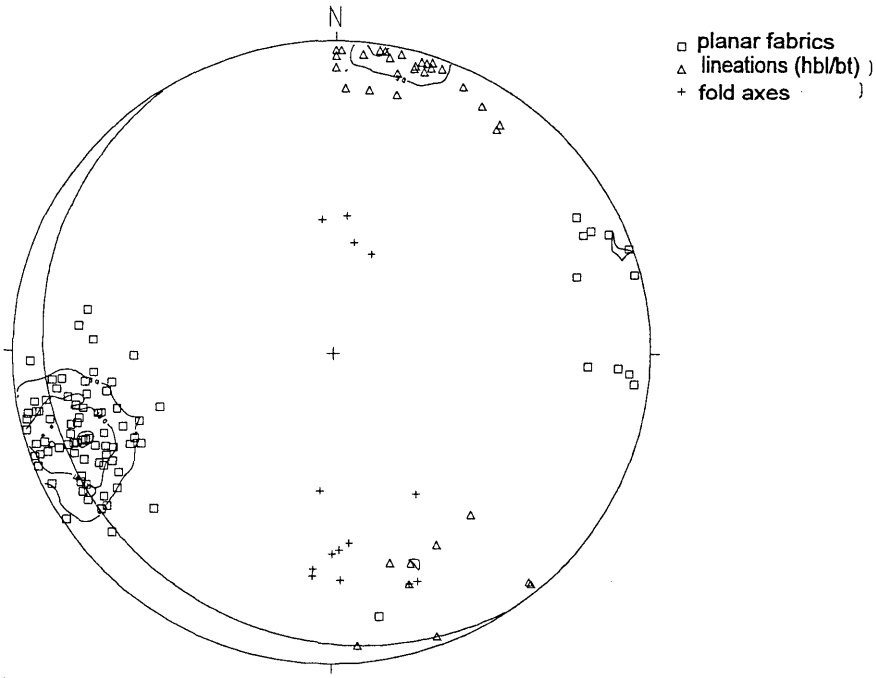

Figure 11.10: Poles to mineral foliations, mineral lineations and fold axes measured in the Chimoio Granodioritic Gneiss.

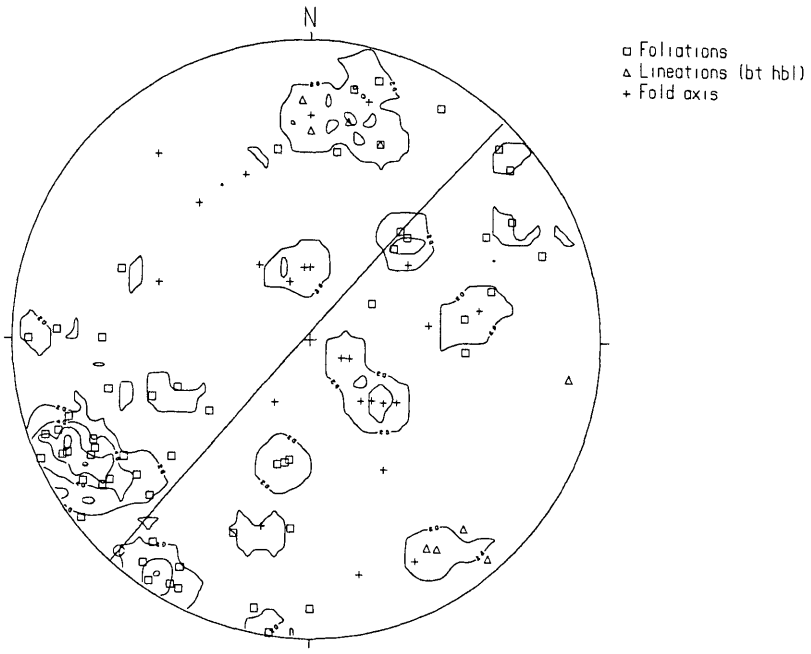

Figure 11.11: Poles to mineral foliations, mineral lineations and fold axes measured in the Tchinhadzandze Granodiorite Gneiss.

11.3 Conclusions

The study area is characterized by structures pertaining, on one hand, to the cratonic Granite-Greenstone Belt and structures pertaining to the Mozambique Metamorphic Province, on the other hand. Structures from the cratonic belt are not traceable into the Mozambique belt. This may suggest that the two belts may have been affected by different deformational episodes.

Within the greenstones, D_1 involved the development of planar fabrics parallel to primary layering which resulted in S_o and S_1 having similar orientation. A latter D_2 folded these planar fabrics about axes plunging shallowly (~30°) to the E suggesting a N-S compression and the steep mineral lineations with plunges towards ESE suggesting a dip-slip movement in an ESE-WNW direction.

Away from the craton, the structures become more complex as one progresses towards E. Thus, within the area underlain by the Messica Granite Gneiss and the Frontier Formation, planar fabrics have strikes essentially oriented N-S and steep dips to E and W. In the Frontier Formation the planar foliations are sub-parallel to primary layering.

Within the Mozambique Belt, two deformational episodes are recorded in the Vanduzi Migmatite Gneiss, east of Messica Granite Gneiss. D_1 is associated with development of planar fabrics parallel to primary layering and the development of planar leucosomes with strikes oriented E-W and steep to moderated dips towards N and S. D_2 folded these planar fabrics about axes that plunge ~45° towards N in a E-W compressional movement and is associated with the development of second stage planar

leucosomes. Towards the E, within the area underlain by the Nhansipfe Granitic Orthogneiss, the planar fabrics are highly variable but show a high concentration with N-S strikes. Present data suggest that the wide range of foliation may be associated with the existence of the two generations of leucosome development because away, in the Chimoio Granodioritic Gneiss the planar fabric have strikes with essentially NNW-SSE orientation. The steep planar fabrics associated with the shallowly to moderately plunging mineral lineations and fold axes in the Chimoio Granodiorite Gneiss, suggests the occurrence of strike-slip deformation.

Chapter 12

METAMORPHIC HISTORY

12.1 Introduction

Petrographic, geothermobarometric and thermochronologic data are used to constrain the metamorphic history of the study area. The area can be subdivided into a low grade metamorphic terrain and a medium- to high grade metamorphic terrain. The low grade terrain includes rocks belonging to the Archaean Greenstone Belt, the Vumba Granite Gneiss and the Early Proterozoic Messica Granite Gneiss. The medium- to high-grade terrain contains rocks of the Mid-to Late Proterozoic Frontier Formation, Vanduzi Migmatite Gneiss, Chimoio Granodioritic Gneiss and the Nhansipfe Granitic Orthogneiss and the Mafic Intrusions.

12.2 Metamorphism

12.2.1 Low Grade Terrain

The rocks in the Manica Greenstone Belt are characterized by a mafic to ultramafic suite containing chlorite+carbonate+serpentine+talc+tremolite+magnetite and a pelitic suite characterized by the quartz+sericite+chloritoid+chlorite+andalusite+fuchsite. Temperatures and pressures of metamorphism were constrained using Figures 3.10 and 3.11 which show that the mineral assemblage above are stable below 500 °C at 2 kbar. The coexistence of carbonate (dol) mostly+talc+serpentine in some samples (eg. mc, scg, 8) suggests that the fluid phase during metamorphism was a mixture of H_2O and CO_2 with $XCO_2 < 0.14$ which is characteristic of low grade or greenschist metamorphism. In the pelitic association, the occurrence of andalusite constrains the pressures of metamorphism below 3.8 kbar and temperatures above 400 °C below which pyrophyllite would be stable. The occurrence of chloritoid suggests temperatures below 525 °C above which it would be replaced by staurolite (Yardly, 1989, p. 86) (Figure 3.12).

Considering the intercalated nature of the pelitic and mafic to ultramafic schists, their combined mineral assemblages suggest P-T conditions of between 400-500 °C, 3.8 Kbar and mixed H_2O-CO_2 with $XCO_2<0.14$, typical of low grade or greenschist facies metamorphism. The occurrence of chloritization, saussuritization, as well as sericitization in the granitoids provides evidence of hydration reactions at low grade. The mineralogical assemblages dominated by Plg+Cpx+Act+Chl+Ep in the mafic intrusions within the Granite-Greenstone Belt are characteristic of basic rocks that have undergone low grade metamorphism of greenschist facies to greenschist-amphibolite transition facies (Bucher and Frey, 1994, p. 263, 273) (Fig. 9.7). The P-T diagram in this figure displays prograde metamorphic evolution of mafic rocks at various geotherms which is represented by chemographic ACF diagrams. The mineral assemblage of the mafic intrusions in Manica is compatible with chemographies 3 to 5.

12.2.2 Medium to High Grade Terrain

High grade rocks occur towards the E of the Granite-Greenstone Belt where the main outcrops are located in the Garuzo-Messica and Mombeza areas (Fig. 2.2). The mineral association include Plg+K-fld+Hbl+Bt, Plg+K-fld+Bt+Grt and Plg+K-fld+Hbl+Bt+Grt in the granitoids and migmatites and Plg+Hbl+Grt±Ilm, Plg+Hbl+Cpx and Plg+Hbl+Cpx±Opx+Grt in the mafic intrusions and enclaves. In the pelitic schist and quartzite of the Frontier Formation in Garuzo and Chimezi the assemblages are Qtz+Bt+Sil+Grt+Ms and Qtz+Sil+Ky+M respectively. In the pelitic schist the assemblage (Bt+Sil+Grt) in presence of quartz and muscovite (Fig.5.5) is typical of upper medium- to high-grade metamorphism (Winkler, 1974, p. 216) or upper amphibolite facies (T=~680 °C; P=~8 kbar) (Bucher and Frey, 1994, p. 273, 279). The application of computer program of Powell and Holland (1988) using present study data, gives a Ky-And-Sil triple point of P=~4.9 kbar and T=~582 °C. In the granitoids the mineral associations with garnet are typical of medium grade metamorphism and in the study area typically occur in the megacrystic granite. In the other granitoids the medium- to high grade metamorphism is supported by the occurrence of bands of partial melts associated with the gneisses. Their nature defines the migmatite gneiss as high grade terranes which in the present study is supported by the presence of garnet in the bands of leucosome supporting the occurrence of metamorphism at high grade. The associations Plg+Hbl+Grt±Ilm, Plg+Hbl+Cpx and Plg+Hbl+Cpx±Opx+Grt in the mafic intrusions and inclusions are characteristic of basic rocks that have been subjected to medium- to high-grade metamorphism (Bucher and Frey, 1994, p. 273, 279) (Fig. 9.7) and P-T conditions are constrained at ~5-8 kbar and ~750-800 °C.

12.3 Thermobarometry

12.3.1 Introduction

Sampling localities as well as sample coordinates are shown in Figure 2.2 and Appendix 1 respectively. Where applicable, the following activities and mineral formula recalculations models were used for the purpose of thermobarometry. Clinopyroxene and orthopyroxene activities were calculated after Wood and Banno (1973), garnet activities after Berman (1990), amphibole end-members activities after Kohn and Spear (1989, 1990) and plagioclase activities after Fuhrman and Lindsley (1988). The mineral formula and cation site allocations in amphibole and pyroxenes were determined using a MINPET 2.02 program. The analytical data used for the thermobarometry are summarized in Table 12.1 and complete microprobe data are shown in Appendix 2. The thermobarometric results are presented in Figures 12.1, for Garuzo-Chibata area (curves 1 to 5) and 12.2, for Mombeza area (curves 6-21). The data used for the construction of curves in this figure are given in Table 12.2 together with other thermobarometric data.

Table 12.1: Summary of analytical data used in thermobarometry.

Amphiboles

Sample	Maamp	Maamp	Maamp	Maamp	mxc	mxc	mbamp	mbamp	mbamp
Analysis	11	14	18	20	6	9	15	45	46
SiO_2	48.72	49.22	49.07	47.75	41.72	42.33	42.01	42.17	42.18
TiO_2	0.84	0.74	0.81	0.94	2.1	1.95	2.21	1.93	2.09
Al_2O_3	7.37	7.44	7.54	8.36	10.49	10.46	11.9	12.22	11.99
FeO	16.27	16.82	16.49	16.84	22.05	21.86	21.09	20.37	20.4
MnO	nd	nd	0.13	0.17	0.14	0.1	0.14	0.12	0.14
MgO	11.14	11.45	11.16	10.65	6.76	6.88	7.85	8.13	8.17
CaO	11.74	11.63	11.71	11.61	11.51	11.44	11.22	11.36	11.2
Na_2O	0.94	0.99	0.82	1.17	1.39	1.23	1.62	1.63	1.68
K_2O	0.59	0.53	0.56	0.64	1.39	1.5	ND	ND	ND
Si	7.192	7.183	7.192	7.05	6.468	6.529	6.38	6.387	6.395
[4]Al	0.808	0.817	0.808	0.95	1.532	1.471	1.62	1.613	1.605
[6]Al	0.473	0.462	0.493	0.503	0.383	0.429	0.509	0.566	0.536
Ti	0.093	0.081	0.089	0.104	0.245	0.226	0.252	0.22	0.238
Mg	2.451	2.491	2.438	2.344	1.562	1.582	1.777	1.836	1.847
Fe2+	2.009	2.053	2.021	2.079	2.859	2.82	2.461	2.378	2.379
Mn	0	0	0.016	0.021	0.018	0.013	0.018	0.015	0.018
sum oct	5.026	5.087	5.057	5.051	5.067	5.07	5	5	5
Ca	1.857	1.818	1.839	1.837	1.912	1.891	1.826	1.844	1.82
Na[M4]	0.117	0.095	0.103	0.111	0.02	0.04	0	0	0
Na[A]	0.152	0.185	0.13	0.224	0.398	0.328	0.477	0.479	0.494
K	0.111	0.099	0.105	0.121	0.275	0.295	0	0	0
Sum_A	0.263	0.284	0.235	0.344	0.673	0.623	0.477	0.479	0.494
Sum_cat	15.263	15.284	15.235	15.344	15.673	15.623	15.538	15.54	15.539

Garnets

Sample	Analysis	XGrs	XAlm	XPy	XSps
gcmx	5	0.039	0.872	0.059	0.03
gcmx	9	0.044	0.871	0.055	0.031
MaAmp	12	0.238	0.619	0.121	0.022
MaAmp	2	0.229	0.635	0.112	0.024
MaAmp	20	0.203	0.648	0.124	0.024
MaAmp	9	0.229	0.633	0.111	0.027
mxc	3	0.19	0.675	0.104	0.031
mxc	5	0.197	0.666	0.108	0.029
mxc	8	0.195	0.664	0.11	0.031
mbamp	21	0.197	0.646	0.122	0.034
mbamp	22	0.196	0.647	0.125	0.033
mbamp	33	0.206	0.641	0.123	0.03
mbamp	34	0.206	0.639	0.124	0.032
mbamp	15	0.202	0.66	0.107	0.031
mbamp	12	0.198	0.657	0.117	0.028
mbamp	11	0.204	0.653	0.114	0.03
mbamp	45	0.207	0.657	0.102	0.035
mbamp	46	0.196	0.642	0.127	0.035

Orthopyroxenes

sample	Analysis	XWo	XEn	XFs	XJd	XAe
mbamp	33	0.01	0.41	0.58	0	0

mbamp	34	0.01	0.4	0.58	0	0

Clinopyroxenes

sample	Analysis	XWo	XEn	XFs	XJd	XAe
mbamp	21	0.45	0.3	0.25	0.04	0
mbamp	22	0.45	0.3	0.24	0.04	0
mbamp	11	0.44	0.3	0.26	0.04	0
mbamp	12	0.44	0.3	0.26	0.04	0

Ilmenites

Sample	Analysis	Mineral	Ti	Fe2	Mn	Mg
mxc	7	ilm	4.037	4.332	0.03	0.06
mxc	8	ilm	4.013	4.325	0.04	0.07

Plagioclases

Sample	Analysis	XAb	XAn	XOr
MaAmp	12	0.46	0.53	0.01
MaAmp	5	0.47	0.52	0.01
mbamp	13	0.6	0.38	0.02
mbamp	41	0.61	0.37	0.02
mbamp	43	0.59	0.4	0.02

ND- not determined and nd- not detected.

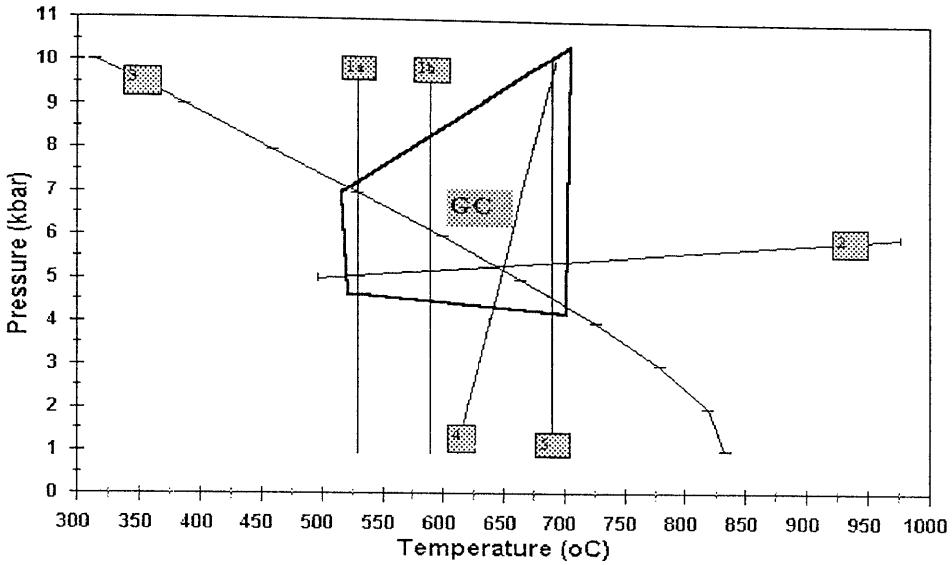

Figure 12.1: Thermobarometric results of mafic dykes and inclusions from the Garuzo-Chibata area, within the Mozambique Metamorphic Province. The prevalent P-T conditions are indicated by the polygon GC.

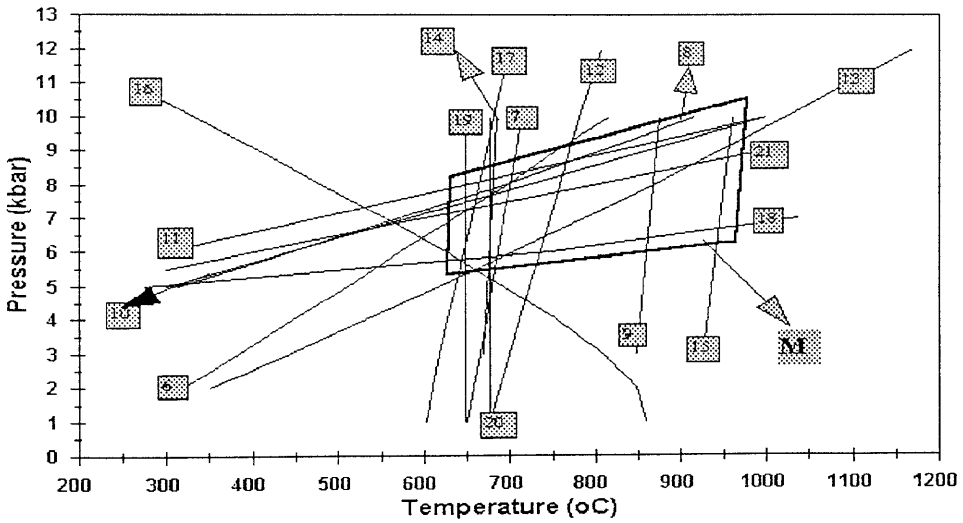

Figure 12.2: Thermobarometric results of mafic dykes from the Mombeza area, east of Chibata, within the Mozambique Metamorphic Province. The prevalent P-T conditions are indicated by the polygon M.

Table 12.2: Results of thermobarometric calculations.

Curve	Sample	Assemblage	T(°C)	P(kbar)
1a	maamp	Grt-Hbl*	529.09	5.1-8.08
1b	"	Grt-Hbl**	589.34	5.52-8.32
2	"	Hbl-Plg-Grt-Qtz	497-976	5-6
3	"	Hbl-Plg-Grt-Qtz	314-833	1-10
4	"	Hbl-Plg-Grt-Qtz	612-692	1-10
5	mxc	Grt-Hbl	690	1-11
6	Mbamp	Alm-Gr-Qtz-An-Hed	319-816	2-10
7	"	Di-Alm-Hed--Py	651-714	1-10
8	"	Py-Gr-Qtz-An-Di	314-917	5-10
9	"	Grt-Cpx	848-876	3-10
10	"	Grt-Cpx-Plg	300-1000	5-10
11	"	Grt-Cpx-Plg	300-1000	6-10
12	"	Hed-En-Alm-Di-Fs-Py	677-806	2-12
13	"	Hed-Alm-Qtz-An-Fs	352-1170	2-12
14	"	Cpx-Opx	670-685	3-10
15	"	Opx	927-961	3-10
16	"	An-Hbl-Py-Gr-Qtz-	256-859	1-11
17	"	Hbl-Alm-Py	602-699	1-12
18	"	Alm-Gr-Qtz-An-Hbl	275-1038	5-7
19	"	Grt-Hbl	648*	1-10
20	"	Grt-Hbl	676**	1-10
21	"	Grt-Hbl-Plg-Qtz	300-1000	5.5-9
	"	Grt-Hbl-Plg-Qtz	300-1000	5.27-10.58
	"	Grt-Cpx-Plg	300-1000	6.02-11.41
	"	Opx	906.23-977.72	
	"	CpX-Opx	635.91-684.69	8.10-12.36
	"	Grt-Cpx	833.13-852.74	3.97-9.37
	"	Grt-Hbl	676.79	5.53-9.13
	"	Grt-Hbl	648.05	5.68-9.00
	mxc	Grt-Hbl	620.34-688.84	5.5-9.22
	mxc	Grt-Ilm	610-645.6	5.41-8.64
	mbamp	Cpx-Plg-Qtz	300-1000	12.2-9

Curves 1-21 were used in the in the construction of the diagram of Figure 12.1. Shown also are other calculated thermobarometric data which were not used in the construction of the curves. *- determination after Perchuck *et al.* (1985); **- calculation after Graham and Powell (1984).

12.3.2 Thermometry

The mineral assemblages used for thermometry in present study include garnet-amphibole, garnet-ilmenite, garnet-clinopyroxene and clinopyroxene-orthopyroxene. Samples maamp, mxc and mbamp contain garnet and hornblende in apparent textural equilibrium and are, therefore, suitable for garnet-hornblende thermometry. The compositions of these minerals were used to estimate the temperatures applying the Graham and Powell (1984) and Perchuck *et al.* (1985) geothermometer calibrations.

In general the Perchuck *et al.* (1985) geothermometer gave relatively lower temperatures in comparison with the Graham and Powell (1984) geothermometer and were, therefore, used for the estimations of minimum temperatures. The thermometry results suggest that a temperature of between ~530 °C and ~570 °C (obtained from assemblages in sample maamp) and between ~620 °C and ~690 °C (estimated from sample mxc) prevailed during the metamorphism in areas around Garuzo-Messica

and Chibata (Fig. 2.1). In Figure 12.1 curves 1a and 1b are plotted using the lower and the higher temperatures obtained using both geothermometers for sample maamp, and curve 5 is plotted using the value from Graham and Powell (1984) for the sample mxc. Thermometry using compositions from sample mbamp from Mombeza area, in the east (Fig.12.2) yield temperature estimates between ~650 °C (curve 19) (Perchuck *et al.* 1985) and ~680 °C (curve 20) (Graham and Powell, 1984) which are higher than those from sample maamp but lower than those from sample mxc.

The sample mxc contains garnet and ilmenite and, therefore, is suitable for Grt-Ilm thermometry. Grt-Ilm geothermometers calibrated by Pownceby *et al.* (1987) and Pownceby *et al.* (1991) yield temperature estimates of ~640 °C and ~615 °C respectively which are slightly lower than those obtained using the Grt-Hbl geothermometer.

The sample mbamp contains the additional suitable assemblages Grt-Cpx, Grt-Opx, Cpx-Opx which were used to estimate the metamorphic temperatures. For the assemblage garnet+clinopyroxene, the Grt-Cpx geothermometer of Sengupta (1989) was used for temperature estimates and gave values between ~830 and ~880 °C whereas for clinopyroxene+orthopyroxene assemblage, the Cpx-Opx and Opx geothermometers of Brey and Kohler (1990) were applied and yielded values of ~670 °C to ~685 °C and ~910 °C to ~980 °C (Table 12.2) respectively. The Cpx-Opx estimates are only slightly higher than those obtained using Grt-Cpx geothermometers whereas the Opx estimates are the highest temperature estimates within the study area. In Figure 12.2, the Grt-Cpx geotherm of 848 °C-876 °C is plotted as curve 9 whereas that of Opx is plotted as curve 15. It is worth mentioning that the curves of these two geothermometers are concordant with the reaction geothermometers (curve 7) containing the assemblages, suggesting that these geothermometers are built up on the same equilibria and are, therefore, reliable temperature estimators.

12.3.3 Barometry

The assemblages used for barometry include garnet-amphibole-plagioclase-quartz, garnet-clinopyroxene-plagioclase and clinopyroxene-plagioclase-quartz. The equilibrium reactions comprising these assemblages were calculated using the computer program THERMOCALC (Powell and Holland, 1988). This program requires the knowledge of minerals end-members activities, which were computed as specified earlier.

For the garnet-amphibole-plagioclase-quartz assemblage, three intersecting reactions were calculated, namely, 9An+6Hbl->8Py+7Gr+15Qtz+H_2O (curves 3, 16), 3Hbl+4Alm->FHbl+4Py (curves 4,17) and 8Alm+7Gr+15Qtz+6 H_2O->An+6Fhbl (curves 2, 18). P-T conditions for the intersecting points are similar, being P=5.2 kbar and T=649 °C and P=5.7 kbar and T=643 °C in samples maamp (Fig. 12.1) and mbamp (Fig. 12.2) respectively. Pressure estimations for the assemblage garnet-amphibole-plagioclase-quartz were done according to Kohn and Spear (1989,1990). Although all samples (mxc, maamp and mbamp) contain the appropriate mineral assemblages, only the compositions of minerals from sample mbamp satisfied the compositional parameters set out in Kohn and Spear(1989,1990). The pressure estimates are ~6.0 kbar for T=300 °C and ~9 kbar for T=1000 °C. These data are plotted in Figure 12.2 as curve 21. The sample mbamp

also contains the assemblages garnet-clinopyroxene-plagioclase and clinopyroxene-plagioclase-quartz, and is, therefore, adequate for Grt-Cpx-Plg and Cpx-Plg-Qtz barometry. Using the computer program THERMOCALC (Powell and Holland, 1988), three intersecting reactions (at P=8 kbar and T=700 °C), two of which containing this assemblage, were determined, namely, Alm+2Gr+3Qtz->An+3Hed (curve 6), Py+2Gr+3Qtz->3An+3Di (curve 8) and 3Di+Alm->3Hed+Py (curve 7) (Fig.12.2).The Grt-Cpx-Plg geobarometer after Eckert *et al.* (1991) (curve 10) suggests pressures of ~5 and ~10 kbar for 300 and 1000 °C respectively, and that of Powell and Holland (1988) (curve 11) suggests similar pressures of ~6 and 10 kbar for the same temperatures. Estimations from Cpx-Plg-Qtz after Ellis (1980), however, provide values of ~12 kbar for T=300 °C and ~9 kbar for T=1000 °C (Table 12.2). From the Figure 12.2 it can be seen that curves 11 and 10 are convergent at high temperatures. The geobarometer almost cut through the intersection point suggesting, consequently, that it may be a good pressure estimator.

In conclusion, the thermobarometric study suggests an increase in P-T conditions during metamorphism within the Mozambique Metamorphic Province, from Garuzo-Chibata to Mombeza of ~5 to ~10 kbar and ~530 to ~980 °C.

12.3.4 Discussion of Petrographic and Thermobarometric Results

Estimations of P-T conditions in the low grade terrain are entirely constrained, using petrographical data, at between 400 and 525 °C and ~4 kbar. Petrographical data within the medium- to high-grade terrain constrain P-T conditions at P=~5 -~8 kbar and T= ~580 -~800 °C. Thermobarometry suggests P-T conditions of ~5 -~10 kbar and ~530 -~980 °C, a bracket which contains the estimations from petrography.

It can be concluded that the study area records a metamorphic history characterized by an increase in P-T conditions from the low-grade greenschist facies metamorphism in the W to the high-grade amphibolitic-granulite facies metamorphism in the E.

12.4 Thermochronology

12.4.1 Introduction

Thermochronological investigations were undertaken using the $^{40}Ar/^{39}Ar$ step heating method in 6 samples from the Vumba Granitoid Gneiss (V Gr2/P and Vgr-3b), the Messica Granite Gneiss (Pd Gr/P), the Chimoio Granodioritic Gneiss (Cv1 Gr/P), the Nhansipfe Granitic Orthogneiss (Nfg/P) and in quartzite from the Frontier Formation (Ch Qtz). Sample locations are shown in Fig. 2.2 and the co-ordinates in Appendix 1.

The step heating method is based on the formation of ^{39}Ar from neutron irradiated ^{39}K-bearing samples and give dates that are calculated from measured $^{40}Ar/^{39}Ar$ ratios. By using the incremental heating technique several dates can be obtained from a single sample by counting the released argon from it in steps of increasing temperature (Berger and York, 1981; Faure, 1986). Like any other radiogenic method, this one is also sensitive to any loss or gain of radiogenic argon because excess argon may give rise to older dates whereas the loss of argon will yield younger ages. In a closed

system, step heating should give rise to plateaus of identical dates and at least 50% of these plateaus should be present for the dates to be considered reliable ages. The ages thus obtainable are mineral closure ages and the method is applicable to dating K-bearing minerals such as biotite, muscovite, hornblende, K-feldspar and plagioclase. Because closure temperatures of these minerals are known, or can be obtained, ultimately the method gives data that can be used for the construction of temperature-time loops. Closure temperatures of the argon system in biotites are estimated at ~350 - ~400 °C (Berger and York, 1981) and in muscovites at ~350-~400 °C (Mezger, 1991).

For the purpose of present study, muscovite separates were extracted from the quartzite (ChQtz) whereas biotite separates were extracted from the granitoids. Samples Vgr2/P and Vgr-3b from the Archaean Vumba Granite Gneiss were selected with the aim of obtaining information on possible mineral resetting due to the Mozambique and Pan-African orogenies. For the younger Mozambique Belt granite gneisses and metasediments of the Frontier Formation, we seek information on possible later orogenies including the Pan-African. The laboratory investigations were conducted by Dr. P. Guise at the Department of Earth sciences, University of Leeds, Leeds, U. K. and the results are presented in Table 12.3 and the diagrams are shown in Figures 12.(A-F).

12.4.2 Discussion of Results

Diagrams in Figs 12.A and 12B show that the plateaus are characterized by weak fluctuations at just above 1000 Ma but no consistent plateaux were obtained. The total gas ages are 1084±4 Ma and 1067±4 Ma respectively and their similarity suggest that they are due to the same geological process. Argon data yield similar mineral resetting ages of 535±2.5 Ma and 558±2.5 Ma respectively in the Early Proterozoic Messica Granite Gneiss and in the Middle Proterozoic Chimoio Granodiorite Gneiss (Figs. 12.C and 12.D) and suggests that this mineral resetting was caused by the same geological event. Argon counts in the diagrams of Figures. 12.E and 12.F yield similar mineral resetting ages of 467±2 Ma and 468±2.7 Ma respectively in the Late Proterozoic Nhansipfe Granitic Orthogneiss and in the possible allochthonous Frontier Formation suggesting that the two units were affected by the same thermal process. It is significant that these younger ages are coincident with areas which have strong planar N-S fabrics. This suggests a degree of young re-activation along these zones.

Similarities between the mineral resetting ages in the Archaean granitoids and age of emplacement of the Nhansipfe gneisses of ~980±83 Ma suggest that the heat that caused the mineral resetting in the Archaean granitoids was possibly derived from the intrusion of Nhansipfe Granitic Orthogneiss. The ages in the metasediments and younger granitoids are consistent with the Pan-African orogeny time span of about ~550 Ma -~450 Ma. The age difference of about ~100 Ma observed in these units is geologically significant and suggests the occurrence of a localized thermal process at about ~460 Ma. This event is supported by the occurrence of a zone of extensive migmatites in the area (Fig. 2.1) and the intrusion of the syn-to post-tectonic Tchinhadzandze Granodiorite Gneiss.

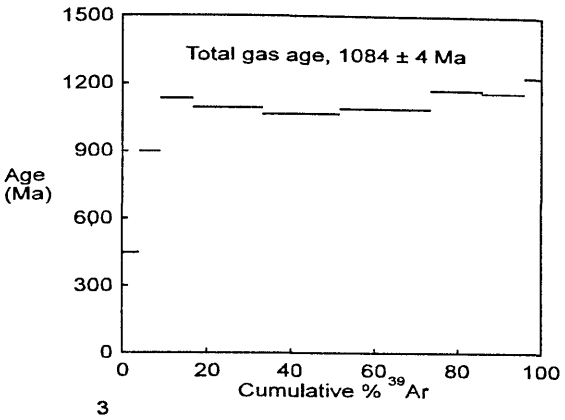

3

Figure 12.A: Cumulative Ar versus age diagram of Vumba granitoids.

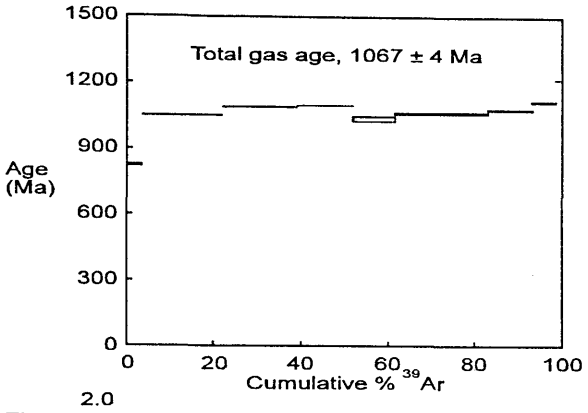

2.0

Figure 12.B: Cumulative Ar versus age diagram of Vumba granitoids.

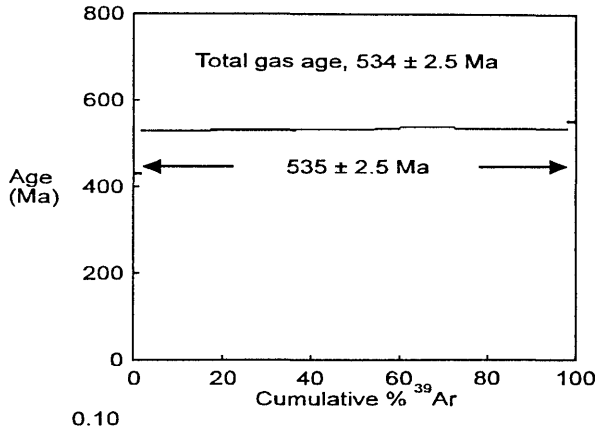

0.10

Figure 12.C: Cumulative Ar versus age diagram of Messica granitoids.

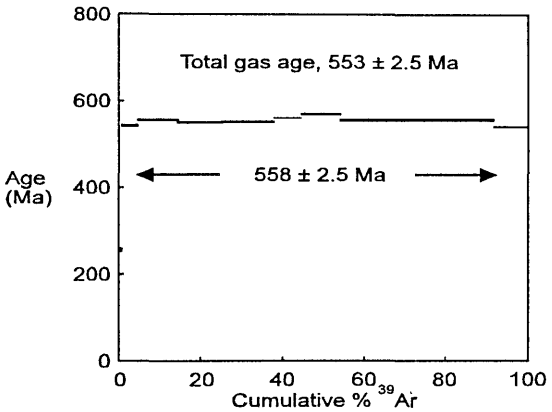

Figure 12.D: Cumulative Ar versus age diagram of Chimoio granitoids.

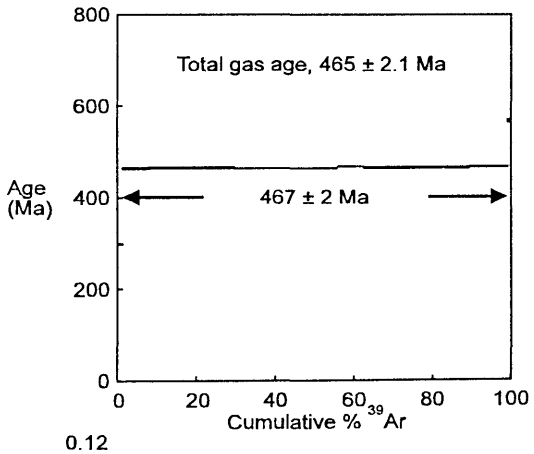

0.12

Figure 12.E: Cumulative Ar versus age diagram of Nhansipfe granitoids.

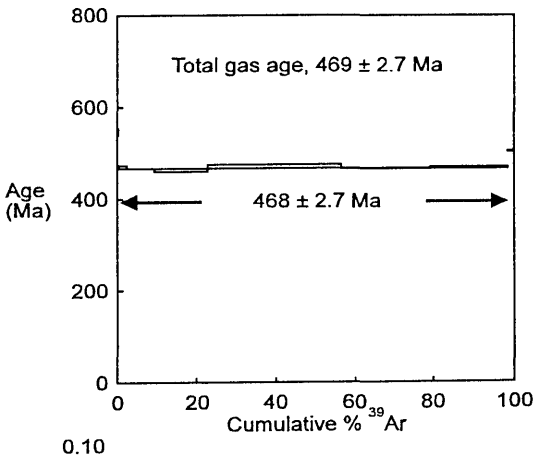

0.10

Figure 12.F: Cumulative Ar versus age diagram of the Frontier Formation quartzite.

Table 12.3: Thermochronological data of various lithological units.

Lithological unit	Mineral	Age (Ma)	Closure temperature (°C)
Barue Group	biotite	425±20[a]	350-400
Frontier Formation	muscovite	465±20[a]	"
Nhansipfe Granitic Orthogneiss	biotite	467±2	"
Frontier Formation	muscovite	468±2.7	"
Gairezi Group	biotite	526±30[a]	"
Messica Granite Gneiss	biotite	535±2.5	"
Chimoio Granodioritic Gneiss	biotite	558±2.5	"
Vumba Granite Gneiss	biotite	1067±4[b]	"
Vumba Granite Gneiss	biotite	1084±4[b]	"

([a]) after Vail(1965), ([b]) total gas age. Biotite and muscovite closure temperatures after Berger and York (1981) and Mezger (1991) respectively.

In conclusion, mineral resetting investigations by the $^{40}Ar/^{39}Ar$ method suggest that the Archaean Vumba Granite Gneiss was affected by a thermal event at about the same time the Nhansipfe Granitic Orthogneiss was intruded. Younger thermal events did take place between ~460 Ma and ~550 Ma in the Mozambique Belt, with the youngest thermal events only affecting a very localized zone, possibly in response to a later Pan-African related heating event. Closure temperatures of the systems are estimated at ~350-400 °C. The calculated mineral resetting ages are similar to those determined by K/Ar method in muscovite from quartzite of Frontier Formation in Chicamba (465 ± 20 Ma) within the study area, in biotite from gneiss (425 ± 20 Ma) and schist (526 ± 30 Ma) within the Barue and Gairezi Groups in Macossa and Gairezi respectively (Vail, 1965), localities which are located reasonably close and are geologically similar to the study area. They are equally correlatable to those determined in Antarctica (Grantham *et al.*, 1988; Grantham *et al.*, 1991 and Grantham *et al.*, 1995). These similarities suggest that the areas were affected by the same thermotectonic events.

12.5 Metamorphic History

The low grade greenschist metamorphism is the oldest metamorphism episode (M_1) overprinted in the study area and is mostly recorded in the Archaean greenstone rocks in the west (Fig. 2.1). The maximum P-T conditions were ~4 kbar and ~525 °C and as a result, low grade mineral paragenesis were formed. As a result of the Kibaran tectonothermal Mozambique Orogenesis during 950 - 1100 Ma (Petters, 1991, p. 15) areas towards the E (Fig. 2.1) were affected by the orogeny which along with deformation, submitted the rocks to medium-high-grade metamorphism (M_2) at P-T conditions of ~5-~10 kbar and ~530 -~980 °C). These P-T conditions did not affect the rocks in the low grade terrane where only mineral resetting is registered at about ~1100 Ma. The third (M_3) metamorphic episode is associated with the Pan-African orogeny which ended at ~450 Ma (Petters, 1991, p. 15: Pinna *et al.* 1993) and resulted in mineral resetting and, possibly, in granitoid emplacement such as the Tchinhadzandze Granodiorite Gneiss.

Chapter 13

SUMMARY OF CONCLUSIONS

13.1 Lithologies

The geology of the study area is essentially the geology of cratons and mobile belts. The cratonic areas are the Archaean Zimbabwe Province dominated by granite-gneisses and greenstone rocks, whereas the Proterozoic Mozambique Metamorphic Province is dominated by granitoids. This structural framework is consistent with the Precambrian geology of Southern Africa (Petters, 1991, p. 5).

The greenstone belt comprises the Macequece and the M'Beza/Vengo Formations. Rock types in the Macequece Formation include talc-chlorite schists, carbonate antigorite fels, quartz-sericite and chloritoid-andalusite schists, gabbroic rocks and felsic to mafic tuffs. The M'Beza/Vengo Formation comprises metaconglomerate, metagreywackes, pelitic schists, locally interlayered with conglomerates, greywackes, shales, mudstones and carbonate lenses. Chemically the mafic to ultramafic schists are peridotitic komatiites. Similar rock types are described in the greenstone belts of South Africa (Viljoen and Viljoen, 1969; Viljoen *et al.*, 1982) and in the greenstone belts of Zimbabwe (Wilson *et al.*, 1978).

The Archaean Vumba Granite Gneiss vary from metaluminous to peraluminous whereas the Early Proterozoic Messica Granite Gneiss is metaluminous. They vary from tonalites throughout the granodiorites to monzogranites and constitute the typical tonalite-trondjhemite-granodiorite (TTG) association common in the Archaean granitoids (Martin, 1987; Clarke, 1992, p. 198). The chemistry of Vumba Granite Gneiss is typical of mantle fractionates whereas that of the Messica Granite Gneiss is typical of a crustal melt. These characteristics are similar to those described in the Barbarton granite suite in South Africa and Swaziland by Viljoen and Viljoen (1969) and Hunter (1973) and in Zimbabwe by Wilson *et al.* (1978).

The Frontier Formation is, possibly, an allochthonous metasedimentary sequence comprising quartzite and pelitic schist units which were metamorphosed to medium grade amphibolite facies. Towards the northwest, the Frontier Formation is thrust over the greenstones. In this area the occurrence of kyanite in the schist suggests higher pressures than those in the underlying andalusite bearing greenschist. Although allochthonous, the Frontier Formation does not overlie the rocks of the Mozambique Metamorphic Province and, consequently could predate the Mozambique Orogeny.

The high grade Vanduzi Migmatite Gneiss is characterized by the development of two stages of leucosomes associated with respective gneissose planar fabrics. Petrographically, the leucosome are a Qtz±Fld±Bt±Hbl variety and a Grt+Qtz+Fld variety.

The Middle Proterozoic Chimoio Granodioritic Gneiss is banded and interlayered with amphibolitic and migmatite gneisses. The mineralogy of the gneiss is characterized by low proportions of quartz and structurally by the combination of zones of steep and shallow fabrics and is metamorphosed to medium grade amphibolite facies. It is metaluminous and has a chemical signature typical of

volcanic-arc granitoids and, consequently, this formation may be compared to the Jutulrora Formation in western H. U. Sverdrupfjella in Antarctica described by Grantham *et. al.* (1995) and Grantham *et al.* (1997).

The megacrystic A-type and Late Proterozoic Nhansipfe Granitic Orthogneiss has undergone metamorphism to medium grade amphibolite facies and local tectonic grain size reduction. The fact that partial melting is seen in these gneisses shows that they have been metamorphosed to high-grade but now have medium-grade assemblages. Mafic boudins included in this gneiss, preserve high grade granulite assemblages. The gneisses vary chemically from metaluminous to peraluminous and have had some trace elements redistributed by metasomatism which result in its plotting as anomalous granite in the classification diagram of El Bouseilly and El Sokkary (1975). These megacrystic gneisses may be similar to the Kirwanveggen Megacrystic Orthogneiss in the Dronning Maud Land , Antarctica (Grantham *et al.*, 1995).

The mafic rocks intruding rocks of the granite-greenstone belt are metamorphosed to greenschist facies and preserve an igneous texture whereas the mafic dykes intruding rocks of the Mozambique Metamorphic Province are metamorphosed to medium to high grade amphibolite up to granulite facies, and record granoblastic metamorphic textures and planar fabrics oriented N-S. Despite their differences in terms of petrography and the crust they intrude, the mafic rocks are chemically similar, being subalkaline and tholeiitic and have chemical signatures typical of ocean floor basalts. The mafic intrusions in Jutulrora, mainly, and Brekkerista and Roerkulten in Antarctica comprise N-S deformed and undeformed dykes (Grantham *et al.* 1988), with the metamorphosed ones having a Plg+Hbl+Grt amphibolite facies paragenesis and a planar foliation defined by oriented hornblende and biotite, resulting in these dykes being similar to the dykes within the Mozambique belt.

The Tchinhadzandze Granodiorite Gneiss comprises syn-to post-tectonic plutons that have undergone retrogressive hydration reactions. It is metaluminous and has a chemical composition typical of volcanic-arc tectonic setting. Late- to post-tectonic granites are described in the Dronning Maud Land, Antarctica. The Dalmantian Granite (Grantham *et al.*, 1991) is one of the best known. However, the chemistry and genesis of this granite as described by Grantham *et al.* (1991) differs from the Tchinhadzandze Granodiorite Gneiss in that the former is a typical S-type granite with SiO_2 contents of ~73-~75 wt%, is biotite-muscovite bearing, forms sheet-like sills commonly parallel to layering and has Rb, Nb and Y contents typical of syn-collisional granites.

13.2 Deformation

The planar structures in the Archaean granite-greenstone belt are dominantly oriented E-W whereas in the Mozambique Metamorphic Province are E-W and N-S.

In the greenstones two deformation episodes are recognized, namely D_1 associated with the development of an S_1 foliation parallel to the S_0 primary layering, and D_2 which folds these fabrics about axes which plunge shallowly to the east implying a N-S compression. Towards the E, in the Messica-Garuzo area, the D_1 episode gave rise to S_1 planar fabrics which are sub-parallel to S_0 primary layering preserved in the metasediments of the Frontier Formation.

Within the Mozambique Metamorphic Province the structures are more complex. Thus, in the Vanduzi Migmatite Gneiss two deformation events are preserved. D_1 produced a more or less E-W striking S_1 planar fabric parallel to S_0 primary layering and the development of leucosomes with similar orientation to the foliation. D_2 deformed the S_0 and S_1 planar fabrics about more or less N-S axes resulting in the development of N-S planar fabrics which include the S_2 foliation and second stage leucosomes. Farther east, within the megacrystic Nhansipfe Granitic Orthogneiss both planar and linear structures have highly variable orientations which possibly record complex deformation processes. In the Chimoio Granodioritic Gneiss the planar fabrics strike N-S and linear fabrics suggest the development of zones of shallow and steep fabrics possibly as a result of oblique strike-slip movement imposed on an earlier shallow dipping fabric. The Tchinhadzandze Granodiorite Gneiss have weak , variable planar and linear fabrics consistent with its syn-to post-tectonic granite nature.

13.3 Metamorphism

The metamorphism in the greenstone reached the low -grade greenschist facies and P-T conditions are constrained at 400-500 °C and <4 kbar. In the granites a later heating is recorded by biotite resetting at ~1100 Ma (Fig. 13.2) and was, possibly, caused by intrusions of granitoids in the Mozambique Metamorphic Province or by Umkondo related mafic intrusions.

The Frontier Formation is characterized by two different metamorphic grades. The block around Garuzo is defined by a paragenesis including Sil+Grt whereas in the block in Chimezi the paragenesis include the higher pressure assemblage Sil+Ky . The medium -grade high pressures assemblage of Sil+Ky in the Chimezi area can be considered anomalous because the Frontier Formation rocks overlie the Manica Greenstone Belt rocks which have a relatively low pressure andalusite-bearing low-grade assemblages. The assemblage Sil+Grt+Bt in the presence of Qtz and Ms in the pelitic schists suggests metamorphic constraints of T=~680 °C and P=~8 kbar typical of medium- to high-grade metamorphism (Winkler, 1974, p. 216). The Early Proterozoic Messica Granite Gneiss, which underlies the Frontier Formation does not record obvious metamorphic mineral growth. This anomaly may, therefore, suggest that the Frontier Formation has been overthrust onto the Archaean granite-greenstone belt and would support the possible allochthonous nature of the unit.

Within the Mozambique Metamorphic Province the metamorphism reached medium- to high-grades whereby higher degrees are registered farther east. P-T conditions are constrained at ~530-~980 °C and
~5-~10 kbar. There is evidence of later thermal processes as is suggested by mineral resetting. The Messica Granite Gneiss and the Chimoio Granodioritric Gneiss record biotite resetting at ~550 Ma significantly different, in terms of geological time, to ~460 Ma recorded by biotite and muscovite resetting in the Nhansipfe Granitic Orthogneisses and the Garuzo Frontier Formation quartzite. This mineral resetting took place in localized zones coinciding with the Messica Granite Gneiss, Vanduzi Migmatitic Gneiss and Nhansipfe Granitic Orthogneiss where strong N-S partial melt bands occurred, suggesting that the partial melts may be a result of same process that caused the mineral resetting.

In conclusion, there is an increase of metamorphic grade from low greenschist facies within the

greenstone belt in the W to medium - to high-grade amphibolitic facies within the Mozambique Metamorphic Province in the E. This, combined with the structural data, can be summarized in Figure 13.1. The figure suggests that the blocks of low (LG), medium (MG) and high (HG) grades are separated from each other by N-S steep zones. The lineations in these steep zones commonly plunge shallowly suggesting that they represent oblique shear zones with combined lateral and vertical displacements.

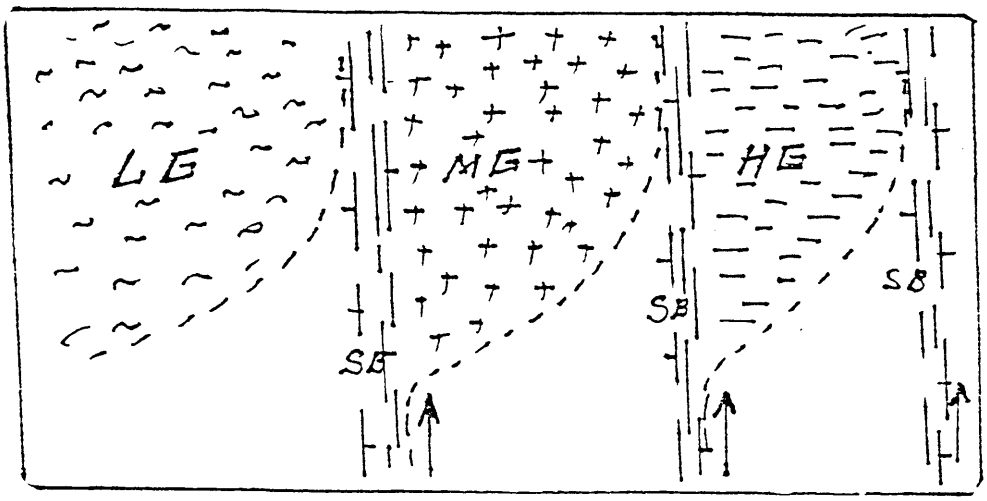

Figure 13.1: Sketch of metamorphic blocks separated by steep zones defining narrow shear belts (SB). LG- block of low grade, MG- block of medium grade and HG- block of high grade. Arrows indicate lateral movement.

Similar deformational and metamorphic conditions as described for the Mozambique belt are observed in Antarctica (Grantham *et al.*, 1988; Grantham *et al.*, 1991; Groenwald *et al.*, 1991; Groenwald, 1993; Grantham *et al.*, 1994; Grantham *et al.*, 1995 and Grantham *et al.*, 1997).

13.4 Isotope Chemistry

The chronological aspects of radiogenic isotope analyses have been discussed in the relevant chapters. This section will consider the implications for the sources of the various granitoids arising from the isotope analyses.

The initial $^{87}Sr/^{86}Sr$ ratios data including those of Manuel (1992) are plotted versus age in the diagram of Figure 13.2. The diagram includes a curve showing the evolution of initial $^{87}Sr/^{86}Sr$ ratios with time in the mantle. The crosses are proportional to the error of either Ro and ages. It can be seen that both the old granites and the Chimoio gneisses have initial $^{87}Sr/^{86}Sr$ ratios close to that of the mantle suggesting their derivation from it. Conversely, the initial $^{87}Sr/^{86}Sr$ ratios of the remaining units are high above the mantle growth curve which suggest that their sources probably had a significant component of older continental crust.

The R_o of ~0.6947 in the ~3400 Ma in the northern Vumba Granitic Gneiss is compatible with the derivation of this gneiss from the mantle (Rollinson, 1993).

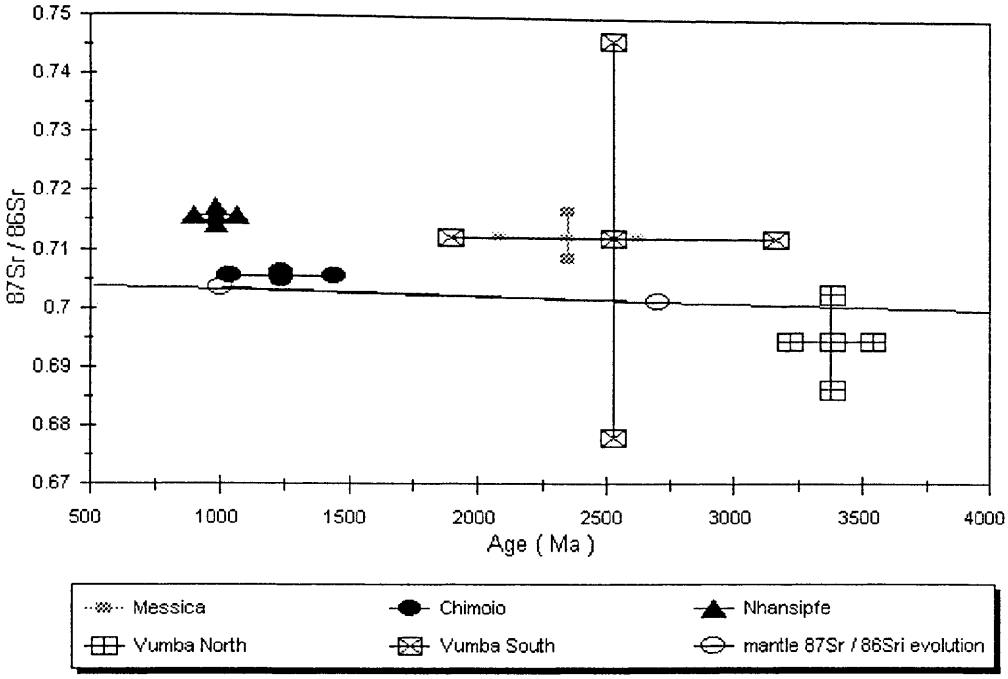

Figure 13.2: Initial $^{87}Sr/^{86}Sr$ ratios versus age of some lithological units. The mantle initial $^{87}Sr/^{86}Sr$ ratios evolution curve is drawn, modified from Rollinson (1993).

The ~2900 Ma non-foliated granite has a R_0 of ~0.7052 (Manuel, 1992) which is very high for the determined age, falling within the limits of subduction related arc-volcanics of 0.7033-0.7095 (Rollinson, 1993), and implies that the magma has been produced from an enriched source. Indistinguishable initial $^{87}Sr/^{86}Sr$ ratios of ~0.7122 and ~0.71241 from the ~2527 Ma granite south of the greenstone (Manuel, 1992) and the ~2347 Ma Messica Granite Gneiss respectively are very high and clearly suggest that their source had high Sr/Rb ratios.

The R_0 of ~0.7056 in the ~1236 Ma Chimoio Granodiorite Gneiss falls within the limits of the arc-volcanic ratios of 0.7033 -0.7095 (Rollinson, 1993) and is consistent with its subduction related arc-volcanic genesis as suggested from geochemistry. The Ro is only marginally higher than the mantle growth curve at the that time suggesting that the Chimoio Granodioritic Gneiss is relatively juvenile.

The R_0 of 0.7157 of Nhansipfe Granitic Othogneiss is compatible with the magma source from an already enriched crust which is consistent with the plate margins of a within-plate tectonic environment of formation of this granite.

13.5 Summary of the Geology of The Study Area and a Comparison with Antarctica

The summary and comparison of the geology are given in Table 13.1 and the temperature-time conditions are shown in Figures 13.3 and 13.4. The table shows that the geology of the study area is so similar to that of Antarctica and that correlations between the two areas are possible. Similarly, for the equivalent period of time, comparison of temperature-time diagrams of the two regions (Fgs. 13.3 and 13.4) show that they experienced similar thermal conditions.

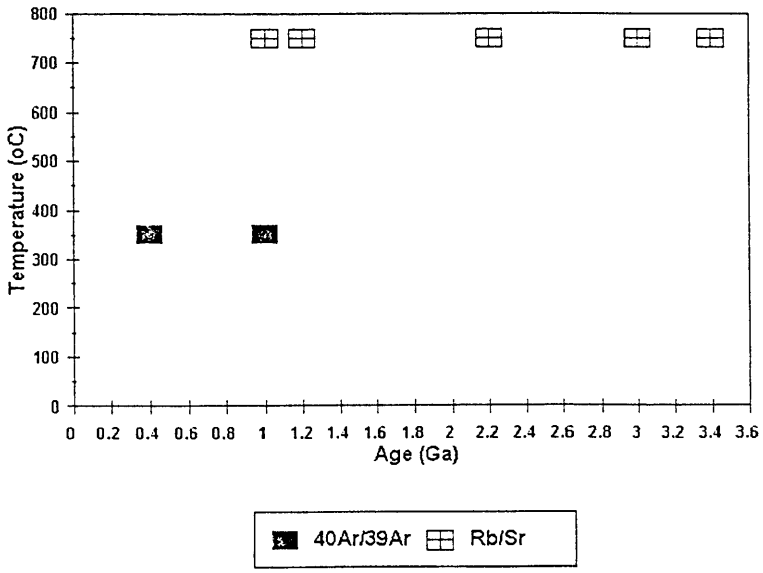

Figure 13.3: Temperature-time diagram for the mineralogical Ar/Ar and whole rock Rb/Sr data determined from the granites and the metasediments in Manica.

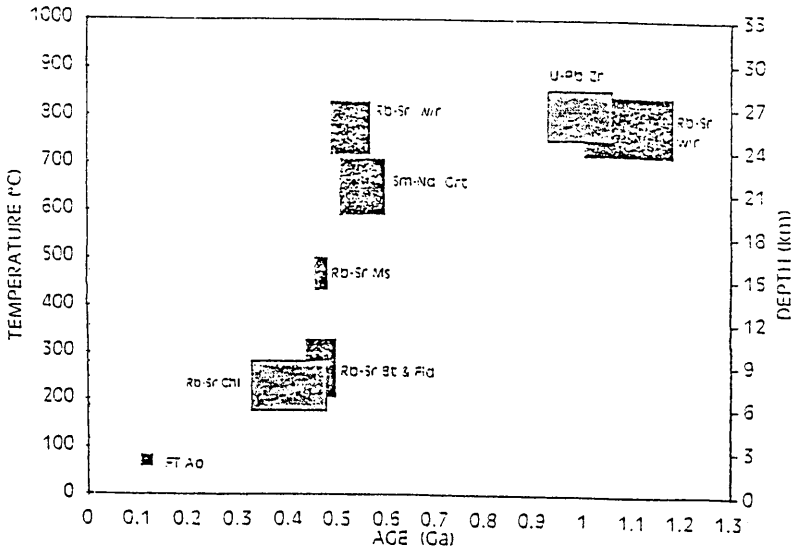

Figure 13.4: Temperature-time diagram for the various mineralogical and whole rock data determined from H.U. Sverdrupfjella. Grt- garnet, Bt- biotite, Chl- chlorite, Ms- muscovite, Zr- zircon and Fld- feldspar; W/r- whole rock; FT- fission track. Diagram reproduced from Grantham *et al.* (1995).

Table 13.1: Summary and comparison of the geologies of study area and Antarctica.

Lithology	Mozambique	Antarctica
	Vumba Granite Gneiss medium to coarse-grained metaluminous Hbl and Bt granodiorite to tonalite gneiss **Manica Greenstones** serpentinites, mafic to ultramafic schist, pelitic schist and felsic schist. **Chimoio Granodiorite Gneiss** medium -grained metaluminous Bt-Hbl quartz feldspathic gneiss **Nhansipfe Granitic Orthogneiss** megacrystic metaluminous to peraluminous Bt+Grt±Hbl quartzo-feldspathic augen gneiss **Mafic Intrusions** N-S oriented medium grained Plg+Hbl+Grt±Cpx±Opx amphibolitic dykes **Syn-to Post Tectonic Intrusions** Thcinhadzandze Granodiorite Gneiss	**Annandagstoppane Granite** medium - to coarse-grained peraluminous Bt tonalitic to granodioritic gneiss (Barton *et al.* 1987). No equivalent exposed **Jutulrora Formation** Ep-Bt-Hbl tonalitic quartz feldspar gneisses (Grantham *et al.*, 1988; Grantham *et al.*, 1995; Grantham *et al.*, 1997) **Kirwanveggen Megacrystic Orthogneiss** Bt±Grt±Hbl quartzo-feldspathic augen gneiss (Grantham *et al*, 1988; Grantham *et al.*, 1995) **Mafic Intrusions** Plg+Hbl+Grt±Cpx±Opx metabasites (Grantham *et al.*, 1988) **Syn-Tectonic Intrusions** Dalmatian Granite (Grantham *et al.*, 1991)

Structural Geology	**In the Archaean Zimbabwe Craton** Early deformation associated with metamorphism in the old granites resulting in their transformation into gneisses. Deformation associated with the greenschist metamorphism which resulted in the N and S moderately dipping, S_1 planar fabrics Deformation associated with the folding of S_1 along an E-W axis **In the Proterozoic Mozambique Metamorphic Province** Deformation associated with E and W moderately and steeply dipping S_1 planar fabrics Deformation associated with the amphibolitic facies metamorphism which resulted in the E and W steeply dipping S_2 planar fabrics which were transposed onto S_1 Deformation associated with the N-S shear zones and linear fabrics trending N and S mostly with shallow to moderate angles	**In the Archaean** Early deformation associated with metamorphism in the old granites resulting in their transformation into gneisses (Barton *et al.*, 1987) no equivalent recognized **In the Proterozoic** Deformation associated with S_1 N-S trending and gently dipping to both east and west planar fabrics Deformation associated with shear zones and folds which deform S_1, shallowly plunging mineral lineation towards 110° and 290°, in Haag Nunataks (Grantham *et al.*, 1997) Deformation associated with the south, mostly, dipping planar fabrics, shallowly plunging lineations towards 110°, in Western Sverdrupfjella (Grantham *et al.*,1988; Grantham *et al.*, 1995) Deformation associated with the southeast east and west dipping planar fabrics Lineations plunging shallowly towards 120° and 130° in Kirwanveggen (G* *et al*, 1988; G* *et al.*, 1991; Grantham *et al.*,1995)

Metamorphic History	**In the Archaean Zimbabwe Craton** Medium grade and retrogressive hydration reactions in the Vumba Granite Gneisses Mineral (biotite) resetting at ~1.1 Ga (Fig. 13.3) Greenschist facies metamorphism in the greenstones **In the Proterozoic Mozambique Metamorphic Province** Medium grade amphibolite facies Mineral (biotite and muscovite) resetting suggest heating at ~470 Ma and ~550 Ma (Fig. 13.3)	**In the Archaean** Medium grade and retrogressive hydration reactions in the Annandagstoppane Granite Gneisses (Barton *et al.*, 1987) mineral resetting at ~1.1-~1.2 Ga (Fig. 13.4) no equivalent recognized **In the Proterozoic** Medium grade amphibolite facies mineral resetting In H.U. Sverdrupfjella data indicate mineral setting at ~450 Ma (Fig. 13.4) (Grantham *et al.*, 1988 ; Grantham *et al.* 1994; Grantham *et al.* (1995)

G*=Grantham.

13.6 Proposed Geological Evolution Model for the Study Area

These data suggest that the geological evolution of the study area comprises:

1- The Emplacement of the Vumba old granitoids (~3300 -~3000 Ma) as mantle derivatives and the consequent formation of an old granitic basement

2- The emplacement of the ophiolitic komatiites from mantle peridotites

4- Deposition of pelitic sediments in a deep still water environment

5- ---------- **Metamorphism (M_1) / Deformation (D_1/D_2)** ----------

Low grade metamorphism to greenschist facies of the komatiites and sediments

retrogressive dehydration reactions in the granitoids

development of schistosity in the komatiites and sediments (D_1)

folding of planar fabrics in the pelitic schist (D_2)

6- Emplacement of Messica Granite Gneiss and Vumba younger granitoids (~2650 -~2350 Ma) from partial melting of the already formed granitic crust

7- ---------- **Cratonization** ----------

Formation of the Zimbabwe Craton

8- Emplacement of the possible allochthonous Frontier Formation

9- ---------- **Subduction related processes / Mozambique Orogeny** ----------

Formation of an island-arc to the east of Zimbabwe Craton (eg. Pinna *et al.* 1993)

Collision of Zimbabwe Craton (ZC) with the island arc which resulted in:

Accretion of the island onto the craton to form the Chimoio Granodiorite Gneiss (~1200 Ma)

Emplacement of the Nhansipfe Granitic Orthogneiss (~1000 Ma)

Metamorphism (M_1)/Deformation (D_1/D_2)

- medium to high grade amphibolite to granulite facies metamorphism (M_1)
- migmatization (Vanduzi Migmatitic Gneiss)
- development of S_1 E-W planar fabrics (D_1)
- development of S_2 N-S planar fabrics (D_2)

9- Intrusion of mafic dykes in an extensional/rifting environment

10- ---------- **Pan-African Orogeny** ----------

Metamorphism (M_2)

- medium to high grade metamorphism and development of second stage leucosomes in the Vanduzi Migmatitic Gneiss

-Syn- to post-tectonic emplacement of Tchinhadzandze Granodiorite Gneiss

REFERENCES

Afonso, R.S., 1978: *Noticia explicativa da Carta Geologica de Mocambique 1:2000 000*, Direccao dos Servicos de geologia e Minas, 191 pp.

Allegre, C. J., Hart, S.R. and Minster, J.F., 1983a: Chemical structure and the evolution of the mantle and continents determined by inversion of Nd and Sr isotopic data, I. Theorethical models. *Earth and Planetary Science Letters*, **66**, 191-213.

Allegre, C. J. and Lewin, E., 1995: Isotopic systems and stirring times of earth's mantle. *Earth and Planetary Science Letters*, **136**, 629 - 646.

Allsop, H.L., Kramers, J.D., Jones, D.L. and Erlank, A.J., 1989: The age of the Umkondo Group, eastern Zimbabwe, and implications for palaeomagnetic correlations. *South African Journal of Geology*, **92**, 11-19.

Araujo, J.R. and Gouveia, J. C., 1965: Contribuicao para o Estudo da Geologia do Distrito de Manica e Sofala. Formacoes Precambricas. *Boletim dos Servicos Geologicos e Mineiros de Mocambique,* **53**, pp. 45 - 60.

Arndt, N.T. and Nisbet, E.G., 1982: What is a komatiite? pp. 19-27. In "*Komatiites*", Arndt, N.T. and Nisbet, E.G. (Eds), George Allen and Unwin (Publishers) Ltd., London WC1A 1LU, 526 pp.

Barker, F., 1979: Trondhjemite: Definition, environment and hypothesis of origin, pp 1-12.. In: *Trondhjemites, dacites and related rocks*, Barker, F. (ed). Elsevier Scientific Publishing, Amesterdam, 659 pp.

Barr, M.W.C., Donning, K.N., Hammil, M., Harding, A.E., Loughlin, W.P., Potts, J.G.,1983: Geological and prospecting survey in north eastern Mozambique. Unpubl. Hunting report, ING, Maputo.

Barton, J.M.Jr., Klemd, R., Allsopp, H.L., Auret, S.H. and Copperthwaite, Y.E., 1987: The geology and geochronology of the Annandagstoppane granite, Western Dronning Maud Land, Antarctica. *Contribution Mineralogy and Petrology*, **97,** 488-496.

Berger, W.G. and York, D., 1981: Geothermometry from $^{40}Ar/^{39}Ar$ dating experiments. *Geochemica and Cosmochimica Acta*, **45**, pp. 795-811.

Berman, R.G., 1990: Mixing properties of Ca-Mg-Fe-Mn garnets. *American Mineralogist*, **75**. 328-344.

Berman, R.G., 1991: Thermobarometry using multiequilibrium calculations: a new technique with petrologic applications. *Canadian Mineralogist*, **29**, 833 - 855.

Brey, G. T. and Köhler, T., 1990: Geothermobarometry in four phase lherzolites, part II: new thermobarometers, and practical assessment of existing thermobarometers. *Journal of Petrol.*, **31**, 1353-1378.

Bucher, K., Frey, M., 1994: *Petrogenesis of Metamorphic Rocks*. Springer-Verlag, New York, 318 pp.

Clarke, D.B., 1992: *Granitoids Rocks*, Chapman and Hall, 2-6 Boundary row, London, 283 pp.

Dalziel, I.W.D., 1991: Pacific margins of Laurentia and east Antarctica-Australia as a conjugate rift pair: Evidence and mplications for an Eocambrian supercontinent. *Geology*, **19**, 598-601.

Deer, W.A., Howie, R.A. and Zussman, J., 1992: *An introduction to rock-forming minerals*. Longman Group UK Limited, 696 pp.

Dirks, P.H.GM., Jelsma, M. Vinyu and Munyanyiwa, H., (1998): The structural history of the Zambezi Belt in northeast Zimbabwe; evidence for crustal extension during the early Pan-African. *South African Journal of Geology*, **101 (1)**, 1-16.

Ebadi A, Johannes W (1991) Beginning of melting and components of first melts in the system Qz-Ab-Or-H_2O-CO_2. *Contributions to Mineralogy and Petrology* **106**, 286-295

Eby, G.N., 1990: The A-type granitoids: A review of their occurrence and chemical characteristics and speculations on their petrogenesis. *Lithos,* **26**, 115-134.

Eby, G.N., 1992: Chemical subdivision of the A-type granitoids: Petrogenetic implications. *Geology*, **20**, 641-644.

Eckert, J.O. Newton, R.C. and Kleppa, O.J., 1991: The ΔH of reaction and recalibration of garnet-pyroxene-plagioclase-quartz geobarometers in the CMAS system by solution calorimetry. *American Mineralogist*, **76**, 148-160.

El Bouseily, A.M. and El Sokkary, A.A. 1975: The relationship between Rb, Ba and Sr in granitic rocks. *Chemical Geology*, **16**, 207-219.

Ellis, D. J., 1980: Osumilite-sapphirine-quartz granulites from Enderby Land, Antartica: P-T conditions of metamorphism, implications for garnet-cordierite equilibria and the evolution of the deep crust. *Contribution Mineralogy and Petrology*, **74**, 201-210.

Evensen, N.M., Hamilton, P.J. and O'Nions, R.K., 1978: Rare earth abundfances in chondritic meteorites. *Geochimica and Cosmochimica Acta*, **42**, 1199-1212.

Faure, G., 1986: *Principles of isotope geology*. John Wiley, New York, 589 pp.

Fuhrman, M.L. and Lindsley, D.H., 1988: Ternary-feldspar modeling and thermometry. *Am. Mineral.*, **73**: 201-215

Gouveia, J. A. C. *et al.*1968: Carta Geologica da Regiao de Vila Manica - Vila Gouveia, Grau Quadrado 1833, 1:250 000. *Servico Geologicoe Mineiro de Mocambique.*

Graham, C.M. and Powell, R., 1984: A garnet-hornblende geothermometer: calibration, testing and application to the Pelona schist, Southern California. *J. Metamorphic Geol.*, **2**. 13-31.

Grantham, G.H., Groenewald, P.B. and Hunter, D.R., 1988: Geology of the northern H.U. Sverdrupfjella,
western Dronning Maud Land and implications for Gondwana reconstructions. *S. Afr. T. Nav. Antarkt., Deel* **18, No. 1**, 2-10.

Grantham, G.H., Moyes, A.B. and Hunter, D.R., 1991: The age, petrogenesis and emplacement of the Dalmatian Granite, H.U. Sverdrupfjella, Dronning Maud Land, Antarctica. *Antarctica Science* **3**, 197-204.

Grantham G.H., Thomas, R.J. and Mendonidis, P., 1994: Contrasting P-T-t loops from southern East Africa, Natal and East Antartica. *Journal of African Earth Sciences*, **19**, 225-235.

Grantham G.H.,Jackson, C., Moyes, A.B., Groenewald, P.B., Harris, P.D., Ferrar, G. and

Krynauw, J.R., 1995: The tectonothermal evolution of the Kirwanveggen-H.U. Sverdrupfjella areas, Dronning Maud Land, Antarctica. *Precambrian Research*, **75**, 209-229.

Grantham, G.H., Storey, B.C., Thomas, R.J. and Jacobs, J., 1997: The Pre-Break-Up of Haag Nunataks within the Gondwana: Possible Correlatives in Natal and Dronning Maud Land. *The Antactica Region: Geological Evolution and processes*, 13-20.

Green, T.H. and Pearson, N.J., 1986: Ti-rich accesssory phase saturation in hydrous mafic-felsic compositions at high P,T. *Chemical Geology*, **54**, 185-201.

Groenewald, P.B., Grantham, G.H. and Watkeys, M.K., 1991: Geological evidence for a Proterozoic to Mesozoic link between southeastern Africa and Dronning Maud Land, Antarctica. *Journal of the Geological Society, London*, **148**, 1115-1123.

Groenewald, P.B., 1993: Correlation of cratonic and orogenic provinces in southeastern Africa and Dronning Maud Land, Antarctica. *Gondwana Eight, Findlay, Unrug, Banks and Veevers (eds)*, Balkema, A.A., Rotherdam.
pp. 111-122.

Harmer, R.E.and Eglington, B.M., 1987: The mathematics of geochemistry: Equations for use in regression calculations. *National Physical Research Laboratory, Geochronology Division C.S.I.R., South Africa*.

Harrison, T.M. and Watson, E.B., 1984: The behaviour of apatite during crustal anatexis: Equilibrium and kenetic considerations. *Geochemica and Cosmaquimica Acta*, **48**, 167 - 1477.

Hunter, D.R., 1973: The granitic rocks of the Precambrian in Swaziland. *Spec. Publs Geol. Soc. S. Africa*, **3**, 131-145.

Irvine, T. N. And Baragar, W. R. A., 1971: A Guide to the Chemical Classification of the Common Volcanic Rocks. *Canadian Journal of Earth Sciences*, **8**, pp. 523 - 548.

Jahn, B.M.,Glickson, A.Y., Peucat, J.J., and Hickman,A.H., 1981: REE geochemistry and isotopic data of Archaean silicic volcanics and granitoids from Pilbara Block, western Australia: implications for the early crustal evolution. *Geochim. Cosmochim. Acta*, **45**, 1633-1652.

Jensen, L.S., 1976: A New Cation Plot for Classifying Subalkaline Volcanic Rocks. Ontario Div. Mines. Misc. Pap. 66.

Johannes W & Holtz F., 1990: Formation and composition of H_2O-undersaturated granitic melts pp. 87-104. In: *High Temperature Metamorphism and Crustal Anatexis*, Ashworth J.R. & Brown M. (eds), Unwin Hyman, London, 407pp.

Johannes, W.,1985: The significance of experimental studies for the formation of migmatites. pp. 36-85. In: Migmatites, Ashworth, J.R. (ed), Blackie, Glasgow pp. 301.

Kohn, M.J. and Spear, F.S., 1989: Empirical calibration of geobarometers for the assemblage garnet+hornblende+plagioclase+quartz. *Am. Mineral.*, **74**, 77-84

Kohn, M.J. and Spear, F.S., 1990: Two new geobarometers for the garnet amphibolites, with applications to southeastern Vermont. *Am. Mineral.*, **75**, 89-96.

Le Maitre, R.W., 1976: Some problemss of the projection of chemical data into mineralogical classifications. Contrib. Mineral. Petrol. **56**, 181-189.

Le Maitre, R.W., 1989: *A Classification of Igneous Rocks and Glossary of Terms*. Blackwell Scientific Publications, Oxford, 193 pp.

Manuel, I.R.V., 1992: Geologie, *Petrgraphie, Geochemie und Lagerstatten der Manica-Greenstone-Belt (Mozambique)*. Ph.D. thesis, unpubl., Rheinisch-Westfalishen Technishen Hochschule Aachen, 210 pp.

Martin, H., 1987: Petrogenesis of Archaean trondhjemites, tonalites and granodiorites from Eastern Finland: Major and trace elements geochemistry. *Journal of Petrology*, **28/5**, 921 - 953.

McCulloch, M.T. and Black, L.P. (1984): Sm-Nd isotopic systematics of Ebderby Land granulites and evidence for redistribution of Sm and Nd during metamorphism. *Earth Planetary Science Letters*, **71**, 46-58.

Mehnert, K.R., 1968: *Migmatites and the origin of granitic rocks*. Elssevier, Amsterdam, 405 pp.

Mehnert, K.R., 1987: The granitization problem- revisited. *Fortschritte der Mineralogie*, **65**, 285-306.

Mezger, K., 1991: Geochronology in granulites, pp. 451-470. In: *Granulites and crustal evolution*. Vielzeuf, D. And Vidal, Ph. (eds). Kluwer Academic Publisher, Dordrecht, 585pp.

Moyes, A.B., Barton Jr, J.M. and Groenewald, P.B., 1993: Late Proterozoic to Early Palaeozoic tectonism in the Dronning Maud Land, Antarctica: supercontinental fragmentation and amalgamation. *Journal of the Geological society, London*, **150**, 833 - 842.

Oberlholzer, W.F., 1964: A geologia da Mancha de Manica.Unpubl, *Direccao dos servicos de Geologia e Minas*, 44 pp.

Obretenov, N., 1977: Regiao de Manica. Relatorio sobre os resultados do estudo geologico e dos trabalhos da prospeccao e pesquisa executados em 1976. Unpubl, *Direccao Nacional de Geologia*, 14 pp.

O'Connor, J.T., 1965: A classification of quartz-rich igneous rocks based on feldspar ratios. *U.S. Geol. Surv. Prof. Paper* **525B**, B79-B84.

Pearce, J.A., 1983: The role of subcontinental lithosphere in magma genesis at destructive plate margins, pp. 230-249. In: *Continental basalts and mantle xenoliths*, Hawesworth, C.J., and Norry, M.J. (eds.). Nantwich, Shiva Publications.

Pearce, J.A., Harris, N.B.W. and Tindle, A.G., 1984: Trace elements discrimination diagrams for the tectonic interpretation of granitic rocks. *Journal of Petrology*, **25 / part 4**, 956-983.

Perchuck, L.L., Aronovich, L.Ya., Podlesskii, K.K., Lavranteva, I.V., Gerasimov, V.Yu. and Fedkin, V.V., (1985): Precambrian granulites of Aldan shield, eastern Siberia, USSR. *Journal of Metamorphic Geol*ogy, **3**, 265-310.

Petters, S., 1991: *Regional geology of Africa,* Springer-Verlag berlin Heidelberg, 722 pp.

Phaup, A.E., 1937: The geology of the Umtali Gold Belt. *Geol. Surv. Bull. S. Rhod.*, **45**

Pinna, P., Jourde, G., Calvez, J.Y., Mroz, J.P. and Marques, J.M., 1993: The Mozambique Belt in northern Mozambique: Neoproterozoic (1100-850) crustal growth and tectogenesis, and

superimposed Pan-african (800-550 Ma) tectonism. *Precambrian Research* **62**, 1-59.

Pinna, P., Marteau, P., Beco-Giraudon, J.F. and Manigault, B., 1986: *Notice explicative de la Carte geologique a 1/1 000 000 de la Republique Populaire du Mozambique*. Unpubl., Instituto Nacional de Geologia, 261 pp.

Pitcher, W.S., 1993: *The nature and origin of granite,* Blackie Academic and Professional, Chapman and Hall, 321 pp.

Powell, R. and Holland, T.J.B., 1988: An internally consistent data set with uncertainties and correlations: Applications to geobarometry, worked examples and a computer program. *Jnl. Metamorphic Petrol.*, **6**, 173-204.

Pownceby, M. I., Wall, V. J. and O'Neill, H. St. C., 1987 : Errata. Fe-Mn partitioning between coexisting garnet and ilmenite: experimental calibration and applications. *Contrib. Mineral. Petrol.*, **97**, 539.

Pownceby, M. I., Wall, V. J. and O'Neill, H. St. C., 1991: An experimental study of the effect of Ca upon garnet-ilmenite Fe-Mn exchange equilibria. *American Mineralo*gist, **76**, 1580-1588.

Rollinson, H.R., 1993: Using Geochemical Data: *Evaluation, Presentation, Interpretation*. Longman London, 341 pp.

Schwarz, H., 1994: Geology and Mineralization of an Alluvial Gold Deposit, Odzi - Manica-Greenstone Belt, Mozambique. *Z. angew. Geol*, **40** (1994) 2, 80-86.

Sengupta, P., 1989: Mixxing behavior in quaternary garnet solid solution and an extended Ellis and Green garnet-clinopyroxener geothermometer. *Contribution Mineralogy and Petrology*, **103**, 223-227.

Servicos de Geologia e Minas da Provincia de Mocambique (1969): Carta Geologica da Regiao de Vila Manica-Vila Gouveia, Grau Quadrado 1833, Scale 1:250 000

Shand, S.J., 1947: *Eruptive Rocks. Their genesis, composition, classification, and their relation to ore deposits*, J. Wiley and sons, New York, 448 pp.

Shelley, D., 1993: *Igneous and metamorphic rocks under the microscope, classification, textures, microstructures and mineral preferred-orientations*, Chapman and Hall, 2-6 Boundary Row, London, 445 pp.

Smith, J.V. and Mackenzie, W.S., 1959: The alkaline feldspars. *Am. Mineral.*, **44**, 1169-1186.

Spry, A., 1969: *Metamorphic Textures.* Pergamon Press, Ltd., Oxford, 350 pp.

Streckeisen, A., 1976: To each plutonic rock its proper name. *Earth Sci. Rev.* **12**, 1-33.

Sun, S., 1980: Lead isotopic study of young volcanic rocks from mid-ocean ridges, ocean islands and island arcs. *Phil. Trans. R. Soc. London*, **A 279**, 409-445.

Vail, J.R., 1964: Esboco geral da geologia da regiao entre os rios Lucite e Revue, distrito de Manica e Sofala, Mocambique. *Bol. Sev. Geol. Minas*, **32**. 47-59

Vail, J.R., 1965: Estrutura e geochronologia da parte oriental da Africa Central, com referencia a Mocambique. *Bol. Sev. Geol. Minas*, **33**, 15-31

Viljoen, M.J. and Viljoen, R.P., 1969: An introduction to the geology of the Barberton granite-greenstone terrain. *Sp. Publ. Geol. Soc. S. Africa*. **2**, 9-28.

Viljoen, M.J., Viljoen, R.P. and Pearton, T.N., 1982: The nature and distribution of Archaean komatiite volcanics in South Africa, pp. 53-79, in "*Komatiites*", Arndt,N.T. and Nisbet, E.G. (eds). George Allen and Unwin (Publishers) Ltd, 40 Museum Street, London, 526 pp.

Watson, E.B. and Harrison, T.M., 1983: Zircon saturation revisited: temperature and composition effects in a variety of crustal magma types. *Earth and Planetary Science Letters*, **64**, 295 - 304.

Whalen, J.B., Currie, K.L. and Chappell, B.W., 1987: A - Type granites: geochemical characteristics, discrimination and petrogenesis. *Contributions to Mineralogy and Petrology*, **95**, 407 - 419.

Wilson. J.F., Bickle, M.J., Hawkesworth, C.J., Martin, a., Nisbet, E.G. and Orpen, J.L., 1978: Granite-greenstone terraines of the Rhodesian Archean craton. *Nature*, **271**, 23-27.

Windley, B.F., 1993: Proterozoic anorogenic magmatism and its orogenic connections. *Journal of the Geological society, London*, **150**,39 - 50.

Winkler, H.G.F., 1974: *Petrogenesis of Metamorphic Rocks*. Springer-Verlag New York Inc., 320 pp.

Wood, B.J. and Banno, S., 1973: Garnet-Orthopyroxene and Orthopyroxene-clinopyroxene relationships in simple and complex systems. *Contributions to Mineralogy and Petrology*, **42**, 109-124.

Wood, D.A., Joron, J. And Treuil, M., 1979: A Re-appraisal of the use of trace elements to classify and discriminate between magma series erupted in different tectonic settings. *Earth and Planetary Science Letters*, **45,** 326 - 336.

Yardley, B.W.D., 1989: *An Introduction to Metamorphic Petrology*. Longman, London, 248 pp.

Appendix 1: Samples per lithological unit, locality and coordinates of samples used in geochronology, geothermobarometry and thermochrology as referred to in the respective sections.

Lithological Unit	Sample	Locality	Coordinates
Vumba Granite Gneiss	VGI	Vumba	
	VGII	Vumba	
	VGIII	Vumba	
	VGIV	Vumba	
	VGV	Vumba	
	VG3-1	Vumba	
	VG3-2	Vumba	18°57'52"/32°50'24"
	VG3-3	Vumba	
	VG3-4	Vumba	
	VG3-5	Vumba	
	VG3-6	Vumba	
	VGr1	Vumba	
	VGr2	Vumba	18°57'20"/32 °54'59"
	MpG	Machipanda	
	MkG	M'kwananda	
Macequece Formation	ma	Manica	
	ba	Manica	
	mb	Manica	
	mc	Manica	
	scg	Manica	
	8	Manica	
	epsc1	Manica	
	26aga	Penhalonga	
	26scg	Penhalonga	
	Ndqtz	Ndirire	
M'Beza/Vengo Formation	21sc	Vengo	
	mbsh	M'Beza	
	zash	Zambuzi	
Messica Granite Gneiss	PdGr1	Messica	19°00'50"/33°05'18"
	PdGr2	Messica	19°00'52"/33°07'18"
	PdGr3	Messica	
	PdGr4	Messica	
	PdGr5	Messica	

	PdGr6	Messica	
	CNO1	Messica	
	CNO2	Messica	
	CNO3	Messica	
	CNO4	Messica	
	CNO5	Messica	
	CNO6	Messica	
	MGn3	Messica	
	Mgn5	Messica	
	M'SKg	Messica	
Frontier Formation	GQZ	Garuzo	
	GSC	Garuzo	
	GMSC	Garuzo	19°02'16"/33°09'48"
	GAQZ1	Garuzo	
	CHQZ	Chicamba	19°09'28"/33°08'32"
	31CHQ1	Chimezi	
	31CHQ2	Chimezi	
Vanduzi Migmatite Gneiss	mh'gn	Matsinho	
	grR	Vanduzi	
	nzgg1	Vanduzi	
	mggnv	Vanduzi	
	gr5	Vanduzi	
Chimoio Granodioritic Gneiss	cvgna	Chimoio	19°06'06"/33°30'15"
	cvgnb	Chimoio	
	cvgnc	Chimoio	
	cvgnd	Chimoio	
	cvgne	Chimoio	
	cvgnf	Chimoio	
Nhansipfe Granitic Gneiss	nfgn1	Nhansipfe	
	nfgn2	Nhansipfe	19°06'28"/33°18'31"
	nfgn3	Nhansipfe	
	nfgn4	Nhansipfe	
	nfgn5	Nhansipfe	19°06'26"/33°18'33"
	nfgn6	Nhansipfe	
	mggn1	Nhansipfe	
	mggn2	Nhansipfe	

	nggn2	Nhansipfe	
	ndgn1	Nhansipfe	
	nzgg1	Nhansipfe	
	nzgn2	Nhansipfe	
	nzgn3	Nhansipfe	
	mrgn	Mombeza	
	chgn	Chibata	
	mhgn1	Matsinho	
	mhgn2	Matsinho	
	mhgn3	Matsinho	
	mhgn4	Matsinho	
	mhgn5	Matsinho	
	mhgn6	Matsinho	
	mhgr	Matsinho	
	mhgn6	Matsinho	
	agn1	Almada	
	agn2	Almada	
	agn3	Almada	
	agn4	Almada	
	agn5	Almada	
	agn6	Almada	
	pcy	Chibata	
	mcgr	Chibata	
	mxc	Chibata	
	GRP	Chibata	
	GRF	chibata	
Mafic Dykes	18S	Manica	
	MDo	Vumba	
	15M	Penhalonga	
	12T	Penhalonga	
	maamp1	Messica	
	maamp	Messica	19°00'29"/33°06'27"
	maamp2	Messica	
	amp*	Manica	
	mramp	Mombeza	
	chm	Chicamba	

	mbamp	Mombeza	18°59'53"/33°24'50"
	MXC	Chibata	19°03'54"/33°18'52"
	MX2	Chibata	
	MX	Chibata	
Tchinhadzandze Granodiorite Gneiss	ygr1	Tchinhadzandze	
	ygr2	Tchinhadzandze	
	ygr3	Tchinhadzandze	
	ygr4	Tchinhadzandze	
	ygr5	Tchinhadzandze	
	ygr6	Tchinhadzandze	

Appendix 2: Complete microprobe analyses, cation site allocations and recalculations of of mineral end-members proportions..

Garnets

Sample	mbamp	mbamp	mbamp	mbamp	mbamp	mbamp	mbamp	mbamp	mbamp
Analysis	21	22	33	34	15	12	11	45	46
SiO_2	37.67	37.87	38.12	37.57	38	38.18	38.06	38.12	38.34
TiO_2	nd	nd	nd	nd	nd	0.05	Nd	0.05	nd
Al_2O_3	21.6	21.77	21.44	21.14	21.31	21.51	21.44	21.33	21.83
FeO	30.51	30.23	29.8	29.41	30.55	30.14	29.78	30.53	29.46
MnO	1.61	1.52	1.39	1.46	1.42	1.26	1.33	1.6	1.61
MgO	3.23	3.28	3.22	3.19	2.77	3	2.91	2.65	3.27
CaO	7.26	7.13	7.47	7.38	7.29	7.1	7.26	7.51	7.02
TSi	2.938	2.953	2.982	2.977	2.987	2.997	3.001	2.985	2.994
[4]Al	0.062	0.047	0.018	0.023	0.013	0.003	0	0.015	0.006
Sum_T	3	3	3	3	3	3	3	3	3
[6]Al	1.922	1.952	1.957	1.95	1.959	1.986	1.991	1.952	2.002
Ti	0	0	0	0	0	0.003	0	0.003	0
Fe2+	1.99	1.971	1.949	1.949	2.008	1.979	1.964	1.999	1.924
Mg	0.376	0.381	0.375	0.377	0.325	0.351	0.342	0.309	0.381
Mn	0.106	0.1	0.092	0.098	0.095	0.084	0.089	0.106	0.106
Ca	0.607	0.596	0.626	0.627	0.614	0.597	0.613	0.63	0.587
Sum_cat	8	8	8	8	8	8	8	8	8
XGrs	0.197	0.196	0.206	0.206	0.202	0.198	0.204	0.207	0.196
XAlm	0.646	0.647	0.641	0.639	0.66	0.657	0.653	0.657	0.642
XPy	0.122	0.125	0.123	0.124	0.107	0.117	0.114	0.102	0.127
Xps	0.034	0.033	0.03	0.032	0.031	0.028	0.03	0.035	0.035

Garnets (cont.)

Sample	MaAmp	MaAmp	MaAmp	MaAmp	Gcmx	Gcmx	Mxc	mxc	mxc
Analysis	2	9	12	20	5	9	8	5	3
SiO_2	37.68	37.69	37.75	37.36	36.14	36.34	37.06	37.07	36.98
TiO_2	nd	0.11	nd	nd	ND	ND	nd	nd	nd
Al_2O_3	21.55	21.49	21.42	21.62	20.98	21.2	21.3	21.37	21.22
FeO	28.81	28.77	28.3	29.51	38.83	38.47	30.19	30.4	30.64
MnO	1.08	1.22	0.97	1.09	1.31	1.34	1.41	1.29	1.38
MgO	2.85	2.82	3.11	3.16	1.48	1.36	2.81	2.77	2.65
CaO	8.12	8.11	8.49	7.23	1.37	1.5	6.92	7	6.72
TSi	2.984	2.983	2.984	2.963	2.947	2.959	2.959	2.954	2.961
[4]Al	0.016	0.017	0.016	0.037	0.053	0.041	0.041	0.046	0.039
Sum_T	3	3	3	3	3	3	3	3	3
[6]Al	1.994	1.987	1.978	1.982	1.962	1.992	1.962	1.96	1.962
Ti	0	0.007	0	0	0	0	0	0	0
Fe2+	1.908	1.904	1.871	1.957	2.648	2.62	2.016	2.026	2.052
Mg	0.336	0.333	0.367	0.374	0.18	0.165	0.334	0.329	0.316
Mn	0.072	0.082	0.065	0.073	0.09	0.092	0.095	0.087	0.094
Ca	0.689	0.688	0.719	0.614	0.12	0.131	0.592	0.598	0.576
Sum_cat	8	8	8	8	8	8	8	8	8
XGrs	0.229	0.229	0.238	0.203	0.039	0.044	0.195	0.197	0.19
XAlm	0.635	0.633	0.619	0.648	0.872	0.871	0.664	0.666	0.675
XPy	0.112	0.111	0.121	0.124	0.059	0.055	0.11	0.108	0.104
XSps	0.024	0.027	0.022	0.024	0.030	0.031	0.031	0.029	0.031

Ilmenites

sample	Analysis	SiO_2	TiO_2	FeO	MnO	MgO	Ti	Fe^{2+}	Mn	Mg
mxc	7	0	49.84	48.1	0.35	0.39	4.037	4.332	0.032	0.063
mxc	8	0.18	49.85	48.32	0.4	0.46	4.013	4.325	0.036	0.073

Plagioclase feldspars

Sample	MaAmp	MaAmp	mbamp	mbamp	mbamp
Analysis	12	5	13	41	43
SiO_2	54.51	54.92	59.18	58.78	58.6
Al_2O_3	28.61	28.44	25.94	26.27	26.42
CaO	11.33	10.83	7.73	7.79	7.96
Na_2O	5.51	5.4	6.67	6.95	6.47
K_2O	0.15	0.14	0.34	0.32	0.25
Si	2.461	2.481	5.277	5.241	5.226
Al	1.521	1.513	2.724	2.759	2.775
Ca	0.548	0.524	0.738	0.744	0.761
Na	0.482	0.473	1.153	1.202	1.119
K	0.009	0.008	0.039	0.036	0.028
XAb	0.464	0.471	0.597	0.606	0.586
XAn	0.527	0.521	0.382	0.375	0.399
XOr	0.009	0.008	0.02	0.018	0.015

Pyroxenes

mineral	Opx	Opx	Cpx	Cpx	Cpx	Cpx
sample	mbamp	mbamp	mbamp	mbamp	mbamp	mbamp
Analysis	33	34	21	22	11	12
SiO_2	49.93	50.57	50.6	50.7	50.7	50.59
TiO_2	0.05	0.09	0.15	0.18	0.13	0.22
Al_2O_3	0.85	1.01	1.76	2	1.93	1.99
FeO	34.41	34.77	14.74	14.57	15.54	15.54
MnO	0.61	0.58	0.3	0.24	0.23	0.28
MgO	13.93	13.84	10.43	10.21	10.26	10.18
CaO	0.66	0.7	21.49	21.47	20.79	20.74
Na_2O	nd	nd	0.51	0.51	0.49	0.48
Si	1.963	1.968	1.929	1.935	1.935	1.933
[4]Al	0.037	0.032	0.071	0.065	0.065	0.067
[6]Al	0.002	0.014	0.008	0.025	0.022	0.023
Ti	0.001	0.003	0.004	0.005	0.004	0.006
Fe2+	1.132	1.132	0.47	0.465	0.496	0.497
Mg	0.816	0.803	0.593	0.581	0.584	0.58
Mn	0.02	0.019	0.01	0.008	0.007	0.009
Ca	0.028	0.029	0.878	0.878	0.85	0.849
Na	0	0	0.038	0.038	0.036	0.036
Sum_cat	4	4	4	4	4	4

Amphibole

Sample	Maamp	Maamp	Maamp	Maamp	mxc	mxc	mbamp	mbamp	mbamp
Analysis	11	14	18	20	6	9	15	45	46
SiO_2	48.72	49.22	49.07	47.75	41.72	42.33	42.01	42.17	42.18
TiO_2	0.84	0.74	0.81	0.94	2.1	1.95	2.21	1.93	2.09
Al_2O_3	7.37	7.44	7.54	8.36	10.49	10.46	11.9	12.22	11.99
FeO	16.27	16.82	16.49	16.84	22.05	21.86	21.09	20.37	20.4
MnO	nd	nd	0.13	0.17	0.14	0.1	0.14	0.12	0.14
MgO	11.14	11.45	11.16	10.65	6.76	6.88	7.85	8.13	8.17
CaO	11.74	11.63	11.71	11.61	11.51	11.44	11.22	11.36	11.2
Na2O	0.94	0.99	0.82	1.17	1.39	1.23	1.62	1.63	1.68
K2O	0.59	0.53	0.56	0.64	1.39	1.5	ND	ND	ND
Si	7.192	7.183	7.192	7.05	6.468	6.529	6.38	6.387	6.395
[4]Al	0.808	0.817	0.808	0.95	1.532	1.471	1.62	1.613	1.605
[6]Al	0.473	0.462	0.493	0.503	0.383	0.429	0.509	0.566	0.536
Ti	0.093	0.081	0.089	0.104	0.245	0.226	0.252	0.22	0.238
Mg	2.451	2.491	2.438	2.344	1.562	1.582	1.777	1.836	1.847
Fe2+	2.009	2.053	2.021	2.079	2.859	2.82	2.461	2.378	2.379
Mn	0	0	0.016	0.021	0.018	0.013	0.018	0.015	0.018
sum oct	5.026	5.087	5.057	5.051	5.067	5.07	5	5	5
Ca	1.857	1.818	1.839	1.837	1.912	1.891	1.826	1.844	1.82
Na[M4]	0.117	0.095	0.103	0.111	0.02	0.04	0	0	0
Na[A]	0.152	0.185	0.13	0.224	0.398	0.328	0.477	0.479	0.494
K	0.111	0.099	0.105	0.121	0.275	0.295	0	0	0
Sum_A	0.263	0.284	0.235	0.344	0.673	0.623	0.477	0.479	0.494
Sum_cat	15.263	15.284	15.235	15.344	15.673	15.623	15.538	15.54	15.539

ND=not determined, nd=not detected.

Appendix 3: Description of analytical techniques

1. In all tables of chemical analyses, iron oxide is presented as FeO which was calculated from Fe_2O_3 analyses, according to Le Maitre (1976).
2. X-Ray fluorescence analyses were executed using an ARL 8420 wavelength dispersive XRF Spectrometer.
   The samples were dried and roasted at 950 °C to determine loss on ignition.
   Major element analyses were executed on fused beads in which to 1g sample were added 6g of lithium tetraborate flux.
   Trace elements were analysed on pressed pellets.
   The XRF Spectrometer was calibrated with certified reference materials, and NBSGSC fundamental parameter was used for matrix correction.
3. Microprobe analyses were done using a Jeol 733 Superprobe with 4 wavelength spectrometers and Iemas Energy Dispersive System (EDS) from OXFORD/LINK, controlled by OXFORD/LINK ex1ll system.
   The analytical conditions were set for EDS mode with beam current of 20 nA, acceleration voltage of 20 kw, and beam size of <1.5 μm (de-focused beam for plagioclase and micas). Counting times on all silicates were 100 seconds (livetime acquisition).